DISSERTATION

CATALYZED CHEMICAL SYNTHESIS OF DESIGNER POLY(3-HYDROXYALKANOATE)S: TUNING FUNCTION, MICROSTRUCTURE, AND ARCHITECTURE OF BIODEGRADABLE POLYMERS

Submitted by

Andrea Hope Westlie

Department of Chemistry

In partial fulfillment of the requirements

For the Degree of Doctor of Philosophy

Colorado State University

Fort Collins, Colorado

Fall 2022

Doctoral Committee:

Advisor: Eugene Y.-X. Chen

Garret Miyake
Nancy Levinger
Margarita Herrera-Alonso

ABSTRACT

CATALYZED CHEMICAL SYNTHESIS OF DESIGNER POLY(3-HYDROXYALKANOATE)S: TUNING FUNCTION, MICROSTRUCTURE, AND ARCHITECTURE OF BIODEGRADABLE POLYMERS

This dissertation describes the development of a chemocatalytic route towards biodegradable poly(hydroxyalkanoate)s (PHAs) based on the ring-opening polymerization of eight-membered cyclic diolide, 8DL, by discrete yttrium complexes. This chemocatalytic platform has transformed the brittle, poly(3-hydroxybutyrate) (P3HB) to high performance, "designer" PHAs through the use of molecular catalysts and the development of a precision polymerization methodology. There continues to be a pressing need for biodegradable polymers in applications where material recovery is unlikely or impossible or where environmental leakage of the plastic waste is highly likely. PHAs are truly biodegradable polyesters that can degrade in ambient conditions such as aerobic soil and marine environments and these polyesters are laden with tunability enabled by their chirality, composition, and architecture. A major challenge in implementing PHAs is to achieve truly tunable thermomechanical properties for any application, coupled with desirable processing conditions at scale.

A critical literature review overviews the decades-long history of various chemocatalytic routes towards PHAs with either controlled tacticity or composition. To demonstrate the scope of our chemocatalytic platform, extensive study of homo- and copolymerization of three $8DL^{R}$ (R = Me, Et, Bu) has been performed. Judicious choice of catalyst to match the steric bulk of the monomer results in high activity and high stereoselectivity ROP of these uncommon PHA

homopolymers and allows for highly precise random copolymers of *rac*-8DL^{Me} with targeted compositions ranging from 5 ~ 40 % incorporation of 8DL^{R} (R = Et, Bu). Moving from aliphatic to aromatic substituents allowed for the synthesis of unnatural and previously unknown PHA with a glass transition (T_g) above room temperature (RT). Aliphatic-aromatic copolymers with designed architecture as random or block copolymers could be synthesized as well. And finally, recently we have designed and synthesized discrete PHA triblock copolymers towards achieving thermoplastic elastomer materials.

Overall, this work has used fundamental investigation into a stereoselective, coordination-insertion polymerization mechanism and the resulting structure-property relationships to design higher-performance PHAs that are, in some cases, competitive with commodity polyolefins. This work serves as a platform for further development of PHAs using this chemocatalytic route towards new topologies, compositions, and functions.

ACKNOWLEDGEMENTS

Chapter 2. This dissertation chapter contains the manuscript of a full review article submitted to Progress in Polymer Science [Westlie, A. H.; Quinn, E. C.; Parker, C. R.; Chen, E. Y.-X. Progress in Polymer Science. *Submitted July, 2022*]. The work was supported in part by the US National Science Foundation (NSF-1955482) and by the U.S. Department of Energy, Office of Energy Efficiency and Renewable Energy (EERE), Advanced Manufacturing Office (AMO) and Bioenergy Technologies Office (BETO), as part of the BOTTLE™ Consortium, which includes the members from Colorado State University, under contract no. DE-AC36-08GO28308 with the National Renewable Energy Laboratory.

Chapter 3. This dissertation chapter contains parts of the manuscript of a full paper published in Angewandte Chemie International Edition. [Tang, X.; Westlie, A. H.; Caporaso, L.; Cavallo, L.; Falivene, L.; Chen, E. Y.-X. Angew. Chem. Int. Ed. 2020, 59, 7881-7890.] Author contributions: X.T. designed and conducted experiments related to monomer and polymer synthesis as well as polymer characterizations. A.H.W. performed experiments related to initial copolymerization studies, monomer synthesis, and multi-gram scale copolymerizations. X.T., L.F. and E.Y.-X.C. wrote the initial manuscript and revised subsequent versions of the manuscript, and all authors contributed to the revised manuscript. This work was supported by the U.S. National Science Foundation (NSF-1664915) for the study carried out at Colorado State University. This work made use of the Central Instrument Facilities of Colorado State University and the polymer characterization instruments of the Chen and G. Miyake research groups.

Chapter 4. This dissertation chapter contains the manuscript of a full paper published in Macromolecules [Westlie, A.H. and Chen, E. Y.-X. Macromolecules 2020, 53, 9906-9915]. The work was supported by the US National Science Foundation (NSF-1955482).

Chapter 5. This dissertation chapter contains the prepared manuscript for submission Fall 2022. This work was performed as part of the BOTTLE™ Consortium, which includes the members from Colorado State University, and funded under contract no. DE-AC36-08GO28308 with the National Renewable Energy Laboratory, operated by Alliance for Sustainable Energy. This work made use of the Analytical Resources Core of Colorado State University and the polymer characterization instruments of the Chen and G. Miyake research groups. We thank R. W. Clarke and C. Shi of the Chen group for assistance with polymer analysis and R. M. Cywar of the NREL for insightful discussions. Author contributions: E.Y.-X.C. conceived the project and directed research. A.H.W. designed and conducted experiments related to monomer and polymer synthesis, and X.T. performed experiments related to monomer and polymer synthesis. E.C.Q. and C.R.P. performed experiments related to monomer and catalyst synthesis. A.H.W., S.A.H., C.J.T., and C.T. performed experiments related to polymer characterization.

Thank you to my committee members, Garret, Nancy, and Margarita for being supportive of me throughout my big milestones throughout graduate school. Garret, thank you for being like a second mentor to me and always having an open door and being willing to chat. Thank you Nancy for always being willing to listen and encouraging me throughout the years.

Thank you to my Chen group colleagues who have been such a light these past few years. The group has grown to be so supportive and collaborative and it is my privilege to have gotten to work alongside you all. Thank you, Ryan, for being the best coworker and friend I could have asked for during this PhD and Reid for always being so supportive and lending an ear when I'm stressed out.

Thanks, Robin, for being such a strong scientist to look up to and a friend throughout the years. Thanks Celine and Ethan for joining a few years ago with your positive and bright energy and reminding me how cool the research is and inspired me to help foster a better environment to learn.

Thank you to the folks at NREL who I've been lucky enough to work with while part of the BOTTLE consortium: Gregg, Kat, and Bob you have helped to elevate my confidence as a scientist to a place I didn't know I could ever find. Thank you for valuing me and always encouraging me.

Thank you to my wonderful friends, near and far, who have never failed to pick up a Facetime call. Sarah, Emma, Bridget, Ruth, Mariel, Sam, and Diane – thank you for being my rocks throughout the past five years. I wouldn't have been able to get through this without you.

Thank you to my family: Mom, Dad, Tyler, Claire, Bryan, Ava, and Hannah for loving me unconditionally and supporting me through anything. I will miss spending easy weekends with you, Tyler and Hannah, but thank you for always welcoming me in your home. To my grandma who I wish could have seen me become Dr. Dre, thanks for believing in me more than I think I believed in myself at times. And, of course, thanks to all of my extended family who have been my cheerleaders as I make it through these milestones.

Thank you Xiaoyan for being my mentor the first few years of graduate school. You are an incredible woman and it is truly an honor to have learned from you. Thank you for always believing in me and encouraging me when times were tough and for never failing to say the perfect thing to get me out of feeling like an imposter: Lucky is for the hardworking.

Thank you Eugene for believing in me as a bright-eyed bushy tailed idiot and allowing me the opportunity to learn about and contribute to sustainable polymers. My passion only continues to grow and I'm grateful to have been mentored as a PhD student by one of the Greats.

DEDICATION

To the women who came before me and who I surround myself with, who hold the ladder for me to stand on the shoulders of giants

TABLE OF CONTENTS

Chapter 1

Introduction

The work presented in this dissertation explores structure/activity relationships of catalysts and monomers, structure/property relationships of resulting novel polymers, and structure/function relationships of designed, competitive polymers endowed with biological recycling as an end-of-life option. Fundamental discovery of these unique relationships between catalysts/monomers/polymers is imperative for expanding materials properties to meet more high-performance applications.

As the polymer community redefines a materials life cycle from linear to circular, biodegradability as an end-of-life option remains crucial for several applications where collection/sorting/recycling is either undesirable or impossible. The Nova Institute compiled a list of 25 products that would be ideal for biodegradability. The list includes packaging film for dishwasher tabs, lawn trimmer threads, seed coatings, leg bands for birds and wild animals, teabags, biowaste bags, non-durable products for fishery, fruit and vegetable stickers, floral foam, wet wipes, bristles for sweeping brushes, microplastics in cosmetics, coffee capsules, mulch films, and more.

Synthesizing a biodegradable polymer with the desired thermal and mechanical properties required for its function as well as the required processibility (extrusion, compression molding, injection molding, etc) is not trivial. As polymer chemists we have handles of tunability including polymer microstructure (tacticity and pendant group structure) and polymer architecture (homopolymer, random copolymers, block copolymers). Manipulating a polymer's tacticity (chirality of the repeat group) from atactic to isotactic can drastically change the crystallinity from

amorphous to highly crystalline which effects characteristics such as strength, ductility, and barrier properties. Replacing a small pendant group with a bulky pendant group changes the crystallinity and rigidity of the resulting polymer. Copolymerization can often blend the advantageous properties of each homopolymer to overcome specific disadvantages. Polymer chemists can also control the molecular weight and dispersity of the polymer chain length which effects the processibility and performance properties of the resulting polymers.

Polyhydroxyalkanoates (PHAs) are an incredibly diverse class of biorenewable, microbially produced, biodegradable polyesters. Biosynthesis and large-scale production of PHAs via fermentation routes have been extensively studied but presents several challenges including high cost and low volume production, no tacticity tunability, limited pendant structure scope and control, and lack of architectural diversity. The development of a catalyzed chemical synthesis of these polyesters can address these challenges by accessing precision control of the polymer microstructure and architecture. Taking advantage of the high activity of molecular organometallic complexes, the synthetic tunability of cyclic ester structure and substituents, and the fast kinetics of ring-opening polymerization can address limitations of the biosynthetic pathways and allow precise control over the resulting polymer microstructure and architecture.

A critical literature review, followed by results of fundamental investigations are presented and discussed in detail in the following chapters:

2) Synthetic Biodegradable Polyhydroxyalkanoates (PHAs): Recent Advances and Future Challenges.

3) Biodegradable Polyhydroxyalkanoates by Stereoselective Copolymerization of Racemic Diolides: Stereocontrol and Polyolefin-like Properties.

4) Catalyzed chemical synthesis of unnatural Aromatic PHA and aromatic-aliphatic PHAs with record-high glass transition and decomposition temperatures.

5) Elastomeric PHAs by precision architectural control via the stereoselective synthesis of isotactic ABA triblock copolymers

6) Conclusions and Outlook

Chapter 2 reviews the advances made over the past five decades of research in developing effective chemocatalytic pathways to synthesize polyhydroxyalkanoates (PHAs), a prominent class of biodegradable polyesters found in nature and considered as sustainable alternatives to petroleum-based non-degradable plastics. This chapter focuses on recent efforts that seek to address the key challenges facing the biosynthetic routes by taking advantage of precision in synthesis, expedient tunability in polymer stereomicrostructures and structures of monomers and molecular catalysts, as well as scalability and speed in polymer production that chemical catalysis can offer. This chapter is organized by poly(3-hydroxybutyrate) (P3HB) stereomicrostructures (tacticities), from isotactic to syndiotactic to atactic P3HB materials, followed by other PHA homopolymers and copolymers. Under each type of stereochemically defined PHAs, monomers, catalysts, and polymerizations employed for the synthesis, as well as mechanistic aspects when possible, are described. Next, recent advances in expanding the PHA scope and developing functionalized, uncommon or unnatural PHAs, inaccessible by biological methods, especially block and stereoblock or stereosequenced PHAs, are highlighted in their synthetic methods and advanced materials properties. Lastly, four key remaining challenges, and thus corresponding future directions directed at addressing those challenges, are discussed.

Chapter 3 reports on the catalyzed chemical synthesis of PHAs, using the metal-catalyzed stereoselective ring opening copolymerization of racemic cyclic dioldies (*rac*-8DL^{R}, R = alkyl group). In this experimental study, the copolymerization characteristics and the properties of the resulting PHAs have been examined. Most notably, stereoselective copolymerizations of *rac*-8DL^{Me} with *rac*-8DL^{R} (R=Et, Bu) have yielded high-molecular-weight, crystalline isotactic PHA copolymers that are hard, ductile, and tough plastics, and exhibit polyolefin-like thermal and mechanical properties.

The catalyzed chemical synthesis of polyhydroxyalkanoates (PHAs) via stereoselective ring-opening polymerization (ROP) of 8-membered cyclic diolides (8DL^{R}, R denotes the two substituents on the ring) has shown its ability to synthesize a variety of stereoregular aliphatic PHAs, but its utility for the synthesis of aromatic PHAs has not yet been demonstrated and will be discussed within Chapter 4. This chapter reports that the controlled ROP of *meso*-8DL^{Bn} (Bn = benzyl)—catalyzed by metal-based complexes supported by C_2-Salen ligands—affords syndiotactic ([*rr*] = 92%) poly(3-hydroxy-4-phenylbutyrate) (*st*-P3H4PhB) with a high molar mass (M_n up to 147 kg mol^{-1}) and the highest glass-transition temperature (43 °C) reported in the PHA family, whereas the ROP of *rac*-8DL^{Bn} leads to essentially pure isotactic ([*mm*] > 99%) *it*-P3H4PhB. With thoughtful selections of catalysts, monomers, and procedures, copolymerizations of *meso*-8DL^{Bn} with *rac*-8DL^{R} (R = Me, ^{n}Bu) produces aromatic-aliphatic random, stereotapered, or crystalline stereodiblock PHA copolymers. In particular, the copolymer of *meso*-8DL^{Bn} with *rac*-8DL^{Bu}—P3H4PhB-*co*-P3HHp (M_n = 205 kg mol^{-1}) —is a strong, hard, but ductile (~191% elongation at break) material, displaying perhaps the highest decomposition temperature (281 °C) reported for PHAs to date.

The controlled, chemocatalytic route towards synthetic polyhydroxyalkanoates (PHAs) via the stereoselective ring-opening (ROP) of 8-membered cyclic diolides (8DLR, R = R denotes the two substituents on the ring) has been found to synthesize highly isotactic homopolymers and random copolymers with aliphatic and aromatic substituents as well as tapered or gradient stereodiblock by simultaneous copolymerization of two or more diastereomers, but this stereoselective ROP utility for the synthesis of discrete ABA triblock copolymers (tri-BCPs) has not yet been demonstrated. Chapter 5 reports the controlled ROP of *rac*-8DL^{R} (R = Et, Bu) catalyzed by metal-based complexes supported by a suitable C_2-Salen ligand and difunctional initiator followed by addition of *rac*-8DL^{Me} affords isotactic P3HB-*b*-P3HV-*b*-P3HB (when R = Et) or P3HB-*b*-P3HHp-*b*-P3HB (when R = Bu) with high molecular weight, narrow chain dispersity, and high crystallinity. Mechanical analysis of these tri-BCPs show either tough thermoplastics or elastomeric PHA depending on the composition of the midblock. To our knowledge, this is the first example of a tri-BCP containing only 3-hydroxybutyrate repeat units to target biodegradable thermoplastic elastomers.

Chapter 6 discusses the overall impact of the presented work including the major insights that have paved way to new challenges and opportunities.

The dissertation presented hereinafter was conceived in a "journals-format" style, in agreement with the Graduate School guidelines at Colorado State University. The first presented manuscript is a review article which has been prepared and submitted to *Progress in Polymer Science*; the remaining manuscripts are original research articles, two of which have been published as full papers in the peer-reviewed journals *Angnewante Chemie International Edition* and *Macromolecules*, and a third full paper has been prepared and is ready to submit. Experimental details, including methods, materials characterization, and supporting figures corresponding to

each of the individual chapters are consecutively included in Appendixes at the end of this dissertation. This arrangement maintains consistency with the previously published work and provides a readable format of the research presented in the main chapters.

Chapter 2

Synthetic Biodegradable Polyhydroxyalkanoates (PHAs): Recent Advances and Future Challenges

2.1. Synopsis

This article reviews the advances made over the past five decades of research in developing effective chemocatalytic pathways to synthesize polyhydroxyalkanoates (PHAs), a prominent class of biodegradable polyesters found in nature and considered as sustainable alternatives to petroleum-based non-degradable plastics. Focused in this review are recent efforts that seek to address the key challenges facing the biosynthetic routes by taking advantage of precision in synthesis, expedient tunability in polymer stereomicrostructures and structures of monomers and molecular catalysts, as well as scalability and speed in polymer production that chemical catalysis can offer. This article is organized by poly(3-hydroxybutyrate) (P3HB) stereomicrostructures (tacticities), from isotactic to syndiotactic to atactic P3HB materials, followed by other PHA homopolymers and copolymers. Under each type of stereochemically defined PHAs, monomers, catalysts, and polymerizations employed for the synthesis, as well as mechanistic aspects when possible, are described. Next, recent advances in expanding the PHA scope and developing functionalized, uncommon or unnatural PHAs, inaccessible by biological methods, especially block and stereoblock or stereosequenced PHAs, are highlighted in their synthetic methods and advanced materials properties. Lastly, four key remaining challenges, and thus corresponding future directions directed at addressing those challenges, are discussed.

2.2. Introduction

Polyhydroxyalkanoates (PHAs) are biologically produced, biocompatible polyesters that are ubiquitous in Nature and living systems, and they have thus gained increasing attraction as

biodegradable plastic alternatives for a variety of applications that emphasize better end-of-life (EoL) options and environmental protection.[1–7] PHAs have been shown to be biodegradable under ambient conditions in both managed and unmanaged environments.[8–11] The most commonly produced PHA in the large PHA family that includes more than 150 known structures—which are defined as, and limited to, poly(3-hydroxyacid)s in this review, poly(3-hydroxybutyrate) (P3HB), exhibits several desirable materials characteristics including its high crystallinity, perfect isotacticity with each pendant group having exclusively (*R*)-configuration, high melting-transition temperature (T_m) up to ~180 °C, good ultimate tensile strength (σ = ~40 MPa), and excellent barrier to oxygen and moisture transport.[12,13] Despite those attractive performance properties, P3HB suffers from low thermostability towards melt-processing, with a degradation temperature (T_d, defined as the temperature at 5% weight loss) around 250 °C, and brittleness, with an extremely low elongation at break (ε_B ~3-6%), therefore largely limiting its wider industrial applications as a commodity plastic.

The development of fermentation routes from biorenewable feedstocks to P3HB and copolymers of P3HB with short-chain length (*scl*, C_4–C_5) and medium-chain length (*mcl*, C_6–C_{14}) comonomers has resulted in the commercial utilities of PHAs (**A**, Figure 2.1). There are several reviews highlighting the developments and advancements of biological routes towards PHAs.[14–26] However, the high cost of the current biological production of PHAs represents a major bottleneck in their large-scale commercialization.[27] In addition, biological routes are limited by the step-growth polymerization mechanism where incorporation of 3-hydroxybutryate is most common, thus engineering of the metabolic pathways is typically required for tuning of PHA compositions.[3,28] For example, bacteria synthesize different PHAs from coenzyme-A thioesters of hydroxyalkanoic acids via polycondensation, which produce PHAs with a high dispersity ($Đ$) ≥

2.0, thus not suitable for synthesizing well-defined block copolymers (BCPs). There is evidence that periodic feeding of microorganisms can result in some "blocky" PHA copolymers that can be fractionated out of the whole polymer product.[29,30] Although the thermal and mechanical properties of these fractionated blocky copolymers were different than the homo- and random copolymers, the evidence overall is lacking for the formation of well-defined BCPs. Furthermore, despite the tunability of the chiral repeat units of the backbone, which allows for generation of various stereomicrustructures (tacticities) including isotactic (*it*), syndiotactic (*st*), atactic (*at*), and stereoblock (*sb*) microstructures (Fig.1), biologically derived PHAs are exclusively accumulated as *it*-polymers with absolute (*R*)-stereoconfiguration.

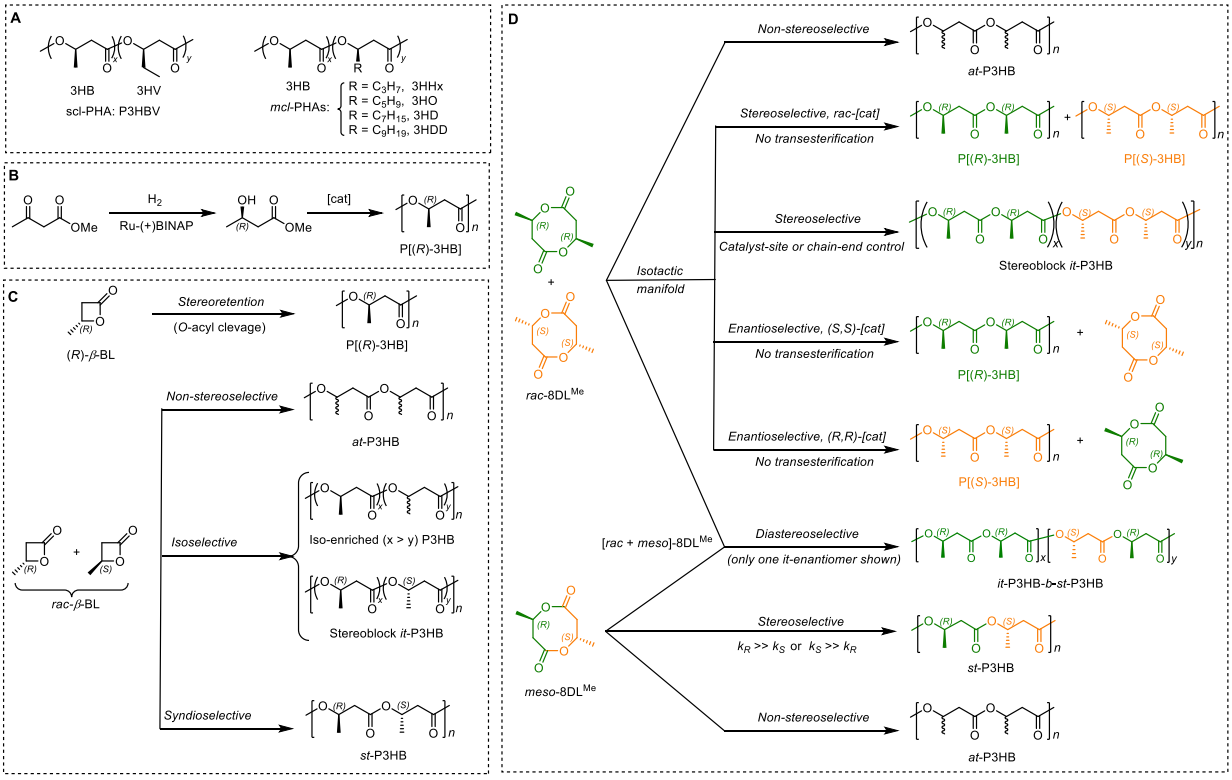

Figure 2.1. Representative common biological PHAs as copolymers: 3HB = 3-hydroxybutyrate, 3HV = 3-hydroxyvalerate, 3HHx = 3-hydroxyhexanoate, 3HO = 3-hydroxyoctanoate, 3HD = 3-hydroxydecanoate, 3HDD = 3-hydroxydodecanoate **A**) and three major chemocatalytic routes towards PHAs, represented by P3HB materials with various tacticities: **B**) step-growth

polymerization, **C**) chain-growth polymerization by ROP of four-membered β-BL, and **D**) chain-growth polymerization by ROP of *eight-membered dimethyl diolide (rac-8DL^{Me} and meso-8DL^{Me}).*

Like other classes of polymers, thermal and mechanical properties of polyesters can generally be tuned by manipulating the polymer stereomicrostructure,[31–34] topology,[35] and pendant group structure.[36] In this context, several advantages of chemocatalytic routes towards PHAs can be envisioned, in principle, including: (i) *precision in synthesis* (control of chain length (M_n) and $Đ$, comonomer sequence, and architecture); (ii) *tunability* in polymer stereomicrostructure (*it, st, at, sb*-tacticities and *R* or *S* stereoconfigurations) and molecular catalyst structure (symmetry and chirality, thus, stereoselectivity); and (iii) *scalability and speed* in production (ease in processing and fast reaction kinetics typically associated with catalyzed ring-opening polymerization (ROP) processes). However, currently a major challenge for the chemocatalytic route to PHAs is the need to develop cost-effective synthesis of monomers (from renewable feedstocks) and catalysts and ideally establish "monomer-polymer-monomer" closed-loop lifecycles of PHAs, in addition to their biodegradation EoL option. The key differentiating and overlapping features of both biological and chemical synthetic routes towards PHAs are highlighted in Figure 2.2.

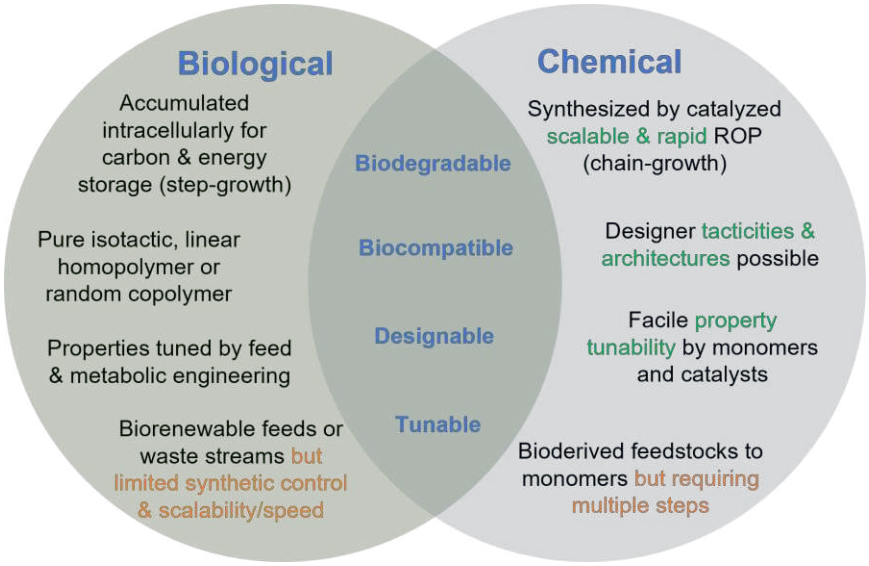

Figure 2.2. Differentiating and overlapping features of biological and chemical routes to PHAs.

Three key chemocatalytic routes towards PHAs, represented by P3HB herein, are summarized in Figure 2.1. The direct route is polycondensation of (*R*)-3-hydroxybutyric acid, which affords *it*-P[(*R*)-3HB] (**B**, Figure 2.1). However, this method is prone to crotonization, the formation of crotonate end groups through transesterification side reactions or elimination/termination reactions (Figure 2.4); hence, polycondensation is not a suitable route towards high-molecular-weight P3HB.[2,37–39] On the other hand, the ROP, which proceeds via a chain-growth mechanism with fast initiation and propagation kinetics, can produce P3HB with high molecular weights, low $Đ$ values, and tunable tacticities. In this context, the ROP of the 4-membered β-butyrolactone (β-BL) leads to P3HB with various tacticities, depending on the stereoselectivity of the catalyst (**C**, Figure 2.1). In comparison, the ROP of the 8-membered cyclic dimer of 3-hydroxybutyric acid, $8DL^{Me}$ (**D**, Figure 2.1), which bears two chiral centers and thus exists in three diastereomeric forms (*R,R/S,S racemic (rac)* and *R,S meso*), allowing access to a more diverse set of possible stereomicrostructures (**D**, Figure 2.1).

This review intends to focus on the chemocatalytic routes towards PHAs, including investigations of the various stereomicrostructures that can be accessed through different catalytic ROP strategies, the design of different organometallic and organic catalysts to synthesize P3HB, as well as the controlled synthesis of various homo- and copolymer PHAs that are challenging to produce or inaccessible, biologically. Several recent reviews offer complementary perspectives that explore discrete metal catalysts for the ROP of cyclic esters in general to various stereomicrostructures,[40–46] but this review focuses on PHAs, poly(3-hydroxyacid)s, specifically, encompassing and analyzing all of the three chemocatalytic routes towards various types of PHA materials.

2.3. Isotactic P3HB

2.3.1. Mechanistic considerations

The desire to make a synthetic analog to bacterial derived, perfectly *it*-P3HB has inspired research efforts spanning 60^+ years since the initial report on the ROP of β-BL in 1961.[47] It has well-established by now that the most facile synthetic approach towards high-molecular-weight polyesters is the ROP of cyclic esters (or lactones). For the synthesis of P3HB, the simplest lactone monomer is the highly strained, four-membered β-BL. There are two general mechanistic pathways for ring-opening of β-lactones: *O*-acyl bond cleavage or *O*-alkyl bond cleavage (Figure 2.3). The former allows the stereo-retention of the chirality at the β-carbon, while the latter leads to either chiral inversion or racemization at the chiral center.

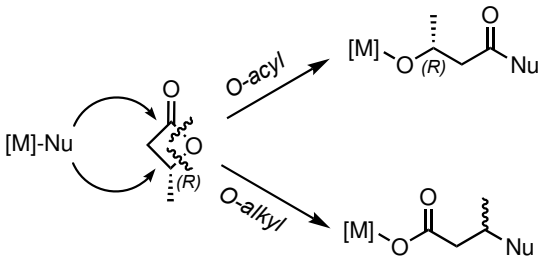

Figure 2.3. General mechanism of ring-opening of β-BL resulting in stereo-retention via *O*-acyl bond cleavage and chiral inversion or racemization via *O*-alkyl bond cleavage. [M] denotes a metal-based catalyst center and Nu a nucleophile, typically an alkoxy or amide ligand.

As β-BL has one stereogenic center, it is available in either an enantiopure or *rac* form. A convenient, albeit expensive, strategy to produce purely isotactic, optically active *it*-P3HB is to use the enantiopure form of β-BL, thereby avoiding the need to control the stereoselectivity of the polymerization, provided that the ROP proceeds via *O*-acyl bond cleavage (**C**, Figure 2.1).[48–51]

The most common termination pathway is through formation of crotonate end groups, resulting in generation of low-molecular-weight polymers and undesirable, non-biomimetic end groups (Figure 2.4).[2]

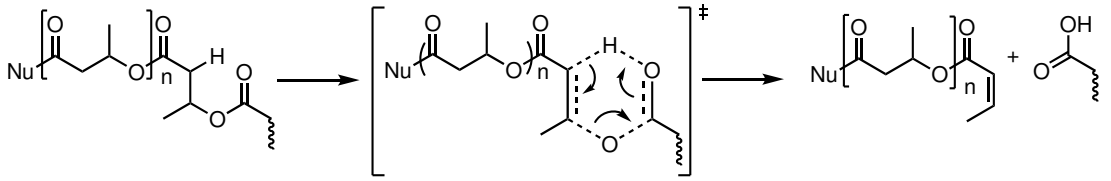

Figure 2.4. A common termination pathway in chemocatalytic synthesis of P3HB from *β*-BL, which leads to crotonate end group formation.

2.3.2. ROP of β-BL

Shelton *et al.* first reported the polymerization of (*R*)-*β*-BL with the $AlEt_3/H_2O$ mixture.[52] The polymerization was presumed to proceed via the *O*-acyl bond scission because the stereochemistry was retained resulting in optically active P[(*R*)-3HB]; however, due to the poorly resolved monomer (~73% optical clarity) the resulting polymer had lower optical activity compared to biologically derived P3HB.[50] Lenz hypothesized a route towards P[(*R*)-3HB] by inversion of stereochemistry via ROP of (*S*)-*β*-BL;[48] with the $AlEt_3/H_2O$ initiator, the inversion of stereochemistry was observed, which is opposite to what Shelton *et al*. observed.[50] These conflicting results highlight the lack of control over this catalyst structure and thus the polymer stereochemistry by the non-discrete AlR_3/H_2O system. Lenz also used $ZnEt_2/H_2O$ as the initiator for ROP of (*S*)-*β*-BL but observed retention of stereochemistry to give P[(*S*)-3HB].[48] Doi *et al.* polymerized chiral *β*-BL of different enantiomeric excess using $ZnEt_2/H_2O$ and obtained *it*-diad fractions, with P_m (defined as the probability of *meso* linkages between two consecutive monomer units) up to 0.85, thanks to retention of the original *S* and *R* configurations of the *β*-BL monomer. This *it*-polymer showed a T_m of 135 °C and an enthalpy of fusion (ΔH) = 64.3 J/g.[53] By

comparison, the biologically produced P3HB has T_m ~ 170 °C and ΔH ~ 80 J/g. Gross *et al.* employed the similar strategy using $ZnEt_2/H_2O$ and produced various stereo-copolymers by adjusting the enantiopurity of the *β*-BL monomer.[54]

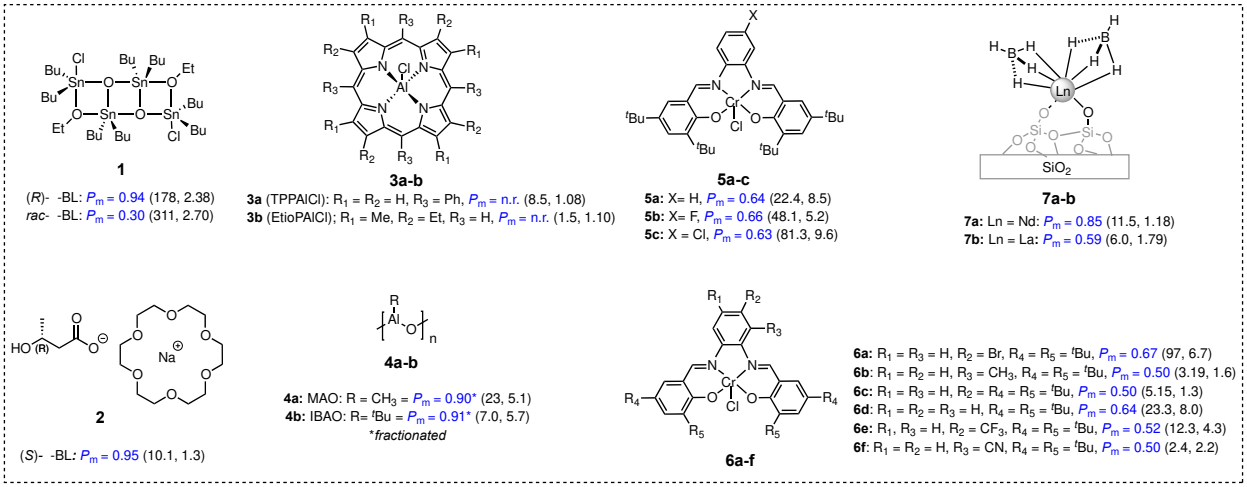

Figure 2.5. Catalyst or initiator systems that produced isotactic ($P_m \geq 0.85$) or iso-rich P3HB from the ROP of (*R*)-*β*-BL or *rac*-*β*-BL (n.r. = not reported in the original literature). M_n in kg/mol and $Đ$ values are placed in parenthesis for each system.

Even with the chiral *β*-BL monomer, achieving synthetic analogs of the biologically derived P3HB via the ROP is not straightforward due to competing *O*-acyl and *O*-alkyl bond cleavage pathways (*vide supra*). In one example, a distannoxane complex initiated the ROP of (*R*)-*β*-BL, proceeding via the *O*-acyl bond cleavage with retention of configuration and thus producing P[(*R*)-3HB] (**1**, Figure 2.5).[55] Ring-opening copolymerization of (*R*)-*β*-BL with *ε*-caprolactone, *γ*-valerolactone, *β*-methyl-*γ*-valerolactone, and L-lactide by such a distannoxane complex yielded copolyesters of high M_n (> 100 kg/mol comprising mostly (*R*)-3-hydroxybutyrate units.[56] ROP of (*R*)-*β*-BL mediated by potassium alkoxide crown ether complexes proceeds via stereo-inversion (i.e. *O*-alkyl bond cleavage) to afford *it*-poly[(*S*)-3HB].[49] This finding led to the synthesis of P[(*R*)-3HB] with a high P_m up to 0.95 through regioselective anionic polymerization of (*S*)-*β*-BL using (*R*)-3-hydroxybutyric acid sodium salt and 18-crown-6 ether initiator (**2**, Figure 2.5) via *O*-alkyl-bond

scission with an inversion of stereochemistry.[51] Overall, the methods of polymerizing chiral *β*-BL to biomimetic *it*-P3HB by the anionic ROP remained largely ineffective, due to often competing stereo-retention vs inversion pathways, and also produced *it*-P3HB with relatively low molecular weights (typically M_n ~ 10 kg/mol).

A more economical but challenging route to produce *it*-P3HB is the stereoselective polymerization of *rac*-*β*-BL. A number of organometallic compounds have been employed in this endeavor since the first example of the ROP of *rac*-*β*-BL to a "powdered polymer" by $ZnEt_2/O_2$ was reported by Inoue in 1961.[47] One of the first examples of stereoselective polymerization of *rac*-*β*-BL was enabled by the use of a coordinative alkyl aluminum complex (formulated as $Et_2Al•O•CPh:NPh$) which yielded a mixture of iso-enriched and *at*-polymer materials.[57] This mixture was then fractionated with acetone to give the insoluble, crystalline *it*-fraction that had high T_m values of 167-169 °C. Although this method produced the crystalline *it*-P3HB, it also afforded large fractions of soluble, *at*-polymer and took up to 7 days at 60 °C to achieve appreciable polymer yields. There are several examples of using mixtures of trialkylaluminum complexes, especially triethylaluminum, with water to polymerize *rac*-*β*-BL over several days to fractions of the crystalline, relatively high molecular weight polymer that was thermally similar to that of biologically produced P3HB, plus large fractions of soluble, low molecular weight polymer products.[52,58,59] The isotacticity of the P3HB produced by trialkylalumum complexes was quantitatively characterized by ^{13}C NMR.[60] The acetone insoluble crystalline fraction had a P_m up to 85%, T_m values of 165-170 °C, and a high ΔH up to 95 J/g.

Subsequent efforts seeking to achieve *it*-P3HB from the ROP of *rac*-*β*-BL focused on the development and utilization of well-defined, discrete catalyst or initiator systems. In this context, aluminum porphyrins, such as (tetraphenylporphinato)(TPP)aluminum chloride (TPPAlCl) (**3a**,

Figure 2.5), were found to mediate living ROP of *β*-BL, but these catalysts suffered from very low activity, requiring 6 days to reach quantitative monomer conversion at room temperature to yield only low-molecular-weight polymer (M_n = 8.5 kg/mol).[61] Changing the porphyrin from TPP to etioporphyrin (EtioP) (**3b**, Figure 2.5) further reduced the activity and the polymer molecular weight.[62] Although the tacticity of the resulting polymer was not described, it was hypothesized the mechanism of initiation resulted in loss of control of the stereogenic center: the chloride of TPPAlCl was proposed to attack the *β*-carbon of the monomer which leads to lactone insertion through *O*-alkyl bond scission,[62] and this resulting carboxylate anion propagates via the *O*-alkyl bond scission to regenerate the porphinatoaluminum carboxylate.[61] Despite the ability to mediate the living ROP of *β*-BL, aluminum porphyrin complexes are poor catalysts in terms of activity and stereoselectivity.

Methylaluminoxane (MAO) (**4a**, Fig 3) and isobutylaluminoxane (IBAO) (**4b**, Figure 2.5), commonly employed as co-catalysts in the metal-catalyzed olefin polymerization,[63] were also utilized to initiate the ROP of *rac*-*β*-BL.[64] Despite the need for high catalyst loadings (10 mol%), the ROP led to 60% of the crude polymer product being the insoluble, crystalline (T_m =163 °C and ΔH = 21 J/g) polymer fraction with P_m ranging between 0.78-0.91.[64]

Polymerization of *rac*-*β*-BL with chiral initiators, such as a complex of *R*(-)-3,3-dimethyl-1,2-butanediol and $ZnEt_2$, resulted in the partial kinetic resolution of the racemic monomer because the catalyst preferentially polymerizes (*R*)-*β*-BL to P[(*R*)-3HB] and leaves (*S*)-*β*-BL partially resolved (Figure 2.6).[65] Initiation and propagation proceed via *O*-acyl bond cleavage thus retaining stereoconfigureation of the enchained monomer. The insoluble fraction of the resulting polymer showed two endotherms with T_m = 122 °C and 166 °C by DSC, and the latter predominant crystalline fraction indicates the presence of an extended distribution of *it*-sequences (P_m ~ 0.75).

Noteworthy also is that this catalyst system was much more active than the previous Al or Zn systems (often mixed with water or common alcohol) – achieving up to 84% conversion at room temperature in 5.5 h. Different metal alkyls including $AlEt_3$ and $CdMe_2$ were also studied; $AlEt_3$ had drastic reduction in activity (13% polymer yield after 18 days of reaction) but maintained the stereoselectivity, while $CdMe_2$ was much more reactive but preferentially produced the opposite enantiomeric poly[(*S*)-3HB].[65]

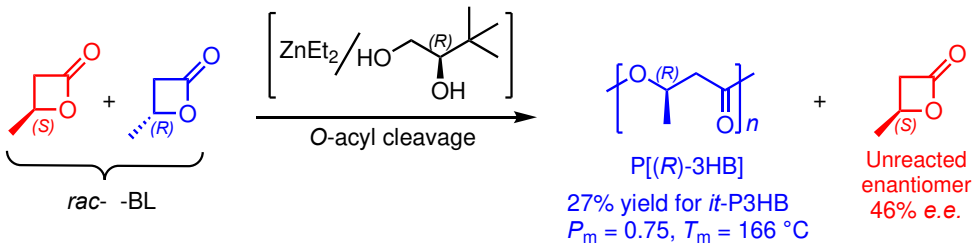

Figure 2.6. Partial kinetic resolution polymerization of *rac*-*β*-BL with a chiral Zn-based initiator system comprising *R*(-)-3,3-dimethyl-1,2-butanediol and $ZnEt_2$.

Mixing alkyl aluminum and zinc complexes with water or alcohol often resulted in formation of oligomeric species or non-discrete complexes. To address this issue, Rieger *et al.* employed discrete chromium salophen complexes (**5**, Figure 2.5) for the ROP of *rac*-*β*-BL and achieved appreciable isoselectivities (P_m up to 0.66).[66] These complexes produced moderately isotactic polymers due to the binuclear mechanism involved that preferentially allows entry of an incoming *β*-BL enantiomer based on the stereoconfiguration of the previous enchained enantiomer (i.e., chain-end control). Adding a halogen to the bridging phenyl ring improved activity and selectivity of the polymerization as well as molecular weight of P3HB substantially. For example, fluorination at the 4-position (**5b**, Figure 2.5) yielded a catalyst that is not only twice as active as the non-halogenated derivative, but also produced P3HB with M_n (48.1 kg/mol) that is 2x of the P3HB produced by the parent catalyst. Chlorination (**5c**, Figure 2.5) showed the similarly enhanced

activity and further increased M_n to 81.3 kg/mol, but the dispersity of the resulting P3HB is very high ($Đ$ = 9.6).[66]

Rieger *et al.* further explored these profound electronic effects and found that, while electron withdrawing halogens, such as Br (**6a**, Figure 2.5), increased reactivity, electron donating groups such as methyl (**6b**, Figure 2.5) and *tert*-butyl (**6c**, Figure 2.5) completely inhibited polymerization, relative to the parent, model catalyst **(6d**, Figure 2.5).[67] This activity inhibition was attributed to increasing the electron density on the Lewis acidic metal center which weakens the Lewis acid bonding to monomer and the growing polymer chain.[67] The use of strongly electron withdrawing groups such as CF_3 (**6e**, Figure 2.5) and CN (**6f**, Figure 2.5) also decreased activity because of enhancing chain affinity towards one catalyst center thus hindering transfer of the activated monomers to the second complex.[67] Further study revealed these chromium complexes even transformed *in situ* into a heterogeneous catalytic process,[68] which can also explain the formation of the polymer with high dispersity values. More specifically, the Cr complex crystalizes into a polymeric form during polymerization, which allows for fast, enantiomorphic, bimetallic or multinuclear stereoinduction of *rac*-*β*-BL by specially arranged chromium centers. It was also suggested that water is important, not as a chain transfer agent but in the formation of the active polymeric chromium species. Changing the ligand substituents alters the complex's ability to transform into the polymeric form and thus reduces activity. Although the polymers with relatively high molecular weights could be achieved, they were accompanied by high dispersities, because of the continual initiation of new polymer chains by newly generated catalyst centers during propagation.[68]

A more common way of generating a heterogenous catalyst system is through anchoring of a molecular catalyst onto an inorganic support. In this context, lanthanide borohydrides were

supported on silica, and the resulting heterogenous catalyst was examined for the ROP of *rac*-*β*-BL.[69] Specifically, a grafted neodymium borohydride complex, $Nd(BH_4)_3(THF)/SiO_2$ (**7a**, Figure 2.5), exhibited good activity (82% monomer conversion in 24 h) and stereoselectivity ($P_m = 0.85$). The corresponding lanthanum complex with a large ionic radius, $La(BH_4)_3(THF)/SiO_2$ (**7b**, Figure 2.5), showed poor activity and also lower stereoselectivity ($P_m = 0.59$). Worth noting here is that the trend for the molecular catalysts performed in solution is often the opposite. In comparison, the (unsupported) molecular version of these complexes led to totally *at*-polymer.

2.3.3. ROP of *rac*-8DL^{Me}

Achieving P3HB with high isotacticity ($P_m > 0.90$ for the bulk polymer without fractionation) remained elusive until 2018 when Tang and Chen developed a new chemocatalytic route to P3HB via the ROP of a *rac*-diolide, the 8-membered cyclic dimer of 3-hydroxybutyrate (*rac*-8DL^{Me}), to perfectly *it*-P3HB ($P_m > 0.99$) (Figure 2.7).[70] The ROP of *rac*-8DL^{Me} was evaluated using a series of discrete, molecular catalysts including $La[N(SiMe_3)_2]_3$ (**8**, Figure 2.7) and yttrium amido complexes supported by tetradentate [O^-,*N*,*O*,O^-] ligands (**9**-**10**, Figure 2.7). These complexes had been utilized for other ROP reactions [12,71,72] and their use to polymerize *rac*-*β*-BL to *st*-P3HB [73–75] will be discussed in Sections 2.4.1.2 and 2.6.2. The investigation of the stereo, electronic, and symmetry effects of the salen-ligand framework (*rac*-**11a-b**, **11e**, Figure 2.7) highlighted the ideal match between the C_2-symmetric, trityl-*ortho*-substituted salen ligated yttrium complex and *rac*-8DL^{Me} resulting in the formation of essentially stereo-perfect *it*-P3HB (*rac*-**11d**, Figure 2.7). This *it*-P3HB had a high T_m of 171 °C and ΔH ~80 J/g, thus exhibiting the high crystallinity and thermal properties similar to those of the microbial P3HB.[70]

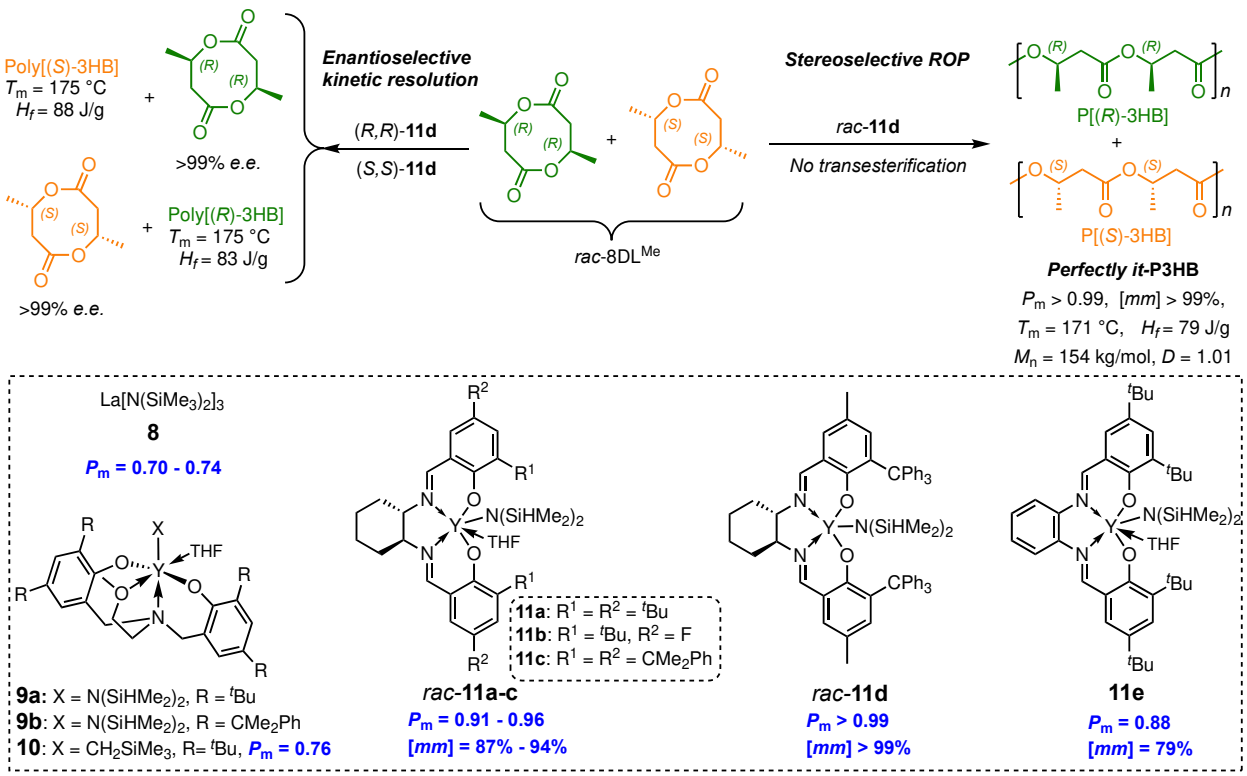

Figure 2.7. Stereoselective ROP and enantioselective kinetic resolution polymerization of *rac*-8DL^{Me} by discrete chiral and non-chiral lanthanum and yttrium complexes.

Further investigation into the stereocontrol of the ROP revealed an enantiomorphic-site control mechanism, pointing to the possibility of kinetic resolution of *rac*-8DL^{Me} if an enantiomerically pure catalyst is used. Indeed, the polymerization of *rac*-8DL^{Me} with enantiopure (*R,R*)-**11d** resulted in 50% conversion of the monomer where all of the (*S,S*)-8DL^{Me} was polymerized to P[(*S,S*)-3HB], leaving (*R,R*)-DL^{Me} unreacted. For typical kinetic resolution polymerization, the reaction needs to be monitored and stopped manually when the monomer conversion approaches ~50%, thereby avoiding stereo-tapering when the concentration factor of the slow-reacting enantiomer overrides the kinetic preference of the fast-reacting enantiomer with its concentration diminishes as the reaction progresses. If the reaction is allowed to continue to completion, then a stereo-tapered diblock copolymer is typically produced. Fascinatingly, the polymerization of *rac*-8DL^{Me} by (*R,R*)-**11d** automatically stopped at 50% monomer conversion, without further incorporating the other enantiomeric monomer that would lead to a stereodiblock or stereo-tapered BCPs, thus

achieving essentially perfect enantioselectivity in the kinetic resolution polymerization (Figure 2.7).[70] When enantiopure (*S,S*)-**11d** was employed, the ROP of *rac*-8DL^{Me} gave the results of mirror-image products: P[(*R,R*)-3HB] and (*R,R*)-DL^{Me} (Figure 2.7). The resulting pure *it*-P3HB exhibited a high T_m up to 175 °C, essentially identical to that the microbial P3HB, but the synthetic P3HB by the ROP exhibits extremely narrow *Đ* values (<1.03), relative to typically high *Đ* values (> 2.0) of the biological P3HB.[70]

When *rac*-8DL^{Me} is polymerized by a racemic catalyst such as *rac*-**11d**, the resulting *it*-P3HB was shown to be a mixture of enantiomeric polymers P[(*R*)-3HB] and P[(*S*)-3HB] (Figure 2.8), thanks to the complete enantioselectivity of (*R,R*)-catalyst for addition of (*S,S*)-8DL^{Me} and (*S,S*)-catalyst for addition of (*R,R*)-8DL^{Me} and no transesterification upon full monomer conversion. Note that transesterification would lead to stereo(multi)block copolymer. This methodology is an important leap forward in discovering a scalable chemocatalytic route towards biomimetic P3HB.

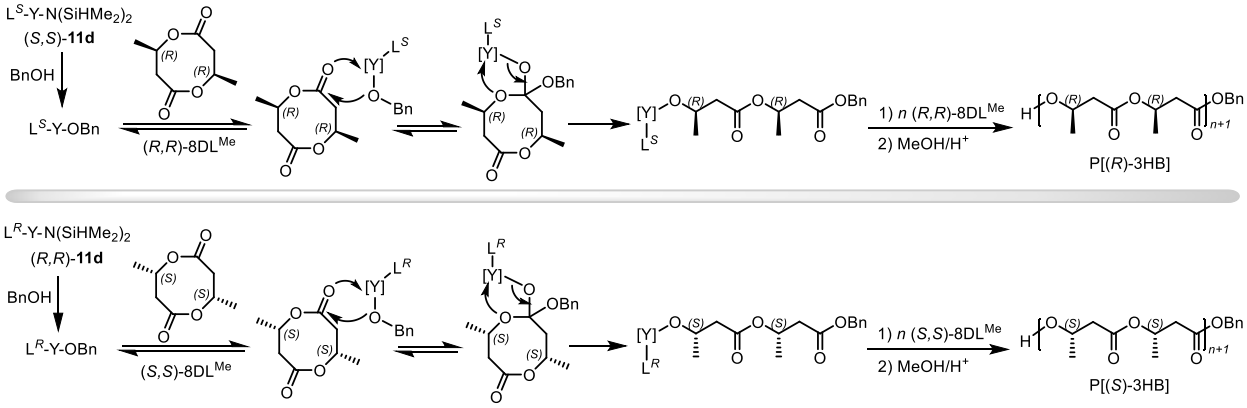

Figure 2.8. Outlined fundamental steps proposed for the stereoselective ROP of *rac*-8DL^{Me} by the racemic catalyst, *rac*-**11d**, to produce a mixture of enantiomeric P[(*R*)-3HB] and P[(*S*)-3HB].

2.4. Syndiotactic P3HB

2.4.1. ROP of β-BL

2.4.1.1. Sn-based initiators

Although microorganisms produce exclusively *it*-P3HB, chemocatalytic ROP of *rac*-*β*-BL can produce unnatural *st*-P3HB. Throughout the 1990s, Sn complexes were examined for the ROP of *rac*-*β*-BL because they had been shown to be active in the polymerization of various lactones.[76,77] The use of $^{n}Bu_3Sn$-OCH_3 (**12a**, Figure 2.9) led to a notable preference for *st*-placement, P_r (defined as the probability of *rac* linkages between monomer units) up to 0.70, but the activity was extremely low.[78] Room temperature polymerization required 55 days to achieve only 37% yield; while increasing the temperature to 90 °C reduced the reaction time to 13 days, this condition consequently decreased the stereoselectivity (P_r = 0.61), yielding the syndio-enriched P3HB with a low T_m of only ~50 °C.

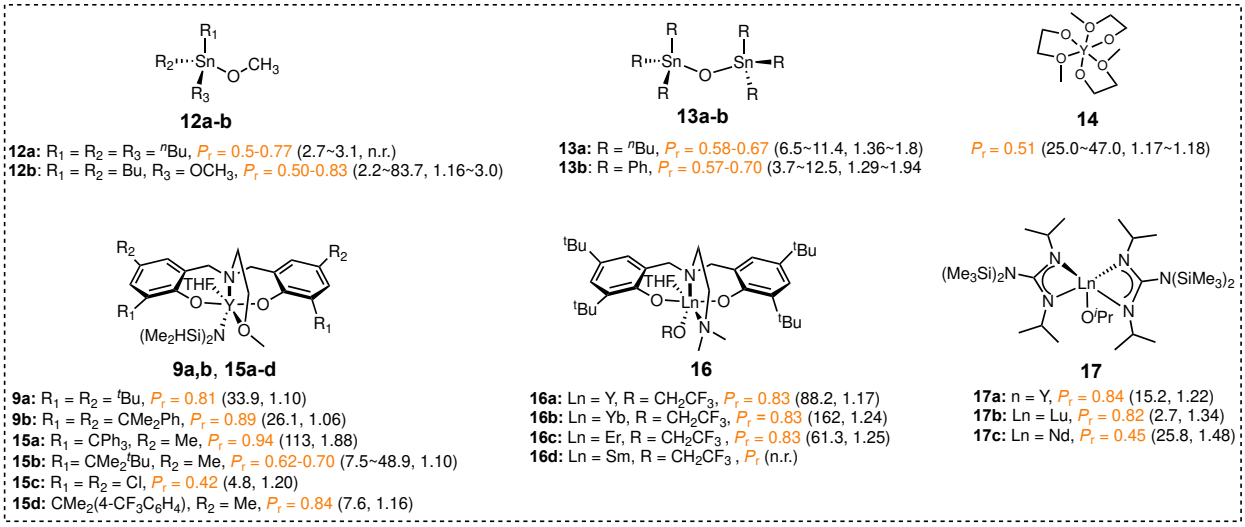

Figure 2.9. Catalyst or initiator systems that produced syndiotactic or syndio-rich P3HB from the ROP of *rac*-*β*-BL (n.r. = not reported). M_n in kg/mol and $Đ$ values are placed in parenthesis for each initiator.

Different Sn(IV) complexes were employed for tuning the syndioselectivity of the ROP of *rac*-*β*-BL. Using $^{n}Bu_2Sn(OMe)_2$ (**12b**, Figure 2.9), $(^{n}Bu_3Sn)_2O$, and $(Ph_3Sn)_2O$ (**13a** and **13b**, Figure 2.9) under various conditions reached a maximum P_r value of 0.83 when the polymerization temperature was lowered to -17 °C.[78–80] The activity of these complexes was extremely low, however, taking 13 to 75 days of reaction time when the reaction was carried out at this temperature

for the highest P_r value.[79] The observed syndioselectivity was attributed to be resulted from the asymmetry of the chain end coordinated to the respective Sn catalysts, thus a chain-end control mechanism.[80]

Use of cyclic dibutyltin resulted in noticeably higher molecular weights but the syndiotacticity remained only modest ($P_r = 0.62$).[81] Polymers with higher molecular weights (M_n up to 80 kg/mol) and syndiotacities (P_r up to 72) were obtained with dialkyltin(IV) oxides, $R_2Sn{=}O$, in particular when R = ^{n}Bu (50 °C) and Et (100 °C).[82] As distannoxane complexes (**1**, Figure 2.5) were found to polymerize (*R*)-*β*-BL with retention of stereochemistry to form *it*-P3HB,[56] they were also utilized for the ROP of *rac*-*β*-BL to give syndio-enriched P3HB ($P_r = 0.67$), attributed to the steric control resulted from diastereomeric interactions between the Sn-coordinated P3HB chain ends and the incoming enantiomeric *β*-BL monomers.[83]

2.4.1.2. Rare-earth metal catalysts

As can be seen from the above selected examples of the initiator systems, classical organometallic complexes of Zn, Al, and Sn are sluggish and often require high temperatures to bring about useful activities for either isoselective or syndioselective ROP of *β*-BL. Discrete, rare earth metal-based molecular catalysts have been shown to exhibit exceptional efficiency and activity in the ROP of *ε*-caprolactone and lactide under mild conditions and, naturally, such catalysts were employed to polymerize *β*-BL.[40,42] Spassky *et al.* in 1994 polymerized *rac*-*β*-BL with yttrium 2-methoxyethoxide (**14**, Figure 2.9) and achieved high activity (100% conversion in 20 min at room temperature) and living polymerization characteristics, including the preparation of homopolymers and well-defined BCPs with lactide.[84] The resulting P3HB was shown to be atactic, however, based on NMR analysis.

Carpentier and co-workers subsequently explored multi-dentate ancillary ligands to tune the catalytic properties of the rare earth metal complexes, minimize catalyst aggregation, and limit transesterification reactions, thereby enhancing activity and stereochemical control.[40,42] In particular, yttrium bis(dimethylsilyl)amido and bis(trimethylsilyl)methyl complexes supported by a tetradentate bis(phenoxy) ligand (**9a** and **9b**, Figure 2.7 and **15a-d,** Fig 5.[85] have been shown to be highly active and efficient catalysts for syndioselective polymerization of *rac*-*β*-BL. With a bulky cumyl group placed at the position ortho to the phenoxy oxygen (**9b**, Figure 2.9), this well-defined, C_s-symmetric single-site bis(phenolate) yttrium complex converted *rac*-*β*-BL in toluene at -20 °C to highly *st*-P3HB (P_r = 0.94, M_n = 113 kg/mol, $Đ$ = 1.88).[74] The less sterically encumbered yttrium complex with *tert*-butyl group at the ortho position (**9a**, Figure 2.9) displayed an appreciable loss in stereoselectivity (P_r = 0.81). Changing the temperature and/or concentration of the polymerization reaction notably affected the activity and selectivity of the ROP. The highly *st*-P3HB (P_r = 0.94) exhibited a high T_m of 178 °C.[74]

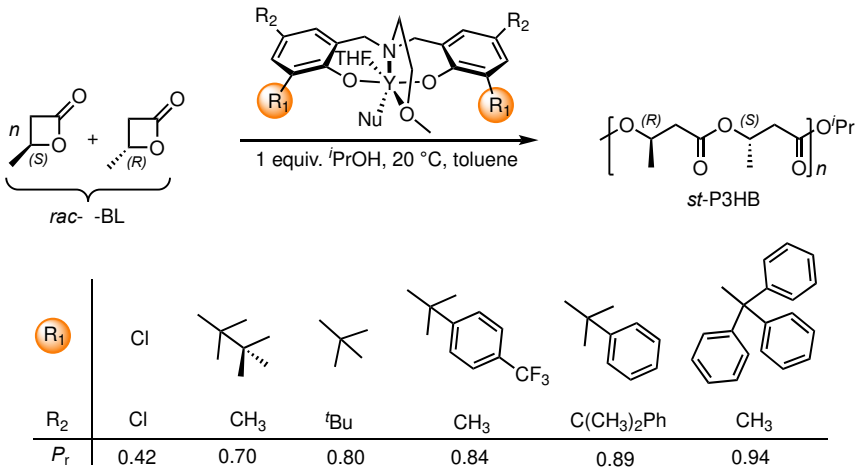

Figure 2.10. Syndioselective polymerization of *rac*-*β*-BL in toluene by C_s-symmetric catalysts **15** to *st*-P3HB with various degrees of syndiotacticity as a function of ortho-substituents on the bis(phenolate) rings.

The impressively high syndioselectivity was further investigated by close analysis of the steric and electronic effects of this class of methoxy-amino bis(phenolate)-yttrium complexes (with the appendant *ether* side arm) on their activity, syndioselectivity, and living behavior (Figure 2.10).[73] It was discovered that, when bulky, aryl-containing substituents are placed at the *ortho* positions, steric interactions are involved, and the P_r value was increased compared to sterically smaller substituents. For example, when running the polymerization at 20 °C in toluene, switching from the cumyl substituted complex (**9b**, Figure 2.9) to trityl substituted analog (**15a**, Figure 2.9) enhanced the syndiotacticity considerably from P_r = 0.89 to P_r = 0.94. Alkyl *ortho* substituents, including those that are rather bulky, gave lower P_r values (**9a** and **15b**, Figure 2.9). Electron withdrawing Cl substituents resulted in loss of stereoselectivity (**15c**, P_r = 0.42, Figure 2.9). Introducing a para-trifluoromethyl group on the phenyl ring of the cumyl substituent (**15d**, Figure 2.9) achieved higher stereoselectivity than the *tert*-butyl substituent (**9a**, Figure 2.9), most likely due to increasing sterics, but placing this electron-withdrawing group on the cumyl phenyl ring lowered stereoselectivity compared to the parent cumyl complex (P_r = 0.84 vs. P_r = 0.89, Figure 2.10).[73] The beneficial effect of the phenyl group in *ortho* substituents prompted further investigation by DFT calculations, indicating C-H--π interactions between one methylene hydrogen of the 3-hydroxybutyrate moiety and the *ortho* and *meta* carbon atoms of a phenyl ring of the cumyl (-Me_2Ph) substituent which appeared as the most stable structure.[73]

The previously described studies[73,74] showed that ligand substituents are essential for stereochemical control through a chain-end control mechanism and that the ROP of *rac*-*β*-BL by metal alkoxides can proceed via a coordination-insertion mechanism or an anionic mechanism. However, the ROP by these bis(phenolate) yttrium complexes proceeds via a coordination-insertion mechanism; as a result, there was no clear crotonate formation (*c.f.,* Figure 2.4) which

would indicate an anionic mechanism.[74] Further mechanistic investigation elucidated a chain-end-control mechanism responsible for the resulting stereochemistry.[75]

Carpentier *et al.* also synthesized a series of neutral amine-bridged bis(phenolate)-lanthanide alkoxide complexes (**16**, Figure 2.9) for the ROP of *rac*-*β*-BL. These complexes with the appendant *amine* side arm effected a controlled polymerization to produce *st*-P3HB with narrow $Đ$ values (<1.25) and P_r = 0.83. The ROP carried out in toluene showed higher activity and syndioselectivity, as compared to the ROP in coordinating solvent THF. The size of ionic metal radii had no notable effects on stereoselectivity, but it did affect the catalytic activity, with Yb > Er > Y >> Sm (**16a-d,** Figure 2.9).[86] The influence of bimetallic complexes on stereoselectivity was also investigated and similar activity and selectivity were observed.[87] Furthermore, bis(guanidinate) alkoxide complexes of lanthanides (**17**, Figure 2.9) were employed for the ROP of *rac*-*β*-BL. Complexes of group 3 metals with smaller atomic radii (Y and Lu) were active and produced *st*-PHB with P_r up to 0.84 (**17a** and **17b**, Figure 2.9).[88] The neodymium complex (**17c**, Figure 2.9) was also active, but it lacked stereoselectivity and produced *at*-P3HB. Combining both the guanidinato and bis(phenolate) ligands for the metal center did not enhance polymerization activity.[89]

2.4.2. ROP of *meso*-8DL^{Me}

Another route to *st*-P3HB is via the stereoselective ROP of *meso*-8DL^{Me}, which is the diastereomeric co-product in the synthesis of *rac*-8DL^{Me} and generally discarded in favor of *rac*-8DL^{Me} that is utilized to produce *it*-P3HB. As described above, the ROP of *rac*-8DL^{Me} results in perfectly *it*-P3HB, thanks to the enantiomorphic site control by the C_2-symmetric, chiral salen-ligated yttrium complexes. These results suggested that such racemic catalysts should also be stereoselective toward *meso*-8DL^{Me}, as the (*R,R*)-catalyst should selectively ring-open *meso*-

8DL^{Me} at the (*S*)-site of the ester (*O*-acyl) bond while the (*S,S*)-catalyst should selectively cleave the ester bond of *meso*-8DL^{Me} at the (*R*)-site, thus affording *st*-P3HB (Figure 2.11). Indeed, the catalyst with the bulky, trityl-substituted ligand complexed to the larger lanthanum ion (**11f**, Figure 2.11) showed good activity and high syndioselectivity, affording *st*-P3HB with a high T_m of 170 °C and P_r up to 0.92.[90]

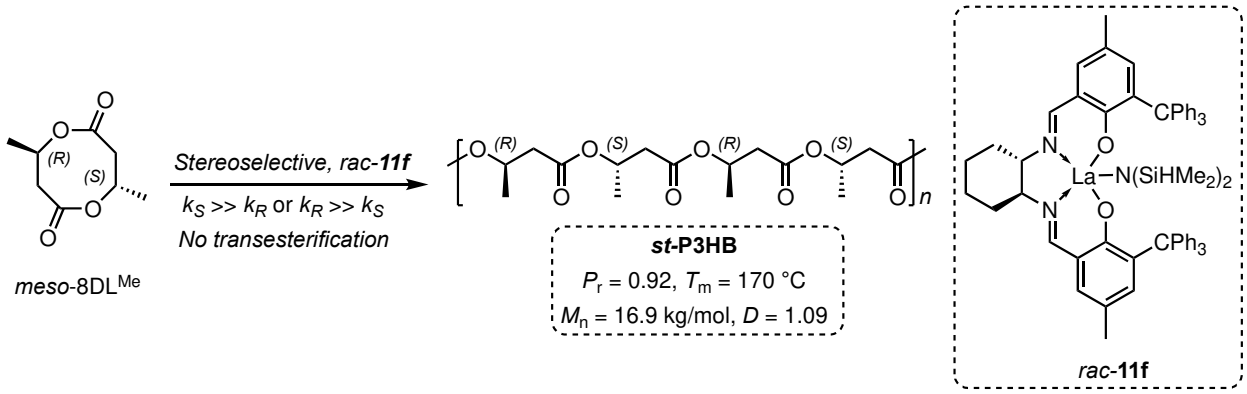

Figure 2.11. Stereoselective ROP of *meso*-8DL^{Me} to *st*-P3HB by racemic catalyst *rac*-**11f** rendered by the catalyst-controlled enantiomeric-site selectivity.

2.5. Atactic P3HB

2.5.1. Organocatalytic ROP of *rac*-β-BL

Metal-free approaches to polyesters via the ROP of cyclic esters are important for accessing metal-free polyesters specifically for microelectronics and biomedical applications, which can also take advantage of mechanistic pathways unique to organocatalysts.[91,92] In 2002, Hedrick and co-workers first reported the organic ROP of cyclic esters using *N*-heterocyclic carbenes (NHCs) as catalysts.[93] In that communication, the authors included one example that 1,3-bis(2,4,6-trimethylphenyl)imidazole-2-ylidene (IMes, **19**, Figure 2.12) effectively polymerizes *rac-β*-BL to *at*-P3HB with a narrow *Đ* (1.15).

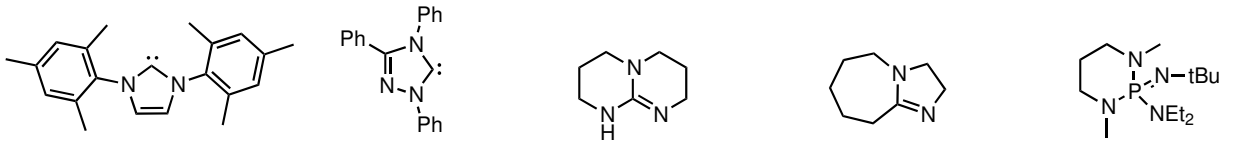

Figure 2.12. Selected organocatalysts for non-stereoselective ROP of *rac*-*β*-BL to *at*-P3HB.

Another NHC, TPT (1,3,4-triphenyl-4,5-dihydro-*1H*-1,2,4-triazol-5-ylidene) (**20**, Figure 2.12), together with methanol, was employed for the ROP of *rac*-*β*-BL at 80 °C, yielding an uncontrolled polymerization due to both postulated alkoxide and carboxylate initiation pathways (Figure 2.13).[94,95] The basicity of the NHC was also attributed to some undesired elimination reactions with unreacted *rac*-*β*-BL that generate crotonate initiators.[94] To circumvent this issue, *tert*-butyl alcohol was added as cosolvent to favor adduct formation and minimize the concentration of the free carbene. Such conditions allowed for the controlled formation of *at*-P3HB although, when higher monomer loadings (>200 equiv.) were used to achieve higher molecular weights, the control was apparently lost. Mechanistic investigations revealed that the *β*-BL-carboxy anion, paired with the protonated carbene, was the initiating species (Figure 2.13).[95] Using *tert*-butyl alcohol in combination with TPT for the ROP of *rac*-*β*-BL brought about a living process absent of the crotonation side reaction, affording higher molecular weight polymer (32 kg/mol) with narrow *Đ* values. This living process allowed for the synthesis of BCPs by the ROP of *rac*-*β*-BL initiated from poly(ethylene glycol)-α-methoxy,ω-carboxylic acid.[95]

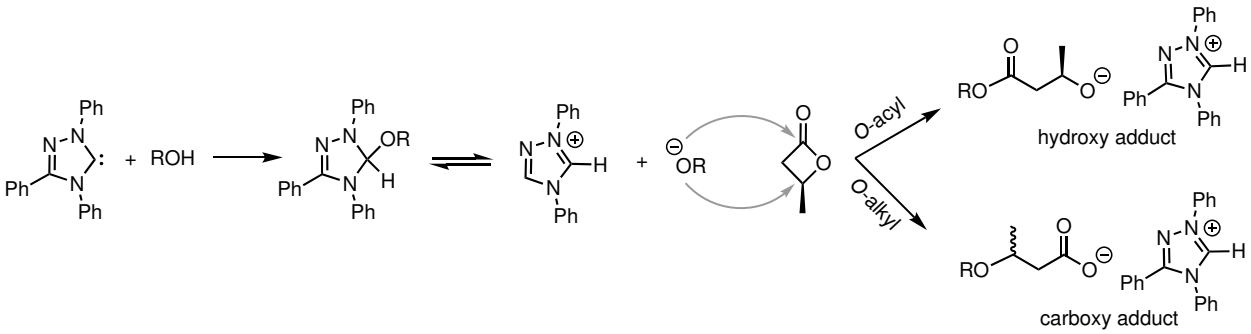

Figure 2.13. Proposed mechanism of carbene initiation of *rac*-*β*-BL where the carboxy anion stabilized by the protonated carbene initiates ROP of *rac*-*β*-BL.

In comparison, TBD (1,5,7-triazabicyclo[4.4.0]dec-5-ene; **21**, Figure 2.12), *N*-methyl-TBD, and DBU (1,8-diazabicyclo[5.4.0]-undec-7-ene; **22**, Figure 2.12) were found to promote uncontrolled ROP of *rac*-*β*-BL.[96] This behavior was ascribed to a 1:1 adduct formation between *β*-BL and the guanidine/amidine organocatalyst, promoted by a strong hydrogen bonding of the hydroxy proton of the ring-opened *β*-BL to the adjacent nitrogen atom of the catalyst (Figure 2.14). This 8-membered ring competes for hydrogen bond formation of the incoming alcohol of the initiator. Attempts to disrupt this adduct formation by increasing the temperature of the reaction resulted in the formation of oligomers with crotonate end-groups, highlighting the uncontrolled nature of the polymerization.[96] Carpentier *et al.* overcame this problem with these basic organocatalysts by using specific reaction conditions and found that a reaction temperature of 60 °C was crucial for enabling the controlled polymerization.[97] TBD had good control over molecular weight and dispersity, but BEMP, 2-*tert*-butylimino-2-diethylamino-1,3-dimethylperhydro-1,3,2-diazaphosphorine (**23**, Figure 2.12), performed better overall.

Two mechanisms were proposed in the above study (Figure 2.14). The first was the formation of the guanidine-*β*-BL adduct, followed by relatively fast dehydration to the corresponding *N*-acyl-α,*β*-unsaturated species, which then further propagates the chain via a living process (*Pathway 1*, Figure 2.14). The alternative mechanism involves a zwitterion formed by partial dissociation of the organic base-*β*-BL adduct that ring-opens an incoming *β*-BL monomer (*Pathway 2*, Figure 2.14). This second insertion is followed by propagation of the resulting zwitterion, and the crotonate end-groups would form via dehydration of the propagating species thus terminating the polymerization.[97] Coulembier *et al.* refuted this mechanism and instead contended that *rac*-*β*-BL is deprotonated by TBD, generating a crotonate anion stabilized by the large cation (the protonated TBD), and this stabilized carboxylate acts as the initiating species.[98] In 2020, Carpentier *et al.*

reinvestigated this mechanism with alkoxymethylene-substituted β-BL,[99] which will be discussed in Section 5 of this article. Nonetheless, the investigations above reveal that the mechanism operating in an organocatalyzed ROP of β-BL is highly dependent on the monomer substituent identity and the organocatalyst used, as well as the reaction conditions.[97–99]

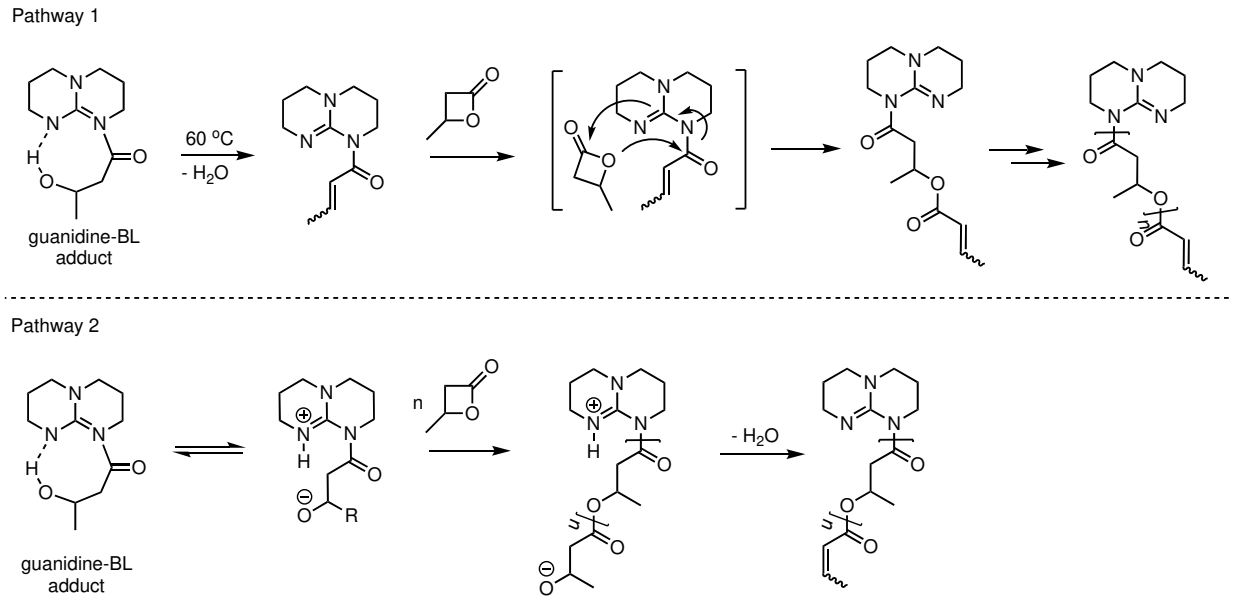

Figure 2.14. Proposed two mechanistic pathways for the ROP of *rac*-β-BL by TBD.

2.5.2. Carbonylative polymerization of epoxides

The metal-catalyzed carbonylative ring-expansion reactions of heterocyclic compounds represent efficient one-step procedures to synthesize lactams, lactones, and thiolactones. Alper *et al.* observed that use of $Co_2(CO)_8$ and 3-hydroxypyridine (**27**, Figure 2.15) as a cocatalyst for carbonylative ring-expansion of propylene oxide resulted in 75% polyester and only 15% β-BL formation.[100] On the other hand, ion pair $[PPN]^+[Co(CO)_4]^-$ (PPN = bis(triphenylphosphine)iminium, **24**, Figure 2.15), in conjunction with a Lewis acid such as BF_3•Et_2O, effectively catalyzed a range of regioselective carbonylation of aliphatic epoxides to afford β-lactones with yields ranging 57-87%.[100]

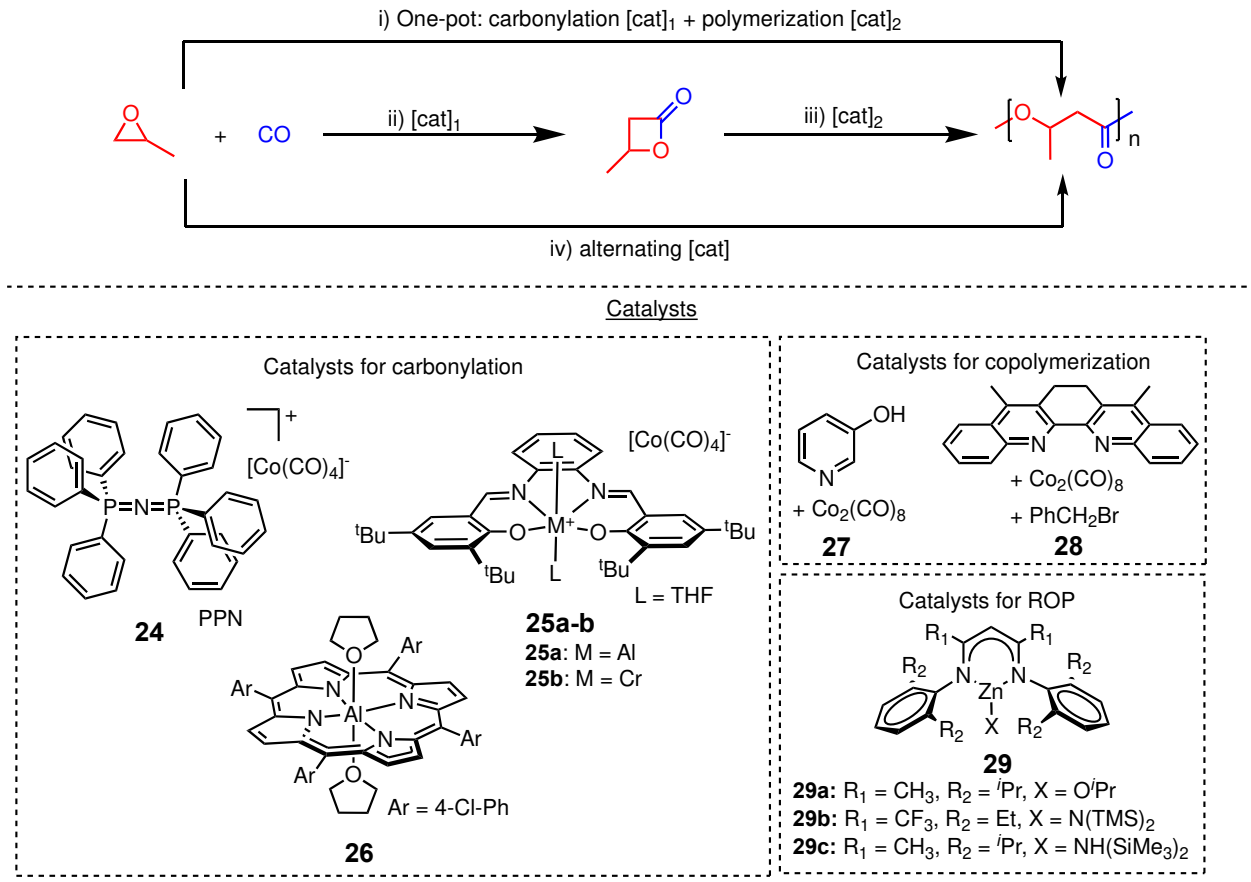

Figure 2.15. Three routes to P3HB using carbonylation of epoxides with CO: i) one-pot carbonylation and polymerization of the resulting *β*-BL by tandem catalytic transformations; ii) first carbonylation of epoxide with CO, followed by iii) ROP of the isolated *β*-BL; iv) direct alternating copolymerization of propylene oxide epoxide and CO.

Coates *et al.* improved the yield of *β*-BL in carbonylation of epoxides by Lewis acids and oxyphilic cations capable of ether coordination.[101] Specifically, cationic aluminum salen-cobaltate complex, $[(salph)Al(THF)_2]^+[Co(CO)_4]^-$ (**25a**, Figure 2.15) exhibited high activity (95% conversion of propylene oxide to *β*-BL in 1 h) with limited formation of polyester side products. The primary mechanistic pathway was proposed to undergo the nucleophilic attack of the activated epoxide at the less hindered site by anion $[Co(CO)_4]^-$ to give the *β*-lactone.

The above described carbonylative ring-expansion catalyzed by $Co_2(CO)_8$ and 3-hydroxypyridine (**27**, Figure 2.15) afforded P3HB as the major product,[100,102] which was reasoned through the direct alternating copolymerization of propylene oxide and CO, rather than by *in situ* ROP of the

β-BL intermediate.[102] This mechanism was corroborated by three lines of evidence: 1) The rate of P3HB formation is independent of the presence of *β*-BL; 2) in fact, repeating the exact reaction conditions without the epoxide but with *β*-BL resulted in no P3HB formation, but the polymerization proceeded after addition of the epoxide to the reaction mixture; and 3) using the enantiopure epoxide resulted in exclusively *it*-P3HB even when *rac*-*β*-BL was present. More specifically, the mechanism was thought to be ring-opening of the epoxide and CO insertion at a tetracarbonyl cobaltate species. Pyridine appeared to be an essential part of the process, but its role was more obscure. Pyridine may assist in the electrophilic attack of the cobalt-bonded acyl carbon of the epoxide, and it may be involved in a back-biting reaction by deprotonating the –OH group to form *β*-BL as a side reaction.[102] In a subsequent study to better understand the mechanism of propagation and the chain termination events that shortened the resultant molecular weights, Rieger *et al.* observed retention of stereochemistry when using the enantiopure epoxide, thus supporting the mechanism previously suggested where CO inserts on the less sterically hindered side of the epoxide.[103] The major chain termination event observed was the hydrolysis of Co-acyl bonds and crotonic ester group formation via dehydration. There was also evidence for the direct coupling of two polymer chains which eliminated $Co_2(CO)_8$ and thus acting as another termination event.

While atom economy is preserved by the direct copolymerization of propylene oxide and CO, this method did not convert monomer at high rates, only produced low-molecular-weight polymers, and also resulted in the formation of *β*-BL as the side product. In an effort to increase the molecular weight, Alper *et al.* changed 3-hydroxypyridine to the bulkier and more basic diamine, 6,7-dihydro-5,8-dimethyldibenzo[*b,j*]-1,10-phenanthroline and 2,9-dimethyl-4,7-diphenyl-1,10-phenanthroline which were used in conjunction with $Co_2(CO)_8$ and benzyl bromide in benzene

(**28**, Figure 2.15), P3HB was formed in higher molecular weight (M_n = 19 kg/mol).[104] This method still achieved only a maximum of 55% P3HB yield after 20 h.

Coates *et al.* developed a one-pot tandem catalytic transformation where *β*-BL is synthesized from propylene oxide and CO by carbonylation catalysts and subsequently polymerized to *at*-P3HB with ROP catalysts *in situ*.[105] Multiple carbonylation catalysts were examined, but aluminum complex $[(ClTPP)Al(THF)_2]^+[Co(CO_4]^-$ (ClTPP = *meso*-tetra(4-chlorophenyl)porphyrinato) (**26**, Figure 2.15) combined with the highly active zinc complex supported by bulky *β*-diiminate (BDI) ligands [(BDI)ZnO^{i}Pr; **29a**, Figure 2.15] showed high activities for both carbonylation and ROP. Tuning the substituents on the Zn complex led to an optimized the system, and higher molecular weight polymers (M_n up to 52 kg/mol) were produced. This process appeared to be living and, when the enantiopure epoxide was used, the tandem carbonylation/ROP process resulted in highly *it*-P3HB.[105]

2.5.3. Metal-mediated coordinative-insertion ROP of *rac*-β-BL

As described in previous sections of this article, prior to the 2000s, most organometallic complexes studied for the ROP of *β*-BL were extremely slow or only resulted in low molecular weight P3HB. In 2002, Coates and co-workers employed discrete zinc alkoxy complex (BDI)ZnO^{i}Pr (**29a**, Figure 2.15) to initiate the ROP of *rac-β*-BL and *rac-β*-valerolactone (*β*-VL) via a coordinative-insertion mechanism at unprecedented rates at that time to controlled, high molecular weight (M_n > 100 kg/mol), *at*-P3HB and P3HV, respectively.[106]

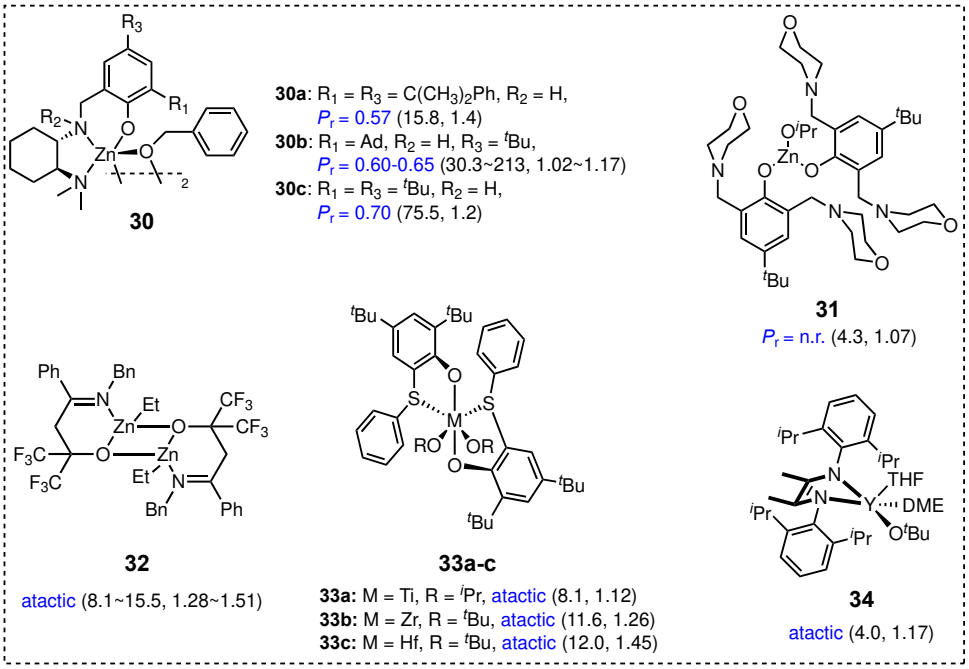

Figure 2.16. Representative metal complexes for controlled, living, or immortal polymerization of *rac*-*β*-BL to largely *at*-P3HB. Dotted lines in **30** indicate a dimer. Ad = Adamantyl; n.r. = not reported, "atactic" = mention of the atactic microstructure based on ^{13}C NMR but no P_r values reported. M_n in kg/mol and $Đ$ values are placed in parentheses for each initiator.

A dimeric diaminophenolate zinc complex (**30**, Figure 2.16) effectively polymerized up to 2,000 equiv. of *rac*-*β*-BL in less than 30 min.[107] The resulting P3HB is syndio-enriched atactic, but tuning the steric bulk on the ligand changed the syndiotacticity of the resulting polymer. For example, changing the *ortho* substituent from a cumyl (**30a**, Figure 2.16) to adamantyl (**30b**, Figure 2.16) increased the P_r value from 0.57 to 0.65.[107] Immortal polymerization, where chain transfer is rapid and reversible thus forming polymers catalytically with narrow $Đ$ values,[108] was achieved using the most syndioselective Zn complex, **30c** (Figure 2.16) and up to 5,000 equiv. of benzyl alcohol as the effective chain transfer agent.[107] A Zn complex supported by the bulky bis(morpholinomethyl)phenoxy ligand (**31**, Figure 2.16) is also effective for immortal polymerization of cyclic esters, converting 500 equiv. of *rac*-*β*-BL with 10 equiv. of ^{i}PrOH in 95% conversion within 3 h. The resulting *at*-P3HB had observed molecular weights similar to those calculated theoretically, indicating good control.[109]

Another Zn(II) complex stabilized by a bidentate fluorous tertiary alkoxide-imino ligand (**32**, Figure 2.16) promoted controlled ROP of *rac*-*β*-BL to *at*-P3HB.[110] This fluorous alkoxide ligand overcame the weakness of other alkoxide ligands which often produce highly aggregated polynuclear species due to the bridging tendency of the more basic alkoxide species compared to the phenoxide ligands. However, complex **32** (Figure 2.16) showed a tendency to catalyze transesterification with prolonged reaction times, which resulted in broader dispersities and decreased molecular weights over time.[110]

Group 4 (Ti, Zr, and Hf) complexes supported by 4,6-di-*tert*-butyl-2-phenylsulfanylphenol ligands (**33a-c**, Figure 2.16) were also examined as catalysts for the ROP of *rac*-*β*-BL.[113] When combined with 5 equiv. of ^{i}PrOH, these complexes were moderately active and promoted "living" polymerization of *rac*-*β*-BL to *at*-P3HB.[111] Group 3 yttrium borohydride and alkoxide complexes supported by rigid dianionic bis(amide) ligands derived from 1,4-diaza-1,3-butadiene (**34**, Figure 2.16) were also investigated for their catalytic performance for the ROP of *rac*-*β*-BL to *at*-P3HB.[112] Generally, the ROP was very slow, but the observed molecular weights were in good agreement with the calculated values and the P3HB dispersities were narrow.

2.6. Other PHA homopolymers and copolymers

2.6.1. Uncommon or unnatural PHAs

To understand the diversity of material properties of the PHA family and discover new PHA materials through PHA structure-property relationship studies, tuning the R pendant groups must be explored. One of the advantages of the chemocatalytic routes is the facile tuning of the monomer substituents that can lead to new PHAs, often uncommon or unnatural homopolymer PHAs and random or block copolymers.

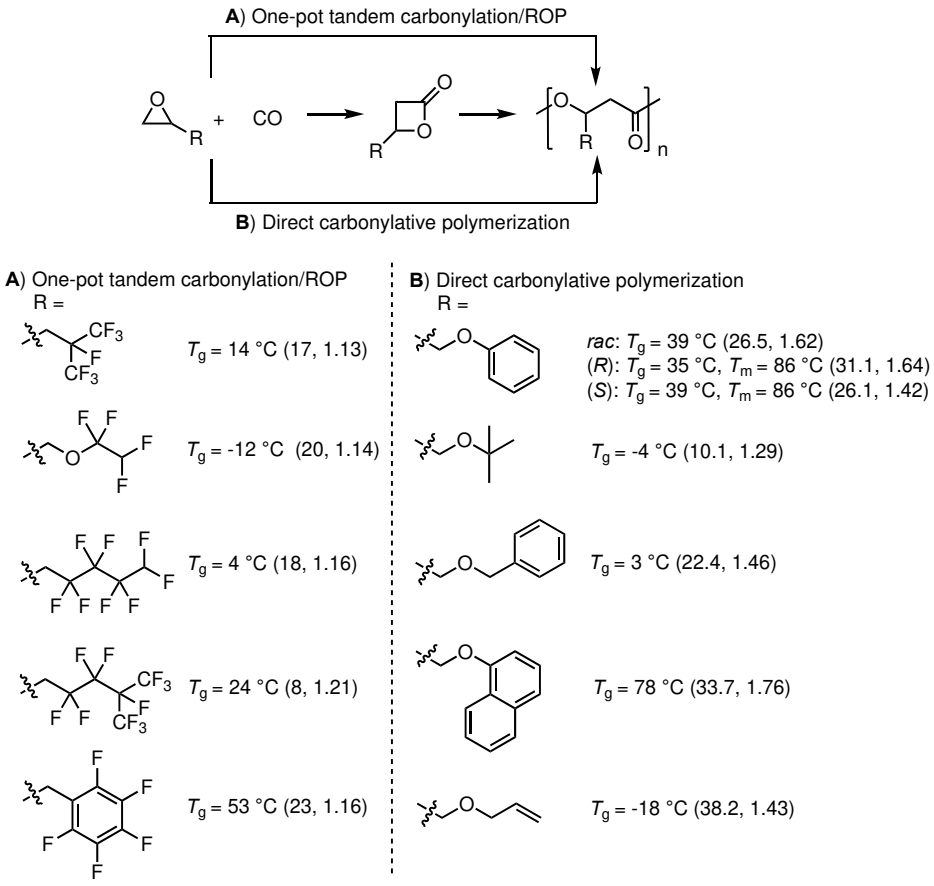

Figure 2.17. A) Tandem carbonylation/ROP and **B**) direct carbonylative polymerization of epoxides for the synthesis of a wide range of fluoroalkyl-substituted and other alkyl- or oxo-alkyl (-CH_2-OR(Ar))-substituted PHAs. M_n in kg/mol and $Đ$ values are placed in parenthesis for each initiator.

Through the catalytic carbonylation of epoxides, which are often commercially available, a wide range of β-lactones, including β-lactones with fluorinated substituents were made available. The highly active (BDI)ZnO^{i}Pr (**29a**, Figure 2.15) effectively polymerized such β-lactones into the resultant fluorinated PHAs (**A**, Figure 2.17).[113] In general, the fluorinated PHAs have higher T_g values than their non-fluorinated analogs. For example, naturally produced poly(β-hydroxyoctanoate) (P3HO) has a T_g of -35 °C, while the fluorinated analog has a higher T_g of 4 °C. The direct carbonylative polymerization of a wide range of epoxides by a trimetallic (Cr) salen complex in combination with $Co_2(CO)_8$ led to generation of 17 new PHAs (M_n up to 38.2 kg/mol)

with various structures, high regioselectivity (toward ring-opening of epoxides), diverse functionalities, and tunability as reflected in the wide ranging T_g values from as low as -45 °C to as high as 78 °C (**B**, Figure 2.17).[114] These examples further highlight the ability of the chemocatalytic route for facile tuning of the PHA structures.

Through stereoselective ROP of *rac*-8DL^R (R = Et, ^{n}Bu) by C_2-salen ligated yttrium complexes (**11c** and **11d**), Chen *et al.* extended the chemocatalytic synthesis of PHAs to isotactic poly(3-hydroxyvalerate) (*it*-P3HV) and poly(3-hydroxyheptanoate) (*it*-P3HHp) (Figure 2.18). These homopolymer PHAs are uncommon biologically, typically only found as random copolymers with *it*-P[(*R*)-P3HB]; thus, this simple chemical synthesis provides access to discrete homopolymer PHAs. It should be noted that P3HV and its copolymers can also be synthesized by the ROP of ethyl-substituted β-VL,[106] but P3HHp is an uncommon PHA previously only accessible by highly engineered biological methods.[115]

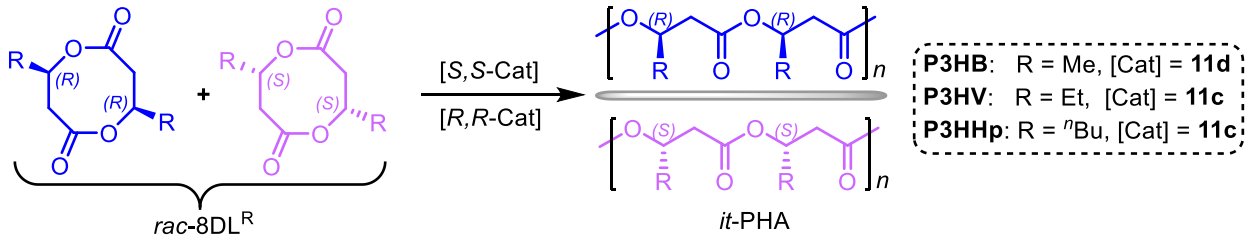

Figure 2.18. Stereoselective ROP of *rac*-8DL^R to *it*-PHAs: R = Me, P3HB; R = Et, P3HV; R = ^{n}Bu, P3HHp.

The stereoselective copolymerization of *rac*-8DL^{Me} with *rac*-8DL^R (R = Et, ^{n}Bu) yields high molecular weight (M_n >100 kg/mol, $Đ$ ~ 1.10), crystalline *it*-PHA copolymers (**A**, Figure 2.19).[116] As expected, increasing incorporation of *rac*-8DL^R decreases the crystallinity, T_m, and T_g of the resulting PHA copolymers. The mechanical properties of the random copolymers, poly(3-hydroxybutyrate-*co*-hydroxyvalerate) (P3HBV) and poly(3-hydroxybutyrate-*co*-hydroxyheptanoate) (P3HBHp) with ~7%, ~10%, and ~20% incorporation of *rac*-8DL^R, were

analyzed via tensile testing of specimens prepared by compression molding (**B** and **C**, Figure 2.19). P3HBV with 19.8% 3HV incorporation showed polypropylene-like thermal and mechanical properties with σ = 25 ± 0.2 MPa, Young's Modulus (*E*) = 669 ± 45 MPa, and ε = 374 ± 19% (**B**, Figure 2.19). On the other hand, the P3HBHp with 19.6% 3HHp incorporation exhibited polyethylene-like thermal and mechanical properties with σ = 20.5 ± 0.4 MPa, *E* = 226 ±9 MPa, and ε = 578 ± 15% (**C**, Figure 2.19). These results highlight the versatility and efficiency of the chemocatalytic synthesis via the stereoselective ROP of *rac*-8DL^{R} towards crystalline, *it*-PHA homopolymers and copolymers with tunable thermal and mechanical properties.

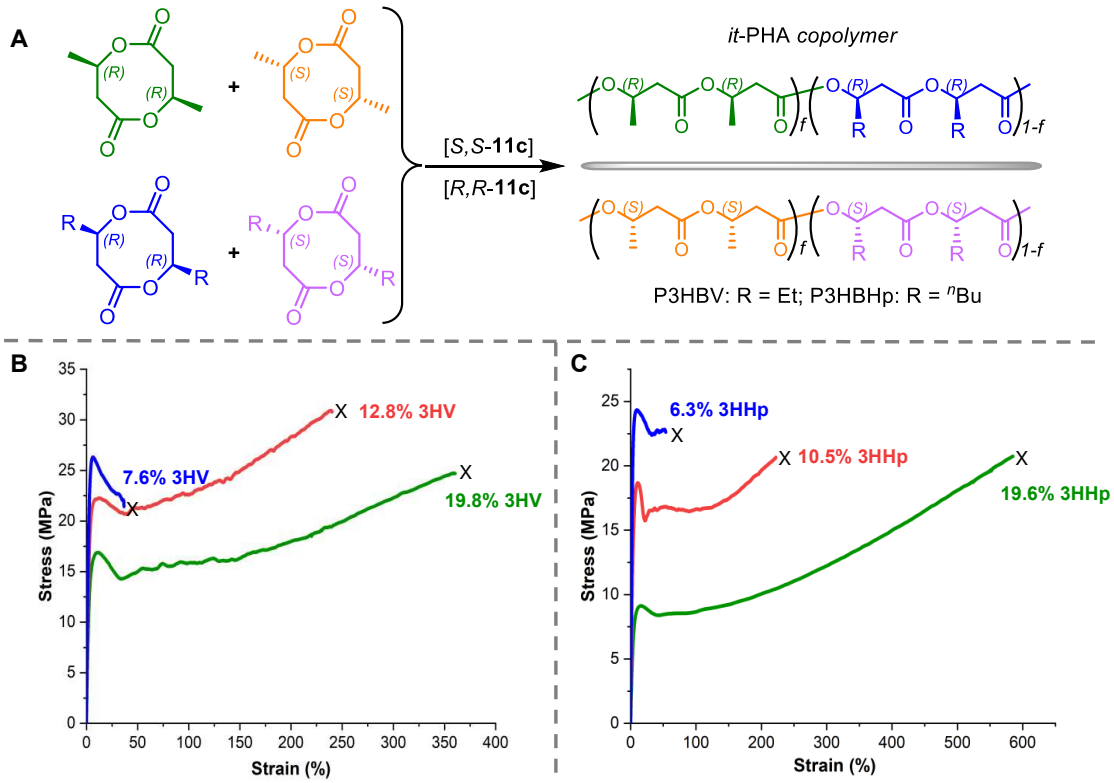

Figure 2.19. A) Stereoselective copolymerization of *rac*-8DL^{Me} with *rac*-8DL^{R} towards *it*-PHA copolymers. **B**) Stress-strain overlay plots of P3HBV copolymers with varying 3HV incorporation. **C**) Stress-strain overlay plots of P3HBHp copolymers with varying 3HHp incorporation.

This catalyzed chemical synthesis was extended further to produce unnatural, aromatic PHAs with relatively high T_g and T_d (Figure 2.20).[117] Specifically, the ROP of benzyl substituted *meso*-8DL^{Bn}

with Y and La complexes supported by C_2-Salen ligands affords syndiotactic ([*rr*] = 92%) poly(3-hydroxy-4-phenylbutyrate) (*st*-P3H4PhB) with high molecular weight (M_n = 147 kg/mol, $Đ$ = 1.19) and a high (relative to common PHAs) T_g of 43 °C (**B**, Figure 2.20).[117] Careful selection of catalyst, monomer, and conditions allowed for copolymerization of *meso*-8DL^{Bn} and *rac*-8DL^{R} (R = Me, ^{n}Bu) to produce aromatic-aliphatic random, stereotapered, or crystalline stereo-diblock PHA copolymers (**A**, Figure 2.20). The statistical copolymerization of *meso*-8DL^{Bn} and *rac*-8DL^{Bu} gave high molecular weight (M_n = 205 kg/mol) copolymer, P3H4PhB-*co*-P3HHp, which is strong, hard, and ductile (ε = 191%) material, and displayed a high decomposition temperature, T_d = 281 °C (**C**, Figure 2.20) (compared to ~250 °C for PHAs generally).

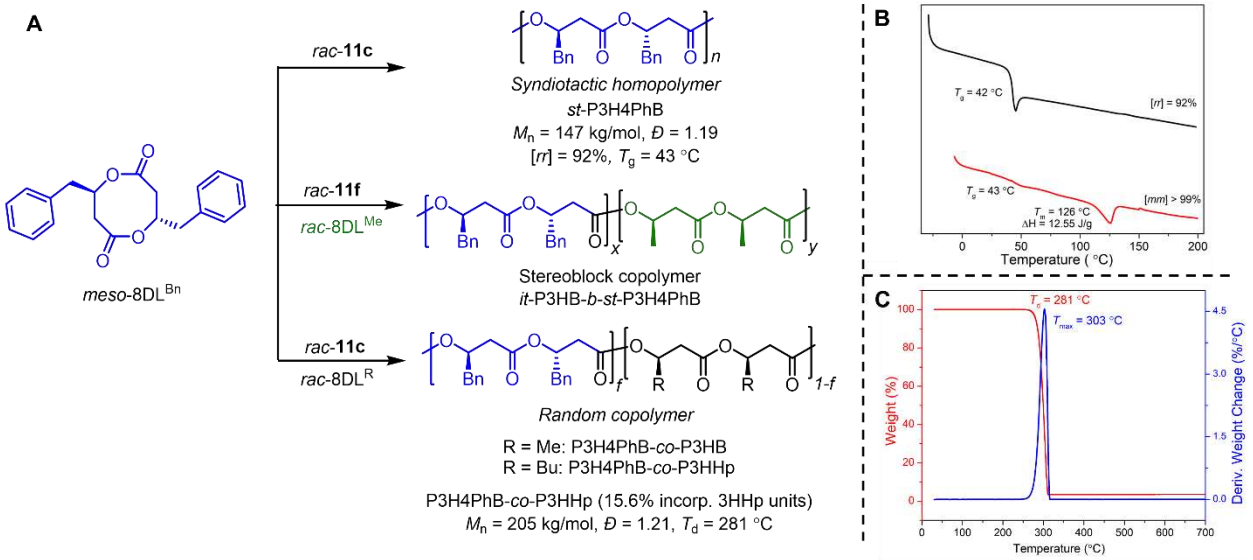

Figure 2.20. A) Aromatic PHAs from ROP of *meso*-8DL^{Bn}. **B**) DSC of *st*-P3H4PhB from ROP of *meso*-8DL^{Bn} (black) and *it*-P3H4PHB from ROP of *rac*-8DL^{Bn} (red, first heating scan). **C**) TGA of P3H4PhB-*co*-P3HHp with 15.6% incorporation of 3HHp units. Reprinted (adapted) with permission from [117]. Copyright 2020 American Chemical Society.

Lu *et al.* reported a *β*-lactone fused with a five-membered ring at the α- and *β*-positions from the carbonylation of cyclopentene oxide with CO.[118] The coordinative-insertion ROP of this monomer using yttrium complex **10** with BnOH as initiator proceeds via *O*-acyl cleavage and produces a *cis*-PHA with a high T_m of ~ 185 °C (ΔH = 21 J/g) and a T_d of ~ 268 °C (Figure 2.21).

On the other hand, the organocatalyzed ROP with TBD (**21**) proceeds via *O*-alkyl cleavage and yields an amorphous, *trans*-PHA with a mixture of linear and cyclic topologies. Using yttrium complex **10** alone (i.e., without an alcohol initiator) also produced a mixture of linear and cyclic topologies, and lanthanum complex **8** afforded the cyclic polymer as the major product. Thermal degradation (pyrolysis) of this α,*β*-cyclopentane fused PHA led to the formation of an α,*β*-unsaturated carboxylic acid, presenting a route for open-loop chemical recycling (Figure 2.21).[118]

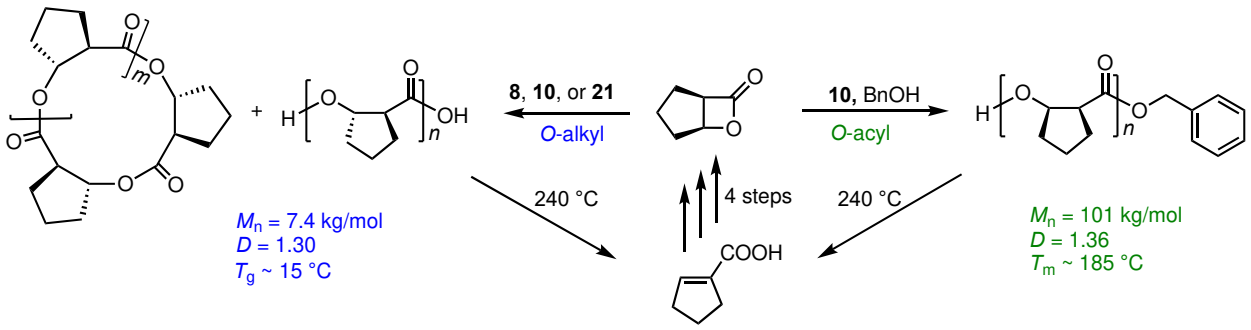

Figure 2.21. ROP of α,*β*-substituted *β*-lactone to an α,*β*-cyclopentane-fused PHA with either linear or cyclic topology and its thermal degradation to cyclopentene carboxylic acid.

2.6.2. Functionalized or alternating PHAs

PHAs with functional groups can significantly modulate their physical, chemical, and mechanical properties, thereby becoming sought-after targets from chemocatalytic routes. The routes using functionalized *β*-BLs are commonly coupled with subsequent post-polymerization transformations of the resulting functionalized PHAs. For example, allyl-functionalized PHAs were synthesized by the ROP of *rac*-*β*-BL^{allyl} and its copolymerization with *rac*-*β*-BL using discrete amino-methoxy-bis(phenolate) yttrium-amido complex **9a** (Figure 2.9).[75] As expected, the ROP of *rac*-*β*-BL^{allyl} is slower than that of *rac*-*β*-BL, but the copolymers with various ratios of *rac*-*β*-BL and *rac*-*β*-BL^{allyl} are accessible by the controlled copolymerization that resulted in *st*-copolymer PHAs. Straightforward chemical transformations of the allyl pendant groups to respective alcohol,

dihydroxyl, and epoxy derivatives were achieved (**A**, Figure 2.22), showcasing the tunability offered by the allyl-functionalized PHA.

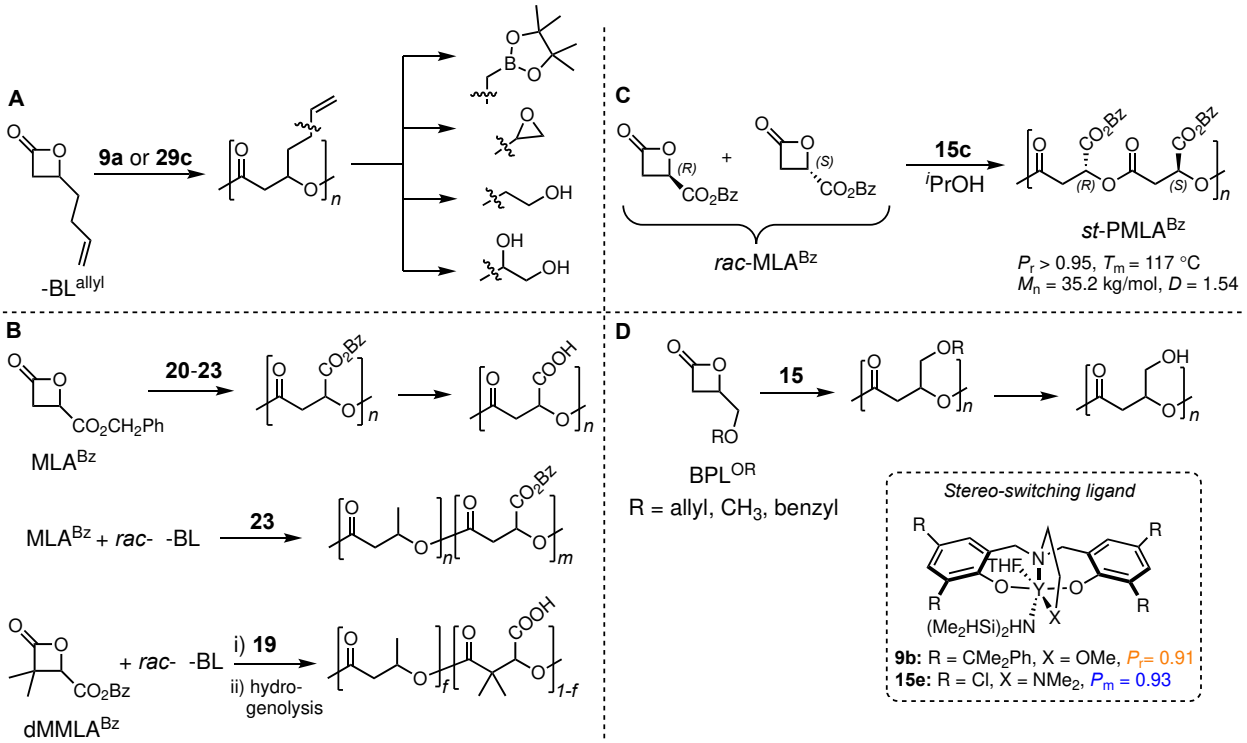

Figure 2.22. ROP of functionalized *β*-BLs and chemical transformations of the resulting PHAs. **A**) allyl-functionalized PHA and its post-polymerization functionalization into boron, epoxy, alcohol, and dihydroxyl PHA derivatives. **B**) Carboxylic acid functionalized PHAs derived from benzyl-*β*-malolactone (MLA^{Bz}) and dimethyl benzyl *β*-malolactone (dMMLA^{Bz}). **C**) Syndiotactic PMLA^{Bz} from stereoselective polymerization of *rac*-MLA^{Bz}. **D**) Alkoxy functionalized *β*-propiolactone (*rac*-BPL^{OR}) and its stereoselective ROP en route to isotactic and syndiotactic PBPL^{OR} and the corresponding hydroxyl functionalized PHAs.

Certain functional pendant groups such as protic (-OH and -COOH) groups cannot be introduced until after polymerization because of catalyst's functional group intolerance that can lead to suppression or inhibition of catalyst activity. Therefore, developing PHAs with pendant groups that can undergo post-polymerization modifications offers a promising route to accessing functional PHAs. With this strategy in mind, Guilaume *et al.* envisioned boron-containing PHAs for their use in the biomedical field, but attempts to polymerize a boron-functionalized *rac*-*β*-BL with Zn complex **29c** was unsuccessful, presumably due to catalyst inhibition by the polar boronate

groups.[119] To solve this issue, the ROP of *rac*-β-BL^{allyl} with Zn complex **29c** mixed *in situ* with BnOH, or Y complex **9a** mixed *in situ* with ^{i}PrOH, was employed first to the allyl functionalized PHA, followed by hydroboration to afford the targeted boron-functionalized PHA (**A**, Figure 2.22).

Through the ROP of benzyl-β-malolactone (MLA^{Bz}), followed by deprotection of *O*-benzyl groups via hydrogenolysis, hydrophilic PHAs carrying the carboxylic acid function have been developed (**B**, Figure 2.22). The organocatalyzed ROP of MLA^{Bz} at 60 °C with organic bases such as DBU and BEMP was efficient and controlled.[120] DBU and BEMP appeared to be more efficient than TBD for the ROP of MLA^{Bz}, and investigation into the mechanism revealed that the β-lactones are initiated by a 1:1 crotonate/TBD adduct or by a DBU/BEMP-*N*-acyl crotonate intermediate.[120] Simultaneous copolymerization of MLA^{Bz} with β-BL by BEMP led to di-BCP P(MLA^{Bz}-*b*-BL), due to drastic kinetic differences between MLA^{Bz} and β-BL (**B**, Figure 2.22). On the other hand, the same copolymerization procedure by TBD and DBU resulted in only MLA^{Bz} conversion, thus yielding only the homopolymer (**B**, Figure 2.22).[121] Subsequently, a copolymerization procedure by sequential addition of MLA^{Bz} and β-BL afforded BCPs regardless of the order of addition for the above organic bases studied. These amphiphilic PMLA-*b*-P3HB copolymers as well as the BCPs from cyclic carbonates and MLA^{Bz} were identified as biocompatible nanovectors for potential use for systemic drug delivery.[122,123] ROP of MLA^{Bz} by organometallic complex **15** results in highly syndiotactic polymer (**C**, Figure 2.22) [124]

Poly([*R/S*]-3,3-dimethylmalic acid) (PdMMLA) is another attractive, water-soluble, aliphatic polyester with carboxylic pendant groups along the chain (**B**, Figure 2.22), thanks to its biocompatibility and degradation to 3,3-dimethylmalic acid, a nontoxic molecule. The copolymerization of dimethyl benzyl β-malolactone (dMMLA^{Bz}) and *rac*-β-BL with triazole

carbene **20** (Figure 2.12) and ethylene glycol initiator proceeds via *O*-acyl cleavage of both dMMLA^{Bz} and *β*-BL with preferential incorporation of dMMLA^{Bz} but affords a random copolymer P(dMMLA^{Bz} -*co*-BL (**B**, Figure 2.22).[125] Because of the diol initiation, the α,ω-dihydroxy (P(dMMLA^{Bz} -*co*-BL) copolyester acts as a difunctional macroinitiator for *L*-lactide ROP to give an amphiphilic A-B-A tri-BCP after the *O*-benzyl groups were removed by hydrogenolysis.

PHAs with the hydroxyl function in the pendant group was produced by the ROP of *rac*-4-alkoxymethylene-*β*-propiolactone (*rac*-BPL^{OR}) derivatives, followed by chemical modifications of the resultant polymers with debenzylation, desilylation, or hydrogenolysis (**D**, Figure 2.22).[126] Contrary to the ROP of MLA^{Bz} by discrete yttrium complexes **15** where even small substituents on the *ortho* position of the phenoxy ligand can achieve high syndioselectivity,[124] the ROP of *rac*-BPL^{OR} to highly syndiotactic polymer (P_r = 0.9) requires bulky *ortho* substituents on the phenolate ring.[127] Thus, the stereoselectivity was found to be strongly influenced by the nature of the *ortho* and *para* substituents on the phenolate ligand, due to steric and electronic secondary interactions between the ligand and monomer. In an intriguing twist, simply switching these *ortho* substituents from the bulky aromatic groups to halogens switches the stereochemical outcome from highly *st*- to *it*-polymer with P_m up to 0.93 (**D**, Figure 2.22).[127] For example, the cumyl substituted catalyst with an ether pendant arm (**9b**) resulted in highly *st*-PHB^{OR} with P_r = 0.91, but the chloride substituted catalyst with an amine pendant arm (**15c**) resulted in *it*-PHB^{OR} with P_m = 0.93 (**D**, Figure 2.22).[127,128] This stereo-switching strategy was extended to the ROP of *rac*-*β*-BL by yttrium complexes supported by a series of salan-like ligands with different R groups on the ligand framework of the bridging *N* atoms.[129] Aromatic phenyl groups on bridging *N* atoms afford iso-enriched P3HB (P_m > 0.66). When the phenyl groups were replaced by aliphatic cyclohexyl groups, syndio-rich P3HB (P_r = 0.77) was obtained instead. Replacing this group with a *tert*-butyl

group resulted in *at*-P3HB with P_m around 0.50,[129] providing another example showing that simple tuning of the ligand architecture can switch the stereoselectivity in the ROP of *rac*-*β*-BL.

Thomas, Coates, and co-workers developed a unique approach to access alternating syndiotactic PHA copolymers through copolymerization of a mixture of two enantiomerically pure, different *β*-lactones of opposite stereoconfiguration by a syndioselective yttrium-based catalyst (**35**, Figure 2.23).[130] These enantiopure *β*-lactones can be readily produced from carbonylation of the corresponding enantiopure epoxides, which were subject to copolymerization by the yttrium catalyst to produce various PHA copolymers with 90-94% alternation and T_m ranging from 47 °C to 210 °C, depending on the substituents (Me, Et, ^{n}Bu, $CH_2C_4F_9$, $CH_2OC_2H_5$) and their combinations.

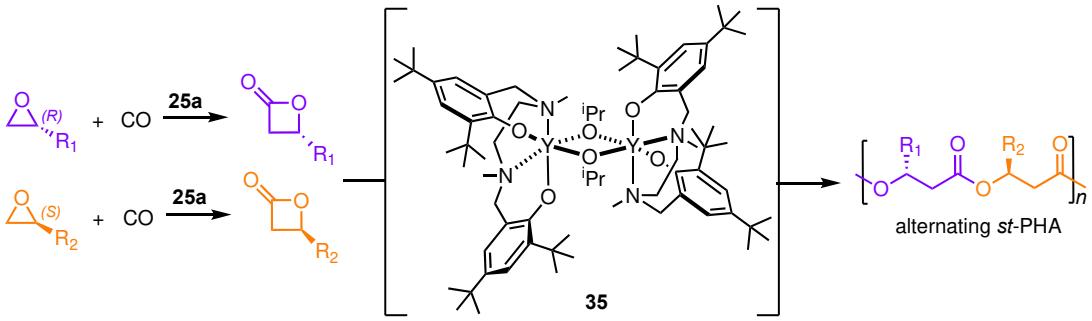

Figure 2.23. Alternating *st*-PHA copolymers via syndioselective copolymerization of a pair of enantiopure *β*-lactones of opposite stereo-configuration.

This strategy has been extended to ROP of *rac*-BPL^{OR} using syndioselective catalyst **9b**, alternating PHA copolymers, P(HB^{OR1}-*alt*-HB^{OR2}), can be conveniently synthesized via copolymerization of equimolar mixtures of (*R*)-BPL^{OR1} and (*S*)-BPL^{OR2} (**A**, Figure 2.24).[131] Changing to the isoselective Cl-substituted Y complex (**15c**) in combination with clever tuning of the monomer mixture can drastically change the resulting copolymer microstructures (**B**-**C**, Figure 2.24). One such example is the polymerization of a 1:1 mixture of two differently substituted monomers of opposite stereo-configuration, (*R*)-BPL^{OR1} + (*S*)-BPL^{OR2} into a mixture of two

isotactic homopolymers, *it*-PHB^{OR1} + *it*-PHB^{OR2} (**B**, Figure 2.24). On the other hand, when using differently substituted monomers of the same absolute configuration, (*S*)-BPL^{OR1} + (*S*)-BPL^{OR2}, *it*-(*S*)-chain random copolymer, (*S*)-P(BPL^{OR1}-*co*-BPL^{OR2}), was produced (**C**, Figure 2.24). Lastly, using a racemic mixture of the differently substituted monomers, *rac*-BPL^{OR1} + *rac*-BPL^{OR2}, a mixture of *it*-(*S*)-chain random copolymers and *it*-(*R*)-chain random copolymers was produced (**D**, Figure 2.24).[131]

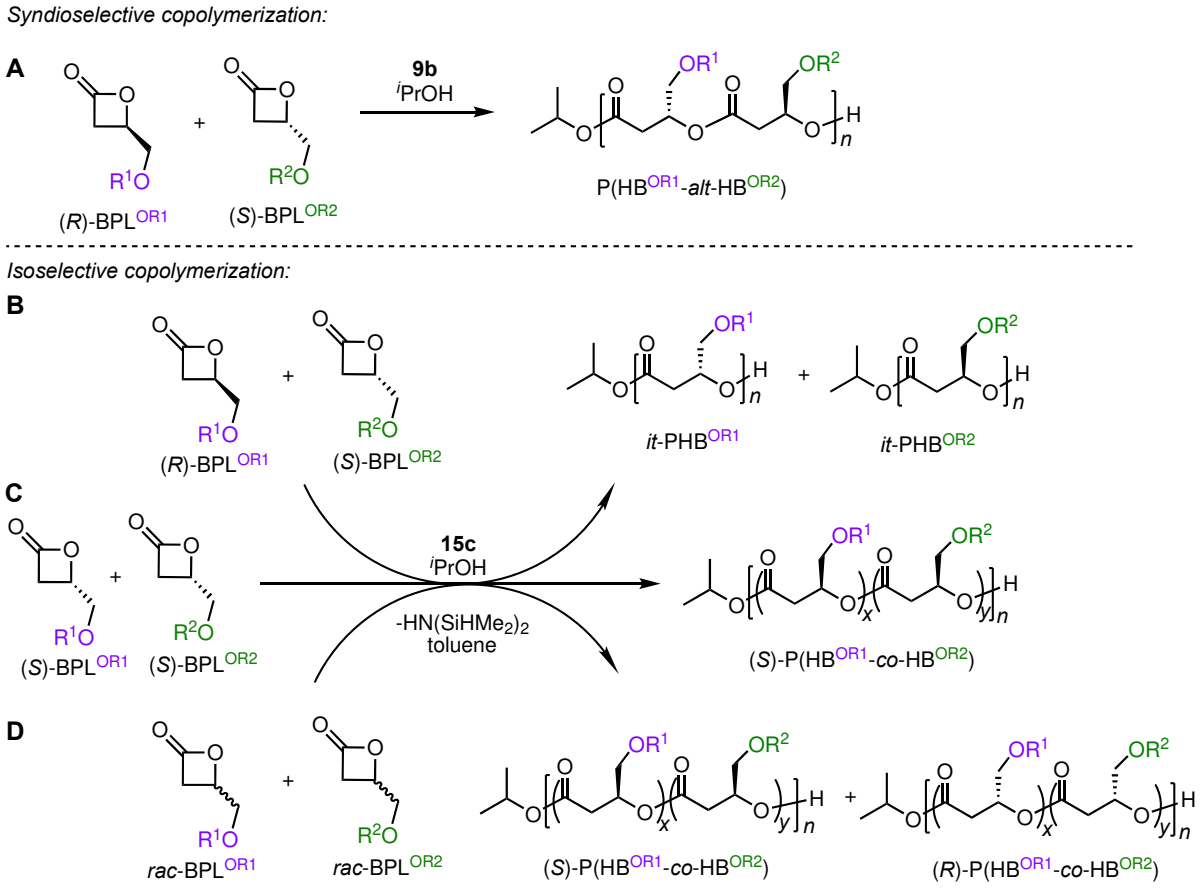

Figure 2.24. A. Alternating copolymerization of different BPL comonomers of opposite stereo-configuration by syndioselective catalyst **9b**. **B**-**D**. Various homopolymer and copolymer compositions that can be achieved by copolymerizing mixtures of BPL^{OR1} + BPL^{OR2} with isoselective catalyst **15c**, depending on the configuration of paring comonomers.

As in the organocatalyzed ROP of *rac*-*β*-BL (*c.f.* Figure 2.14), a recent investigation of the organocatalyzed ROP of BPL^{OR} using TBD, DBU, and BEMP to produce *at*-PHB^{OR} revealed that each organocatalyst carries a different mechanism of initiation.[99] Specifically, BEMP acts as a

base and deprotonates the monomer to form the [carboxylate anion / protonated BEMP cation] ion pair which is the initiating species. Highly nucleophilic TBD forms a 1:1 *N*-acyl-α,*β*-unsaturated adduct via *O*-acyl cleavage of BPL^{OR} and this adduct propagates in a similar manner to BEMP. Lastly, DBU, which is both a nucleophile and base, favors scission of both *O*-acyl and *O*-alkyl bonds of BPL^{OR}, thus forming alkoxy and carboxylate active species.

2.6.3. Stereoblock or stereosequenced PHAs

A common practice for polymerizing a monomer bearing two stereogenic centers is to first separate its *racemic* and *meso* diastereomers and then subject the *rac*- or *meso*-diastereomer to different stereoselective catalysts to *it*- or *st*-polymer, respectively. In the case of $8DL^{Me}$, the stereoselective ROP of *rac*-$8DL^{Me}$ can produce perfectly *it*-polymer ($P_m > 0.99$)[70] while the stereoselective ROP of *meso*-$8DL^{Me}$ can lead to highly *st*-polymer ($P_r \sim 0.92$).[90] One might expect that the polymerization of the mixture of these diastereomers would result in a stereorandom, *at*-polymer. But in the diastereoselective polymerization system developed by Chen and co-workers, the racemic (*R,R*/*S,S*) yttrium and lanthanium complexes supported by C_2-symmetric salcy ligands with bulky, trityl *ortho* substituents (**11d**, Figure 2.7 and **11f**, Figure 2.11) were found to be both highly enantioselective[70] and diastereoselective, thus producing *it/st*-stereotapered diblock P3HB when directly polymerizing a *rac/meso*-$8DL^{Me}$ mixture (Figure 2.25).[90]

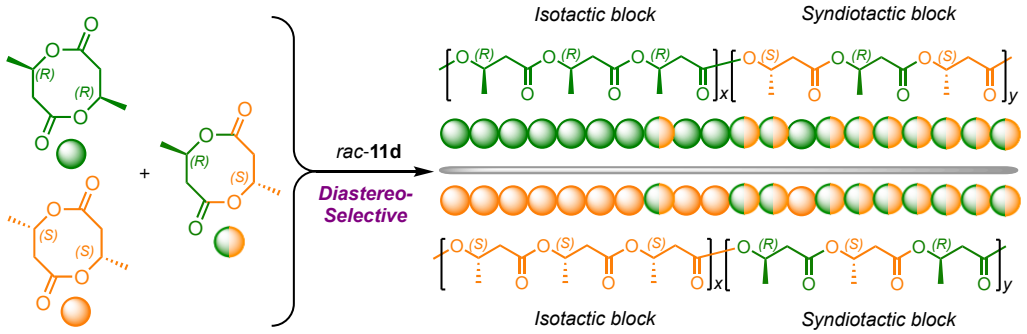

Figure 2.25. Schematic representation of diastereoselective polymerization of the *rac/meso*-$8DL^{Me}$ mixture to *it/st*-stereotapered diblock, crystalline P3HB, *it-sb-st*-P3HB.

The diastereoselectivity that renders the formation of the tapered stereodiblock was revealed by monitoring of the polymerization of the 1:1 *rac/meso*-8DL^{Me} mixture, showing that *rac*-8DL^{Me} was rapidly polymerized within 30 seconds whereas *meso*-8DL^{Me} was much slower to react and required an additional 35 min to reach near quantitative conversion.[90] The monomer reactivity ratios of the copolymerization indicated a tendency for comonomers to form long, blocky segments. The isolated *it-sb-st*-P3HB was semicrystalline, having two T_c values of 87° and 69 °C and two corresponding T_m values of 135° and 115 °C associated with the respective *it*- and *st*-crystalline domains. Changing the *rac/meso*-8DL^{Me} ratio to 2:1 gave *it-sb-st*-P3HB with higher T_m values of 150° and 133 °C. The T_m values were further enhanced (by 6 to 10 °C) in the authentic stereodiblock P3HB synthesized by sequential addition of each diastereomer, due to the absence of the stereotapered junctions in this strereodiblock P3HB.[90]

The *it-sb-st*-P3HB (50% *it*) showed enhanced ductility (ε_B = 17 ± 5 %) compared to *it*-P3HB (ε_B < 5 %), and the *it-sb-st*-P3HB (86% *it*) was similarly brittle to *it*-P3HB, thus highlighting the importance of the *st*-P3HB fraction in modulating mechanical properties. The ductility was drastically enhanced by copolymerizing 8DL^{Me} with 8DL^{Et} (*meso*-8DL^{Me} with *rac*-8DL^{Et}, as an example), which yielded a gradient stereo-BCP, *st*-P3HB-*sb-it*-P3HV (**A**, Figure 2.26), due to the inherent diastereoselectivity between faster reacting *meso*-8DL^{Me} compared to *rac*-8DL^{Et} (**B**, Figure 2.26). This stereo-BCP (18% 8DL^{Et} or 3HV incorporation) was shown to be a strong, ductile, and tough material with relatively high ultimate strength (σ = 24.1 ± 1.5 MPa) and impressive elongation at break (ε_B = 564 ± 24%) (**C**, Figure 2.26).[90]

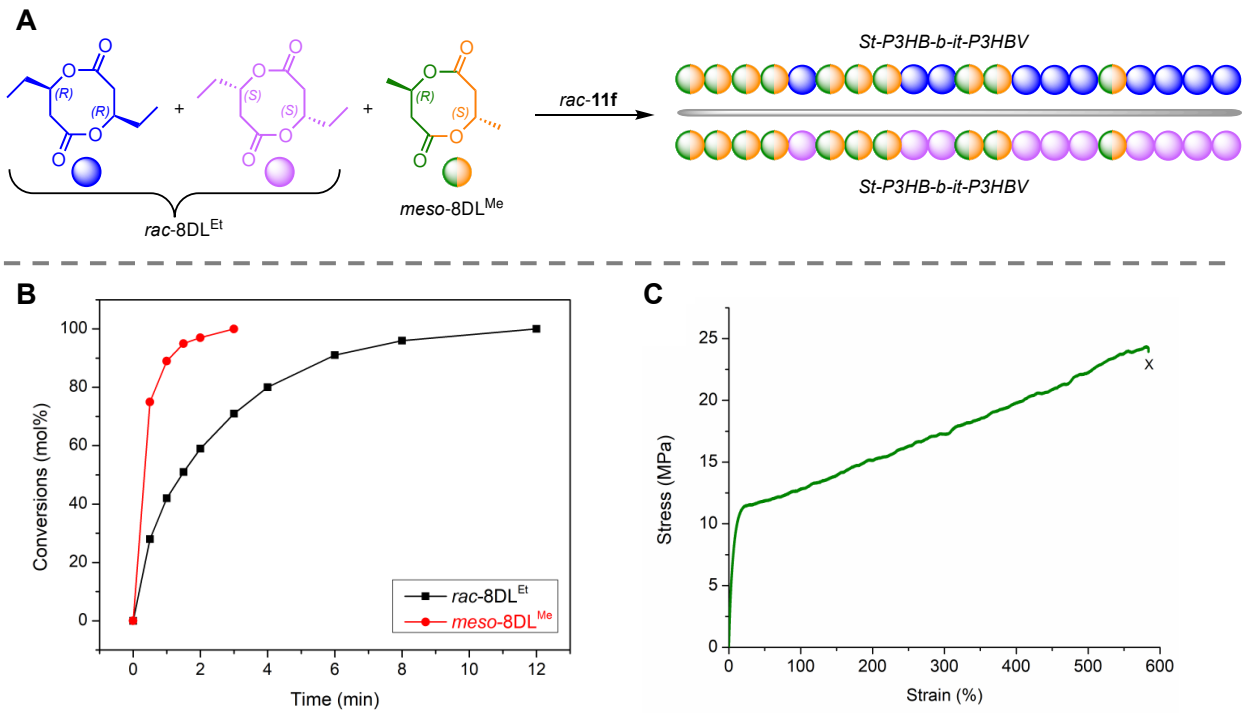

Figure 2.26. A. Stereoblock copolymerization of *rac*-8DL^{Et} and *meso*-8DL^{Me} to produce a gradient stereo-BCP, *st*-P3HB-*sb*-*it*-P3HV. **B**. Kinetic plot of simultaneous polymerization of *rac*-8DL^{Et} and *meso*-8DL^{Me}. **C**. Stress-strain curve of *st*-P3HB-*sb*-*it*-P3HV (M_n = 113 kDa, $Đ$ = 1.27, 18% 3HV incorporation). Reprinted (adapted) with permission from [90]. Copyright 2019 AAAS.

Direct polymerization of all six 8DL$^{Me/Et}$ diastereomers all together with a selective catalyst (*rac*-**11f**) yielded a stereogradient di-BCP consisting of the iso-rich P3HBV block and syndio-rich P3HBV block (Figure 2.27).[90] This sequencing was attributed to the established reactivity where *rac*-8DL^{Me} > *rac*-8DL^{Et}, *meso*-8DL^{Me} > *meso*-8DL^{Et}, and the catalyst's enantioselectivity toward the *rac* monomers and diastereoselectivity toward the *rac/meso* diastereomers. This stereogradient di-BCP is a semicrystalline material with a narrow $Đ$ value of 1.07. The scope was extended further to the synthesis of semicrystalline BCP *it*-P3HBHp-*sb*-*st*-P3HBHp, through copolymerization of a 1/1/1/1 diastereomeric mixture of *rac*/*meso*-8DL^{Bu} and *rac*/*meso*-8DL^{Me}. Overall, the unique catalyst-site-controlled diastereoselective methodology enables direct polymerization of diastereomeric mixtures of the same or different 8DL^{R} monomers (R = Me, Et, ^{n}Bu) into stereosequenced crystalline PHAs with tunable properties.

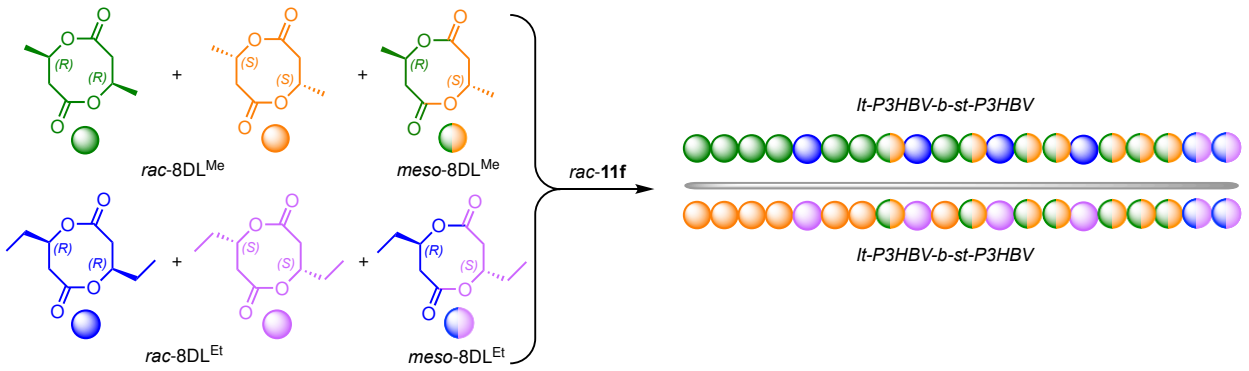

Figure 2.27. Stereoblock copolymerization of diastereomeric mixtures of *rac/meso*-8DL^{Me} and *rac/meso*-8DL^{Et} to stereogradient di-BCP PHA.

2.6.4. PHAs copolymers with other polyesters or polycarbonates

Copolymers of P3HB with other polymer segments or units through copolymerizations should substantially tailor the PHA properties by incorporating complementary comonomer units. Several examples of copolymerizing *rac*-*β*-BL with other lactones have been mentioned previously in this article.[56,84,95] One particularly interesting example is terpolymerization of mixed monomer feedstocks consisting of *rac*-*β*-BL, cyclohexene oxide (CHO), and CO_2 using (BDI^{CF3})Zn[N(SiMe$_3$)$_2$] (**29b**, Figure 2.15).[132] This Zn complex catalyzes the alternating copolymerization of CHO and CO_2 to make poly(cyclohexene carbonate) (PCHC), and the presence of CO_2 effectively turns off the ROP of *rac*-*β*-BL. This inhibition is attributed to CO_2 insertion into the Zn-O bond, leading to a carbonate chain end that is unable to ring-open an incoming *rac*-*β*-BL monomer. Thus, once CO_2 is released, the ROP of *rac*-*β*-BL begins again. Leveraging this on/off switch, tri-BCPs were synthesized by a one-pot method simply by increasing CO_2 pressure when *rac*-*β*-BL conversion reached 50% to produce P3HB-*b*-PCHC (**A**, Figure 2.28). The CO_2 pressure was then released so that *rac*-*β*-BL continued polymerizing to full conversion to give the tri-BCP, P3HB-*b*-PCHC-*b*-P3HB. Low CO_2 pressure resulted in similar rates of both CHO/CO_2 copolymerization and ROP of *rac*-*β*-BL, thus forming statistical copolymers (**A**, Figure 2.28).[132]

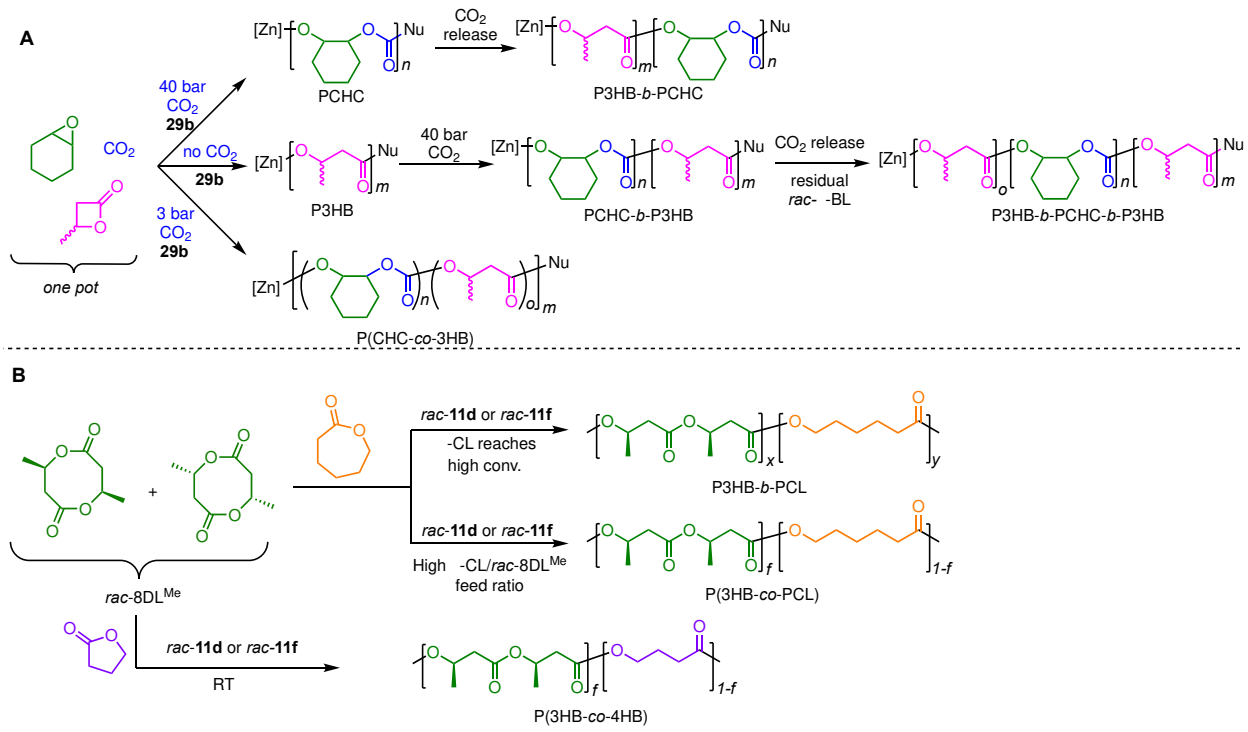

Figure 2.28. Copolymers with other polyesters or polycarbonates. **A**. One-pot terpolymerization of CHO (green), *rac*-*β*-BL (pink), and CO_2 (blue) at varying CO_2 pressures to produce random or block copolymers. **B**. Copolymerization of *rac*-8DL^{Me} with ε-CL (orange) to block or random copolymers and with γ-BL (purple) to a random copolymer.

Copolymerization of *rac*-8DL^{Me} with ε-caprolactone (*ε*-CL) and *γ*-butyrolactone (*γ*-BL) combines the desirable high crystallinity, high T_m, and low gas permeability of P3HB with the high ductility of poly(*ε*-caprolactone) (PCL) and poly(*γ*-butyrolactone) (P4HB), thus making tougher biodegradable materials. In this context, a one-pot copolymerization of *rac*-8DL^{Me} and *ε*-CL comonomer mixture resulted in a di-BCP P3HB-*b*-PCL, thanks to the substantially higher rate of polymerization of *rac*-8DL^{Me} than that of *ε*-CL (the estimated initial k_p,*rac*-8DL^{Me}/ k_p,*ε*-CL is 28.8) (**B**, Figure 2.28).[133] By simply changing the conditions and comonomer feed ratio (using the *ε*-CL/*rac*-8DL^{Me} feed ratio ≥ 5/1 and quenching the reaction before *rac*-8DL^{Me} reaches full conversion to prevent formation of the long PCL block), semicrystalline random copolymers, P(3HB-*co*-CL) and P(3HB-*co*-4HB), can also be formed (**B**, Figure 2.28). Mechanical testing of

the BCP P3HB-*b*-PCL showed a strong and tough material with σ_B of 20.5 MPa, E of 1.45 GPa, and ε_B of 106%.

2.7. Conclusions and Outlook

PHAs, thanks to their biodegradability in either managed or unmanaged environment and high structural tunability, are attracting ever increasing attention because they hold great potential to offer a practical solution to address the plastics pollution crisis and ever-growing needs for more sustainable materials that our society will rely on. However, the current high production costs and undesired performance properties of the PHAs produced by the biological routes largely limit their broader applications as commodity plastics. These challenges prompted the development of the chemocatalytic routes that can offer precision in synthesis—enabled by the living or controlled chain-growth ROP mechanism, greater tunability in polymer stereomicrostructures and the structures of monomers and molecular catalysts, as well as scalability and speed in polymer production. Advances to-date in the catalyzed chemical synthesis of PHAs have offered rapid access to highly *it*- and *st*-P3HB through the stereoselective ROP of β-BL and $8DL^{Me}$ enabled by the highly tunable chiral and achiral metal-based complexes that promote, often living or controlled, coordinative-insertion ROP. Rationally designed catalyst and monomer structures and insights obtained from mechanistic investigations have realized the precision synthesis of a wide range of PHAs, including PHA homopolymers of diverse stereomicrostructures as well as random, block and stereosequenced PHA copolymers that are often uniquely functionalized and uncommon or unnatural and inaccessible by biological methods. Some of the advanced, synthetic PHA materials offer thermal and mechanical properties that rival those of commodity polyolefins. Organic catalysts such as NHCs and superbases have offered new avenues towards the synthesis of *at*-PHAs that target sensitive applications in microelectronics and biomedical devices.

Despite tremendous advances made in the chemocatalytic routes to PHAs over the past five decades, four key challenges are yet to be addressed:

First, concerning the cyclic ester monomers used for the two major routes, *β*-BL is toxic (possibly carcinogenic to humans), while $8DL^{R}$ monomers are currently prepared from a four-step synthesis starting from succinic acid but require the use of an alkyl halide and an oxidant, calling for more cost-effective and environmentally benign monomer synthesis.

Second, the closed-loop chemical recycling of PHAs to their monomers is presently not realized. Base-catalyzed depolymerization of P3HB with catalysts such as $Mg(OH)_2$ afforded the dehydration product, *trans*-crotonic acid, in essentially quantitative yield (>97%),[134] but not the original lactone monomer (*β*-BL or $8DL^{Me}$), while the acid-catalyzed depolymerization of P3HB with catalysts such as *p*-toluenesulfonic acid led to the formation of cyclic oligomers, with the major product being the highly stable, cyclic trimer (~50% yield).[135] The ROP of this cyclic trimer reformed only oligomeric 3-hydroxybutyrate with low molecular weights (~5 kg/mol),[136] which cannot be considered a feasible route for closed-loop chemical recycling. Hence, there is a pressing need to develop an efficient, "monomer-polymer-monomer" closed-loop chemical recycling of PHAs, ultimately establishing the PHA-based circular materials economy.

Third, PHAs suffer from low thermostability towards melt-processing, particularly P3HB, with T_d values typically around 250 °C. This thermal property appears to be inherent to those unsubstituted PHAs at the 2 (or β)-position.

Fourth, the current synthetic PHAs are limited to offering properties of thermoplastics and elastomers. Endowing PHAs to deliver performance properties of other polymer classes, such as

thermoplastic elastomers, reprocessable thermosets, and adhesives, will further broaden utilities of PHA-based materials and thus represents an exciting direction.

By way of critical analysis, the development of a biocatalytic route to the monomers for the ROP of the chemocatalytic route to PHAs should provide a desirable solution to meet the above stated first challenge of the chemocatalytic route. On the other hand, the second, third, and fourth challenges face both biocatalytic and chemocatalytic routes. Meeting those challenges will require innovative designs of new monomer and catalyst structures, as well as the development of novel selective, catalytic processes. Therefore, ultimately, the above challenges should be solved more effectively by coupling biocatalytic and chemocatalytic routes—the use of this preferred, synergistic catalysis mode to address the plastics problems,[137] including the above described challenges still facing PHAs.

2.8. References

[1] Sudesh K, Abe H, Doi Y. Synthesis, structure and properties of polyhydroxyalkanoates: biological polyesters. Prog Polym Sci 2000;25:1503–55.

[2] Müller H -M, Seebach D. Poly(hydroxyalkanoates): A Fifth Class of Physiologically Important Organic Biopolymers? Angew Chem Int Ed 1993;32:477–502.

[3] Lenz RW, Marchessault RH. Bacterial Polyesters: Biosynthesis, Biodegradable Plastics and Biotechnology. Biomacromolecules 2005;6:1–8.

[4] Li Z, Yang J, Loh XJ. Polyhydroxyalkanoates: Opening doors for a sustainable future. NPG Asia Mater 2016;8:e265-20.

[5] Muhammadi, Shabina, Afzal M, Hameed S. Bacterial polyhydroxyalkanoates-eco-friendly next generation plastic: Production, biocompatibility, biodegradation, physical properties and applications. Green Chem Lett Rev 2015;8:56–77.

[6] Chen G-Q. A microbial polyhydroxyalkanoates (PHA) based bio- and materials industry. Chem Soc Rev 2009;38:2434–46.

[7] Taguchi S, Iwata T, Abe H, Doi Y. Poly(hydroxyalkanoate)s. Polym Sci A Compr Ref 10 Vol Set 2012;9:157–82.

[8] Narancic T, Verstichel S, Reddy Chaganti S, Morales-Gamez L, Kenny ST, De Wilde B, Padamati RB, O'Connor KE. Biodegradable Plastic Blends Create New Possibilities for End-of-Life Management of Plastics but They Are Not a Panacea for Plastic Pollution. Environ Sci Technol 2018;52:10441–52.

[9] Dilkes-Hoffman LS, Lant PA, Laycock B, Pratt S. The rate of biodegradation of PHA

bioplastics in the marine environment: A meta-study. Mar Pollut Bull 2019;142:15–24.

[10] Meereboer KW, Misra M, Mohanty AK. Review of recent advances in the biodegradability of polyhydroxyalkanoate (PHA) bioplastics and their composites. Green Chem 2020;22:5519–58.

[11] Suzuki M, Tachibana Y, Kasuya K. Biodegradability of poly(3-hydroxyalkanoate) and poly(ε-caprolactone) via biological carbon cycles in marine environments. Polym J 2021;53:47–66.

[12] Laycock B, Halley P, Pratt S, Werker A, Lant P. The chemomechanical properties of microbial polyhydroxyalkanoates. Prog Polym Sci 2013;38:536–83.

[13] Sangroniz A, Zhu J-B, Tang X, Etxeberria A, Chen EY-X, Sardon H. Packaging materials with desired mechanical and barrier properties and full chemical recyclability. Nat Commun 2019;10:3559.

[14] Li M, Wilkins MR. Recent advances in polyhydroxyalkanoate production: Feedstocks, strains and process developments. Int J Biol Macromol 2020;156:691–703.

[15] Amadu AA, Qiu S, Ge S, Addico GND, Ameka GK, Yu Z, Xia W, Abbew A-W, Shao D, Champagne P, Wang S. A review of biopolymer (Poly-β-hydroxybutyrate) synthesis in microbes cultivated on wastewater. Sci Total Environ 2021;756:143729.

[16] Chen G-Q, Patel MK. Plastics derived from biological sources: Present and future: A technical and environmental review. Chem Rev 2012;112:2082–99.

[17] Madison LL, Huisman GW. Metabolic Engineering of Poly(3-Hydroxyalkanoates): From DNA to Plastic. Microbiol Mol Biol Rev 1999;63:21–53.

[18] Tan D, Wang Y, Tong Y, Chen G-Q. Grand Challenges for Industrializing Polyhydroxyalkanoates (PHAs). Trends Biotechnol 2021;39:953–63.

[19] Zia KM, Noreen A, Zuber M, Tabasum S, Mujahid M. Recent developments and future prospects on bio-based polyesters derived from renewable resources: A review. Int J Biol Macromol 2016;82:1028–40.

[20] Anjum A, Zuber M, Zia KM, Noreen A, Anjum MN, Tabasum S. Microbial production of polyhydroxyalkanoates (PHAs) and its copolymers: A review of recent advancements. Int J Biol Macromol 2016;89:161–74.

[21] Suriyamongkol P, Weselake R, Narine S, Moloney M, Shah S. Biotechnological approaches for the production of polyhydroxyalkanoates in microorganisms and plants - A review. Biotechnol Adv 2007;25:148–75.

[22] Wang Y, Yin J, Chen G-Q. Polyhydroxyalkanoates, challenges and opportunities. Curr Opin Biotechnol 2014;30:59–65.

[23] Kumar G, Ponnusamy VK, Bhosale RR, Shobana S, Yoon J-J, Bhatia SK, Banu JR, Kim S-H. A review on the conversion of volatile fatty acids to polyhydroxyalkanoates using dark fermentative effluents from hydrogen production. Bioresour Technol 2019;287:121427.

[24] Adeleye AT, Odoh CK, Enudi OC, Banjoko OO, Osiboye OO, Odediran ET, Louis H. Sustainable synthesis and applications of polyhydroxyalkanoates (PHAs) from biomass. Process Biochem 2020;96:174–93.

[25] Tan D, Yin J, Chen G-Q. Production of Polyhydroxyalkanoates. In: Pandey A, Negi S,

Soccol CR, editors. Current Developments in Biotechnology and Bioengineering Elsevier 2017. p. 655-692

[26] Chee J, Yoga S-S, Lau N-S, Ling S-C, Abed RMM, Sudesh K. Bacterially Produced Polyhydroxyalkanoate (PHA): Converting Renewable Resources into Bioplastics. Curr. Res. Technol. Educ. Top. Appl. Microbiol. Microb. Biotechnol., 2010, p. 1395–404.

[27] Bedade DK, Edson CB, Gross RA. Emergent approaches to efficient and sustainable polyhydroxyalkanoate production. Molecules 2021;26:3463..

[28] Steinbüchel A. Perspectives for Biotechnological Production and Utilization of Biopolymers: Metabolic Engineering of Polyhydroxyalkanoate Biosynthesis Pathways as a Successful Example. Macromol Biosci 2001;1:1–24.

[29] Pederson EN, McChalicher CWJ, Srienc F. Bacterial synthesis of PHA block copolymers. Biomacromolecules 2006;7:1904–11.

[30] Li S, Cai L, Wu L, Zeng G, Chen J, Wu Q, Chen G-Q. Microbial synthesis of functional homo-, random, and block polyhydroxyalkanoates by β-oxidation deleted Pseudomonas entomophila. Biomacromolecules 2014;15:2310–9.

[31] Ovitt TM, Coates GW. Stereoselective Ring-Opening Polymerization of meso-Lactide: Synthesis of Syndiotactic Poly(lactic acid). J Am Chem Soc 1999;121:4072–3.

[32] Coates GW, Waymouth RM. Oscillating Sterocontrol: A Strategy for the Synthesis of Thermoplastic Elastomeric Polypropylene. Science 1995;267:217–9.

[33] Natta G. Properties of Isotactic, Atactic, and Stereoblock Homopolymers, Random and Block copolymers of α-Olefins. J Polym Sci 1959;34:531–49.

[34] Farina M. The Stereochemistry of Linear Macromolecules. In: Eliel EL, Wilen SH, editors. Topics in Stereochemistry. John Wiley & Sons, Inc. 1987. p. 1-111.

[35] Hoskins JN, Grayson SM. Cyclic polyesters: Synthetic approaches and potential applications. Polym Chem 2011;2:289–99.

[36] Steinbüchel A, Valentin HE. Diversity of bacterial polyhydroxyalkanoic acids. FEMS Microbiol Lett 1995;128:219–28.

[37] Seebach D, Bürger HM, Müller H-M, Lengweiler UD, Beck AK. 104 . Synthesis of Linear Oligomers of (R) -3-Hydroxybutyrate and Solid-State Structural Investigations by Electron Microscopy and X-Ray Scattering. Helv Chim Acta 1994;77:1099–123.

[38] Kobayashi T, Hori Y, Kakimoto M, Imai Y. Synthesis of biodegradable polyesters by polycondensation of methyl (R)-3-hydroxybutyrate and methyl (R)-3-hydroxy- valerate. Makromol Chem, Rapid Commun 1993;14:785–90.

[39] Lengweiler von UD, Fritz MG, Seebach D. 61 . Synthese monodisperser hearer und cyclischer Oligomere der (R)-3-Hydroxybuttersaure mit bis zu 128 Einheiten. Helv Chim Acta 1996;79:670–701.

[40] Carpentier J-F. Discrete Metal Catalysts for Stereoselective Ring-Opening Polymerization of Chiral Racemic β-Lactones. Macromol Rapid Commun 2010;31:1696–705.

[41] Li H, Shakaroun RM, Guillaume SM, Carpentier J-F. Recent Advances in Metal-Mediated Stereoselective Ring-Opening Polymerization of Functional Cyclic Esters towards Well-Defined Poly(hydroxy acid)s: From Stereoselectivity to Sequence-Control. Chem Eur J 2020;26:128–38.

[42] Carpentier J-F. Rare-Earth Complexes Supported by Tripodal Tetradentate Bis(phenolate) Ligands: A Privileged Class of Catalysts for Ring- Opening Polymerization of Cyclic Esters. Organometallics 2015;34:4175–89.

[43] Jerome C, Lecomte P. Recent Developments in Ring-Opening Polymerization of Lactones. In: Rieger B, Kunkel A, Coates GW, Reichardt R, Dinjus E, Zevaco TA, editors. Advances in Polymer Science, vol. 245. 2012, p. 173–217.

[44] Tang X, Chen EY-X. Toward Infinitely Recyclable Plastics Derived from Renewable Cyclic Esters. Chem 2019;5:284–312.

[45] Thomas CM. Stereocontrolled ring-opening polymerization of cyclic esters: Synthesis of new polyester microstructures. Chem Soc Rev 2010;39:165–73.

[46] Okada M. Chemical syntheses of biodegradable polymers. Prog Polym Sci 2002;27:87–133.

[47] Inoue S, Tomoi Y, Tsuruta T, Furukawa J. Organometallic-Catalyzed Polymerization of Propiolactone. Makromol Chemie 1961;48:229–33.

[48] Zhang Y, Gross RA, Lenz RW. Stereochemistry of the Ring-opening polymerization of (S)-β-butyrolactone. Macromolecules 1990;23:3206–12.

[49] Jedlinski Z, Kowalczuk M, Kurcok P, Matuszowicz A, Sikorska W, Gross RA, Xu J, Lenz RW. Stereochemical Control in the Anionic Polymerization of β-Butyrolactone Initiated with Alkali-Metal Alkoxides. Macromolecules 1996;29:3773–7.

[50] Shelton JR, Agostini DE, Lando JB. Synthesis and Characterization of poly-β-hydroxybutyrate. II. Synthesis of d-poly-β-hydroxybutyrate and the mechanism of ring-

opening polymerization of β-butyrolactone. J Polym Sci Part A 1971;9:2789–99.

[51] Jedlinski Z, Kurcok P, Lenz RW. First Facile Synthesis of Biomimetic Poly-(R)-3-hydroxybutyrate via regioselective anionic polymerixation of (S)-β-butyrolactone. Macromolecules 1998;31:6718–20.

[52] Agostini DE, Lando JB, Shelton JR. Synthesis and Characterization of Poly-β-Hydroxybutyrate. I. Synthesis of Crystalline DL-Poly-β-hydroxybutyrate from DL-β-Butyrolactone. J Polym Sci Part A 1971;9:2775–87.

[53] Tanahashi N, Doi Y. Thermal Properties and Stereoregularity of Poly(3-hydroxybutyrate) Prepared from Optically Active β-Butyrolactone with a Zinc-Based Catalyst. Macromolecules 1991;24:5732–3.

[54] Kemnitzer JE, Mccarthy SP, Gross RA. Poly (β-hydroxybutyrate) Stereoisomers : A Model Study of the Effects of Stereochemical and Morphological Variables on Polymer Biological Degradability. Macromolecules 1992;25:5927–34.

[55] Hori Y, Suzuki M, Yamaguchi A, Nishishita T. Ring-Opening Polymerization of Optically Active β-Butyrolactone Using Distannoxane Catalysts: Synthesis of High Molecular Weight Poly(3-hydroxybutryate). Macromolecules 1993;26:5533–4.

[56] Hori Y, Takahashi Y, Yamaguchi A, Nishishita T. Ring-opening copolymerization of optically active β-butryolactone with several lactones catalyzed by distannoxane complexes: synthesis of new biodegradable polyesters. Macromolecules 1993;26:4388–90.

[57] Tani H, Yamashita S, Teranishi K. Stereospecific Polymerization of β-Methyl-β-

propiolactone. Polym J 1972;3:417–8.

[58] Teranishi K, Iida M, Araki T, Yamashita S, Tani H. Stereospecific Polymerization of β-alkyl-β-propiolactone. Macromolecules 1974;7:421–7.

[59] Iida M, Araki T, Teranishi K, Tani H. Effect of Substituents on Stereospecific Polymerization of β-alkyl- and β-chloroalkyl-β-propiolactones. Macromolecules 1977;10:275–84.

[60] Bloembergen S, Holden DA, Bluhm TL, Hamer GK, Marchessault RH. Stereoregularity in Synthetic β-Hydroxybutyrate and β-hydroxyvalerate homopolyesters. Macromolecules 1989;22:1656–63.

[61] Yasuda T, Aida T, Inoue S. Living polymerization of β-butyrolactone catalysed by tetraphenylporphinatoaluminum chloride. Die Makromol Chemie, Rapid Commun 1982;3:585–8.

[62] Asano S, Aida T, Inoue S. Polymerization of Epoxide and β-lactone catalyzed by aluminum porphyrin. Exchange of alkoxide or carboxylate group as growing species on aluminum porphyrin. Macromolecules 1985;18:2057–61.

[63] Chen EY-X, Marks TJ. Cocatalysts for metal-catalyzed olefin polymerization: Activators, activation processes, and structure-activity relationships. Chem Rev 2000;100:1391–434.

[64] Wu B, Lenz RW. Stereoregular Polymerization of [R,S]-3-Butyrolactone Catalyzed by Alumoxane--Monomer Adducts. Macromolecules 1998;31:3473–7.

[65] Le Borgne A, Spassky N. Stereoelective polymerization of β-butyrolactone. Polymer (Guildf) 1989;30:2312–9.

[66] Zintl M, Molnar F, Urban T, Bernhart V, Preishuber-Pflügl P, Rieger B. Variably isotactic poly(hydroxybutyrate) from racemic β-butyrolactone: Microstructure control by achiral chromium(III) salophen complexes. Angew Chem Int Ed 2008;47:3458–60.

[67] Reichardt R, Vagin S, Reithmeier R, Ott AK, Rieger B. Factors Influencing the Ring-Opening Polymerization of Racemic β -Butyrolactone Using Cr III(salphen). Macromolecules 2010;43:9311–7.

[68] Vagin S, Winnacker M, Kronast A, Altenbuchner PT, Deglmann P, Sinkel C, Loos R, Rieger B. New Insights into the Ring-Opening Polymerization of β-Butyrolactone Catalyzed by Chromium(III) Salphen Complexes. ChemCatChem 2015;7:3963–71.

[69] Ajellal N, Durieux G, Delevoye L, Tricot G, Dujardin C, Thomas CM, Gauvin RM. Polymerization of racemic β-butyrolactone using supported catalysts: A simple access to isotactic polymers. Chem Commun 2010;46:1032–4.

[70] Tang X, Chen EY-X. Chemical synthesis of perfectly isotactic and high melting bacterial poly(3-hydroxybutyrate) from bio-sourced racemic cyclic diolide. Nat Commun 2018;9:2345.

[71] Hong M, Tang X, Newell BS, Chen EY-X. "Nonstrained" γ-Butyrolactone-Based Copolyesters: Copolymerization Characteristics and Composition-Dependent (Thermal, Eutectic, Cocrystallization, and Degradation) Properties. Macromolecules 2017;50:8469–79.

[72] Tang X, Hong M, Falivene L, Caporaso L, Cavallo L, Chen EY-X. The Quest for Converting Biorenewable Bifunctional α-Methylene-γ-butyrolactone into Degradable and Recyclable Polyester: Controlling Vinyl-Addition/Ring-Opening/Cross-Linking

Pathways. J Am Chem Soc 2016;138:14326–37.

[73] Bouyahyi M, Ajellal N, Kirillov E, Thomas CM, Carpentier J-F. Exploring electronic versus steric effects in stereoselective ring-opening polymerization of lactide and β-butyrolactone with amino-alkoxy-bis(phenolate)-yttrium complexes. Chem A Eur J 2011;17:1872–83.

[74] Amgoune A, Thomas CM, Ilinca S, Roisnel T, Carpentier J-F. Highly active, productive, and syndiospecific yttrium initiators for the polymerization of racemic β-butyrolactone. Angew Chem Int Ed 2006;45:2782–4.

[75] Ajellal N, Bouyahyi M, Amgoune A, Thomas CM, Bondon A, Pillin I, Grohens Y, Carpentier J-F. Syndiotactic-enriched poly(3-hydroxybutyrate)s via stereoselective ring-opening polymerization of racemic β-butyrolactone with discrete yttrium catalysts. Macromolecules 2009;42:987–93.

[76] Kricheldorf HR, Berl M, Scharnagl N. Poly(lactones). 9. Polymerization Mechanism of Metal Alkoxide Initiated Polymerizations of Lactide and Various Lactones. Macromolecules 1988;21:286–93.

[77] Kricheldorf HR, Sumbél M V, Kreiser-Saunders I. Polylactones. 20. Polymerization of ε-Caprolactone with Tributyltin Derivatives : A Mechanistic Study. Macromolecules 1991;24:1944–9.

[78] Kemnitzer JE, Mccarthy SP, Gross RA. Preparation of Predominantly Syndiotactic Poly (β-hydroxybutyrate) by the Tributyltin Methoxide Catalyzed Ring-Opening Polymerization of racemic β-butyrolactone. Macromolecules 1993;26:1221–9.

[79] Kricheldorf HR, Lee S, Scharnagl N. Polylactones. 28. Syndiotactic Poly(β-D,L-butyrolactone) by Ring-Opening Polymerization of β-D,L-Butyrolactone with Butyltin Methoxides. Macromolecules 1994;27:3139–46.

[80] Kemnitzer JE, Mccarthy SP, Gross RA. Syndiospecific Ring-Opening Polymerization of β-Butryolactone to form predominantly syndiotactic Poly(β-hydroxybutryate) using Tin(IV) catalysts. Mactromolecules 1993;26:6143–50.

[81] Kricheldorf HR, Lee S. Polylactones. 35. Macrocyclic and stereoselective Polymerization of β-D,L-Butyrolactone with Cyclic Dibutyltin Initiators. Macromolecules 1995;28:6718–25.

[82] Kricheldorf HR, Eggerstedt S. Polymerizations of β-D,L-Butyrolactone with Dialkyltinoxides as Initiators. Macromolecules 1997;30:5693–7.

[83] Hori Y, Hagiwara T. Ring-opening polymerisation of β-butyrolactone catalysed by distannoxane complexes: study of the mechanism. Int J Biol Macromol 1999;25:237–45.

[84] Le Borgne A, Pluta C, Spassky N. Highly reactive yttrium alkoxide as new initiator for the polymerization of β-butyrolactone. Macromol Rapid Commun 1994;15:955–60.

[85] Cai C-X, Toupet L, Lehmann CW, Carpentier J-F. Synthesis, structure and reactivity of new yttrium bis(dimethylsilyl)amido and bis(trimethylsilyl)methyl complexes of a tetradentate bis(phenoxide) ligand. J Organomet Chem 2003;683:131–6.

[86] Nie K, Fang L, Yao Y, Zhang Y, Shen Q, Wang Y. Synthesis and Characterization of Amine-Bridged Bis(phenolate)lanthanide Alkoxides and Their Application in the Controlled Polymerization of rac-Lactide and rac -β -Butyrolactone. Inorg Chem

2012;51:11133–43.

[87] Nie K, Feng T, Song F, Zhang Y, Sun H, Yuan D, Yao Y, Shen Q. Bimetallic amine-bridged bis (phenolate) lanthanide aryloxides and alkoxides : synthesis, characterization, and application in the ring-opening polymerization of rac-lactide and rac -β-butyrolactone. Sci China Chem 2014;57:1106–16.

[88] Ajellal N, Lyubov DM, Sinenkov MA, Fukin GK, Cherkasov A V, Thomas CM, Carpentier J-F, Trifonov AA. Bis(guanidinate) Alkoxide Complexes of Lanthanides: Synthesis, Structures and Use in Immortal and Stereoselective Ring-Opening Polymerization of. Chem Eur J 2008;14:5440–8.

[89] Zeng T, Qian Q, Zhao B, Yuan D, Yao Y, Shen Q. Synthesis and characterization of rare-earth metal guanidinates stabilized by amine-bridged bis(phenolate) ligands and their application in the controlled polymerization of rac-lactide and rac-β-butyrolactone. RSC Adv 2015;5:53161–71.

[90] Tang X, Westlie AH, Watson EM, Chen EY-X. Stereosequenced crystalline polyhydroxyalkanoates from diastereomeric monomer mixtures. Science 2019;366:754–8.

[91] Kamber NE, Jeong W, Waymouth RM, Pratt RC, Lohmeijer BGG, Hedrick JL. Organocatalytic ring-opening polymerization. Chem Rev 2007;107:5813–40.

[92] Kiesewetter MK, Shin EJ, Hedrick JL, Waymouth RM. Organocatalysis: Opportunities and challenges for polymer synthesis. Macromolecules 2010;43:2093–107.

[93] Connor EF, Nyce GW, Myers M, Mock A, Hedrick JL. First Example of N-Heterocyclic Carbenes as Catalysts for Living Polymerization: Organocatalytic Ring-Opening

Polymerization of Cyclic Esters. J Am Chem Soc 2002;124:914–5.

[94] Coulembier O, Lohmeijer BGG, Dove AP, Pratt RC, Mespouille L, Culkin DA, Benight SJ, Dubois P, Waymouth RM, Hedrick JL. Alcohol Adducts of N-Heterocyclic Carbenes: Latent Catalysts for the Thermally-Controlled Living Polymerization of Cyclic Esters. Macromolecules 2006;39:5617–28.

[95] Coulembier O, Delva X, Hedrick JL, Waymouth RM, Dubois P. Synthesis of Biomimetic Poly(hydroxybutyrate): Alkoxy- and Carboxytriazolines as Latent Ionic Initiator. Macromolecules 2007;40:8560–7.

[96] Lohmeijer BGG, Pratt RC, Leibfarth F, Logan JW, Long DA, Dove AP, Nederberg F, Choi J, Wade C, Waymouth RM, Hedrick JL. Guanidine and Amidine Organocatalysts for Ring-Opening Polymerization of Cyclic Esters. Macromolecules 2006;39:8574–83.

[97] Jaffredo CG, Carpentier J-F, Guillaume SM. Controlled ROP of β-Butyrolactone Simply Mediated by Amidine, Guanidine, and Phosphazene Organocatalysts. Macromol Rapid Commun 2012;33:1938–44.

[98] Moins S, Henoumont C, Winter JD, Khalil A, Laurent S, Cammas-Marion S, Coulembier O. Reinvestigation of the mechanism of polymerization of β-butyrolactone from 1,5,7-triazabicyclo[4.4.0]dec-5-ene. Polym Chem 2018;9:1840–7.

[99] Shakaroun RM, Jehan P, Alaaeddine A, Carpentier J-F, Guillaume SM. Organocatalyzed ring-opening polymerization (ROP) of functional β-lactones: new insights into the ROP mechanism and poly(hydroxyalkanoate)s (PHAs) macromolecular structure. Polym Chem 2020;11:2640.

[100] Lee JT, Thomas PJ, Alper H. Synthesis of β-Lactones by the Regioselective, Cobalt and Lewis Acid Catalyzed Carbonylation of Simple and Functionalized Epoxides. J Org Chem 2001;66:5424–6.

[101] Getzler YDYL, Mahadevan V, Lobkovsky EB, Coates GW. Synthesis of β-Lactones: A Highly Active and Selective Catalyst for Epoxide Carbonylation. J Am Chem Soc 2002;124:1174–5.

[102] Allmendinger M, Eberhardt R, Luinstra G, Rieger B. The Cobalt-Catalyzed Alternating Copolymerization of Epoxides and Carbon Monoxide: A Novel Approach to Polyesters. J Am Chem Scoiety 2002;124:5646–7.

[103] Allmendinger M, Eberhardt R, Luinstra GA, Rieger B. Alternating Copolymerization Reaction of Propylene Oxide and CO: Variation of Polymer Stereoregularity and Investigation into Chain Termination. Macromol Chem Phys 2003;204:564–9.

[104] Lee JT, Alper H. Alternating Copolymerization of Propylene Oxide and Carbon Monoxide to form Aliphatic Polyesters. Macromolecules 2004;2:2417–21.

[105] Dunn EW, Coates GW. Carbonylative Polymerization of Propylene Oxide: A Multicatalytic Approach to the Synthesis of Poly(3-Hydroxybutyrate). J Am Chem Soc 2010;132:11412–3.

[106] Rieth LR, Moore DR, Lobkovsky EB, Coates GW. Single-Site β-Diiminate Zinc Catalysts for the Ring-Opening Polymerization of β-Butyrolactone and β-Valerolactone to Poly(3-hydroxyalkanoates). J Am Chem Scoiety 2002;124:15239–48.

[107] Ebrahimi T, Aluthge DC, Hatzikiriakos SG, Mehrkhodavandi P. Highly Active Chiral

Zinc Catalysts for Immortal Polymerization of β-Butyrolactone Form Melt Processable Syndio-Rich Poly(hydroxybutyrate). Macromolecules 2016;49:8812–24.

[108] Inoue S. Immortal Polymerization: The Outset, Development, and Application. J Polym Sci Part A Polym Chem 2000;38:2861–71.

[109] Poirier V, Roisnel T, Carpentier J-F, Sarazin Y. Versatile catalytic systems based on complexes of zinc , magnesium and calcium supported by a bulky bis(morpholinomethyl)phenoxy ligand for the large-scale immortal ring-opening polymerisation of cyclic esters. Dalt Trans 2009:9820–7.

[110] Grunova E, Roisnel T, Carpentier J-F. Zinc complexes of fluorous alkoxide-imino ligands: Synthesis, structure, and use in ring-opening polymerization of lactide and β-butyrolactone. Dalt Trans 2009:9010–9.

[111] Luciano E, Buonerba A, Grassi A, Milione S, Capacchione C. Thioetherphenolate Group 4 Metal Complexes in the Ring Opening Polymerization of rac-β-Butyrolactone. J Polym Sci Part A Polym Chem 2016;54:3132–9.

[112] Mahrova T V, Fukin GK, Cherkasov A V, Trifonov AA, Ajellal N, Carpentier J-F. Yttrium Complexes Supported by Linked Bis(amide) Ligand: Synthesis, Structure, and Catalytic Activity in the Ring-Opening Polymerization of Cyclic Esters. Inorg Chem 2009;48:4258–66.

[113] Kramer JW, Coates GW. Fluorinated β-Lactones and Poly(β-hydroxyalkanoate)s: Synthesis via Epoxide Carbonylation and Ring-Opening Polymerization. Tetrahedron 2008;64:6973–8.

[114] Yang J-C, Yang J, Li W-B, Lu X-B, Liu Y. Carbonylative Polymerization of Epoxides Mediated by Tri-metallic Complexes: A Dual Catalysis Strategy for Synthesis of Biodegradable Polyhydroxyalkanoates. Angew Chem Int Ed 2022;61:e202116208.

[115] Wang H, Li X, Chen G-Q. Production and characterization of homopolymer polyhydroxyheptanoate (P3HHp) by a fadBA knockout mutant Pseudomonas putida KTOY06 derived from P. putida KT2442. Process Biochem 2009;44:106–11.

[116] Tang X, Westlie AH, Caporaso L, Cavallo L, Falivene L, Chen EY-X. Biodegradable Polyhydroxyalkanoates by Stereoselective Copolymerization of Racemic Diolides: Stereocontrol and Polyolefin- Like Properties Research Articles. Angew Chem Int Ed 2020;59:2–12.

[117] Westlie AH, Chen EY-X. Catalyzed Chemical Synthesis of Unnatural Aromatic Polyhydroxyalkanoate and Aromatic − Aliphatic PHAs with Record- High Glass-Transition and Decomposition Temperatures. Macromolecules 2020;53:9906–15.

[118] Li Y-T, Yu HY, Li W-B, Liu Y, Lu X-B. Recyclable Polyhydroxyalkanoates via a Regioselective Ring-Opening Polymerization of α,β-Disubstituted β-Lactone Monomers. Macromolecules 2021;54:4641–8.

[119] Guillaume C, Ajellal N, Carpentier J-F, Guillaume SM. Boron-Functionalized Poly(3-hydroxybutyrate)s from Hydroboration of Poly(allyl-β-hydroxyalkanoate)s: Synthesis and Insights into the Microstructure. J Polym Sci Part A Polym Chem 2010;49:907–17.

[120] Jaffredo CG, Carpentier J-F, Guillaume SM. Organocatalyzed controlled ROP of β-lactones towards benzyl β-malolactone polymers. Polym Chem 2013;4:3837–50.

[121] Jaffredo CG, Carpentier J-F, Guillaume SM. Poly(hydroxyalkanoate) Block or Random Copolymers of β-Butyrolactone and Benzyl β-Malolactone: A Matter of Catalytic Tuning. Macromolecules 2013;46:6765–76.

[122] Barouti G, Jarnouen K, Cammas-Marion S, Loyer P, Guillaume SM. Polyhydroxyalkanoate-based amphiphilic diblock copolymers as original biocompatible nanovectors. Polym Chem 2015;6:5414–29.

[123] Barouti G, Khalil A, Orione C, Jarnouen K, Cammas-Marion S, Loyer P, Guillaume SM. Poly(trimethylene carbonate)/Poly(malic acid) Amphiphilic Diblock Copolymers as Biocompatible Nanoparticles. Chem Eur J 2016;22:2819–30.

[124] Jaffredo CG, Chapurina Y, Kirillov E, Carpentier J-F, Guillaume SM. Highly Stereocontrolled Ring-Opening Polymerization of Racemic Alkyl β-Malolactonates Mediated by Yttrium [Amino-alkoxy-bis(phenolate)] Complexes. Chem Eur J 2016;22:7629–41.

[125] Coulembier O, Mespouille L, Hedrick JL, Waymouth RM, Dubois P. Metal-Free Catalyzed Ring-Opening Polymerization of β-Lactones: Synthesis of Amphiphilic Triblock Copolymers Based on Poly(dimethylmalic acid). Macromolecules 2006;39:4001–8.

[126] Ligny R, Hänninen MM, Guillaume SM, Carpentier J-F. Highly Syndiotactic or Isotactic Polyhydroxyalkanoates by Polymerization of Functional Racemic β-Lactones. Angew Chem Int Ed 2017;56:10388–93.

[127] Ligny R, Hänninen MM, Guillaume SM, Carpentier J-F. Steric vs. electronic stereocontrol in syndio- or iso-selective ROP of functional chiral β-lactones mediated by achiral

yttrium-bisphenolate complexes. Chem Commun 2018;54:8024–31.

[128] Ligny R, Hänninen MM, Guillaume SM, Carpentier J-F. Highly Syndiotactic or Isotactic Polyhydroxyalkanoates by Ligand-Controlled Yttrium-Catalyzed Stereoselective Ring-Opening Polymerization of Functional Racemic β-Lactones. Angew Chem Int Ed 2017;56:10388–93.

[129] Zhuo Z, Zhang C, Luo Y, Wang Y, Yao Y, Yuan D, Cui D. Stereo-selectivity switchable ROP of rac-β-butyrolactone initiated by salan-ligated rare-earth metal amide complexes: the key role of the substituents on ligand frameworks. Chem Commun 2018;54:11998–2001.

[130] Kramer JW, Treitler DS, Dunn EW, Castro PM, Roisnel T, Thomas CM, Coates GW. Polymerization of Enantiopure Monomers Using Syndiospecific Catalysts : A New Approach To Sequence Control in Polymer Synthesis. J Am Chem Soc 2009;131:16042–4.

[131] Ligny R, Guillaume SM, Carpentier J-F. Yttrium-Mediated Ring-Opening Copolymerization of Oppositely Configurated 4-Alkoxymethylene-β-Propiolactones: Effective Access to Highly Alternated Isotactic Functional PHAs. Chem Eur J 2019;25:6412–24.

[132] Kernbichl S, Reiter M, Adams F, Vagin S, Rieger B. CO2-Controlled One-Pot Synthesis of AB, ABA Block, and Statistical Terpolymers from β-Butyrolactone, Epoxides, and CO2. J Am Chem Scoiety 2017;139:6787–90.

[133] Tang X, Shi C, Zhang Z, Chen EY-X. Toughening Biodegradable Isotactic Poly(3-hydroxybutyrate) via Stereoselective Copolymerization of a Diolide and Lactones.

Macromolecules 2021;54:9401–9.

[134] Ariffin H, Nishida H, Shirai Y, Hassan MA. Highly selective transformation of poly[(R)-3-hydroxybutyric acid] into trans-crotonic acid by catalytic thermal degradation. Polym Degrad Stab 2010;95:1375–81.

[135] Seebach D, Müller H, Bürger HM, Plattner DA. The Triolide of (R)-3-Hydroxybutyric Acid. Direct Preparation from Polyhydroxybutyrate and Formation of a Crown Estercarbonyl Complex with Na Ions. Angew Chem Int Ed 1992;31:434–5.

[136] Zhang D, Hillmyer MA, Tolman WB. A New Synthetic Route to Poly[3-hydroxypropionic acid] (P[3-HP]): Ring-Opening Polymerization of 3-HP Macrocyclic Esters. Macromolecules 2004;37:8198–200.

[137] Ellis LD, Rorrer NA, Sullivan KP, Otto M, McGeehan JE, Román-Leshkov Y, Wierckx N, Beckham GT. Chemical and biological catalysis for plastics recycling and upcycling. Nat Catal 2021;4:539–56.

Chapter 3

Biodegradable Polyhydroxyalkanoates by Stereoselective Copolymerization of Racemic Diolides: Stereocontrol and Polyolefin-like Properties.

3.1. Synopsis

Bacterial polyhydroxyalkanoates (PHAs) are a unique class of biodegradable polymers due to their biodegradability in ambient environments and structural diversity enabled by side-chain groups. However, the biosynthesis of PHAs is slow and expensive, limiting their broader applications as commodity plastics. To overcome such limitation, the catalyzed chemical synthesis of bacterial PHAs has been developed via the metal-catalyzed stereoselective ring-opening (co)polymerization of racemic cyclic diolides (*rac*-8DL^{R}, R = alkyl group). Herein, we report the homopolymers and random copolymers of uncommon composition, copolymerization characteristics, and examination of the resulting PHAs' properties. Most notably, stereoselective copolymerizations of *rac*-8DL^{Me} with *rac*-8DL^{R} (R = Et, Bu) have yielded high-molecular-weight, crystalline isotactic PHA copolymers that are hard, ductile, and tough plastics, and exhibit polyolefin-like thermal and mechanical properties.

3.2. Introduction

Petroleum-derived plastics that have fueled modern economies are the most widely used man-made substances in modern life. Owing to their lightweight, low cost, long-lasting, and high-performance properties, plastics have now become indispensable to daily life and the global economy. However, when disposed or leaked into the environment, their durability and resistance to degradation in ambient environments result in severe plastics pollution to landfills and oceans as well as other environmental consequences.[1] Thus, the development of future polymers including plastics should focus on biorenewable materials that are sustainable in both production

and use and can be recycled or disposed of in ways that are environmentally innocuous.[2] In this context, polyhydroxyalkanoates (PHAs),[3] a unique class of biorenewable aliphatic polyesters that are biodegradable in ambient environments,[4] have shown great potential as a replacement for petroleum-based plastics. Natural PHAs, produced by bacteria and other living microorganisms from biorenewable resources, are purely isotactic polymers containing a chiral site in each repeat unit, and their thermal and mechanical properties span a wide range depending on the length of the pendant group on the β-carbon, making them attractive for a wide range of applications.[3b-d] Among them, bacterial poly[(*R*)-3-hydroxybutyrate], P[(*R*)-3HB], with the methyl group as the side chain, is highly crystalline with a melting temperature (T_m) of 170 ~ 180°C, showing comparable thermal and mechanical properties (especially tensile strength) to isotactic polypropylene (*it*-PP). However, P[(*R*)-3HB] is stiff and brittle, and its high T_m and relatively low degradation temperature (*ca.* 250°C) makes processing by standard methods difficult. Incorporation of comonomers with a longer side chain, such as 3-hydroxyvalerate (3HV) with ethyl (Et) as the pendant group, leads an increase in ductility and a decrease in crystallinity and T_m, resulting in a decrease in stiffness and an increase in toughness. Thus, tuning the copolymer composition leads to PHAs with more desirable properties, better processability, and commercial applications,[3] but broader applications as commodity thermoplastics are limited due to their relatively high production costs and low volumes. Although bacterial PHAs can incorporate various short and longer pendant groups into copolymers with improved elongation relative to P3HB, it requires specific growth substrates or metabolic engineering to adapt incorporation of each type of side groups.

Compared with biosynthetic pathways, chemical catalysis approaches could provide better scalability, more rapid catalyst tuning to accommodate diverse substrate structures, and faster

reaction kinetics. In fact, the chemical synthesis of PHAs via ring-opening polymerization (ROP) of cyclic esters has been developed since 1960s,[5] affording PHAs with different structures and stereoregularities. P3HB, the most common and prominent member of PHAs, was synthesized through ROP of *rac*-*β*-butyrolactone (*rac*-*β*-BL).[5e-h] Highly syndiotactic (*st*) P3HB with P_r (defined as the probability of racemic linkages between adjacent monomer units) up to 0.95 was synthesized by discrete yttrium complexes supported by tetradentate, dianionic alkoxy-amino-bis(phenolate) [O^-,*N*,*O*,O^-] ligands.[6] Iso-enriched P3HB with $P_m \leq 0.85$ was synthesized by the ROP of *rac*-*β*-BL with alkyl aluminoxanes,[7] chiral initiator by *in-situ* reaction of $ZnEt_2$ with (*R*)(-)-3,3-dimethyl-1,2-butanediol,[8] chromium(III) salophen complexes,[9] grafted neodymium borohydrides onto silica,[10] and salan-ligated rare-earth metal amide complexes.[11] There are fewer successful examples on the synthesis of PHAs with a longer side chain,[12] such as P3HV and poly(3-hydroxybutyrate-*co*-3-hydroxyvalerate) (P3HBV).[7c,13]

Inspired by the ROP of the racemic lactide,[14] a cyclic dimer of lactic acid, we recently realized the synthesis of perfectly isotactic P3HB via the stereoselective ROP of the bio-sourced racemic eight-membered diolide (*rac*-8DL^{Me}, the superscripted Me denotes methyl substituents on the 8DL ring), a cyclic dimer of 3-hydroxybutyric acid (3HB), using racemic yttrium catalysts **1**–**4** supported by C_2-symmetric *N,N′*-bis(salicylidene) cyclohexanediimine (salcy) ligands (Chart 1). In particular, racemic catalyst **4** with bulky trityl groups installed at the ortho-phenoxy positions of the salcy ligand produced perfectly isotactic P3HB (isotacticity in *meso* triads, [*mm*], > 99%) with a high T_m up to 171ºC, M_n up to 1.54×10^5 g/mol (Da), and low dispersity ($Đ = 1.01$) under ambient conditions.[15] Kinetic resolution polymerization of *rac*-8DL^{Me} with enantiomeric catalysts (*R,R*)-**4** and (*S,S*)-**4** automatically stops at 50% conversion and yields enantiopure (*R,R*)-8DL^{Me} and (*S,S*)-8DL^{Me} with >99% *e.e.* and the corresponding poly[(*S*)-3HB] and poly[(*R*)-3HB]

with a high T_m of 175ºC. We also developed the diastereoselective polymerization methodology to enable the direct polymerization of diastereomeric mixtures of *rac*/*meso*-8DL^{Me} at varied *rac*/*meso* ratios, or *meso*-8DL^{Me}/*rac*-8DL^{Et} (ethyl-substituted 8DL) into stereosequenced semi-crystalline *it*-P3HB-*sb*-*st*-P3HB or *st*-P3HB-*sb*-*it*-P3HBV with isotactic and syndiotactic stereoblock or tapered stereoblock microstructures.[16] The stereosequenced block copolymers of 8DL$^{Me/Et}$ or 8DL$^{Me/Bu}$, *it*-P3HBV-*sb*-*st*-P3HBV or *it*-P3HBHp-*sb*-*st*-P3HBHp, where P3HBHp = poly(3-hydroxybutyrate-*co*-3-hydroxyheptanoate), can be also prepared through direct copolymerization of six diastereomers of 8DL$^{Me/Et}$ or 8DL$^{Me/Bu}$ (8DL^{Bu}: *n*-butyl-substituted 8DL) all together by racemic catalysts **4**–**5**. However, the stereoselective copolymerization of *rac*-8DL^{Me} with *rac*-8DL^{R} has not been previously studied, which could provide a catalyzed facile chemical synthesis route to crystalline isotactic PHA copolymers with potentially polyolefin-like thermal and mechanical properties; hence, this topic is the central objective of this study.

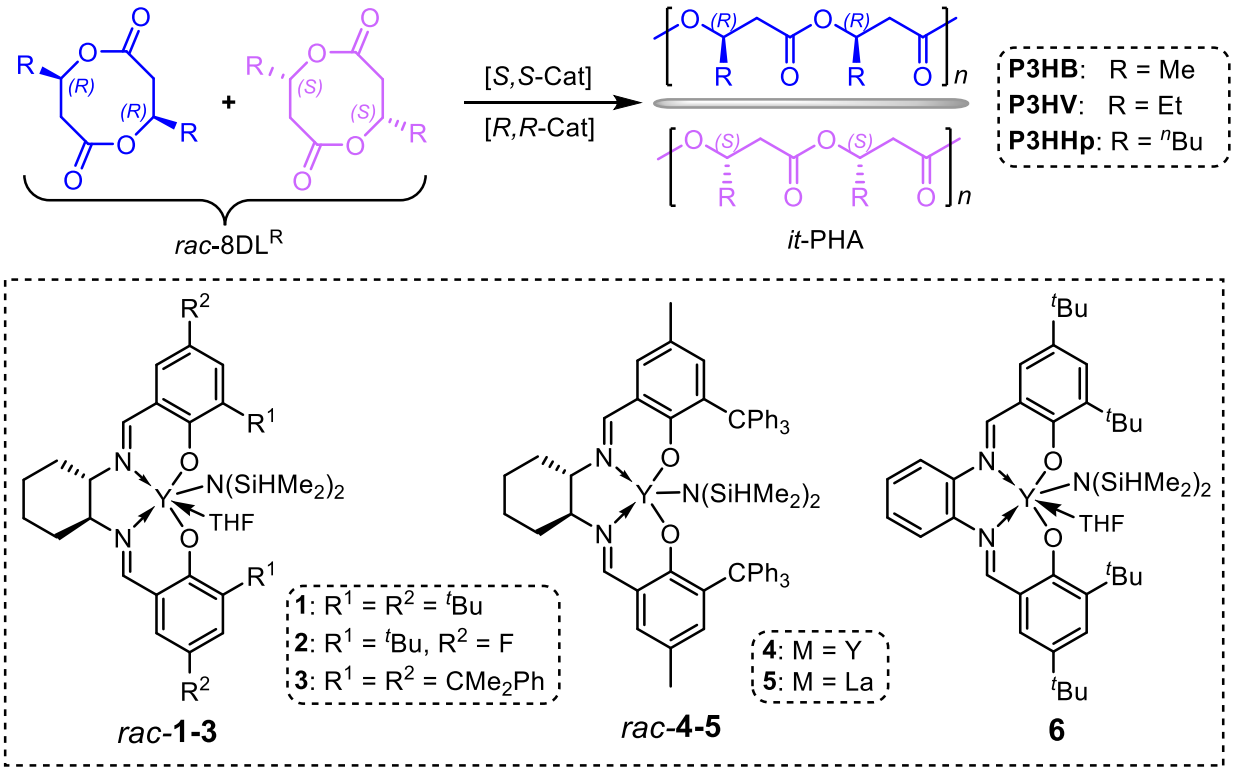

Figure 3.1. Stereoselective ROP of *rac*-8DL^{R} to *it*-PHAs: R = Me, P3HB; R = Et, P3HV; R = ^{n}Bu, P3HHp.

3.3. Results and Discussion

Stereoselective ROP of Longer Alkyl-Substituted rac-8DL^{R} (R = Et, Bu). To probe the generality of the chemical synthesis of PHAs via the stereoselective ROP of *rac*-8DL^{R} and modulate the properties of PHAs, we investigated two longer alkyl-substituted monomers *rac*-8DL^{R} (R = Et, Bu) (Figure 3.1), which were prepared following the procedures for the preparation of *rac*-8DL^{Me}.[16] At the outset, the ROP of *rac*-8DL^{Et} was performed using yttrium catalysts **1**–**4** (Table S3.1), achieving high to near quantitative isotacticity with P_m values ranging from 0.90 to 0.97. Complex **1** with the salen ligand bearing the 3,5-di-*tert*-butyl substituents [20] polymerized 100 equivalents of *rac*-8DL^{Et} to 87% and 98% conversion in 120 and 360 min, respectively, which was much slower than the ROP of *rac*-8DL^{Me}. The molecular weight of the resulting P3HV increased with increasing monomer conversion while keeping the dispersity relatively low ($Đ$ = 1.19 to 1.16) and the calculated initiation efficiency high (from 128% to 104 %, runs 1 and 2, Table S3.1). Based on ^{1}H and ^{13}C NMR analysis[5e, 7c, 21] (Figure S3.3), the P3HV produced by complex **1** exhibited high isotacticity with P_m ~ 0.90–0.91 and [*mm*] triad ~85%, by somewhat lower than that of P3HB by complex **1**. However, with this level of isotacticity, the resulting P3HV showed no T_m on the differential scanning colorimetry (DSC) curve with a cooling and heating rate of as low as 1 °C/min.

Next, we investigated possible effects of the salen ligand framework's *electronics*, *sterics*, and *symmetry* on the *rac*-8DL^{Et} polymerization activity and stereoselectivity. Complex **2** with the electron withdrawing F atoms substituted at the 5-positions of the salcy ligand produced P3HV with P_m and [*mm*] values (run 3, Table S3.1) similar to those by **1**. Turning to the steric perturbation of the catalyst, the bulkier cumyl-substituted complex **3** produced isotactic P3HV more rapidly

and also achieved noticeably higher isotacticity with P_m = 0.96 and [*mm*] = 95%) (run 4, Table S3.1, Figure S3.3). Now the resulting P3HV is semi-crystalline, exhibiting a T_m of 108 ºC and T_g of −18 ºC, while the M_n can be modulated by adjusting the [*rac*-8DL^{Et}]$_0$/[**3**]$_0$ ratio from 100/1 to 400/1 (runs 4–6, Table S3.1). Switching to complex **4** with even bulkier trityl groups substituted at the 3-positions of the salcy ligand, which exhibited extremely high activity and isoselectivity towards *rac*-8DL^{Me}, led to sluggish *rac*-8DL^{Et} polymerization (run 7, Table S3.1), highlighting the importance of the catalyst/monomer steric matching. The use of the corresponding La **5** with a larger metal center improved the activity somewhat but not the isotacticity (P_m = 0.94, [*mm*] = 93%).[16] Lastly, the achiral salph-based complex **6** showed the highest activity in this catalyst series, but it exhibited the lowest isoselectivity with P_m ~ 0.86 and [*mm*] ~ 75% (run 8, Table S3.1) and yielded an amorphous P3HV.

As **3** showed both high activity and isoselectivity for *rac*-8DL^{Et}, it was then chosen for the ROP of *rac*-8DL^{Bu} to produce isotactic poly(3-hydroxyheptanoate) (P3HHp). Indeed, P3HHp with high molecular weight (M_n = 99.3 – 140 kDa, $Đ$ = 1.19–1.24) and high isotacticity (P_m = 0.97, [*mm*] = 93−94%, Figure S3.7) was obtained (runs 1−3, Table S3.2). As in the case of *rac*-8DL^{Et}, the trityl-substituted **4** exhibited only marginal activity towards *rac*-8DL^{Bu} polymerization. La **5** polymerized 50 equivalents of *rac*-8DL^{Bu} to 58% conversion after 20 h, producing P3HHp with isotacticity P_m of 0.97 and [*mm*] of 96% but low molecular weight (M_n = 6.67 kDa, $Đ$ = 1.19, run 5, Table S3.2). The use of achiral **6** brought about the fastest polymerization, but the resulting P3HHp had the lowest P_m of 0.85 and [*mm*] of 74% (run 6, Table S3.2).

To gain insight into the control of the ROP of *rac*-8DL^{Et}, the P3HV samples produced at different times and [*rac*-8DL^{Et}]/[**3**] ratios were analyzed by matrix-assisted laser desorption/ionization time-of-flight mass spectroscopy (MALDI-TOF MS). When a low ratio of 20/1 was used with a longer

reaction time (5 min), the MS spectra showed some transesterification reactions, as evidenced by the appearances of molecular ion peaks with the spacing between the neighboring peaks being that of the half molar mass of the repeat unit (Figure S3.10). When the polymerization was quenched after 1 or 2 min (at which time the conversion was 55% or 87%), its MS spectrum displayed exclusive molecular ion peaks with the spacing between the neighboring peaks being that of *rac*-8DL^{Et} (Figures S3.8-3.9). These results indicate that transesterification occurred when the reaction reached full conversion and thus can be shut down by reducing the time or the catalyst amount in feed. For example, when [*rac*-8DL^{Et}]/[**3**] = 100, no transesterification was observed even after the full conversion of *rac*-8DL^{Et} (Figure S3.11). The intercept of the linear plot of *m*/*z* values (y) *vs* the number of *rac*-8DL^{Et} repeat units (x), 108, indicated that each P3HV chain carries BnO/H as chain ends [M_{end} = 108 (BnO/H) + 23 (Na^+) g/mol], which can be further confirmed by the ^{1}H NMR spectrum of P3HV (Figure S3.13). Similarly, the ROP of *rac*-8DL^{Bu} gave the P3HHp with BnO/H as chain ends, confirmed by its MS and ^{1}H NMR spectra (Figures S3.12 and S3.14). Overall, these results are consistent with the coordination-insertion mechanism proposed for the ROP of *rac*-8DL^{Me}.[15]

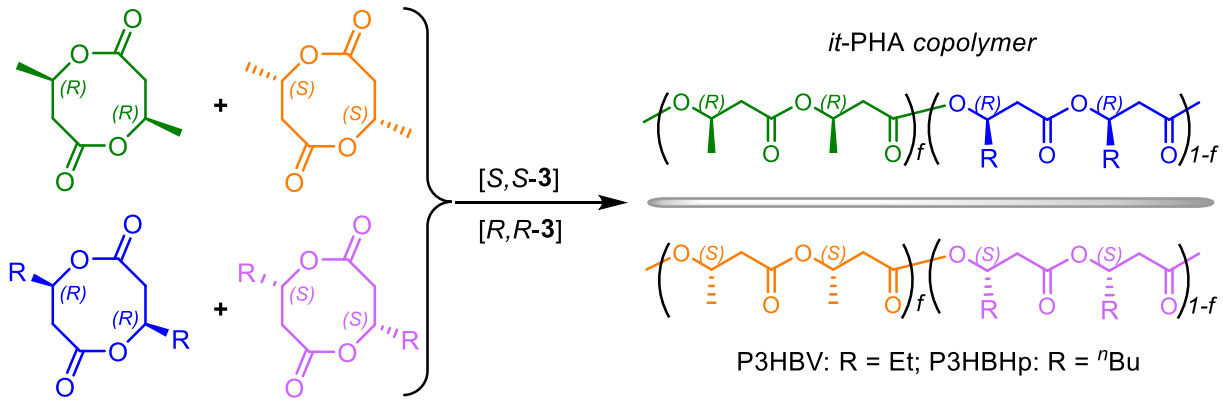

Figure 3.2. Stereoselective copolymerization of *rac*-8DL^{Me} with *rac*-8DL^{R} towards *it*-PHA copolymers.

PHAs from Copolymerization of rac-8DL^{Me} and rac-8DL^{R} (R = Et, Bu). The stereoselective copolymerization of *rac*-8DL^{Me} with *rac*-8DL^{R} using complex **3** under different conditions (Figure

3.2). As a control, homopolymerization of *rac*-8DL^{Me} was examined with **3** (0.5 mol% and 0.25 mol % loading) at r.t. (runs 1 and 2, Table 3.1), achieving 100% and 98% *rac*-8DL^{Me} conversion in 20 and 30 min to give *it*-P3HB ([*mm*] = 94%) with M_n = 52.7 and 121 kg/mol, narrow dispersity $Đ$ = 1.14 and 1.24, and T_m = 156 and 157 °C, respectively.[15] The copolymerization of *rac*-8DL^{Me} with *rac*-8DL^{Et} was then conducted with different *rac*-8DL^{Me}/*rac*-8DL^{Et} ratios at fixed [*rac*-8DL^{Me} + *rac*-8DL^{Et}]/[**3**] = 200. Decreasing the *rac*-8DL^{Me}/*rac*-8DL^{Et} feed ratio from 10/1 to 1/1 significantly enhanced *rac*-8DL^{Et} incorporation (mol%) of the resulting P3HBV from 9.0% to 42.1% (runs 3−7, Table 3.1), while the T_m of P3HBV decreased from 149 to 128 °C with increasing the *rac*-8DL^{Et} incorporation from 9.0% to 23.9%, and no T_m was observed when the *rac*-8DL^{Et} incorporation reached 42.1%. To increase the molecular weight of P3HBV, while keeping the catalyst loading constant (0.25 mol%), the reaction conditions (comonomer feed ratio, time, conversion) were varied to produce P3HBV with *rac*-8DL^{Et} incorporations from 3.9 to 37.6%, M_n from 53.2 to 90.7 kg/mol, and $Đ$ from 1.16 to 1.24 (runs 8−17, Table 3.1 and Figures S3.15). To further increase the molecular weight, the [*rac*-8DL^{Me} + *rac*-8DL^{Et}]/[**3**] molar ratio was increased to 600/1 and 800/1 with *rac*-8DL^{Me}/*rac*-8DL^{Et} feed ratio of 3/1 to 1/1, and the molecular weight of the resulting P3HBV enhanced to 75.1−121 kDa with narrower dispersity of 1.08−1.11, while keeping the *rac*-8DL^{Et} incorporation from 13.7 to 34.6% (runs 18−23, Table 3.1). Highly reactive La **5** was also tested for this copolymerization in a 1/1 feed ratio, producing P3HBV with *rac*-8DL^{Et} incorporation of 5.7% and T_m of 156 °C in 20 s (run 24, Table 3.1). The resulting P3HBV was shown to be a *random copolymer*: (a) monitoring the copolymerization ^{1}H NMR revealed that both monomers were consumed concurrently, although *rac*-8DL^{Me} was consumed more rapidly (runs 8-17, Table 3.1; Table S3.3); (b) the peaks for 3HB-3HV and 3HV-3HB sequences were

observed clearly from the ^{13}C NMR spectra of the copolymers (Figure S3.16); and (c) there showed only one T_m for each crystalline copolymer (vide infra).

Table 3.1. Results of copolymerization of *rac*-8DL^{Me} and *rac*-8DL^{Et} by catalyst **3** [a]

Run	[8DL]/[**3**]	[*rac*-DL^{Me}]/[*rac*-DL^{Et}]	Time (min)	Conv. [b] (%)		*rac*-8DL^{Et} content [c] (mol%)	M_n [d] (kg/mol)	$Đ$ [d] (M_w/M_n)	T_g [e] (°C)	T_m [e] (°C)	ΔH_f [e] (J/g)
				rac-DL^{Me}	*rac*-8DL^{Et}						
1	200/1	1/-	20	100	-	-	52.7	1.14	6.4	156	56.5
2	400/1	1/-	30	99	-	-	121	1.24	4.9	157	53.0
3	200/1	10/1	15	100	89	9.0	71.4	1.29	2.6	149	33.7
4	200/1	5/1	15	99	75	13.4	67.5	1.28	1.6	144	15.6
5	200/1	3/1	15	99	67	18.6	61.8	1.33	-0.6	138	20.2
6	200/1	2/1	15	98	61	23.9	58.0	1.30	-4.3	128	19.4
7	200/1	1/1	20	99	72	42.1	54.3	1.22	-8.6	-	-
8	400/1	10/1	20	75	26	3.9	90.7	1.24	3.6	150	39.7
9	400/1	10/1	30	99	66	6.6	86.6	1.18	3.2	149	36.4
10	400/1	5/1	20	76	28	7.0	82.3	1.21	2.8	144	30.7
11	400/1	5/1	30	97	55	10.8	82.3	1.18	2.4	143	23.7
12	400/1	3/1	20	73	25	11.2	75.3	1.21	1.8	138	14.1
13	400/1	3/1	30	95	53	15.7	76.6	1.18	0.4	138	18.3
14	400/1	2/1	20	72	26	15.4	72.5	1.18	0.1	131	11.2
15	400/1	2/1	30	94	49	21.0	74.4	1.16	-3.3	130	21.7
16	400/1	1/1	20	61	18	26.9	53.2	1.23	-4.7	114	2.6
17	400/1	1/1	40	97	59	37.6	59.6	1.21	-7.9	-	-
18	600/1	3/1	120	95	50	15.0	94.8	1.09	-0.2	137	24.5
19	600/1	2/1	140	91	42	19.9	99.0	1.08	-2.6	131	20.8
20	600/1	1/1	160	95	49	34.6	75.1	1.10	-6.4	-	-
21	800/1	3/1	240	92	44	13.7	121	1.10	1.0	138	27.1
22	800/1	2/1	240	92	44	19.9	107	1.11	-2.2	132	22.3
23	800/1	1/1	240	84	35	29.3	83.6	1.10	-5.5	-	-
24 [f]	400/1	1/1	20 s	97	5.7	5.7	45.0	1.01	2.6	156	64.0

[a] Conditions: *rac*-8DL^{Me} + *rac*-8DL^{Et} = 0.80 mmol in CH_2Cl_2, $V_{solvent}$ = 0.8 mL; r.t.; catalyst to BnOH initiator ratio fixed at 1/1, and the amount varied according to the [*rac*-8DL^{Me}+*rac*-8DL^{Et}]/[**3**] ratio. [b] Monomer conversions measured by ^1H NMR. [c] *rac*-8DL^{Et} content measured by ^1H NMR of the isolated copolymer. [d] Determined by GPC coupled with an 18-angle light scattering detector at 40 °C in chloroform. [e] Measured by DSC with the cooling and second heating rate of 10 °C/min for samples with *rac*-8DL^{Et} incorporations of 0−13.4%, 5 °C/min for 13.7−18.6%, 2 °C/min for 19.9−23.9%, or 1 °C/min for 26.9−42.1%. [f] **5** was used

Table 3.2 summarized the results of copolymerizations of *rac*-8DL^{Me} and *rac*-8DL^{Bu} by catalyst **3**, affording P3HBHp random copolymers with *rac*-8DL^{Bu} incorporation ranging from 7.3 to 44.8%, M_n from 95.6 to 126 kg/mol, and dispersity $Đ$ from 1.13 to 1.24 (runs 1−5, Table 3.2 and Figures S3.17-S3.18). The T_m of P3HBHp decreased from 143 to 118 °C with an increase in the *rac*-8DL^{Bu} incorporation from 7.3 to 24.3%, and no T_m was observed when the *rac*-8DL^{Bu} incorporation reached 44.8%. To increase the molecular weight of P3HBHp, the [*rac*-8DL^{Me} + *rac*-8DL^{Bu}]/[**3**] ratio was increased to 800/1 with varied *rac*-8DL^{Me}/*rac*-8DL^{Bu} feed ratios of 3/1

to 1/1. Indeed, the M_n of the resulting P3HBHp was enhanced to 126−139 kDa with narrower dispersity of 1.08−1.10, while keeping the *rac*-8DL^{Bu} incorporation of 18.1−41.0% (runs 6−8, Table 3.2). In addition, La **5** was used to mediate rapid copolymerization of *rac*-8DL^{Me} and *rac*-8DL^{Bu} in a 1/1 feed ratio, producing P3HBHp with *rac*-8DL^{Bu} incorporation of only 4.6% and a high T_m of 160 °C (run 9, Table 3.2).

Table 3.2. Results of copolymerization of *rac*-8DL^{Me} and *rac*-8DL^{Bu} by catalyst **3** [a]

Run	[8DL]/[**3**]	[*rac*-8DL^{Me}]/[*rac*-8DL^{Bu}]	Time (min)	Conv. (%)		*rac*-8DL^{Bu} content (mol%)	M_n (kg/mol)	$Đ$ (M_w/M_n)	T_g [b] (°C)	T_m [b] (°C)	ΔH_f [b] (J/g)
				rac-8DL^{Me}	*rac*-8DL^{Bu}						
1	400/1	10/1	30	88	69	7.3	126	1.13	0.7	143	28.3
2	400/1	5/1	30	87	63	12.7	96.6	1.24	-3.1	135	17.8
3	400/1	3/1	30	86	61	19.1	108	1.16	-8.7	124	19.6
4	400/1	2/1	30	81	52	24.3	95.6	1.15	-11.5	118	1.3
5	400/1	1/1	40	96	78	44.8	105	1.17	-19.4	-	-
6	800/1	3/1	140	84	56	18.1	139	1.08	-7.6	127	8.4
7	800/1	2/1	140	82	55	25.1	126	1.10	-11.4	-	-
8	800/1	1/1	160	78	54	41.0	135	1.08	-18.4	-	-
9 [c]	400/1	1/1	20 s	98	4.7	4.6	47.2	1.01	2.8	160	59.4

[a] See Table 3.1 footnotes for explanations. [b] Measured by DSC with the cooling and second heating rate of 10 °C/min for samples with *rac*-8DL^{Bu} incorporations of 0−7.3%, 5 °C/min for 12.7%, 2 °C/min for 18.1−19.1%, or 1 °C/min for 24.3−44.8%. [f] **5** was used as the catalyst.

Thermal and Mechanical Properties of PHAs. The DSC curves of P3HV and P3HHp produced by catalyst **3** under identical conditions ([*rac*-8DL^{R}]/[**3**] = 200/1, CH_2Cl_2, r.t., 100% conversion), and copolymers P3HBV and P3HBHp produced by **3** under identical conditions ([*rac*-8DL^{Me} + *rac*-8DL^{R}]/[**3**] = 400/1) were compared in Figures 3.3A, Figure S3.28. For the P3HV with $P_m \leq$ 0.91, no T_m was observed with the cooling and second heating rate of as low as 1 °C/min, and T_m can be only observed on the first heating scan (Figures S3.23-3.24). On the other hand, the P3HV with P_m = 0.94−0.97 exhibited a T_m from 104 to 108 °C with the cooling and second heating rate of 2 °C/min,[16] but no T_m were seen with the cooling and second heating rate of 10 or 5 °C/min (Figures S3.25-3.26 and S3.28), due to the slow crystalline rate of P3HV. For P3HHp with P_m =

0.97, a T_g of -34.3 °C, but no T_m, was observed on the second heating scan. However, there exhibited a T_m of 50.8 °C on the first heating scan (Figures S23.27-3.28).

The T_m of P3HBV copolymers prepared by **3** decreased from 150 °C to 114 °C with an increase in *rac*-8DL^{Et} incorporation from 3.9% to 26.9%, and no obvious T_m was observed when the *rac*-8DL^{Et} incorporation reached 29.3% or higher (Figures 3.3A and S3.29). Similarly, the T_m of P3HBHp produced by **3** decreased from 143 °C to 118 °C with an increase in *rac*-8DL^{Bu} incorporation from 7.3% to 24.3%, and no obvious T_m was observed on the second heating scan when the *rac*-8DL^{Et} incorporation reached 25.1% or higher (Figures 3.3B). Additionally, the T_m of the P3HBV and P3HBHp obtained by **5** (Figure S3.31) was higher than that of the copolymers with similar comonomer incorporation level obtained by **3**, due to the higher isotacticity of the P3HB component by **5**.

Thermal degradation profiles of isotactic P3HV, P3HHp, P3HBV, and P3HBHp produced by **3** were examined by thermal gravimetric analysis (TGA). The TGA curve of P3HV (M_n = 31.8 kDa, $Đ$ = 1.18, Figure S3.32) showed a decomposition temperature (T_d, defined by the temperature of 5% weight loss) of 258 °C and a maximum rate decomposition temperature (T_{max}) of 285 °C, while P3HHp (M_n = 140 kDa, $Đ$ = 1.20) exhibited a somewhat lower T_d of 247 °C and T_{max} of 272 °C. Moreover, P3HBV with the *rac*-8DL^{Et} incorporation of 19.9% (M_n = 107 kDa, $Đ$ = 1.11) exhibited a T_d of 247 °C and T_{max} of 277 °C, and P3HBHp with the *rac*-8DL^{Bu} incorporation of 18.1% (M_n = 139 kDa, $Đ$ = 1.08) showed a similar T_d of 247 °C and T_{max} of 274 °C (Figure S3.35).

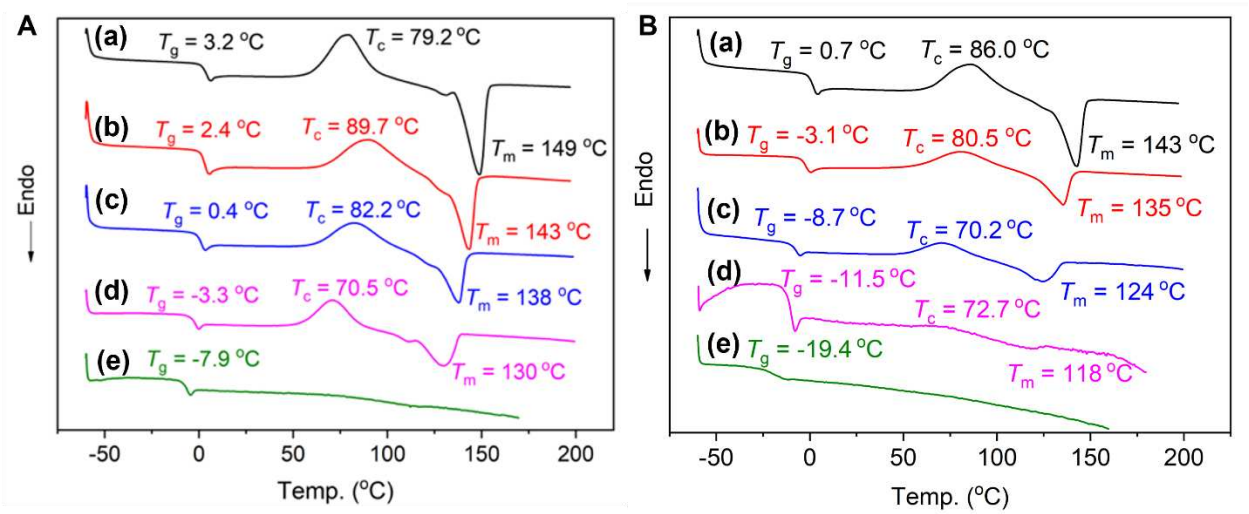

Figure 3.3. A. DSC curves of P3HBV copolymers produced by [*rac*-8DL^{Me} + *rac*-8DL^{Et}]/[**3**] = 400 with different *rac*-8DL^{Et} incorporations: (**a**) 6.6%; (**b**) 10.8%; (c) 15.7%; (**d**) 21.0%; and (**e**) 37.6%. **B.** DSC curves of P3HBHp copolymers produced by [*rac*-8DL^{Me} + *rac*-8DL^{Bu}]/[**3**] = 400 with different *rac*-8DL^{Bu} incorporations: (**a**) 7.3%; (**b**) 12.7%; (c) 19.1%; (**d**) 24.3%; and (**e**) 44.8%.

Table 3.3. Results of multi-gram scale copolymerization of *rac*-8DL^{Me} and *rac*-8DL^{R} by catalyst **3**

Run	[*rac*-8DL^{Me}]/[*rac*-8DL^{R}] [a]	R	Time (min)	Conv. (%)[b]		*rac*-8DL^{R} content [c] (mol%)	M_n [d] (kg/mol)	$Đ$ [d] (M_w/M_n)	E [e] (MPa)	σ [e] (MPa)	ε [e] (%)
				rac-8DL^{Me}	*rac*-8DL^{R}						
1	5/1	Et	350	86	38	7.6	175	1.35	1166	25.8	35
2	3/1	Et	360	88	40	12.8	138	1.08	856	30.9	257
3	2/1	Et	540	92	45	19.8	119	1.16	669	25.0	374
4	10/1	Bu	300			6.3	169	1.02	1056	25.3	58
5	5/1	Bu	330	92	68	10.5	183	1.05	532	20.8	215
6	3/1	Bu	280	n.r.	50	19.6	144	1.15	226	20.5	578

[a] Conditions: *rac*-8DL^{Me} + *rac*-8DL^{Et} = 25 mmol in CH_2Cl_2, $V_{solvent}$ = 25 mL; r.t.; catalyst to BnOH initiator ratio fixed at 1/1, [*rac*-8DL^{Me}+*rac*-8DL^{Et}]/[**3**] = 800/1. [b] Monomer conversions measured by ^{1}H NMR. [c] *rac*-8DL^{R} content measured by ^{1}H NMR of the isolated copolymer. [d] Determined by GPC coupled with an 18-angle light scattering detector at 40 °C in chloroform.. [e] performed on Instron 5966 universal testing system on dog-bone-shaped specimens prepared via compression molding and measured to the point of material break at a grip extension speed of 10.0 mm/min at ambient conditions.

To examine mechanical properties of copolymers, P3HBV and P3HBHp with varying *rac*-8DL^{R} incorporation of 5 ~ 20mol%, the copolymerizations of *rac*-8DL^{Me} and *rac*-8DL^{R} with **3** were carried out in a multi-gram scale under similar conditions and summarized in Table 3.3. ([*rac*-8DL^{Me} + *rac*-8DL^{R}]/[**3**] = 800/1, CH_2Cl_2, r.t.). The copolymerization of *rac*-8DL^{Me} and *rac*-8DL^{Et} conducted with [*rac*-8DL^{Me}]/[*rac*-8DL^{Et}] feed ratio of 5/1 produced P3HBV with *rac*-8DL^{Et}

incorporation of 7.6% and M_n = 175 kDa ($Đ$ = 1.35). A [*rac*-8DL^{Me}]/[*rac*-8DL^{Et}] feed ratio of 3/1 produced P3HBV with *rac*-8DL^{Et} incorporation of 12.8% and M_n = 138 kDal ($Đ$ = 1.08). Finally, a [*rac*-8DL^{Me}]/[*rac*-8DL^{Et}] feed ratio of 2/1 produced P3HBV with *rac*-8DL^{Et} incorporation of 19.8% and M_n = 119 kDa ($Đ$ = 1.16). The copolymerization of *rac*-8DL^{Me} and *rac*-8DL^{Bu} conducted with [*rac*-8DL^{Me}]/[*rac*-8DL^{Bu}] feed ratio of 10/1 produced P3HBHp with *rac*-8DL^{Bu} incorporation of 6.3% and M_n = 169 kDa ($Đ$ = 1.02). Lowering the [*rac*-8DL^{Me}]/[*rac*-8DL^{Bu}] feed ratio to 5/1 produced P3HBHp with *rac*-8DL^{Bu} incorporation of 10.5% and M_n = 183 kDa ($Đ$ = 1.05). Increasing the *rac*-8DL^{Bu} incorporation to 19.6% was achieved with a [*rac*-8DL^{Me}]/[*rac*-8DL^{Bu}] feed ratio of 3/1 and produced P3HBHp with M_n = 144 kDa ($Đ$ = 1.15). These results obtained by the multi-gram scale reactions were consistent with those performed in the small-scale runs in Table 3.1 and Table 3.2.

Tensile testing of dog-bone-shaped copolymer specimens, prepared by compression molding yielded the stress-strain curves in Figure 3.4. P3HBV with *rac*-8DL^{Et} incorporation of 7.6% was quite brittle, an ultimate tensile strength (σ_B) of 25.8 ± 0.6 MPa, Young's modulus (E) of 1166 ± 81 MPa, and elongation at break (ε_B) of 35 ± 4% (**A**, blue curve, Figure 3.4, Table S3.4). Increasing the *rac*-8DL^{Et} incorporation to 12.8% yielded a much more ductile polymer with σ_B = 30.9 ± 4.1 MPa, E = 856 ± 46 MPa, and ε_B = 257 ± 37% (**A**, red curve, Figure 3.4, Table S3.5). Finally, the P3HBV specimen with highest *rac*-8DL^{Et} incorporation of 19.8% exhibited an impressive σ_B = 25.0 ± 0.2 MPa, E = 669 ± 45 MPa, and ε_B = 374 ± 19% (**A**, green curve, Figure 3.4, Table S3.6). In comparison, P3HBHp with low *rac*-8DL^{Bu} incorporation of 6.3% was brittle and exhibited σ_B = 25.3 ± 1.3 MPa, E = 1056 ± 105 MPa, and ε_B = 58 ± 6% (**B**, blue curve, Figure 3.4, Table S3.7). Increasing the *rac*-8DL^{Bu} incorporation to 10.5% resulted in P3HBHp that was more ductile with σ_B = 20.8 ± 2.7 MPa, E = 532 ± 31 MPa, and ε_B = 215 ± 80% (**B**, red curve, Figure 3.4, Table

S3.8). The P3HBHp copolymer with highest *rac*-8DL^{Bu} incorporation of 19.6% exhibited σ_B = 20.5 ± 0.4 MPa, E = 226 ± 9 MPa, and ε_B = 578 ± 15% (**B**, green curve, Figure 3.4, Table S3.9. In addition, P3HBV (19.8% 3HV) showed a yield point at elongation of 11.0 ± 0.05% and tensile strength of 17.3 ± 0.9 MPa, while P3HBHp (19.6% 3HHp) exhibited a higher elongation of 15.7 ± 1.2%, but lower tensile strength of 9.09 ± 0.30 MPa at the yield point.

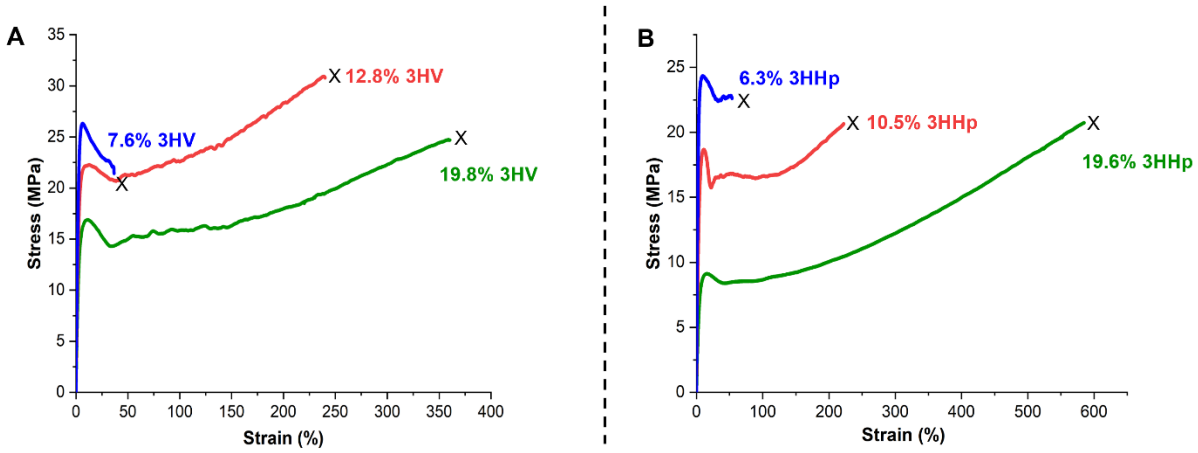

Figure 3.4. Representative Stress-strain curves (10 mm/min, r.t.) of P3HBV with *rac*-8DL^{Et} incorporation of 19.8% (M_n = 119 kDa, $Đ$ = 1.16) and P3HBHp with *rac*-8DL^{Bu} incorporation of 19.6% (M_n = 144 kDa, $Đ$ = 1.15). Break point indicated by "x".

A lower % incorporation of *rac*-8DL^{R} (R= Et & Bu) is a stiff material with a high Young's modulus coupled with brittleness (ε_B < 50%). Increasing the % incorporation of the more flexible monomer unit results in a copolymer with increased ductility and the PHA copolymers with ~20 % incorporation can can be described as hard, ductile, and tough plastics, much like polyethylene and isotactic polypropylene.[22] While P3HBV (19.8% 3HV) is stronger and stiffer due to the higher tensile strength and Young's modulus, P3HBHp (19.6% 3HHp) exhibits considerably higher elongation at break and lower Young's modulus and is thus more ductile and softer.

3.4. Conclusions

The catalyzed chemical synthesis of PHAs using *rac*-8DL^{R} derived from the bio-sourced succinate has been shown to be highly versatile in the efficient and stereoselective synthesis of crystalline,

isotactic PHA homopolymer and copolymers with tunable properties. With a class of readily accessible racemic metal-based catalysts supported by the C_2-salcy ligand, the stereoselective ROP of *rac*-8DL^{R} (R = Me, Et, and Bu) leads to highly to quantitatively isotactic PHAs, including P3HB (R = Me) with P_m or [*mm*] > 99% and T_m up to 171 ºC, P3HV (R = Et) with P_m = 0.97 ([*mm*] = 95%) and T_m = 108 ºC, and P3HHp (R = Bu) with P_m = 0.97 ([*mm*] = 94%) and T_m = 50.8 °C (T_g = −34.3 °C).

The catalyst/monomer steric matching is found to be critical to achieve a highly active and stereoselective ROP of *rac*-8DL^{R}. In the case of the smallest *rac*-8DL^{Me}, the sterically most demanding catalyst **4** with bulky trityl groups exhibits extremely high activity and isoselectivity, leading to purely isotactic, high MW (M_n = 154 kDa) P3HB. However, this sterically encumbered catalyst exhibits only marginal activity for the ROP of *rac*-8DL^{Et} and *rac*-8DL^{Bu}, whereas the less bulky cumyl-substituted **3** exhibits both high activity and isoselectivity for these two bulkier monomers. For example, P3HHp with P_m = 0.97 ([*mm*] = 94%) and M_n = 140 kDa ($Đ$ = 1.19) can be rapidly produced by **3**.

Molecular catalyst **3** effectively copolymerizes *rac*-8DL^{Me} with *rac*-8DL^{Et} or *rac*-8DL^{Bu} to produce high-molecular-weight (> 10^5 Da) PHA random copolymers P3HBV or P3HBHp with various levels of *rac*-8DL^{Et} or *rac*-8DL^{Bu} incorporation. The T_m of P3HBV or P3HBHp decreases with the increase of *rac*-8DL^{Et} or *rac*-8DL^{Bu} incorporation, but they all exhibit similar thermal degradation temperature of *ca.* 250 °C. These copolymerizations can be scaled up to analyze mechanical performance and a clear trend is visible moving from low % incorporation (stiff, brittle materials) to higher % incorporation (ductile and tough plastics). This chemocatalatic route allows precision synthesis of PHA copolymers with targeted % incorporation of the flexible monomer unit, high M_n (>100 kDa) and low chain dispersity (<1.35). Notably, both P3HBV with *rac*-8DL^{Et}

incorporation of 19.8% and P3HBHp with *rac*-8DL^{Bu} incorporation of 19.6% are hard, ductile, and tough plastics having polyolefin-like thermal transition temperatures and mechanical properties, with an ultimate tensile strength of 25.0 ± 0.2 MPa and 20.5 ± 0.4 MPa, Young's modulus of 669 ± 45 MPa and 226 ± 9 MPa, and elongation at break of 374 ± 19% and 578 ± 15%, respectively.

3.5. References

[1] a) R. Geyer, J. R. Jambeck, K. L. Law, *Sci. Adv.* **2017**, *3*, e1700782; b) The new plastics economy: Rethinking the future of plastics. https://www.weforum.org/reports/the-new-plastics-economy-rethinking-the-future-of-plastics; c) C. M. Rochman, A. Andrady, S. Dudas, J. Fabres, Galgani, Hardesty, V. Hidalgo-Ruz, S. Hong, P. Kershaw, L. Lebreton, A. Lusher, R. Narayan, S. Pahl, J. Potemra, C. Rochman, S. A. Sherif, J. Seager, W. Joon Shim, P. Sobral, L. Amaral-Zettler, *Sources, fate and effects of microplastics in the marine environment: Part 2 of a global assessment*, **2016**; d) J. R. Jambeck, R. Geyer, C. Wilcox, T. R. Siegler, M. Perryman, A. Andrady, R. Narayan, K. L. Law, *Science* **2015**, *347*, 768-771; e) C. M. Rochman, M. A. Browne, B. S. Halpern, B. T. Hentschel, E. Hoh, H. K. Karapanagioti, L. M. Rios-Mendoza, H. Takada, S. Teh, R. C. Thompson, *Nature* **2013**, *494*, 169-171.

[2] a) M. Hong, E. Y. X. Chen, *Trends in Chemistry* **2019**, *1*, 148-151; b) X. Zhang, M. Fevre, G. O. Jones, R. M. Waymouth, *Chem. Rev.* **2018**, *118*, 839-885; c) X.-B. Lu, Y. Liu, H. Zhou, *Chem. Eur. J.* **2018**, *24*, 11255-11266; d) D. K. Schneiderman, M. A. Hillmyer, *Macromolecules* **2017**, *50*, 3733-3749.

[3] a) A. Anjum, M. Zuber, K. M. Zia, A. Noreen, M. N. Anjum, S. Tabasum, *Int. J. Biol. Macromol.* **2016**, *89*, 161-174; b) Z. Li, J. Yang, X. J. Loh, *NPG Asia Mater.* **2016**, *8*, e265; c) Muhammadi, Shabina, M. Afzal, S. Hameed, *Green Chem. Lett. Rev.* **2015**, *8*, 56-77; d) B. Laycock, P. Halley, S. Pratt, A. Werker, P. Lant, *Progress in Polymer Science* **2013**, *38*, 536-583; e) M. N. Somleva, O. P. Peoples, K. D. Snell, *Plant Biotechnol. J.* **2013**, *11*, 233-252; f) S. Taguchi, T. Iwata, H. Abe, Y. Doi, in *Polymer Science: A Comprehensive Reference* (Ed.: M. Möller), Elsevier, Amsterdam, **2012**, pp. 157-182; g) G.-Q. Chen, in *Plastics from bacteria: Natural functions and applications, Vol. 14* (Ed.: G.-Q. Chen), Springer-Verlag, Berlin, **2010**,

pp. 17-37; h) G.-Q. Chen, *Chem. Soc. Rev.* **2009**, *38*, 2434-2446; i) R. W. Lenz, R. H. Marchessault, *Biomacromolecules* **2005**, *6*, 1-8; j) K. Sudesh, H. Abe, Y. Doi, *Progress in Polymer Science* **2000**, *25*, 1503-1555; k) Y. Poirier, C. Nawrath, C. Somerville, *Nat. Biotechnol.* **1995**, *13*, 142; l) H.-M. Müller, D. Seebach, *Angew. Chem. Int. Ed. Engl.* **1993**, *32*, 477-502.

[4] A. H. Tullo, *Chem. Eng. News* **2019**, *97*, 20-21.

[5] a) H. Li, R. M. Shakaroun, S. M. Guillaume, J.-F. Carpentier, *Chem. Eur. J.* **2020**, *26*, 128-138; b) X. Tang, E. Y.-X. Chen, *Chem* **2019**, *5*, 284-312; c) J.-F. Carpentier, S. M. Guillaume, H. Li, R. Shakaroun, *Chem. Eur. J.* **2019**, DOI: 10.1002/chem.201904108; d) Z. Jedliński, P. Kurcok, R. W. Lenz, *Macromolecules* **1998**, *31*, 6718-6720; e) M. Iida, T. Araki, K. Teranishi, H. Tani, *Macromolecules* **1977**, *10*, 275-284; f) K. Teranishi, M. Iida, T. Araki, S. Yamashita, H. Tani, *Macromolecules* **1974**, *7*, 421-427; g) D. E. Agostini, J. B. Lando, J. R. Shelton, *Journal of Polymer Science Part A-1: Polymer Chemistry* **1971**, *9*, 2775-2787; h) S. Inoue, Y. Tomoi, T. Tsuruta, J. Furukawa, *Die Makromolekulare Chemie* **1961**, *48*, 229-233; i) M. Hong, E. Y. X. Chen, *Nat Chem* **2016**, *8*, 42-49; j) M. Hong, E. Y. X. Chen, *Angew. Chem., Int. Ed.* **2016**, *55*, 4188-4193; k) S. Liu, C. Ren, N. Zhao, Y. Shen, Z. Li, *Macromol. Rapid Commun.* **2018**, *39*, 1800485.

[6] a) M. Bouyahyi, N. Ajellal, E. Kirillov, C. M. Thomas, J.-F. Carpentier, *Chem. Eur. J.* **2011**, *17*, 1872-1883; b) N. Ajellal, M. Bouyahyi, A. Amgoune, C. M. Thomas, A. Bondon, I. Pillin, Y. Grohens, J.-F. Carpentier, *Macromolecules* **2009**, *42*, 987-993; c) A. Amgoune, C. M. Thomas, T. Roisnel, J.-F. Carpentier, *Chem. Eur. J.* **2006**, *12*, 169-179; d) A. Amgoune, C. M. Thomas, S. Ilinca, T. Roisnel, J.-F. Carpentier, *Angew. Chem. Int. Ed.* **2006**, *45*, 2782-2784.

[7] a) B. Wu, R. W. Lenz, *Macromolecules* **1998**, *31*, 3473-3477; b) C. Jaimes, M. Arcana, A. Brethon, A. Mathieu, F. Schue, J. M. Desimone, *Eur. Polym. J.* **1998**, *34*, 175-185; c) S. Bloembergen, D. A. Holden, T. L. Bluhm, G. K. Hamer, R. H. Marchessault, *Macromolecules* **1989**, *22*, 1656-1663.

[8] A. Le Borgne, N. Spassky, *Polymer* **1989**, *30*, 2312-2319.

[9] M. Zintl, F. Molnar, T. Urban, V. Bernhart, P. Preishuber-Pflügl, B. Rieger, *Angew. Chem., Int. Ed.* **2008**, *47*, 3458-3460.

[10] N. Ajellal, G. Durieux, L. Delevoye, G. Tricot, C. Dujardin, C. M. Thomas, R. M. Gauvin, *Chem. Commun.* **2010**, *46*, 1032-1034.

[11] Z. Zhuo, C. Zhang, Y. Luo, Y. Wang, Y. Yao, D. Yuan, D. Cui, *Chem. Commun.* **2018**, *54*, 11998-12001.

[12] J.-F. Carpentier, *Macromolecular Rapid Communications* **2010**, *31*, 1696-1705.

[13] a) L. R. Rieth, D. R. Moore, E. B. Lobkovsky, G. W. Coates, *J. Am. Chem. Soc.* **2002**, *124*, 15239-15248; b) C. Guillaume, N. Ajellal, J.-F. Carpentier, S. M. Guillaume, *J. Polym. Sci., Part A: Polym. Chem.* **2011**, *49*, 907-917; c) N. Ajellal, C. M. Thomas, J.-F. Carpentier, *J. Polym. Sci., Part A: Polym. Chem.* **2009**, *47*, 3177-3189; d) J. W. Kramer, G. W. Coates, *Tetrahedron* **2008**, *64*, 6973-6978.

[14] a) T.-Q. Xu, G.-W. Yang, C. Liu, X.-B. Lu, *Macromolecules* **2017**, *50*, 515-522; b) D. Myers, A. J. P. White, C. M. Forsyth, M. Bown, C. K. Williams, *Angew. Chem., Int. Ed.* **2017**, *56*, 5277-5282; c) Z. Mou, B. Liu, M. Wang, H. Xie, P. Li, L. Li, S. Li, D. Cui, *Chem. Commun.* **2014**, *50*, 11411-11414; d) N. Maudoux, T. Roisnel, V. Dorcet, J.-F. Carpentier, Y. Sarazin,

Chem. Eur. J. **2014**, *20*, 6131-6147; e) C. Bakewell, A. J. P. White, N. J. Long, C. K. Williams, *Angew. Chem. Int. Ed.* **2014**, *53*, 9226-9230; f) M. J. Stanford, A. P. Dove, *Chem. Soc. Rev.* **2010**, *39*, 486-494; g) N. Nomura, R. Ishii, Y. Yamamoto, T. Kondo, *Chem. Eur. J.* **2007**, *13*, 4433-4451; h) Z. Zhong, P. J. Dijkstra, J. Feijen, *Angew. Chem. Int. Ed.* **2002**, *41*, 4510-4513; i) T. M. Ovitt, G. W. Coates, *J. Am. Chem. Soc.* **2002**, *124*, 1316-1326; j) N. Spassky, M. Wisniewski, C. Pluta, A. Le Borgne, *Macromol. Chem. Phys.* **1996**, *197*, 2627-2637.

[15] X. Tang, E. Y.-X. Chen, *Nat. Commun.* **2018**, *9*, 2345.

[16] X. Tang, A. H. Westlie, E. M. Watson, E. Y.-X. Chen, *Science* **2019**, *366*, 754-758.

[17] a) J. Eppinger, M. Spiegler, W. Hieringer, W. A. Herrmann, R. Anwander, *J. Am. Chem. Soc.* **2000**, *122*, 3080-3096; b) W. A. Herrmann, J. Eppinger, M. Spiegler, O. Runte, R. Anwander, *Organometallics* **1997**, *16*, 1813-1815.

[18] P. T. Altenbuchner, A. Kronast, S. Kissling, S. I. Vagin, E. Herdtweck, A. Pöthig, P. Deglmann, R. Loos, B. Rieger, *Chem. Eur. J.* **2015**, *21*, 13609-13617.

[19] a) A. Duda, A. Kowalski, J. Libiszowski, S. Penczek, *Macromol. Symp.* **2005**, *224*, 71-84; b) C. Alemán, O. Betran, J. Casanovas, K. N. Houk, H. K. Hall, *J. Org. Chem.* **2009**, *74*, 6237-6244.

[20] a) M.-H. Lin, T. V. RajanBabu, *Org. Lett.* **2002**, *4*, 1607-1610; b) Q. Liu, C. Meermann, H. W. Gorlitzer, O. Runte, E. Herdtweck, P. Sirsch, K. W. Tornroos, R. Anwander, *Dalton Trans.* **2008**, 6170-6178.

[21] M. Iida, S. Hayase, T. Araki, *Macromolecules* **1978**, *11*, 490-493.

[22] J. M. Eagan, J. Xu, R. Di Girolamo, C. M. Thurber, C. W. Macosko, A. M. LaPointe, F. S. Bates, G. W. Coates, *Science* **2017**, *355*, 814-816.

Chapter 4

Catalyzed Chemical Synthesis of Unnatural Aromatic Polyhydroxyalkanoate (PHA) and Aromatic-Aliphatic PHAs with Record-High Glass-Transition and Decomposition Temperatures

4.1. Synopsis

The catalyzed chemical synthesis of polyhydroxyalkanoates (PHAs) via stereoselective ring-opening polymerization (ROP) of 8-membered cyclic diolides (8DL^{R}, R denotes the two substituents on the ring) has shown its ability to synthesize a variety of stereoregular aliphatic PHAs, but its utility for the synthesis of aromatic PHAs has not yet been demonstrated. Here we report that the controlled ROP of *meso*-8DL^{Bn} (Bn = benzyl)—catalyzed by metal-based complexes supported by C_2-Salen ligands—affords syndiotactic ([*rr*] = 92%) poly(3-hydroxy-4-phenylbutyrate) (*st*-P3H4PhB) with a high molar mass (M_n up to 147 kg mol^{-1}) and the highest glass-transition temperature (43 °C) reported in the PHA family, whereas the ROP of *rac*-8DL^{Bn} leads to essentially pure isotactic ([*mm*] > 99%) *it*-P3H4PhB. With judicious selections of catalysts, monomers, and procedures, copolymerizations of *meso*-8DL^{Bn} with *rac*-8DL^{R} (R = Me, ^{n}Bu) produces aromatic-aliphatic random, stereotapered, or crystalline stereodiblock PHA copolymers. In particular, the copolymer of *meso*-8DL^{Bn} with *rac*-8DL^{Bu}—P3H4PhB-*co*-P3HHp (M_n = 205 kg mol^{-1}) —is a strong, hard, but ductile (~191% elongation at break) material, displaying perhaps the highest decomposition temperature (281 °C) reported for PHAs to date.

4.2. Introduction

The pressing need to address the end-of-life issues of today's predominately petroleum-based non-degradable plastics, which have accelerated depletion of finite natural resources and caused severe worldwide plastics pollution problems,[1–4] has fueled intense research aiming for sustainable

polymers with closed-loop lifecycles, including the development of biorenewable and biodegradable alternatives.[5–12] In this context, polyhydroxyalkanoates (PHAs), the most versatile polymer class produced from biorenewable resources by living microorganisms,[13–21] have gained increasing attraction as a suitable sustainable alternative to today's commodity plastics due to their comparable physical and mechanical properties to polyolefins[22] and, most importantly, their unique ability to biodegrade in ambient environment.[23] Although more than 150 different PHAs are known,[14,24] microorganisms commonly produce isotactic (*it*-) poly(3-hydroxybutyrate) (P3HB), along with its copolymers with longer aliphatic pendant groups, such as poly(3-hydroxybutyrate-*co*-3-hydroxyvalerate) (PHBV).[21]

In sharp contrast, PHAs bearing an *aromatic pendant group* are much less common, often considered as “unusual” or “unnatural”. The first biosynthesized PHA bearing an aromatic pendant group was reported by Lenz and co-workers in 1990 who described the production of an “unusual” PHA, poly(3-hydroxy-5-phenylvalerate), P(3H5PhV), from 5-phenylvaleric acid by *Pseudomonas oleovorans*.[25] Because of the novelty of aromatic PHAs as well as their ability to alter the physical properties of PHAs drastically, most notably the glass-transition temperature (T_g), while not compromising the biodegradability, further exploration has yielded various aromatic PHAs since. Several aromatic pendant groups with different functionalities, such as phenyl, phenoxy, methyphenyl, methylphenoxy, nitrophenyl, cyanophenoxy, fluorophenoxy, thiophenoxy, and benzoyl groups, have been incorporated into aromatic PHAs.[26] However, only P(3H5PhV)[25,27–29] and poly(3-hydroxy-6-phenylhexanoate)[30] have been biosynthesized as homopolymers, while all other aromatic PHAs have been incorporated as copolymers with P3HB or other aromatic groups.

It is worth mentioning that an aromatic ring pendant group limiting the flexibility of the polymer backbone and thus resulting in a higher T_g is a well-known phenomenon. For example, polystyrene has a drastically higher T_g (100 °C) compared to polyethylene (T_g = –78 °C). In the case of bio-based polyesters, poly(mandelic acid) has a much higher T_g (95–100°C) compared to aliphatic polylactide (T_g = 30–60 °C).[31] Poly(ethylene terephthalate) is a widely used packaging material with a high T_g of 75 °C that contributes to its excellent barrier properties.[32]

The biosynthesis of aromatic PHAs requires specific growth substrates and often metabolic engineering of the microorganism to obtain even low to moderate yields, between 18-40 weight%.[19,27,33,34] This demanding need, coupled with slow reaction kinetics and limited scale, contributes to PHA's current high bio-production costs in general. Polyesters are well-known to be readily accessible by the metal- or organocatalyzed chemical synthesis via ring-opening polymerization (ROP) of cyclic esters (lactones or lactides).[35,36,45,37–44] Utilizing the potential of molecular catalysts' tunability, reaction scalability, and fast reaction kinetics in the typical ROP, PHAs have also been synthesized via the ROP of β-butyrolactone (β-BL), affording iso-enriched P3HB with $P_m \leq 0.85$ (defined as the probability of *meso* linkages between adjacent monomer units) from *rac*-β-BL with various types of catalysts.[46–52] Using discrete yttrium complexes supported by tetradentate, dianionic alkoxy-amino-bis(phenolate) [O^-,N,O,O^-] ligands, Carpentier and co-workers have synthesized highly syndiotactic (*st*-) P3HB with P_r (defined as probability of *rac* linkages between adjacent monomer units) up to 0.95 by the ROP of *rac*-β-BL.[53–59] However, to the best of our knowledge, no chemical synthesis of an aromatic PHA has been reported.

Recognizing an additional, important potential of the chemical route to access *discrete* aromatic PHA homopolymers, which are challenging to accomplish via the biosynthetic pathway (*vide supra*), for fundamental structure-property relationship studies, we undertook this study

aiming to fill in this knowledge gap and uncover properties of new aromatic PHAs. Here, we report the first chemical synthesis of a new, unnatural aromatic PHA homopolymer, poly(3-hydroxy-4-phenylbutyrate) (P3H4PhB) in both *it*- and *st*-stereomicrostructures, as well as aromatic-aliphatic random copolymers with P3HB, P3H4PhB-*co*-P3HB, and with poly(3-hydroxyheptanoate) (P3HHp), P3H4PhB-*co*-P3HHp, and crystalline aliphatic isotactic–aromatic stereoblock copolymer, *it*-P3HB-*b*-*st*-P3H4PhB (Figure 4.1). Most notably, we uncovered that *st*-P3H4PhB and P3H4PhB-*co*-P3HHp exhibit the highest T_g (43 °C) and the highest decomposition temperature (281 °C), respectively, within the PHA family reported to date.

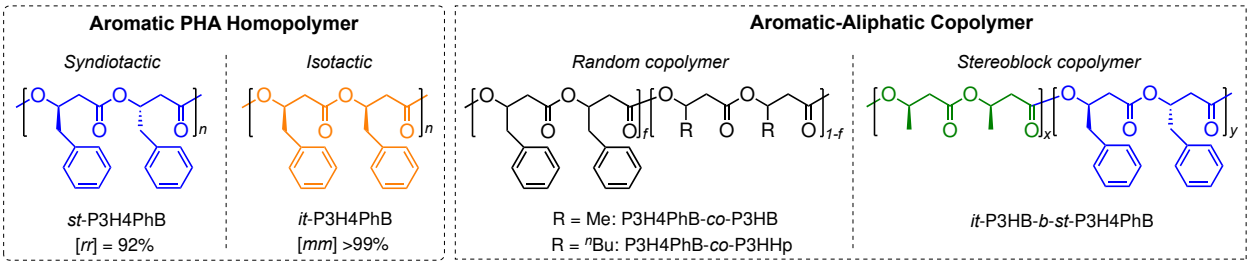

Figure 4.1. Chemical structures of aromatic PHA homopolymer in both *it*- and *st*-forms as well as amorphous random and crystalline stereoblock copolymers synthesized in this work.

4.3. Results and Discussion

Stereoselective ROP Method and Diastereoselective Monomer Synthesis. This work employed the method for the chemical synthesis of highly stereoregular PHAs via the ROP of 8-membered cyclic diolides (8DL^R, where R denotes the two substituents on the diolide ring) we established earlier for PHAs with aliphatic side groups, such as Me, Et, ^{n}Bu.[22,60,61] The most effective precatalysts for the ROP of *rac*-8DL^R were found to be yttrium (Y) and lanthanum (La) catalysts supported by C_2-symmetric *N*,*N*'-bis(salicylidene)cyclohexanediimine (salcy) ligands (Figure 4.2), which exhibit high selectivity of the catalyst structure for *rac*-8DL^R monomers' steric bulk. For example, the most sterically bulky complex of this series with trityl groups on the *ortho*-phenoxy positions on the salcy ligand (i.e., Y **3** or La **4**) exhibits exceptional activity and

stereoselectivity for the ROP of *rac*-8DL^{Me}, affording essentially stereoperfect *it*-P3HB, but it is much less active (and somewhat less stereoselective) towards longer alkyl-substituted diolides including *rac*-8DL^{Et} and *rac*-8DL^{Bu}. On the other hand, less sterically encumbered complex **2** with the cumyl-substituted salcy ligand exhibits high activity and stereoselectivity towards the bulkier monomers, also allowing for efficient copolymerization of monomers with varying steric bulk. This strong catalyst/monomer structure-reactivity relationship has also allowed the diastereoselective polymerization methodology that enables direct polymerizations of diastereomeric mixtures of *rac/meso*-8DL^{Me} at varied *rac/meso* ratios into stereosequenced semi-crystalline isotactic-P3HB-stereoblock-syndiotactic-P3HB (*it*-P3HB-*sb*-*st*-P3HB).[61]

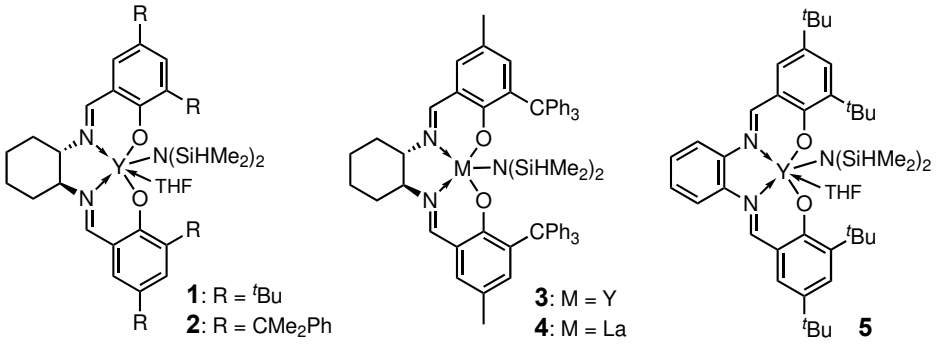

Figure 4.2. Chemical structures of Y and La-based precatalysts (**1**–**4** in racemic form) employed in this work.

The synthesis of the new dibenzyl-substituted diolide monomer, 8DL^{Bn}, followed our previously established general synthetic protocol for *rac*-8DL^{R} and *meso*-8DL^{R},[61] either from dimethyl succinate or dimethyl 2,5-dioxocyclohexane-1,4-dicarboxylate, both of which are commercial reagents. Here we chose the benzyl-substituted diolide rather than the phenyl-substituted one because the second step of the monomer synthesis is a nucleophilic substitution reaction and the benzyl halide, being a better electrophile, enabled this diolide synthesis to follow the established synthetic protocol (Figure 4.3). Interestingly, unlike the aliphatic derivatives where

a typical 2:1 *rac/meso* diastereomeric ratio was retained throughout the synthesis, the decarboxylation of a 1:1 *rac/meso* mixture of the benzyl *β*-ketoester resulted in selective formation of the *trans meso*-dione (90%, vs. 10% *cis rac*-diastereomer, Figure 4.3). This notable *diastereoselectivity* can be attributed to the thermodynamically controlled formation of the *trans*-isomer in the equilibrium tautomerization step of the decarboxylation.[62] The final oxidation to 8DL^{Bn} occurred with retention of stereochemistry thus forming predominately *meso*-8DL^{Bn}, which was confirmed by ^{1}H NMR and also verified by single-crystal X-ray crystallography (Figure 4.3). The overall yield of *meso*-8DL^{Bn} was 35% based on dimethyl succinate, or 54% based on the commercial dicarboxylate intermediate. The corresponding *rac*-8DL^{Bn} was obtained through separation of the *rac*-diastereomer from the *meso*-diasteromer at the dione stage by column chromatography, followed by oxidation of the *rac*-dione with *m*-CPBA (see Supporting Information for details).

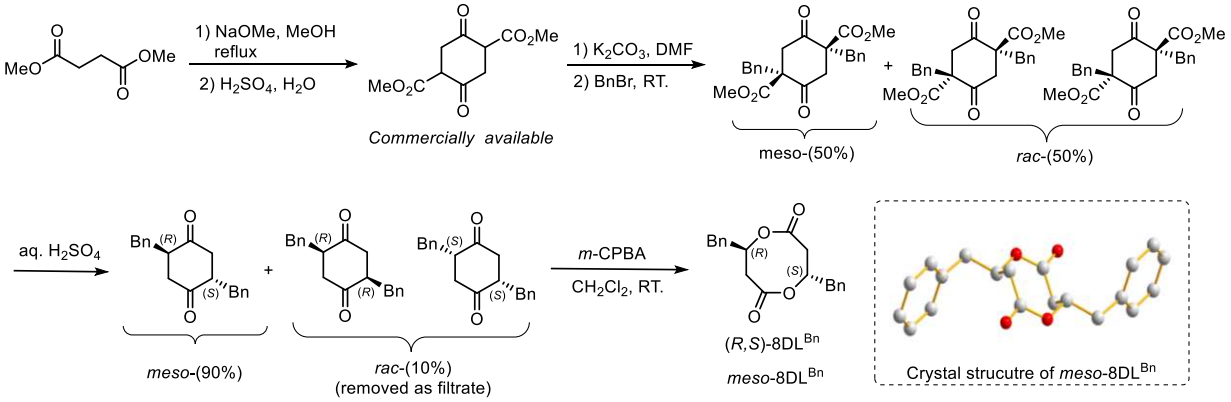

Figure 4.3. Synthetic route for *meso*-8DL^{Bn} and *rac*-8DL^{Bn} from dimethyl succinate. Crystal structure of *meso*-8DL^{Bn} obtained via single-crystal X-ray crystallography.

Stereoselective Polymerization of *Meso*-8DL^{Bn} and *Rac*-8DL^{Bn}. The ROP of *meso*-8DL^{Bn} was performed using five different metal silylamide complexes (Figure 2) varying in salcy ligand sterics [-CMe_3, **1**; -CMe_2Ph, **2**; -CPh_3, **3** and **4**], symmetry (C_2, **1**–**4**; C_{2v}, **5**), and metal centers (Y, **1**–**3**, **5**; La, **4**). These precatalysts, in combination with 1 equiv. of benzyl alcohol (BnOH) that

converts *in situ* the silylamide precatalyst to the alkoxide catalyst, were chosen for this study as they have been shown to be highly active for the syndiospecific polymerization of the parent *meso*-8DL^{Me} in dichloromethane (DCM),[61] affording *st*-P3HB with largely different P_r values ranging from 0.67 by **1**, to 0.72 by **2**, 0.81 by **3**, and 0.92 by **4**. Worth noting here is the innate challenge in producing highly syndiotactic polymers from *meso*-monomers,[63] due to their alternating (*R*,*S*) stereo-sequences in both polymers and monomers. *st*-P3HB is produced by such racemic catalysts because the (*R,R*)-catalyst selectively ring-opens *meso*-8DL^{Me} at the (*S*)-site while the (*S,S*)-catalyst selectively cleaves the ester bond of *meso*-8DL^{Me} at the (*R*)-site, proceeding through the proposed catalyst site-control, coordination-insertion polymerization mechanism.

For the ROP of *meso*-8DL^{Bn} in DCM at room temperature (RT), the least sterically hindered complex **1** of the series mediated rapid polymerization (100% conversion in 15 min, run 1, Table 4.1), yielding P3H4PhB with a modest triad syndiotacticity of [*rr*] = 64%. The more sterically encumbered Y-**2** is also highly active, affording *st*-P3H4PhB with a noticeably higher [*rr*] of 77% (run 2, Table 4.1). The control of the polymerization was demonstrated first by a gradual increase of the P3H4PhB number-average molecular weight (M_n) from medium 52.1 kg mol^{-1} to high 147 kg mol^{-1}, as increasing the [*meso*-8DL^{Bn}]/[**2**] ratio from 100/1 to 800/1, while the resulting PHA's syndiotacticity remained constant (77%) and dispersity ($Đ$) values kept low in a narrow range of 1.11 to 1.19 (runs 2–4, Table 4.1) (Figure S4.18). Second, monitoring the polymerization at [*meso*-8DL^{Bn}]/[**2**]/[BnOH] = 600/1/1 revealed a linear relationship (R^2 = 0.996) between the polymer M_n values and the monomer conversion percentages (black) while maintaining low $Đ$ values throughout the entire conversion range (Figure 4.4). Third, a low-molecular-weight P3H4PhB sample prepared by the [*meso*-8DL^{Bn}]/[**2**] ratio of 20 was analyzed by matrix-assisted laser desorption/ionization time-of-flight mass spectroscopy (MALDI-TOF MS). The mass spectrum

(Figure 4.5) showed no noticeable transesterification side reaction, even when quenched 10 min after the full conversion had already been achieved, as evidenced by the peaks of molecular ions with the spacing between the neighboring peaks being that of the exact (*not half* of the spacing if transesterification occurred) molar mass of the repeat unit, $8DL^{Bn}$ (*m/z* = 324.09). The exclusive chain initiation by BnOH was also evident from the intercept of the linear plot of *m/z* values (y) *vs* the number of $8DL^{Bn}$ repeat units (x): M_{end} = 108.14 (BnO/H) + 23 (Na^+) g mol^{-1} (Figure 4.5). Overall, the above collective results showed that this is a well-controlled polymerization.

Table 4.1. Results of *meso*-$8DL^{Bn}$ polymerization by precatalysts **1**-**5** in DCM [a]

Run no.	Pre-catalyst	[*meso*-$8DL^{Bn}$] /[pre-cat]	Time (min)	Conv. [a] (%)	M_n [b] (kg mol^{-1})	$Đ$ [b] (M_w/M_n)	[*rr*] [c] (%)	T_g [d] (°C)
1	**1**	100/1	15	100	48.5	1.30	64	42
2	**2**	100/1	10	100	52.1	1.11	77	42
3	**2**	400/1	30	100	112	1.15	77	42
4	**2**	800/1	50	100	147	1.19	77	43
5	**3**	100/1	1440	20	[e]	[e]	[e]	[e]
6	**4**	100/1	1400	42	19.8	1.06	79	36
7	**5**	100/1	10	100	64.2	1.08	56	36

Conditions: [*meso*-$8DL^{Bn}$] = 0.77 M (0.100 g in 0.4 mL DCM); RT; [precatalyst]/[BnOH] = 1/1; n.d. = not determined. [a] Monomer conversion measured by ^1H NMR spectra of the quenched solution in benzoic acid/chloroform. [b] Weight-average molecular weight (M_w), number-average molecular weight (M_n), and dispersity ($Đ = M_w/M_n$) values determined by GPC coupled with an 18-angle light scattering detector at 40 °C in chloroform. [c] [*rr*] (syndiotactic triad made up of two adjacent *rac* diads) determined by $^{13}C\{^1H\}$ NMR spectroscopy. [d] T_g values reported from 2nd heating scans measured by DSC with a cooling and second heating rate of 5 °C min^{-1} for all samples (this heating rate used for current low or non-crystalline PHA samples). [e] The polymer by **3** in DCM not completely analyzed due to low yield, and its complete analysis performed on the sample by **3** in toluene (see run 13 in Table 4.2).

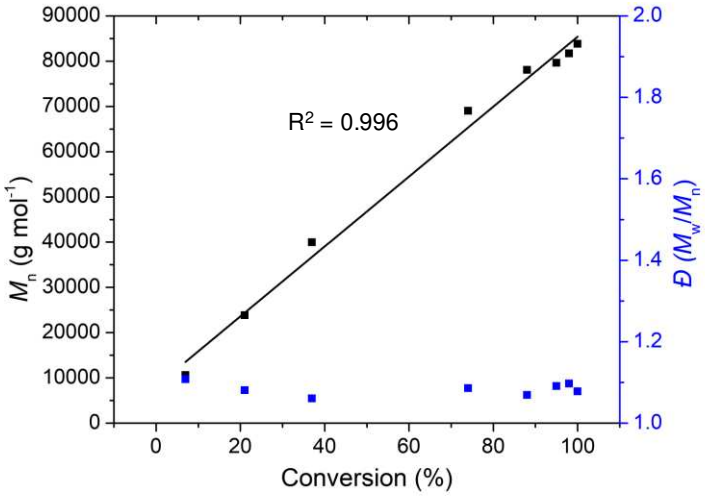

Figure 4.4. Plot of polymer M_n (black) and $Đ$ values (blue, measured by GPC in THF) *vs* conversion percentages (black, measured by ^{1}H NMR) for the ROP of *meso*-8DL^{Bn} by **2** at [*meso*-8DL^{Bn}]/[**2**]/[BnOH] = 600/1/1.

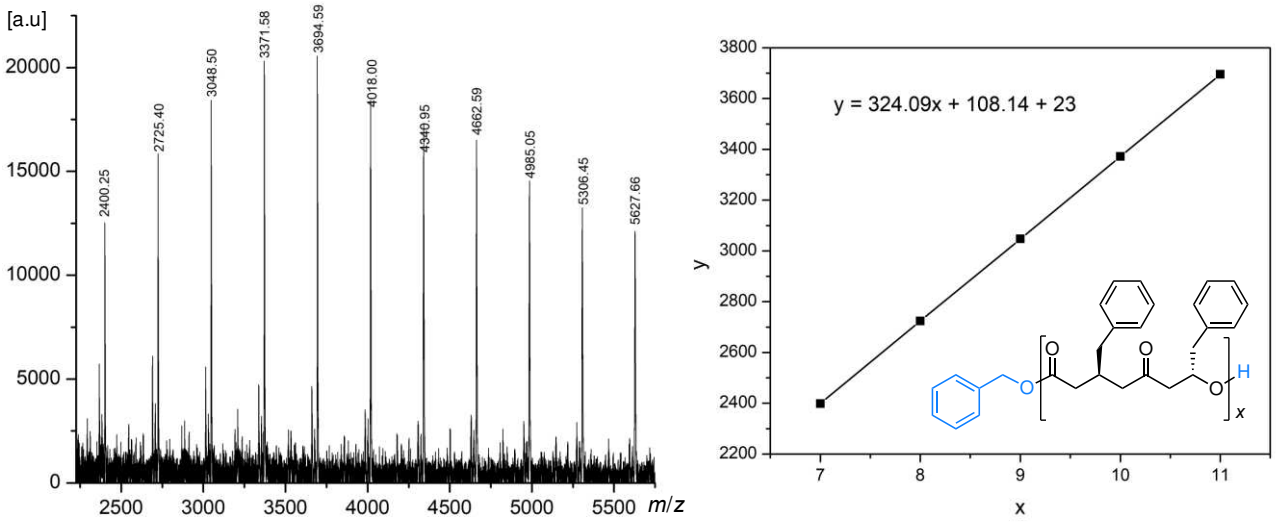

Figure 4.5. MALDI-TOF spectrum of a low-molecular-weight P3H4PhB sample prepared by the [*meso*-8DL^{Bn}]/[**2**] ratio of 20 in DCM and plot of *m/z* values (y) *vs* the number of *meso*-8DL^{Bn} repeat units (x).

The above observation of the enhanced syndioselectivity of *st*-P3H4PhB with increasing catalyst's steric bulk on the *ortho*-positions of the salcy ligand prompted us to investigate next, the most sterically hindered Y-**3**. However, due to steric clash between the bulky monomer and the catalyst, the activity of the ROP by Y-**3** was low, achieving only 20% conversion even after an extended time period of 24 h (run 5, Table 4.1). Switching to La-**4** with the same bulky ligand

framework but a larger metal center (La vs. Y) led to enhanced monomer conversion to 42%. As anticipated, the resulting *st*-P3H4PhB exhibited a higher syndiotacticity of [*rr*] = 79% (run 6, Table 4.1) than the polymer produced by **1** and **2**. Lastly, symmetric salph-based complex **5** is the least selective catalyst of the series; thus, although being highly active (100% conversion in 10 min) and controlled (M_n = 64.2 kg mol^{-1}, $Đ$ = 1.08), it produced the polymer with the lowest syndiotacticity of [*rr*] = 56% (run 7, Table 4.1).

Stereoregulation in syndiospecific polymerization not only depends on catalyst's site-stereoselectivity but also is rather sensitive to polymerization conditions, such as reaction solvent and temperature. Hence, we selected better performing precatalysts **2**–**4** for investigation into potential influences of reaction conditions on their stereoselectivity, and the results of this investigation are summarized in Table 4.2. For complex **2**, simply replacing DCM with THF and toluene resulted in a steady increase in the syndiotacticity of the resulting P3H4PhB from [*rr*] = 77% in DCM to 83% in THF (run 8, Table 4.2) and 92% in toluene (runs 9-10, Table 4.2, Figure 4.6), while maintaining high reactivity with quantitative monomer conversation achieved in 10 min (1 mol% catalyst loading) or 30 min (0.25 mol% catalyst loading). Lowering the temperature from RT to 0 °C drastically decreased the polymerization activity (1 mol% catalyst loading, 50% in 48 h) but the stereoselectivity remained the same ([*rr*] = 92%).

Table 4.2. Results of *meso*-8DL^{Bn} polymerization with different precatalysts and solvents [a]

Run no.	Pre-catalyst	Solvent	[*meso*-8DL^{Bn}] /[pre-cat]	Time (min)	Conv. [a] (%)	M_n [b] (kg mol^{-1})	$Đ$ [b] (M_w/M_n)	[*rr*] [c] (%)	T_g [d] (°C)
8	**2**	THF	100/1	10	100	49.8	1.05	83	40
9	**2**	toluene	100/1	10	100	29.9	1.17	92	36
10	**2**	toluene	400/1	30	100	76.0	1.16	92	43
11	**2**	fluorobenzene	100/1	20	100	26.3	1.14	92	42
12	**2**	fluorobenzene	800/1	50	100	119	1.16	92	43
13	**3**	toluene	100/1	1440	92	18.3	1.05	83	40
14	**4**	toluene	100/1	40	100	15.4	1.06	89	42

Conditions: [*meso*-8DL^{Bn}] = 0.77 M (0.100 g in 0.4 mL solvent); RT; [precatalyst]/[BnOH] = 1/1; [a] Monomer conversion measured by ^{1}H NMR spectra. [b] M_n and $Đ$ values determined by GPC in chloroform. [c] [*rr*] determined by $^{13}C\{^1H\}$ NMR spectroscopy. [d] T_g values reported from 2nd heating scans measured by DSC with a cooling and second heating rate of 5 °C min^{-1} for all samples.

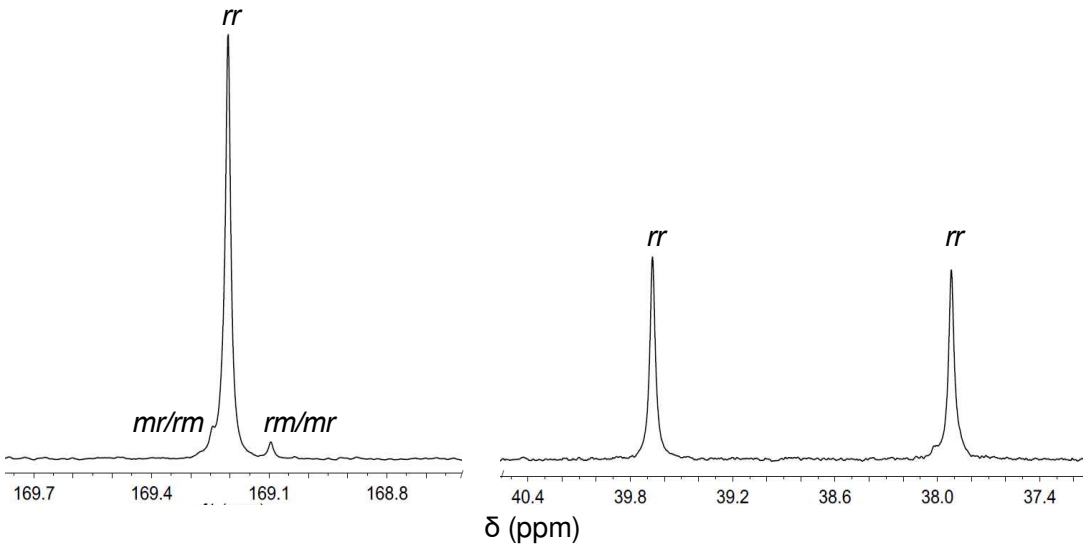

Figure 4.6. Representative ^{13}C NMR spectra ($CDCl_3$) of *st*-P3H4PhB in the carbonyl and (main-chain and side-chain) methylene regions, produced by [*meso*-8DL^{Bn}]/[**2**] = 400/1 in toluene at RT (run 10, Table 4.2).

The polymerization in more polar aromatic solvent fluorobenzene performed similarly to that carried out in toluene, in both activity and syndioselectivity (runs 11-12, Table 4.2). Thus, the ROP with a [*meso*-8DL^{Bn}]/[**2**] ratio of 800/1 in fluorobenzene at RT achieved 100% monomer conversion in 50 min, affording *st*-P3H4PhB with a high syndiotacticity of [*rr*] = 92%, a high molecular weight of M_n = 119 kg mol^{-1}, and a low dispersity of $Đ$ = 1.16. Lastly, performing the polymerization by sterically more hindered complexes **3** and **4** in toluene also brought about higher activity and stereoselectivity relative to that carried out in DCM (runs 13-14 in Table 4.2 vs runs 5-6 in Table 4.1). Overall, there exhibited a strong solvent effect on the syndioselectivity of the polymerization. Using complex **2** as an example, the tacticity trend showed that the syndiotacticity of the resultant P3H4PhB overall decreased as increasing solvent polarity: 92% in toluene (ε = 2.38), 92% in fluorobenzene (ε = 5.55), 83% in THF (ε = 7.58), and 77% in DCM (ε = 8.93). For the current racemic catalyst to produce syndiotactic P3H4PhB from the stereoselective

polymerization of *meso*-8DL^{Bn}, the (*R,R*)-catalyst must selectively ring-open *meso*-8DL^{Me} at either the (*S*)-site or the (*R*)-site, while the (*S,S*)-catalyst must selectively cleave the ester bond of *meso*-8DL^{Me} at the opposite site. In the present system, it appears that the more polar medium lowers the site selectivity, presumably due to a more loosely coordinated catalyst-monomer complex in such a polar medium.

We also investigated the ROP of *rac*-8DL^{Bn} (100 equiv.) with [**2**] + BnOH (1:1) in DCM at RT, achieving full monomer conversion in 20 min. As expected, the resulting polymer is that of the highly isotactic *it*-P3H4PhB with [*mm*] >99%, based on ^{13}C NMR analysis (Figure 4.7).

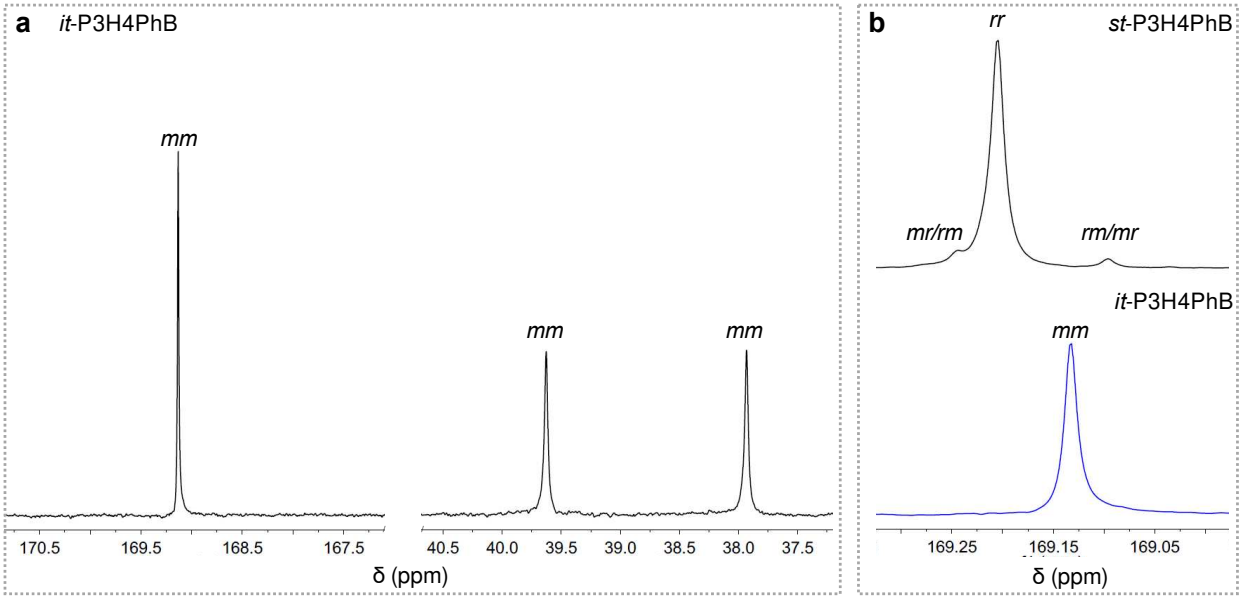

Figure 4.7. (**a**) ^{13}C NMR spectra ($CDCl_3$) of *it*-P3H4PhB in the carbonyl and (main-chain and side-chain) methylene regions, produced by [*rac*-8DL^{Bn}]/[**2**] = 100/1 in DCM at RT. (**b**) Overlay of ^{13}C NMR spectra ($CDCl_3$) of *st*- and *it*-P3H4PhB in the carbonyl region.

Random and Block Copolymerization of *Meso*-8DL^{Bn} with *Rac*-8DL^{R} (R = Me, ^{n}Bu). To produce aromatic and aliphatic PHA copolymers, we first copolymerized *meso*-8DL^{Bn} with 1 and 5 equivalents of *rac*-8DL^{Me} together by **2** in DCM at RT, yielding amorphous, random copolymers P3H4PhB-*co*-P3HB with M_n = 58.9 kg mol^{-1} ($Đ$ = 1.16, run 15, Table 4.3) and M_n = 93.3 kg mol^{-1} ($Đ$ = 1.11, run 16, Table 4.3), respectively. Both monomers were consumed at nearly identical

rates based on kinetic profiling (Figure 4.8**a**), pointing to the formation of a random copolymer. Based on the first-order kinetic plots by catalyst **2**, the ratio of apparent first-order rate constants, k(*rac*-8DL^{Me})/k(*meso*-8DL^{Bn}), was calculated to be 0.81. Next, a well-defined, crystalline isotactic-*b*-syndiotactic stereoblock copolymer, *it*-P3HB-*b*-*st*-P3H4PhB, with M_n = 84.1 kg mol^{-1} and $Đ$ = 1.08 was synthesized in DCM by sequential addition of monomers, first *rac*-8DL^{Me}, followed by *meso*-8DL^{Bn} (run 17, Table 4.3). Excitingly, semi-crystalline tapered block copolymer can also be obtained via one-pot polymerization of *meso*-8DL^{Bn} and *rac*-8DL^{Me} together, using catalyst **4** in toluene (run 18, Table 4.3). This synthesis was made possible by catalyst's diastereoselectivity in toluene, under which conditions *rac*-8DL^{Me} was rapidly consumed in 1 min first, followed by gradual consumption of *meso*-8DL^{Bn} over next 40 min based on kinetic profiling (Figure 4.8**b**). For the copolymerization by catalyst **4**, k(*rac*-8DL^{Me})/k(*meso*-8DL^{Bn}) was calculated to be 175, highlighting large modulation of catalyst structure on the relative reactivity of the comonomers and accordingly the resulting copolymer microstructure.

Table 4.3. Results of copolymerization of *meso*-8DL^{Bn} with *rac*-8DL^{R} (R = Me, ^{n}Bu) [a]

Run no.	Pre-catalyst	Co-M (*rac*-8DL^{R}) (eq.)	[M]/[cat]	Time (min)	Conv. (%)	Co-M [b] Incorp. (%)	M_n (kg mol^{-1})	$Đ$ (M_w/M_n)	T_g [c] (°C)	T_m [c] (°C)
15	**2**	R=Me (1)	100/1	15	100	48	58.9	1.16	28	--
16	**2**	R=Me (5)	100/1	10	100	80	93.3	1.11	14	--
17	**2**	R=Me (1)	100/1	5,40	100	50	84.1	1.08	5, 42	159
18	**4**	R=Me (1)	100/1	40	100	50	18.4	1.22	23	160
19	**2**	R=^{n}Bu (0.2)	800/1	120	100	15.6	117	1.28	33	--
20	**2**	R=^{n}Bu (0.1)	800/1	120	100	8.1	84.0	1.14	37	--

[a] Conditions: RT; [precatalyst]/BnOH = 1/1. Specific conditions for copolymerization runs can be found in the SI. Statistical (runs 15, 16, 19, 20 in DCM) and one-pot block (run 18 in toluene) copolymerizations: *meso*-8DL^{Bn} and comonomer (co-M) ((eq.) of co-M based on 1 eq. of *meso*-8DL^{Bn}) mixed together before polymerization. Sequential block copolymerization (run 17 in toluene): *rac*-8DL^{Me} added first, followed by addition of *rac*-8DL^{Bn}. See footnotes in Table 1 for other explanations. [b] Comonomer incorporation measured by ^{1}H NMR on the isolated copolymers and values deviated slightly from theoretical ones. [c] T_g and T_m measured by DSC from 2nd scans at the heating rate of 5 °C min^{-1}.

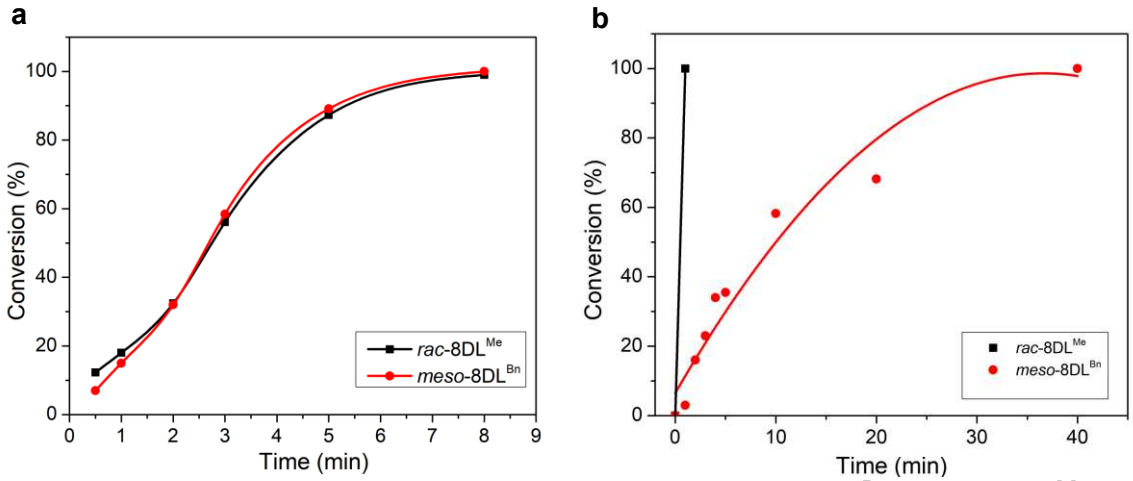

Figure 4.8. Time-conversion plots in the copolymerization of *meso*-8DL^{Bn} and *rac*-8DL^{Me}. (**a**) 1/1 ratio, in DCM, RT, [8DL]/[**2**]/BnOH =100/1/1). (**b**) 1/1 ratio, in toluene, RT, [8DL]/[**4**]/BnOH =100/1/1.

To further modulate properties of aromatic PHA materials derived from *meso*-8DL^{Bn}, particularly ductility (*vide infra*), copolymerization *meso*-8DL^{Bn} with *rac*-8DL^{Bu} was carried out by [**2** + BnOH] with a [8DL]/[**2**] ratio of 800/1 in DCM at RT. Two feed ratios of *meso*-8DL^{Bn} : *rac*-8DL^{Bu}, 5:1 and 10:1, were employed to produce random copolymer P3H4PhB-*co*-P3HHp with *rac*-8DL^{Bu} incorporation of 15.6% (M_n = 117 kg mol^{-1} and $Đ$ = 1.28) and 8.1% (M_n = 84.0 kg mol^{-1} and $Đ$ = 1.14), respectively (runs 19 and 20, Table 4.3). A high-molecular-weight P3H4PhB-*co*-P3HHp sample with M_n = 205 kg mol^{-1}, $Đ$ = 1.21, and 15.6% incorporation of 3HHp units (from *rac*-8DL^{Bu}) for mechanical testing was also prepared from a 3.0-g scale run.

Thermal and mechanical properties of *st*-P3H4PhB and its copolymers with *rac*-8DL^{R}. Polymer thermal properties, including T_g, melting-transition temperature (T_m), and decomposition temperature ($T_{d,5\%}$, defined by the temperature at 5% weight loss) of the P3H4PhB materials with various syndiotacticity values were analyzed by differential scanning calorimetry (DSC) and thermal gravimetric analysis (TGA) measurements. The T_g values measured were in the narrow range of 36 to 43 °C (Tables 4.1 and 4.2) with the syndiotacticity [*rr*] varying largely from low

56% to high 92%, but there was no clear correlation between the T_g and [*rr*] values. To the best of our knowledge, the T_g of 43 °C represents the highest T_g reported to date for any natural PHAs, including those with the rigid aromatic pendant group.[26] However, no T_m was observed for *st*-P3H4PhB, even for samples with a high syndiotacticity of [*rr*] = 92% (Figure 4.9), thus, an amorphous material lacking of crystallinity. On the other hand, the highly isotactic *it*-P3H4PhB ([*mm*] > 99%) displayed an endotherm peak at T_m = 126 °C (ΔH = 18.12 J g^{-1}) on the DSC's first heating scan when the sample was allowed to slowly crystallize from chloroform overnight (8$^+$ hours) (Figure 4.8) but showed no crystallization temperature (T_c) or T_m even with cooling and second heating rates at 1 °C min^{-1} (Figure S4.17), indicating that it can be crystalline but with a very slow crystallization rate. In comparison, highly crystalline P3HB materials produced by ROP of *rac*-8DL^{Me} by **2** ([*mm*] = 94%) and **3** ([*mm*] > 99%) show much higher heat of fusion values with ΔH = 56.5 J g^{-1} and ΔH = 79.3 J g^{-1}, respectively.

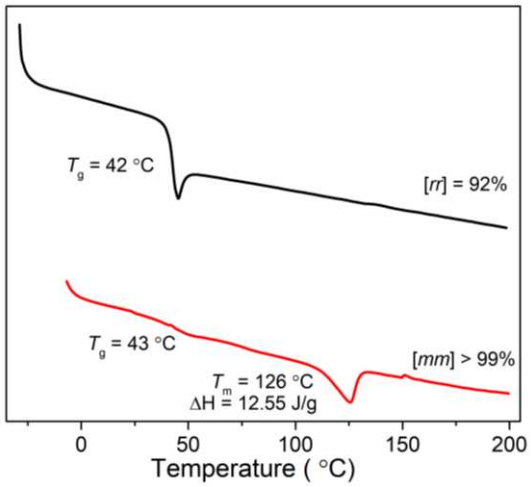

Figure 4.9. DSC curves of *st*-P3H4PhB ([*rr*] = 92%, run 10, Table 4.2; black curve; second heating scan at 5 °C min^{-1}) and *it*-P3H4PhB ([*mm*] > 99%; red curve; first heating scan at 10 °C min^{-1}).

As expected, random copolymers P3H4PhB-*co*-P3HB exhibited no T_m but a single T_g, the value of which depends on the relative ratio of the high T_g (P3H4PhB) and low T_g (P3HB)

compositions: 28 °C for the copolymer with 48% *rac*-8DL^{Me} incorporation and 14 °C for the copolymer with 80% *rac*-8DL^{Me} incorporation (Figure 4.10).[64] Stereoblock copolymer *it*-P3HB-*b*-*st*-P3H4PhB synthesized by the sequential block copolymerization procedure is a semi-crystalline material, exhibiting two T_g values at 5 °C and 42 °C, corresponding to the respective *it*-P3HB and *st*-P3H4PhB domains, as well as a T_c of 101 °C and a T_m of 159 °C, corresponding to the crystalline *it*-P3HB domain (Figure 4.10). In comparison, the stereo-tapered copolymer prepared by the one-pot polymerization of the comonomer mixture exhibited one T_g at 23 °C as well as a T_c at 91 °C and a T_m at 160 °C (Figure 4.10). It is apparent that the crystallinity of the stereo-tapered copolymer prepared by one-pot block copolymerization is much reduced (ΔH = 4.3 J g^{-1}), as compared to the well-defined stereo-diblock copolymer prepared by sequential block copolymerization (ΔH = 17.4 J g^{-1}).

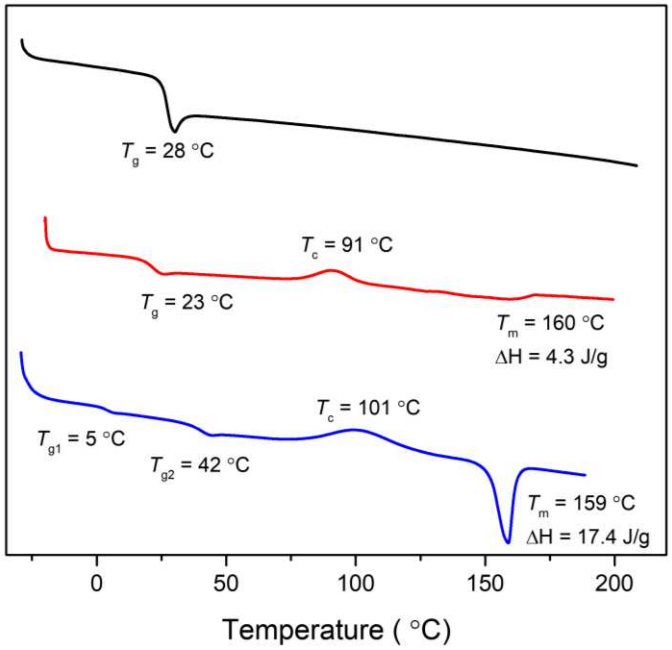

Figure 4.10. DSC curves (second heating scans 5°C min^{-1}) of random copolymer P3H4PhB-*co*-P3HB with 48% *rac*-8DL^{Me} incorporation (black curve, top), stereo-tapered copolymer (red curve, middle), and stereodiblock copolymer *it*-P3HB-*b*-*st*-P3H4PhB (blue curve, bottom).

Aliphatic stereoregular PHA homopolymers and copolymers with medium to high molecular weights prepared in our lab exhibited T_d values typically around 250 °C or lower.[22,60,61] The

current aromatic PHA homopolymer, *st*-P3H4PhB (M_n = 147 kg mol^{-1}, [*rr*] = 77%) shows a similar T_d value of 246 °C (Figure 4.11**a**). Intriguingly, the aromatic-aliphatic PHA random copolymer, P3H4PhB-*co*-P3HHp (M_n = 206 kg mol^{-1}, $Đ$ = 1.13, 9.1% incorporation of 3HHp units), displays a noticeably higher T_d value of 258 °C (Figure S4.24). A further increase in the 3HHp incorporation to 15.6% while maintaining the similar molecular weight (M_n = 205 kg mol^{-1}, $Đ$ = 1.21) gave P3H4PhB-*co*-P3HHp that displays a further enhanced T_d value of 281 °C (Figure 4.11**b**), >30 °C higher than a typical PHA, and a high maximum rate decomposition temperatures (T_{max}) of 303 °C, which, to the best of knowledge, represents the highest degradation temperature recorded to date for the PHA family. In the random copolymer, there are three types of cleavable sites during thermal degradation, continuous 3HPhB and 3HHp homo-sequences and 3HPhB-3HHp hetero-sequences. As the T_d of random copolymer P3HPhB-*co*-P3HHp is noticeably higher than both the homopolymers, the enhanced thermostability is presumably attributed to the PHA backbone containing the hetero-sequences of adjacent bulky butyl and benzyl size-chain groups, but the mechanism of this heightened thermostability has yet to be determined. Nonetheless, the above result, which showed that aromatic-aliphatic PHA copolymers can exhibit higher T_d values than the respective homopolymers, is significant as the relatively low T_d of 250 °C or lower hampers the melt-processability of crystalline PHAs with high T_m values.

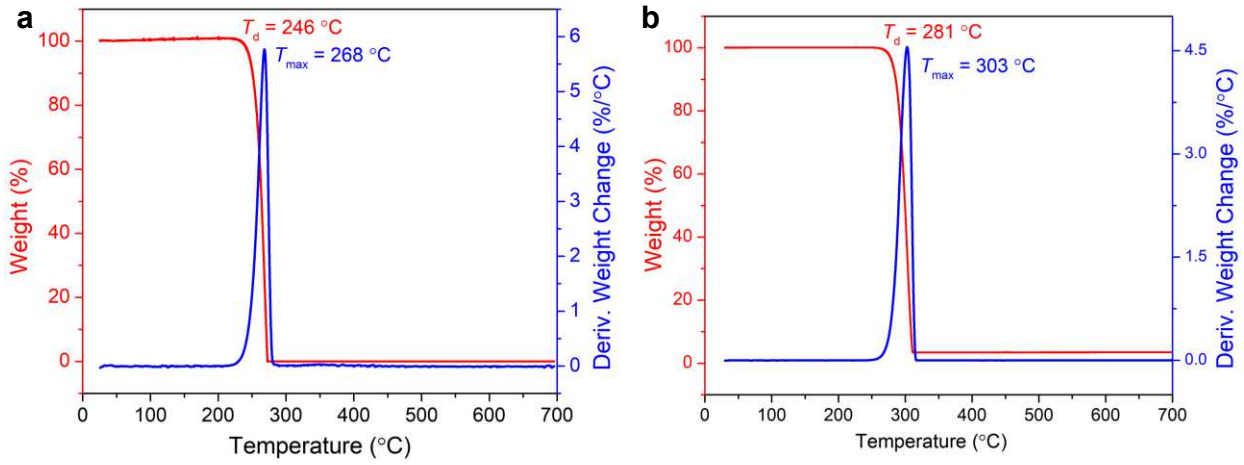

Figure 4.11. TGA curves: (**a**) *st*-P3H4PhB (M_n = 147 kg mol^{-1}, $Đ$ = 1.19, [*rr*] = 92%) and (**b**) random copolymer P3H4PhB-*co*-P3HHp (M_n = 205 kg mol^{-1}, $Đ$ = 1.21, 15.6% incorporation of 3HHp units).

To study the mechanical properties, random copolymer P3H4PhB-*co*-P3HHp (M_n = 205 kg mol^{-1}, $Đ$ = 1.21, 15.6% incorporation of 3HHp units) was prepared in a multi-gram scale using catalyst **2** with 1 eq. BnOH. Tensile testing of dog-bone-shaped P3H4PhB-*co*-P3HHp specimens, prepared by compression molding, showed a ductile material with a high elongation at break of ε_B = 191 ± 16 % (Figure 4.12). This ductile copolymer is still glassy at RT (T_g = 33 °C), thus exhibiting an appreciably high tensile strength of σ_B = 22.7 ± 3.3 MPa and modulus of E = 1.36 ± 0.14 GPa.

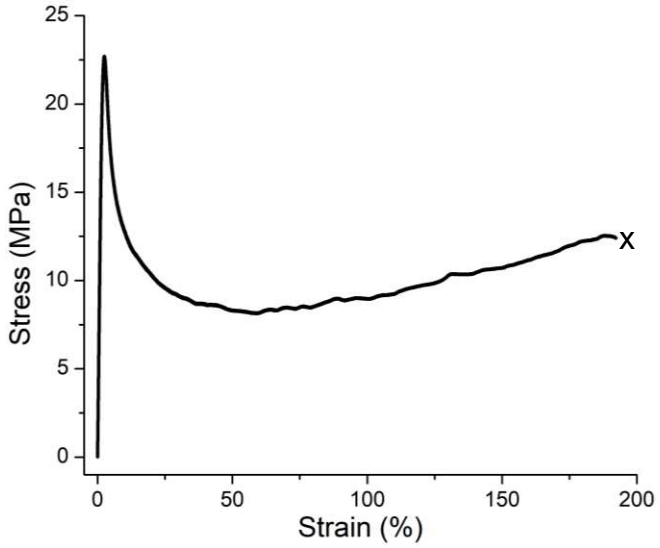

Figure 4.12. Stress-strain curve (10 mm min^{-1}, RT) of random copolymer P3H4PhB-*co*-P3HHp (M_n = 205 kg mol^{-1}, $Đ$ = 1.21, 15.6% incorporation of 3HHp).

4.4. Conclusions

Reported herein is the first catalyzed chemical synthesis of the new, unnatural aromatic PHA stereoregular syndiotactic and isotactic homopolymers, *st*-P3H4PhB and *it*-P3H4PhB, as well as aromatic-aliphatic random/amorphous copolymers P3H4PhB-*co*-P3HB and P3H4PhB-*co*-P3HHp, and crystalline isotactic-syndiotactic stereodiblock copolymer *it*-P3HB-*b*-*st*-P3H4PhB.

On thermal properties, within the natural PHAs reported to date, including those with the rigid aromatic pendant group, *st*-P3H4PhB exhibits the highest T_g (43 °C) and P3H4PhB-*co*-P3HHp displays the highest T_d (281 °C). On mechanical properties, the copolymer with incorporating 15.6% flexible 3HHp units is ductile (ε_B ~ 191%) while maintaining appreciably high strength (σ_B ~ 22.7 MPa) and modulus (E ~ 1.3 GPa) at RT. These results show the thermal and mechanical properties of aromatic PHAs can be readily modulated, thanks to facile tunability of the chemical synthesis route catalyzed by chiral molecular catalysts towards both stereoselective (co)polymerization and monomer structures.

Three notable features of the current monomer and polymerization system enabled the successful chemical synthesis of the above new aromatic PHAs. (1) From the monomer standpoint, the diastereoselectivity in the decarboxylation of the benzyl substituted β-ketoester intermediate allows for the diastereoselective synthesis of *meso*-8DL^{Bn}, thus largely eliminating the need for energy-intensive separation of diastereomers. (2) From the catalyst standpoint, yttrium pre-catalyst **2** supported by the C_2-salcy ligand with the sterically balanced cumyl-substituents is special as it not only exhibits high polymerization activity, but also is both *syndiospecific* in the polymerization of *meso*-8DL^{Bn}, affording *st*-P3H4PhB with high syndiotacticity of [*rr*] = 92% in toluene, and *isospecific* in the polymerization of *rac*-8DL^{Bn}, affording essentially stereo-defect-free *it*-P3H4PhB with [*mm*] > 99% in DCM. The polymerization by this catalyst is also controlled and capable of producing high-molecular-weight polymers, for example, *st*-P3H4PhB with M_n = 147 kg mol^{-1}. (3) From monomer selectivity standpoint, catalysts **2** and **4** can readily copolymerize aromatically and aliphatically substituted diolide monomers to afford either random, stereo-tapered, or stereodiblock copolymers, depending on the copolymerization procedure as well as the catalyst and comonomer employed. The copolymerization by **2** is rapid, achieving quantitative

conversion of comonomers to copolymers with molecular weight up to M_n = 205 kg mol^{-1} (P3H4PhB-*co*-P3HHp with 15.6% 3HHp incorporation). Overall, this work highlights the tunability of the catalyzed chemical synthesis of PHAs by stereoselective ROP of 8DL monomers and its potential for discovering new and interesting PHAs materials currently not available by the biosynthetic pathway.

4.5. References

[1] Geyer, R.; Jambeck, J. R.; Law, K. L. Production, Use, and Fate of All Plastics Ever Made. *Sci. Adv.* **2017**, *3* (7), 25-29. https://doi.org/10.1126/sciadv.1700782

[2] Jambeck, J. R.; Geyer, R.; Wilcox, C.; Siegler, T. R.; Perryman, M.; Andrady, A.; Narayan, R.; Law, K. L. Plastic Waste Inputs from Land into the Ocean. *Science* **2015**, *347*, 768–771. https://doi.org/10.1126/science.1260352

[3] The New Plastics Economy Rethinking the future of plastics, World Economic Forum, United Nations, REF 080116, January 2016. www.ellenmacarthurfoundation.org/publications/ the-newplasticseconomy-rethinking-the-future-of-plastics.

[4] Lamb, J. B.; Willis, B. L.; Fiorenza, E. A.; Couch, C. S.; Howard, R.; Rader, D. N.; True, J. D.; Kelly, L. A.; Ahmad, A.; Jompa, J.; et al. Plastic Waste Associated with Disease on Coral Reefs. *Science* **2018**, *359*, 460–462. https://doi.org/10.1126/science.aar3320

[5] Hong, M.; Chen, E. Y.-X. Future Directions for Sustainable Polymers. *Trends Chem.* **2019**, *1,* 148-151. https://doi.org/10.1016/j.trechm.2019.03.004

[6] Tang, X.; Chen, E. Y.-X. Toward Infinitely Recyclable Plastics Derived from Renewable Cyclic Esters. **2019**, 5, 284–312. https://doi.org/10.1016/j.chempr.2018.10.011

[7] Schneiderman, D. K.; Hillmyer, M. A. 50th Anniversary Perspective: There Is a Great Future in Sustainable Polymers. *Macromolecules* **2017**, *50*, 3733–3749. https://doi.org/10.1021/acs.macromol.7b00293

[8] Zhang, X.; Fevre, M.; Jones, G. O.; Waymouth, R. M. Catalysis as an Enabling Science for Sustainable Polymers. *Chem. Rev.* **2018**, *118*, 839–885. https://doi.org/10.1021/acs.chemrev.7b00329

[9] Hillmyer, M. A. The Promise of Plastics from Plants. *Science* **2017**, *358*, 868–870. https://doi.org/10.1126/science.aao6711

[10] Zhu, Y.; Romain, C.; Williams, C. K. Sustainable Polymers from Renewable Resources. *Nature* **2016**, *540*, 354–362. https://doi.org/10.1038/nature21001

[11] Albertsson, A.-C.; Hakkarainen, M. Designed to Degrade. *Science* **2017**, *358*, 872–873. https://doi.org/10.1126/science.aap8115

[12] Coates, G. W.; Getzler, Y. D. Y. L. Chemical Recycling to Monomer for an Ideal, Circular Polymer Economy. *Nat. Rev. Mater.* **2020**, *5*, 501−516. https://doi.org/10.1038/s41578-020-0190-4

[13] Anjum, A.; Zuber, M.; Zia, K. M.; Noreen, A.; Anjum, M. N.; Tabasum, S. Microbial Production of Polyhydroxyalkanoates (PHAs) and Its Copolymers: A Review of Recent Advancements. *Int. J. Biol. Macromol.* **2016**, *89*, 161–174. https://doi.org/10.1016/j.ijbiomac.2016.04.069

[14] Li, Z.; Yang, J.; Loh, X. J. Polyhydroxyalkanoates: Opening Doors for a Sustainable

Future. *NPG Asia Mater.* **2016**, *8*, e265. https://doi.org/10.1038/am.2016.48

[15] Muhammadi; Shabina; Afzal, M.; Hameed, S. Bacterial Polyhydroxyalkanoates-Eco-Friendly next Generation Plastic: Production, Biocompatibility, Biodegradation, Physical Properties and Applications. *Green Chem. Lett. Rev.* **2015**, *8*, 56–77. https://doi.org/10.1080/17518253.2015.1109715

[16] Laycock, B.; Halley, P.; Pratt, S.; Werker, A.; Lant, P. The Chemomechanical Properties of Microbial Polyhydroxyalkanoates. *Prog. Polym. Sci.* **2013**, *38*, 536–583. https://doi.org/10.1016/j.progpolymsci.2012.06.003

[17] Somleva, M. N.; Peoples, O. P.; Snell, K. D. PHA Bioplastics, Biochemicals, and Energy from Crops. *Plant Biotechnol. J.* **2013**, *11*, 233–252. https://doi.org/10.1111/pbi.12039

[18] Chen, G. A Microbial Polyhydroxyalkanoates (PHA) Based Bio- and Materials Industry. *Chem. Soc. Rev.* **2009**, *38*, 2434–2446. https://doi.org/10.1039/b812677c

[19] Lenz, R. W.; Marchessault, R. H. Bacterial Polyesters: Biosynthesis, Biodegradable Plastics and Biotechnology. *Biomacromolecules* **2005**, *6*, 1–8. https://doi.org/10.1021/bm049700c

[20] Sudesh, K.; Abe, H.; Doi, Y. Synthesis, Structure and Properties of Polyhydroxyalkanoates: Biological Polyesters. *Prog. Polym. Sci.* **2000**, *25*, 1503–1555. https://doi.org/10.1016/S0079-6700(00)00035-6

[21] Müller, H. -M; Seebach, D. Poly(Hydroxyalkanoates): A Fifth Class of Physiologically Important Organic Biopolymers? *Angew. Chem. Int. Ed. English* **1993**, *32*, 477–502. https://doi.org/10.1002/anie.199304771

[22] Tang, X.; Westlie, A. H.; Caporaso, L.; Cavallo, L.; Falivene, L.; Chen, E. Y.-X. Biodegradable Polyhydroxyalkanoates by Stereoselective Copolymerization of Racemic Diolides: Stereocontrol and Polyolefin- Like Properties Research Articles. *Angew. Chem. Int. Ed.* **2020**, *59*, 2–12. https://doi.org/10.1002/anie.201916415

[23] Tullo, A. H. PHA: A Biopolymer Whose Time Has Finally Come. *Chem. Eng. News*. **2019**, *97*, 20-21.

[24] Steinbüchel, A.; Valentin, H. E. Diversity of Bacterial Polyhydroxyalkanoic Acids. *FEMS Microbiol. Lett.* **1995**, *128*, 219–228. https://doi.org/10.1016/0378-1097(95)00125-o

[25] Fritzsche, K.; Lenz, R.; Fuller, R. C. An Unusual Bacterial Polyester with a Phenyl Pendant Group. *Makromol. Chem.* **1990**, *191*, 1957–1965. https://doi.org/10.1002/macp.1990.021910821

[26] Ishii-Hyakutake, M.; Mizuno, S.; Tsuge, T. Biosynthesis and Characteristics of Aromatic Polyhydroxyalkanoates. *Polymers.* **2018**, *10*, 1267. https://doi.org/10.3390/polym10111267

[27] Jae Jun, S.; Choi, M. H.; Yoon, S. C.; Huh, N. E. Cometabolism of ω-Phenylalkanoic Acids with Butyric Acid for Efficient Production of Aromatic Polyesters in *Pseudomonas Putida* BM01. *J. Microbiol. Biotechnol.* **2001**, *11*, 435–442.

[28] Mizuno, S.; Katsumata, S.; Hiroe, A.; Tsuge, T. Biosynthesis and Thermal Characterization of Polyhydroxyalkanoates Bearing Phenyl and Phenylalkyl Side Groups. *Polym. Degrad. Stab.* **2014**, *109*, 379–384. https://doi.org/10.1016/j.polymdegradstab.2014.05.020

[29] Antoun, S.; Grizzi, I.; Lenz, R.W.; Fuller, C. Production of a Chiral Polyester by *Pseudomonas Oleovorans* Grown with 5-Phenyl-2,4-Pentadienoic Acid. *Chirality* **1991**, *3*, 492–494. http://doi.org/10.1002/chir.530030615

[30] Garcia, B.; Olivera, E. R.; Minambres, B.; Fernandez-Valverde, M.; Canedo, L. M.; Prieto, M. A.; Garcia, J. L.; Martinez, M.; Luengo, J. M. Novel Biodegradable Aromatic Plastics from a Bacterial Source. *J. Biol. Chem.* **1999**, *274*, 29228–29241. https://doi.org/10.1074/jbc.274.41.29228

[31] Buchard, A.; Carbery, D. R.; Davidson, M. G.; Ivanova, P. K.; Jeffery, B. J.; Kociok-Köhn, G. I.; Lowe, J. P. Preparation of Stereoregular Isotactic Poly(Mandelic Acid) through Organocatalytic Ring-Opening Polymerization of a Cyclic O-Carboxyanhydride. *Angew. Chem. Int. Ed.* **2014**, *53*, 13858–13861. https://doi.org/10.1002/anie.201407525

[32] De Clerck, K.; Rahier, H.; Van Mele, B.; Kiekens, P. Thermal Properties Relevant to the Processing of PET Fibers. *J. Appl. Polym. Sci.* **2003**, *89,* 3840–3849. https://doi.org/10.1002/app.12543

[33] Steinbüchel, A. Perspectives for Biotechnological Production and Utilization of Biopolymers: Metabolic Engineering of Polyhydroxyalkanoate Biosynthesis Pathways as a Successful Example. *Macromol. Biosci.* **2001**, *1*, 1–24. https://doi.org/10.1002/1616-5195(200101)1:1<1::AID-MABI1>3.0.CO;2-B

[34] Tobin, K. M.; O'Connor, K. E. Polyhydroxyalkanoate Accumulating Diversity of *Pseudomonas* Species Utilising Aromatic Hydrocarbons. *FEMS Microbiol. Lett.* **2005**, *253*, 111–118. https://doi.org/10.1016/j.femsle.2005.09.025

[35] Carpentier, J. F. Rare-Earth Complexes Supported by Tripodal Tetradentate Bis(Phenolate) Ligands: A Privileged Class of Catalysts for Ring-Opening Polymerization of Cyclic Esters. *Organometallics* **2015**, *34*, 4175–4189. https://doi.org/10.1021/acs.organomet.5b00540

[36] Jerome, C.; Lecomte, P. *Recent Developments in Ring-Opening Polymerization of Lactones*; 2012; Vol. 245. https://doi.org/10.1007/978-3-642-27154-0

[37] Carpentier, J. F. Discrete Metal Catalysts for Stereoselective Ring-Opening Polymerization of Chiral Racemic β-Lactones. *Macromol. Rapid Commun.* **2010**, *31*, 1696–1705. https://doi.org/10.1002/marc.201000114

[38] Kiesewetter, M. K.; Shin, E. J.; Hedrick, J. L.; Waymouth, R. M. Organocatalysis: Opportunities and Challenges for Polymer Synthesis. *Macromolecules* **2010**, *43*, 2093–2107. https://doi.org/10.1021/ma9025948

[39] Thomas, C. M. Stereocontrolled Ring-Opening Polymerization of Cyclic Esters: Synthesis of New Polyester Microstructures. *Chem. Soc. Rev.* **2010**, *39*, 165–173. https://doi.org/10.1039/b810065a

[40] Kamber, N. E.; Jeong, W.; Waymouth, R. M.; Pratt, R. C.; Lohmeijer, B. G. G.; Hedrick, J. L. Organocatalytic Ring-Opening Polymerization. *Chem. Rev.* **2007**, *107*, 5813–5840. https://doi.org/10.1021/cr068415b

[41] Dechy-Cabaret, O.; Martin-Vaca, B.; Bourissou, D. Controlled Ring-Opening Polymerization of Lactide and Glycolide. *Chem. Rev.* **2004**, *104*, 6147–6176. https://doi.org/10.1021/cr040002s

[42] Okada, M. Chemical Syntheses of Biodegradable Polymers. *Prog. Polym. Sci.* **2002**, *27*, 87–133. https://doi.org/10.1016/S0079-6700(01)00039-9

[43] Liu, X.; Hua, X.; Cui, D. Copolymerization of Lactide and Cyclic Carbonate via Highly Stereoselective Catalysts to Modulate Copolymer Sequences. *Macromolecules* **2018**, *51*, 930–937. https://doi.org/10.1021/acs.macromol.7b02696

[44] Hua, X.; Liu, X.; Cui, D. Sequence Controlled Copolymerization of Lactide and a Functional Cyclic Carbonate Using Stereoselective Aluminum Catalysts. *Polym. Chem.* **2019**, *10*, 4042–4048. https://doi.org/10.1039/c9py00424f

[45] Mou, Z.; Liu, B.; Liu, X.; Xie, H.; Rong, W.; Li, L.; Li, S.; Cui, D. Efficient and Heteroselective Heteroscorpionate Rare-Earth-Metal Zwitterionic Initiators for ROP of *Rac*-Lactide: Role of σ-Ligand. *Macromolecules* **2014**, *47*, 2233–2241. https://doi.org/10.1021/ma500209t

[46] Wu, B.; Lenz, R. W. Stereoregular Polymerization of [R , S] -3-Butyrolactone Catalyzed by Alumoxane - Monomer Adducts. *Macromolecules* **1998**, *31*, 3473–3477. https://doi.org/10.1021/ma9717698

[47] Jaimes, C.; Arcana, M.; Brethon, A.; Mathieu, A.; Schue, F.; Desimone, J. M. Structure and Morphology of Poly([R,S]-β-Butyrolactone) Synthesized from Aluminoxane Catalyst. *Eur. Polym. J.* **1998**, *34*, 175–185. https://doi.org/10.1016/S0014-3057(97)00106-7

[48] Bloembergen, S.; Holden, D. A.; Bluhm, T. L.; Hamer, G. K.; Marchessault, R. H. Stereoregularity in Synthetic β-Hydroxybutyrate and β-Hydroxyvalerate Homopolyesters. *Macromolecules* **1989**, *22*, 1656–1663. https://doi.org/10.1021/ma00194a027

[49] Spassky, N.; Wisniewski, M.; Pluta, C.; Borgne, A. Le. Highly Stereoelective Polymerization of Rac-(D,L)-Lactide with a Chiral Schiff's Base/Aluminium Alkoxide Initiator. *Macromol. Chem. Phys.* **1996**, *197*, 2627–2637. https://doi.org/10.1002/macp.1996.021970902

[50] Zintl, M.; Molnar, F.; Urban, T.; Bernhart, V.; Preishuber-Pflügl, P.; Rieger, B. Variably Isotactic Poly(Hydroxybutyrate) from Racemic β-Butyrolactone: Microstructure Control by Achiral Chromium(III) Salophen Complexes. *Angew. Chem. Int. Ed.* **2008**, *47*, 3458–3460. https://doi.org/10.1002/anie.200703859

[51] Ajellal, N.; Durieux, G.; Delevoye, L.; Tricot, G.; Dujardin, C.; Thomas, C. M.; Gauvin, R. M. Polymerization of Racemic β-Butyrolactone Using Supported Catalysts: A Simple Access to Isotactic Polymers. *Chem. Commun.* **2010**, *46*, 1032–1034. https://doi.org/10.1039/b923546a

[52] Zhuo, Z.; Zhang, C.; Luo, Y.; Wang, Y.; Yao, Y.; Yuan, D.; Cui, D. Stereo-Selectivity

Switchable ROP of *rac*-β-Butyrolactone Initiated by Salan-Ligated Rare-Earth Metal Amide Complexes: The Key Role of the Substituents on Ligand Frameworks. *Chem. Commun.* **2018**, *54*, 11998–12001. https://doi.org/10.1039/c8cc05469j

[53] Ajellal, N.; Bouyahyi, M.; Amgoune, A.; Thomas, C. M.; Bondon, A.; Pillin, I.; Grohens, Y.; Carpentier, J. F. Syndiotactic-Enriched Poly(3-Hydroxybutyrate)s via Stereoselective Ring-Opening Polymerization of Racemic β-Butyrolactone with Discrete Yttrium Catalysts. *Macromolecules* **2009**, *42*, 987–993. https://doi.org/10.1021/ma8022734

[54] Amgoune, A.; Thomas, C. M.; Ilinca, S.; Roisnel, T.; Carpentier, J. F. Highly Active, Productive, and Syndiospecific Yttrium Initiators for the Polymerization of Racemic β-Butyrolactone. *Angew. Chem. Int. Ed.* **2006**, *45*, 2782–2784. https://doi.org/10.1002/anie.200600058

[55] Bouyahyi, M.; Ajellal, N.; Kirillov, E.; Thomas, C. M.; Carpentier, J. F. Exploring Electronic versus Steric Effects in Stereoselective Ring-Opening Polymerization of Lactide and β-Butyrolactone with Amino-Alkoxy- Bis(Phenolate)-Yttrium Complexes. *Chem. Eur. J.* **2011**, *17*, 1872–1883. https://doi.org/10.1002/chem.201002779

[56] Ligny, R.; Hänninen, M. M.; Guillaume, S. M.; Carpentier, J. F. Highly Syndiotactic or Isotactic Polyhydroxyalkanoates by Ligand-Controlled Yttrium-Catalyzed Stereoselective Ring-Opening Polymerization of Functional Racemic β-Lactones. *Angew. Chem. Int. Ed.* **2017**, *56*, 10388–10393. https://doi.org/10.1002/anie.201704283

[57] Li, H.; Shakaroun, R. M.; Guillaume, S. M.; Carpentier, J. Recent Advances in Metal-Mediated Stereoselective Ring-Opening Polymerization of Functional Cyclic Esters towards Well-Defined Poly(Hydroxy Acid)s: From Stereoselectivity to Sequence-Control. *Chem. Eur. J.* **2020**, *26*, 128–138. https://doi.org/10.1002/chem.201904108

[58] Kricheldorf, H. R.; Eggerstedt, S. Polylactones . 41 . Polymerizations of β-D,L-Butyrolactone with Dialkyltinoxides as Initiators. *Macromolecules* **1997**, *30*, 5693–5697. https://doi.org/10.1021/ma970244c

[59] Kemnitzer, J. E.; Mccarthy, S. P.; Gross, R. A. Syndiospecific Ring-Opening Polymerization of β-Butryolactone to Form Predominantly Syndiotactic Poly(β-Hydroxybutryate) Using Tin(IV) Catalysts. *Macromolecules* **1993**, *26*, 6143–6150. https://doi.org/10.1021/ma00075a001

[60] Tang, X.; Chen, E. Y.-X. Chemical Synthesis of Perfectly Isotactic and High Melting Bacterial Poly(3-Hydroxybutyrate) from Bio-Sourced Racemic Cyclic Diolide. *Nat. Commun.* **2018**, *9*, 2345. https://doi.org/10.1038/s41467-018-04734-3

[61] Tang, X.; Westlie, A. H.; Watson, E. M.; Chen, E. Y.-X. Stereosequenced Crystalline Polyhydroxyalkanoates from Diastereomeric Monomer Mixtures. *Science* **2019**, *366*, 754–758. https://doi.org/10.1126/science.aax8466

[62] Lee, J. Y.; Kim, J.; Lee, K. Y.; Kim, J. N. Diastereoselective Decarboxylation of Cyclopentene Dicarboxylic Acid Derivatives. *J. Phys. Chem. A* **2004**, *108*, 5678–5683. https://doi.org/10.1021/jp0492063

[63] Ovitt, T. M.; Coates, G. W. Stereoselective Ring-Opening Polymerization of Meso -

Lactide : Synthesis of Syndiotactic Poly(Lactic Acid). *J. Am. Chem. Soc.* **1999**, *121*, 4072–4073. https://doi.org/10.1021/ja990088k

[64] Fox, T. G. Influence of Diluent and of Copolymer Composition on the Glass Temperature of a Polymer System. *Bull. Am. Phys. Soc.* **1956**, *1*, 123–125.

Chapter 5

Elastomeric polyhydroxyalkanoates by precision arc.hitecture control via the stereoselective synthesis of isotactic ABA triblock copolymers

5.1. Synopsis

The controlled, chemocatalytic route towards synthetic polyhydroxyalkanoates (PHAs) via the stereoselective ring-opening (ROP) of 8-membered cyclic diolides (8DLR, R = R denotes the two substituents on the ring) has been found to synthesize highly isotactic homopolymers and random copolymers with aliphatic and aromatic substituents as well as tapered or gradient stereodiblock by simultaneous copolymerization of two or more diastereomers, but this stereoselective ROP utility for the synthesis of discrete ABA triblock copolymers (tri-BCPs) has not yet been demonstrated. Here we report that the controlled ROP of *rac*-8DL^{R} (R = Et, Bu) catalyzed by metal-based complexes supported by a suitable C_2-Salen ligand and difunctional initiator followed by addition of *rac*-8DL^{Me} affords isotactic P3HB-*b*-P3HV-*b*-P3HB (when R = Et) or P3HB-*b*-P3HHp-*b*-P3HB (when R = Bu) with high molecular weight, narrow chain dispersity, and high crystallinity. Mechanical analysis of these tri-BCPs show either tough thermoplastics or elastomeric PHA depending on the composition of the midblock. To our knowledge, this is the first example of a tri-BCP containing only 3-hydroxybutyrate repeat units to target biodegradable thermoplastic elastomers.

5.2. Introduction

Polyhydroxyalkanoates (PHAs) are microbially produced polyesters that exhibit biodegradability in ambient environments, and recently have been considered desirable replacements for polyolefin-based packaging materials thanks to their low permeability to gas and moisture.[1–5] The biosynthesis of PHAs by microorganisms is limited in several ways: 1) microbes preferentially produce methyl substituted PHA (P3HB) over other substitutions; 2) microbes

produce exclusively isotactic where all repeat units have R stereo-configuration; and 3) biosynthesis is limited to polycondensation of hydroxy acids where polymers are produced in a step-growth mechanism.[6,7] We recently developed a chemocatalytic route towards PHAs based on the 8-membered cyclic diolide, $8DL^{R}$ (R = Me, Et, ^{n}Bu, Bn) to address these limitations.[8–11] The ring-opening polymerization (ROP) of *rac*-$8DL^{Me}$ results in perfectly isotactic P3HB (as a 1:1 mixture of poly(*R*)3HB and poly(*S*)3HB).[8] We observed the formation of tapered stereoblock copolymers by ROP of the diastereomeric mixture of *rac*-$8DL^{Me}$ and *meso*-$8DL^{Me}$ directly.[9] Increasing the syndiotactic fraction led to a 6 fold increase in ductility. ROP of the mixture of *rac*-$8DL^{Et}$ and *meso*-$8DL^{Me}$ results in a gradient stereodiblock that is highly ductile. In another example, we found that changing the pendant group to longer alkyl (R = Et, ^{n}Bu)[10] or aromatic (R = Bn)[11] substituents can drastically change the thermal and mechanical properties of the resulting isotactic homo- and random copolymers.

More complex polymer architectures, such as block copolymers, remain relatively unexplored for this class of polyesters. Biosynthetic routes can attain "blocky" structures of P3HB blocks and P3HBV blocks (random copolymer) by periodically adding valerate to the bioreactor over time.[12] Blocky P3HB-P3HBV must be fractionated away from the random copolymer and homopolymer products, but displayed two T_m values and different tensile profiles compared to random copolymer alone.[13] Longer chain block copolymer of P3HDD and P3H9D were reportedly produced via periodic feeding of an engineered bacterium, though the DSC, NMR evidence and yield of fractionated block copolymer remained inconclusive in showing block regions.[14]

Thermoplastic elastomers (TPEs) are an important industrial class of polymers as they combine the elasticity of rubbers and thermal reprocessability of plastics. ABA triblock copolymer

(tri-BCP) TPEs typically have a hard (high glass transition (T_g) and/or high melting temperature (T_m)) A blocks and soft (low T_g /rubbery) B blocks. Aliphatic and degradable polyester-based ABA tri-BCP elastomers with bio-based PLA as hard, A blocks and various bio-derived soft block, B polyesters have been investigated by Hillmyer and coworkers.[15–20] Several of these impressive materials show competitive properties in ultimate tensile stress and elongation at breaks to styrenic block polymers.

Chemocatalytic routes to block copolymers containing PHAs present a wide design space and initial studies show promising thermomechanical properties. P3HB via ROP of 4-membered lactone, β-butyrolactone (BL) has been explored, for example the sequential addition or simultaneous polymerization (depending on which catalyst is employed) of BL and the benzyl ester functionalized BL, MLABe, results in diblock copolymers (di-BCP) that can be post-functionalized via deprotection of the benzyl ester moiety to produce amphiphilic block copolymers.[21] ABA tri-BCPs, where the B block is polycarbonate from cyclopentene oxide and CO_2 (poly(cyclohexene carbonate)) (PCHC) and A block is P3HB from BL, have been synthesized using a one-pot copolymerization of cyclopentene oxide, BL, and CO_2 by controlling the CO_2 pressure.[22] Another ABA tri-BCP containing a PHA-based B block and PLA A block was synthesized using a dimethyl substituted benzyl ester PHA, dMMLABz-co-BL, as the midblock. The resulting PLA-*b*-P(dMMLABz-*co*-BL)-*b*-PLA can be deprotected by catalytic hydrogenation of the pendant benzylic ester functions leading to the expected PLA-*b*-P(dMMLA-*co*-BL)-*b*-PLA symmetric tri-BCP.[23] Recently, we reported the synthesis of PHA di-BCP structures from diasteroselective ROP of *meso*-8DL^{Bn} and *rac*-8DL^{Me} to *it*-P3HB-*b*-*st*-P3H4PhB.[11] Further discovery led to the one-pot synthesis of diblock P3HB-*b*-PCL by the catalysts kinetic preference to polymerize *rac*-8DL^{Me} before ε-caprolactone.[24] The resulting di-

BCP was a hard and tough plastic that synergistically combines isotactic P3HB's high modulus with PCL's high ductility. Herein we report the synthesis of ABA tri-BCP PHAs to access PHA-based TPEs. We hypothesized the highly crystalline, high T_m P3HB as a suitable hard A block and the amorphous, low T_g (-30 °C) butyl-substituted PHA, poly(3-hydroxyheptanoate) (P3HHp) as an appropriate soft B block (Figure 5.1). We also investigated an ABA tri-BCP with ethyl-substituted PHA, poly(3-hydroxyvalerate) (P3HV) as a B block (T_g = -19 °C). By moving through method development, tri-BCP formulation, and thermal studies, candidates were selected for scale-up and mechanical study. To our knowledge, this is the first example of discrete highly isotactic, ABA tri-BCP based completely on 3-hydroxybutyrates.

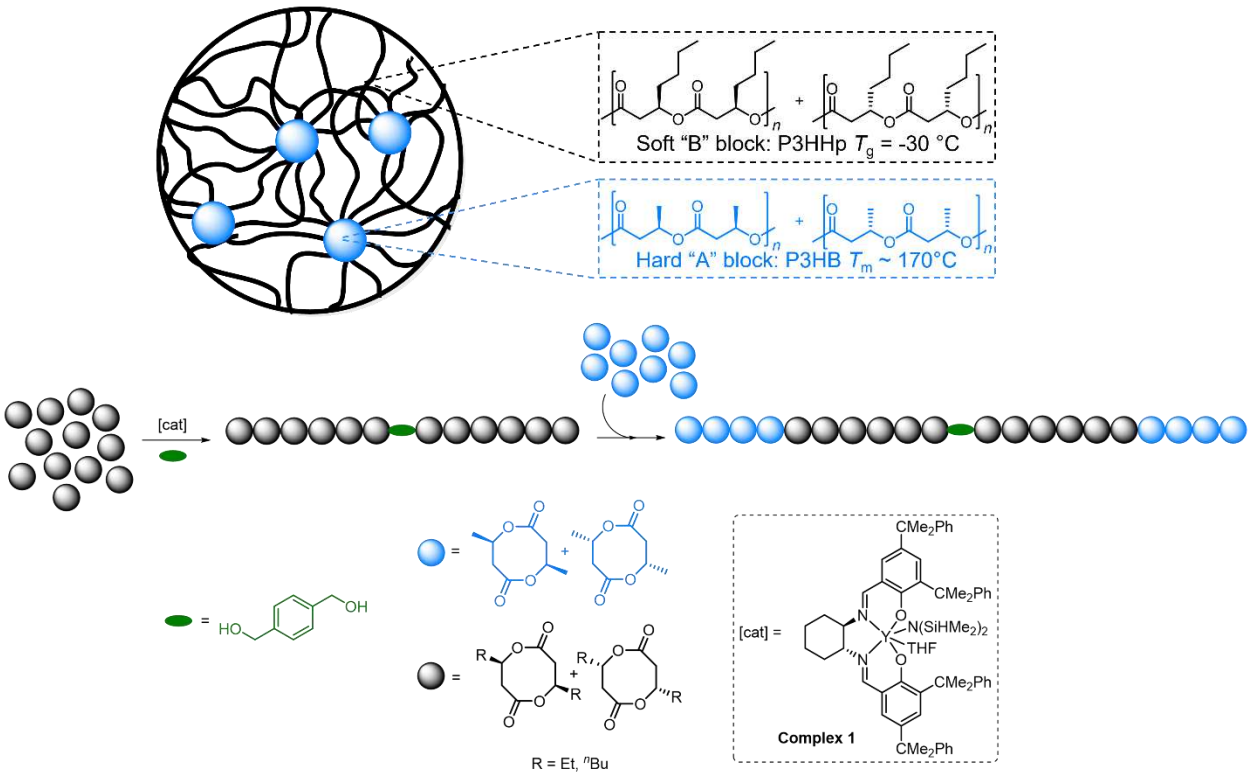

Figure 5.1. Synthesis of isotactic ABA tri-BCP PHAs.

5.3. Results and Discussion

The stereoselective ROP of 8-DL^R (R = alkyl) is catalyzed by racemic yttrium catalysts supported by C_2-symmetric N,N'-bis(salicylidene) cyclohexanediimine (salcy) ligands.[8–10] To maintain both high catalytic activity and high isoselectivity (to retain highly crystalline P3HB blocks) for the 8DLs of contrasting steric bulk, the cumyl-substituted Y complex **1** was chosen for development of tri-BCP synthesis (Figure 5.1). This precatalyst combined with one equivalent of an alcohol (such as benzyl alcohol) initiator undergoes rapid alcoholysis of the Y complex to generate the corresponding Y alkoxide catalyst that produces linear homopolymer, random copolymers, or tapered stereodiblock copolymers. Assuming the system is living, synthesis of multiblock copolymers is also possible though the sequential addition of monomers. For example, ABA tri-BCP would be synthesized via three monomer addition steps: 1) Addition of A, 2) addition of B, 3) addition of A. A more convenient route towards tri-BCPs would be to use a bifunctional initiator, such as 1,4-benzenedimethanol (BDM) where an ABA tri-BCP can be produced in only two monomer addition steps (Figure 5.1).

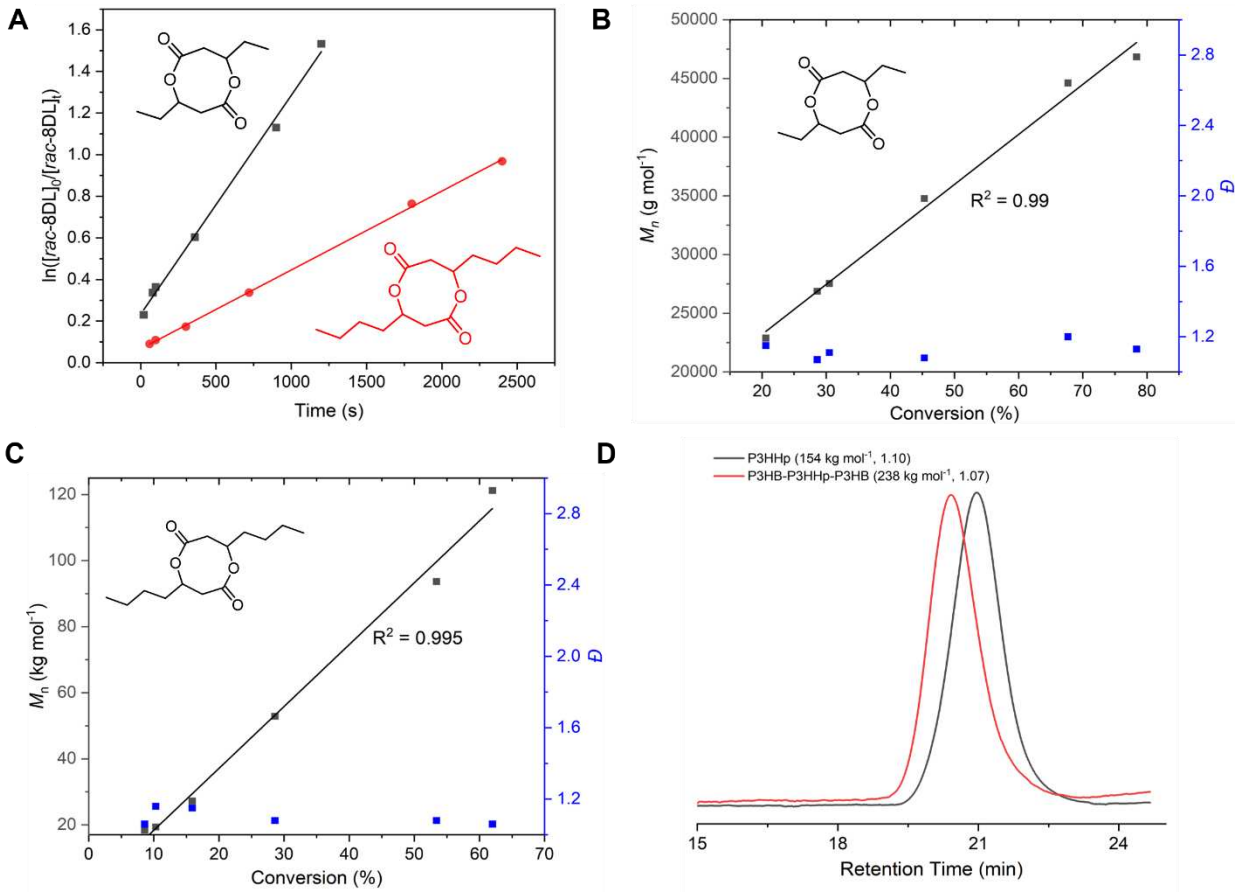

Figure 5.2. ROP of *rac*-8DL^{R} with BDM. A) Linear fit of kinetic data up to 40 minutes ([*rac*-8DL^{R}] = 0.5). Black line = *rac*-8DL^{Et} and red line = *rac*-8DL^{Bu}. B) Linear relationship between conversion and molecular weight of ROP of *rac*-8DL^{Et} ([BDM]$_0$ = 1.22 mM). C) Linear relationship between conversion and molecular weight of ROP of *rac*-8DL^{Bu} ([BDM]$_0$ = 1.22 mM). D) Representative GPC traces. Black curve: P3HHp block M_n = 154 kg mol^{-1}, $Đ$ = 1.10; red curve: P3HB-*b*-P3HHp-*b*-P3HB block, M_n = 238 kg mol^{-1}, $Đ$ = 1.07.

We sought to prepare the tri-BCP with bifunctional initiator and two monomer additions. First, we show that the copolymerization is living and that discrete blocks are produced using this method. One equivalent of BDM is premixed with two equivalents of precatalyst and injected into the B-block monomer, *rac*-8DL^{Et} or *rac*-8DL^{Bu}. After ROP of B-block reaches near 100% conversion, the A-block monomer, *rac*-8DL^{Me}, is added to form a tri-BCP (Figure 5.1). To demonstrate livingness, and thus discrete block formation, kinetic studies were performed: first, the kinetic plot of each B block monomer, *rac*-8DL^{Et} and *rac*-8DL^{Bu}, indicates the polymerization is first order in monomer (Figure 5.2A). As expected, ROP of *rac*-8DL^{Bu} has a slower rate

compared to *rac*-8DL^{Et}, likely due to the longer alkyl substituent sterically hindering the propagating polymer alkoxide chain-end. Second, for both *rac*-8DL^{Et} and *rac*-8DL^{Bu}, a linear relationship between conversion and molecular weight was observed while dispersity (*Đ*) remains below 1.2 throughout ROP (Figure 5.2B and 5.2C). Third, the gel permeation chromatography (GPC) trace is monomodal after polymerization of each block and the observed molecular weight (M_n) is close to that of the theoretical M_n (Figure 5.2D, Figure S5.2-S5.6).

Table 5.1. Synthesis of multi-gram scale tri-BCPs by **1** and BDM.

Run	Midblock	[*rac*-DL] /[I] [a]	$M_{n,P3H(V/HHp)}$ [b] (kg mol^{-1})	$M_{n,P3HB}$ [b] (kg mol^{-1})	$M_{n,total}$ [b] (kg mol^{-1})	% *Midblock*	*Đ* [b] (M_w/M_n)	T_m [c] (°C)	ΔH [c] (J/g)
1	P3HV	600/1	84.4	59.6	144	59	1.14	154	36.6
2	P3HHp	1800/1	154	84	238	64	1.07	154	42.7
3	P3HHp	700/1	172	28	200	86	1.05	145	8.6
4	P3HBHp	800/1	164	66	230	71	1.18	156	24.3

[a]. Conditions: Solvent = DCM, RT [**1**/BDM (I)]=2/1: Run 1: 17.4 mmol 8DL (3.2 g), $V_{solvent}$ = 5.8 mL for midblock, [*rac*-8DL^{Et}]=1M. Run 2: 9.3 mmol 8DL (1.9 g), $V_{solvent}$ = 3.1 mL for midblock, [*rac*-8DL^{Bu}]=1M. Run 3: 6.55 mmol 8DL (1.5 g), $V_{solvent}$ = 4.77 mL for midblock, [*rac*-8DL^{Bu}]=1M. Run 4: 9.2 mmol 8DL (1.8 g), $V_{solvent}$ = 4.6 mL for midblock, [8DL]=1M. [b]. Weight-average molecular weights (M_w), number-average molecular weights (M_n), and dispersity indices ($Đ = M_w/M_n$) determined by GPC coupled with an 18-angle light scattering detector at 40 °C in chloroform. [c]. T_m and ΔH measured by DSC with the cooling and second heating rate of 5 °C/min

With good evidence for the living ROP of *rac*-8DL^{Et} and *rac*-8DL^{Bu} using complex **1** and BDM, synthesis of hard-soft-hard tri-BCPs P3HB-*b*-P3HV-*b*-P3HB and P3HB-*b*-P3HHp-*b*-P3HB, was investigated. At the outset, two tri-BCPs were synthesized at small-scale to test the feasibility of route (Figure 5.1). First, 400 eq. of *rac*-8DL^{Et} was polymerized using **1** and BDM (2/1 ratio) in DCM and allowed to reach full conversion followed by addition of 200 eq. of *rac*-8DL^{Me} (Table S5.3, run 1). Tri-BCP architecture was characterized by an expected molecular weight increase and overall monomodality of GPC traces (Figure 5.2D, Figure S5.2-S5.6). For example, the theoretical M_n of P3HV mid-block was 40 kg mol $^{-1}$ (actual = 60 kg mol^{-1}, *Đ* = 1.07) and the theoretical M_n of resultant tri-BCP was 108 kg mol^{-1} (or 128 kg mol^{-1} based off actual 60

kg mol^{-1} M_n result) (actual = M_n = 150 kg mol^{-1}, $Đ$ = 1.08) (Fig. S5.2). Slightly elevated molecular weights due to initiator efficiencies of 60-70% is common for this ROP system because of high sensitivity to ppm-level protic impurities.[8–11] Tri-BCP with P3HHp midblock was then synthesized by polymerizing 600 eq. of *rac*-8DL^{Bu} using **1** and BDM (2/1 ratio) in DCM and reached 87% conversion before addition of 1200 equiv. of *rac*-8DL^{Me} (Table S5.3, Run 2). *Rac*-8DL^{Me} reached 45% conversion and the polymerization was quenched. Molecular weight increased as expected and monomodality of the GPC trace was maintained (Fig. S5.3).

With good evidence for controlled tri-BCP formation at small scale, the remainder of the analysis presented was performed on specimens produced at the multi-gram scale. By varying the length of the hard end block and the length and flexibility of the soft midblock, design principles (or structure-property relationships) for PHA tri-BCPs can be unveiled (Table 5.1). The carbonyl region of ^{13}C-NMR spectra show discrete block formation, no random copolymer formation, with limited transesterification scrambling the respective blocks (Fig S5.7-S5.8). High isotacticity (P_m > 0.95) can also be seen by analysis of the carbonyl region of ^{13}C-NMR spectra (Figure S5.7-S5.8). Diffusion-Ordered Spectroscopy (DOSY) experiments on a mixture of homopolymers (P3HB and P3HHp) detected two diffusion coefficients related to each respective polymer (Fig. S5.11) whereas the DOSY experiment of the tri-BCPs showed only one diffusion coefficient (Fig. S5.9-S5.10) also supporting the formation of a discrete tri-BCP.

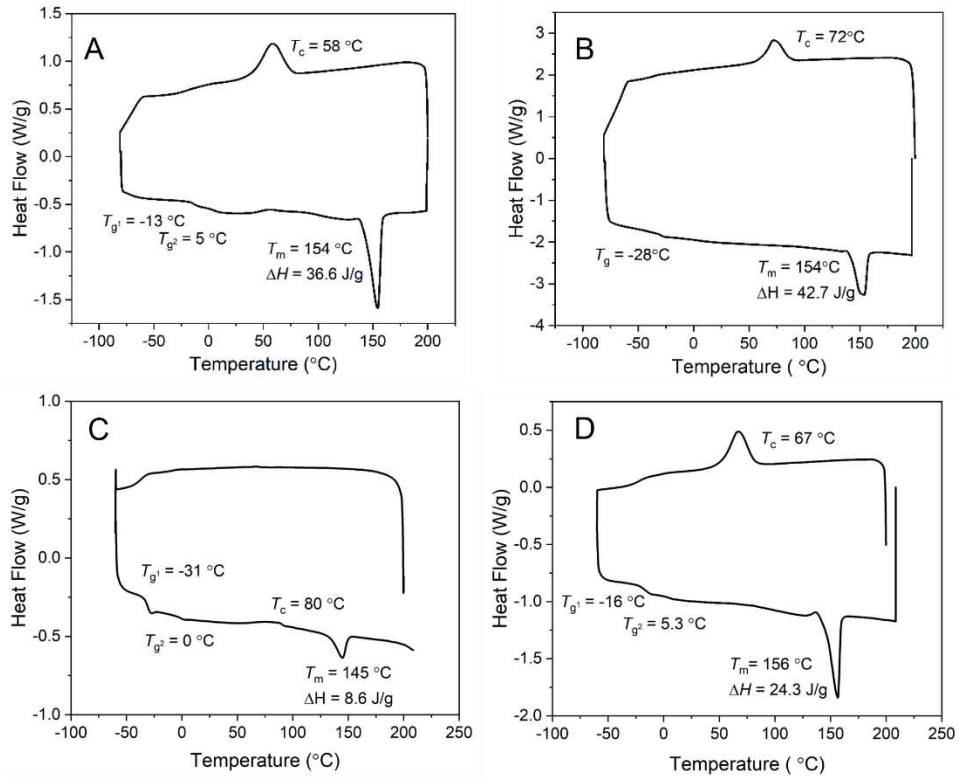

Figure 5.3. Thermal properties of tri-BCP samples. DSC curves (first cooling scan from melt and then second heating scan 5 °C/min) of tri-BCPs produced by **1** (Refer to Table 5.1 for ROP conditions). A) P3HB-*b*-P3HV-*b*-P3HB (59 % midblock). B) P3HB-*b*-P3HHp-*b*-P3HB (64% midblock). C) P3HB-*b*-P3HHp-*b*-P3HB (85% midblock). D) P3HB-*b*-P3HBHp-*b*-P3HB (66% midblock)

Differential scanning calorimetry (DSC) and thermogravimetric analysis (TGA) was used to analyze the thermal properties of synthesized tri-BCPs. The tri-BCP with 59% *rac*-8DL^{Et} showed two T_g values; -11.3 °C for the P3HV block and 8.8 °C for the P3HB block and the cooling and second heating scan revealed a T_c at 58 °C and T_m of 155 °C with an enthalpy of fusion (ΔH) = 36.8 J/g (Figure 5.3) The first heating scan of this material had two T_m values associated with both blocks (Fig S5.1), 74 °C for P3HV (owing to slow crystallization) and 153 °C for P3HB (fast crystallization); only the P3HB block T_m can be seen on the second heating scan (5 °C/min). Unlike the random copolymer where ~40% *rac*-8DL^{Et} resulted in an amorphous material[10], the tri-BCP with 59% *rac*-8DL^{Et} midblock is a highly crystalline material (Figure 5.3A). The tri-BCP copolymer with 64% *rac*-8DL^{Bu} clearly shows one T_g associated with P3HHp block, -28 °C, but

has T_c = 72 °C and T_m = 154 °C with ΔH =42.7 J/g associated with P3HB block (Figure 5.3B). Dynamic mechanical analysis (DMA) of this tri-BCP shows two tan delta peaks at -21.9 °C and 11.8 °C associated with the P3HHp and P3HB blocks, respectively (Fig. S5.18). Importantly, the random copolymer with ~60% *rac*-8DL^{Bu} incorporation is an amorphous, viscous liquid that exhibits a T_g of -30 °C and cannot be made into a film (Fig. S19). Furthermore, increasing the *rac*-8DL^{Bu} midblock to 85% still results in a crystalline material with a small T_c = 80 °C and T_m = 145 °C with ΔH =8.6 J/g (Figure 5.3C). Two T_g values are observed at -31 °C for P3HHp block and 0 °C for P3HB block. To further tune the properties of the midblock, an amorphous, random copolymer midblock was synthesized by copolymerization of *rac*-8DL^{Me} and *rac*-8DL^{Bu} (1/1 feed ratio) using **1** and BDM. The P3HBHp midblock tri-BCP (71% midblock) yielded a material with balanced crystallinity (T_c = 67 °C and T_m = 156 °C with ΔH =24.3 J/g) and the expected two T_g values reflective of the random copolymer midblock (-16 °C) and P3HB hard block (5.3 °C).

The mechanical properties of the tri-BCPs were examined by tensile analysis. Dog bone-shaped specimens were produced via compression molding for stress-strain analysis on an Instron universal testing machine (Figure 5.4). The tri-BCP with 59% *rac*-8DL^{Et} midblock is a tough thermoplastic-like material with ultimate tensile strength (σ) = 26.6 MPa, Young's modulus (E) = 570 MPa, and elongation at break (ε) = 340 % (Figure 5.4, blue). The tri-BCP with 64% *rac*-8DL^{Bu} midblock is an elastomer (no/little yield point) with σ = 7 MPa, E = 0.45 MPa, and ε = 290 % (Figure 5.4, red). Increasing the midblock size to 85% resulted in an even more elastomeric product with σ = 3.9 MPa, E = 1.6 MPa, ε = 380 % (Figure 5.4, blue). With no observable yield point, this material was subjected to hysteresis (20 cycles and strain 50% reached) showing elasticity with 60% elastic recovery (Fig. S5.21). The tri-BCP with random copolymer P3HBHp (50% 3HHp incorp.) midblock is much stronger, exhibiting thermoplastic-like properties with σ = 14.7 MPa, E

= 572 MPa, ε = 250 % (Figure 5.4, green). The effect of tri-BCP architecture is clearly illustrated by comparison of a random copolymer with 40% 3HHp, which shows little strength, but elongates to ~550% (Figure 5.4, black), highlighting the importance of architectural control when synthesizing polymers with desired thermomechanical properties.

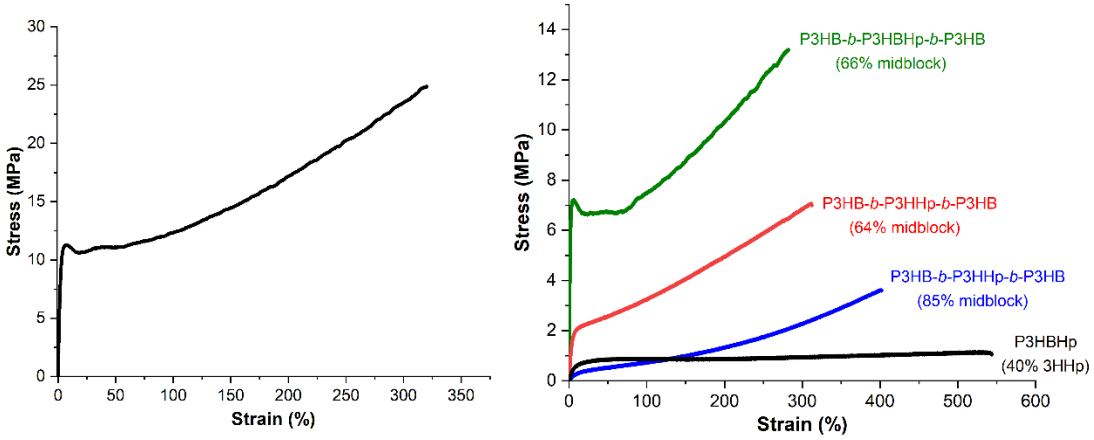

Figure 5.4. Mechanical properties of tri-BCP samples. Left: P3HB-*b*-P3HV-*b*-P3HB (59 % midblock). Right: Black = P3HB-*b*-P3HBHp-*b*-P3HB (66% midblock), Red = P3HB-*b*-P3HHp-*b*-P3HB (64% midblock), Blue = P3HB-*b*-P3HHp-*b*-P3HB (85% midblock), Green = random copolymer P3HB-*co*-P3HHp (40% 3HHp incorp.)

To characterize the phase ordering behavior of our tri-BCPs, we synthesized a series of 4 tri-BCPs (Table S5.9), P3HV midblock 45% (**A**), P3HV midblock 80% (**B**), P3HHp midblock 70% (**C**), P3HHp midblock 78% (**D**) and these samples were sent without prior melt-processing. Initial SAXS at RT indicated no phase separation of these tri-BCPs (Figure 5.5). Once the samples were brought to the melt, no ordering occurred for the tri-BCPs with P3HV midblock, but the tri-BCP with P3HHp midblock showed phase separation in the melt (Figure 5.5). Once the tri-BCPs were cooled to RT, this ordering was lost and unable to be recovered on subsequent heating cycles (Figure S5.20D). A virgin tri-BCP sample with 70% P3HHp sample was prepared and subjected to isothermal holds at 160 °C for 45 min (same conditions the samples experienced during SAXS analysis) and analyzed by both TGA and DSC to determine if decomposition or transesterification

was the cause of disordering (Figure S5.15-S5.17). TGA analysis revealed a 1% loss in weight during the 45 min isothermal hold. This can be attributed to loss of moisture or impurities in the specimen. After an isothermal hold of 45 min at 160 °C, the DSC revealed the T_c increased from 71 °C to 105 °C and ΔH increased from 23.8 to 28.7 J/g. This leads us to the hypothesis that disruptive, breakout crystallization of the hard P3HB phase is causing the loss of ordering. *In-situ* WAXS and ongoing collaboration with the structural analysis team at SLAC is hoping to further understand the cause of this disordering upon cooling.

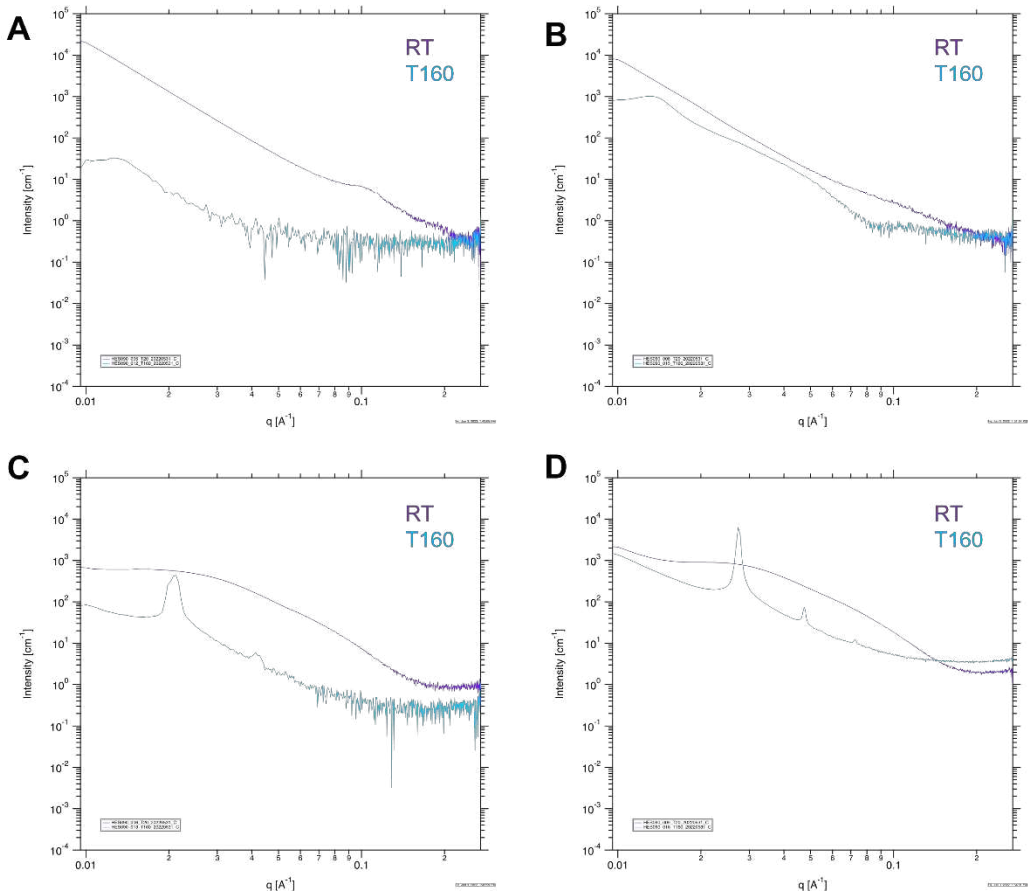

Figure 5.5. SAXS analysis at RT (purple) and in the melt at 160 °C (blue). A) P3HB-*b*-P3HV-*b*-P3HB (45% midblock). B) P3HB-*b*-P3HV-*b*-P3HB (80% midblock). C) P3HB-*b*-P3HHp-*b*-P3HB (70% midblock). D) P3HB-*b*-P3HHp-*b*-P3HB (77% midblock)

5.4. Conclusions

Reported herein is the first synthesis of discrete, high molecular weight, isotactic ABA tri-BCP PHAs with P3HB as the hard block and three different midblocks: P3HV, P3HHp, and P3HBHp. The stereoselective ROP of *rac*-8DL^{R} (R = Et and Bu) by **1** and difunctional initiator BDM is well-controlled, characterized as living and formation of tri-BCP occurs in only two monomer addition steps. Midblock % of greater than 50% show high crystallinity with T_m ~ 160 °C.

P3HB-*b*-P3HV-*b*-P3HB and P3HB-*b*-P3HBHp-*b*-P3HB are crystalline, strong, and tough thermoplastics. Phase separation in the melt is not visible for P3HB-*b*-P3HV-*b*-P3HB specimens, and the most likely explanation for this is the amorphous regions of the semi-crystalline hard P3HB block blending with the amorphous region of the midblock. P3HB-*b*-P3HHp-*b*-P3HB is elastomeric, exhibits strain-hardening with no visible yield point. SAXS characterization showed that ordering occurs in the melt for this tri-BCP but is seemingly lost upon cooling due to disruptive/breakout crystallization of P3HB. Further experiments including *in-situ* WAXS is ongoing.

5.5. References

[1] B. Laycock, P. Halley, S. Pratt, A. Werker, P. Lant, *Prog. Polym. Sci.* **2013**, *38*, 536–583.

[2] Y. Wang, J. Yin, G.-Q. Chen, *Curr. Opin. Biotechnol.* **2014**, *30*, 59–65.

[3] H. -M Müller, D. Seebach, *Angew. Chem. Int. Ed.* **1993**, *32*, 477–502.

[4] A. Anjum, M. Zuber, K. M. Zia, A. Noreen, M. N. Anjum, S. Tabasum, *Int. J. Biol. Macromol.* **2016**, *89*, 161–174.

[5] G.-Q. Chen, *Chem. Soc. Rev.* **2009**, *38*, 2434–2446.

[6] A. Anjum, M. Zuber, K. M. Zia, A. Noreen, M. N. Anjum, S. Tabasum, *Int. J. Biol. Macromol.* **2016**, *89*, 161–174.

[7] A. Arumugam, *Encycl. Renew. Sustain. Mater.* **2020**, *2*, 236–252.

[8] X. Tang, E. Y. X. Chen, *Nat. Commun.* **2018**, *9*, 2345.

[9] X. Tang, A. H. Westlie, E. M. Watson, E. Y.-X. Chen, *Science (80-.).* **2019**, *366*, 754–758.

[10] X. Tang, A. H. Westlie, L. Caporaso, L. Cavallo, L. Falivene, E. Y.-X. Chen, *Angew. Chem. Int. Ed.* **2020**, *59*, 2–12.

[11] A. H. Westlie, E. Y.-X. Chen, *Macromolecules* **2020**, *53*, 9906–9915.

[12] E. N. Pederson, C. W. J. McChalicher, F. Srienc, *Biomacromolecules* **2006**, *7*, 1904–1911.

[13] C. W. J. McChalicher, F. Srienc, *J. Biotechnol.* **2007**, *132*, 296–302.

[14] S. Li, L. Cai, L. Wu, G. Zeng, J. Chen, Q. Wu, G.-Q. Chen, *Biomacromolecules* **2014**, *15*, 2310–2319.

[15] C. L. Wanamaker, L. E. O'Leary, N. A. Lynd, M. A. Hillmeyer, W. B. Tolman, *Biomacromolecules* **2007**, *8*, 3634–3640.

[16] C. L. Wanamaker, M. J. Bluemle, L. M. Pitet, L. E. O. Leary, W. B. Tolman, M. A. Hillmyer, *Biomacromolecules* **2009**, *10*, 2904.

[17] M. T. Martello, M. A. Hillmyer, *Macromolecules* **2011**, *44*, 8537–8545.

[18] D. K. Schneiderman, E. M. Hill, M. T. Martello, M. A. Hillmyer, *Polym. Chem.* **2015**, *6*, 3641–3651.

[19] A. Watts, N. Kurokawa, M. A. Hillmyer, *Biomacromolecules* **2017**, *18*, 1845–1854.

[20] S. Liffland, M. A. Hillmyer, *Macromolecules* **2021**, *54*, 9327–9340.

[21] C. G. Jaffredo, J.-F. Carpentier, S. M. Guillaume, *Macromolecules* **2013**, *46*, 6765–6776.

[22] S. Kernbichl, M. Reiter, F. Adams, S. Vagin, B. Rieger, *J. Am. Chem. Scoiety* **2017**, *139*, 6787–6790.

[23] O. Coulembier, L. Mespouille, J. L. Hedrick, R. M. Waymouth, P. Dubois, *Macromolecules* **2006**, *39*, 4001–4008.

[24] X. Tang, C. Shi, Z. Zhang, E. Y.-X. Chen, *Macromolecules* **2021**, *54*, 9401–9409.

Chapter 6

Conclusions and Outlook

Materials endowed with biodegradability as an end-of-life option for applications where collection and sorting is either undesirable or impossible continues to be an important target for polymer chemists. Synthesizing biodegradable polymers with the required thermal and mechanical properties for its application and processibility is an ongoing challenge and this dissertation work has highlighted various examples where tunability in properties is enabled by a chemocatalytic route to alter the properties and thus applications of biodegradable PHAs.

Tremendous advances in chemocatalytic routes towards synthetic PHAs have offered access to highly isotactic and/or syndiotactic P3HB through the stereoselective ROP of β-BL and 8DL^{Me} by various organometallic complexes. The detailed mechanistic investigations and in-depth study of ligand symmetry, sterics, and electronics has allowed the precision synthesis of novel homopolymer PHAs as well as more complex random, block, and stereosequenced PHA copolymers typically inaccessible by biological methods.

To continue advancing the catalyzed chemical synthesis of PHAs, we further developed the synthesis of PHAs using the *rac*-8DL^{R} (R = Me, Et, Bu) monomer platform derived from the bio-sourced succinate. Stereoselective ROP of *rac*-8DL^{R} using a class of racemic metal-based catalysts supported by the C2-salcy ligand yields highly isotactic PHAs including P3HB (R = Me) with P_m or [*mm*] > 99% and T_m up to 171 ºC, P3HV (R = Et) with P_m = 0.97 ([*mm*] = 95%) and T_m = 108 ºC, and P3HHp (R = Bu) with P_m = 0.97 ([*mm*] = 94%) and T_m = 50.8 °C (T_g = −34.3 °C). Like the syndioselective ROP of β-BL, the steric bulk on the catalyst ligand is crucial in endowing both activity and stereoselectivity in ROP of *rac*-8DL^{R}. For the small *rac*-8DL^{Me}, the sterically most demanding catalyst with bulky trityl groups exhibits extremely high activity and isoselectivity,

leading to purely isotactic, high MW (M_n = 154 kDa) P3HB. However, this sterically encumbered catalyst exhibits very low activity for the ROP of *rac*-8DL^{Et} and *rac*-8DL^{Bu}. The less-bulky cumyl-substituted catalyst exhibits both high activity and isoselectivity for these two bulkier monomers. For example, P3HHp with P_m = 0.97 ([*mm*] = 94%) and M_n = 140 kDa ($Đ$ = 1.19) can be rapidly produced by the cumyl-substituted catalyst. The copolymerization of *rac*-8DL^{Me} with *rac*-8DL^{Et} or *rac*-8DL^{Bu} using the cumyl-substituted complex results in high molecular weight, random copolymers with controlled incorporation of each monomer. The thermal and mechanical properties of these random copolymers can be tuned based on the % incorporation of *rac*-8DL^{Et} (for P3HBV) and *rac*-8DL^{Bu} (for P3HBHp). The T_m of P3HBV or P3HBHp decreases with the increase of *rac*-8DL^{Et} or *rac*-8DL^{Bu} incorporation and copolymers with low % incorporation of *rac*-8DL^{Et} or *rac*-8DL^{Bu} are stiff, brittle materials while increasing these monomer % incorporation results in much more ductile and tough plastics. Excitingly, the precision synthesis of PHA copolymers with targeted incorporation of the flexible monomer unit (~20%) produces PHA copolymers that are polyolefin-like thermally and mechanically. These aliphatic comonomers are capable of being incorporated into biologically-derived PHA, although in the case of 3HHp, it is very uncommon. We then sought to target a PHA with an unnatural microstructure, in both tacticity and pendant structure identity.

Further derivatization of 8DL^{R} platform from aliphatic pendant groups to aromatic pendant groups allowed access to a new, unnatural benzyl-substituted PHA homopolymer with controlled tacticity as well as its aromatic-aliphatic random and block copolymers. Diastereoselective synthesis of *meso*-8DL^{Bn} via the diastereoselective decarboxylation of the benzyl-substituted β-ketoester intermediate eliminates the requirement to separate the diastereomers and using the highly active cumyl-substituted catalyst allows for syndiospecific ROP of *meso*-8DL^{Bn} to highly

syndiotactic ([*rr*] = 92%) P3H4PhB. Judicious selection of catalysts allows for the formation of either random, stereo-tapered, or stereodiblock copolymers. Owing to the rigidity of the benzyl pendant group, syndiotactic P3H4PhB exhibits a T_g above RT (43 °C). The resulting random copolymer when copolymerizing *meso*-8DL^{Bn} and *rac*-8DL^{Bu} (P3H4PhB-co-P3HHp) has a ~30 °C increase in T_d (281 °C) compared to most PHAs (~250 °C) and the copolymer with 15.6% 3HHp units is a tough and ductile material (ε_B ~ 191% and σ_B ~ 22.7 MPa) with high modulus (E ~ 1.3 GPa). Overall, this work highlights the tunability of the catalyzed chemical synthesis of PHAs to discover new and interesting PHA materials currently not accessible via biological methods. This initial exploration into "unnatural" PHA materials inevitably led us to designing new PHA architectures via our precision chemical synthesis.

Tuning polymer microstructure by altering the tacticity or pendant group structure is one way we have altered PHA materials properties, but a rich and unexplored area of discovery is changing PHAs architecture to more complex topologies and block copolymers. The first synthesis of discrete, high molecular weight, isotactic ABA tri-BCP PHAs with P3HB as the hard block and three different midblocks: P3HV, P3HHp, and P3HBHp was investigated. The stereoselective ROP of *rac*-8DL^{R} (R = Et and Bu) by **1** and difunctional initiator BDM is well-controlled, characterized as living and formation of tri-BCP occurs in only two monomer addition steps. P3HB-*b*-P3HV-*b*-P3HB and P3HB-*b*-P3HBHp-*b*-P3HB are crystalline (midblock % of greater than 50% show high crystallinity with T_m ~ 160 °C), strong, and tough thermoplastics. Phase separation in the melt is not visible for P3HB-*b*-P3HV-*b*-P3HB specimens, and the most likely explanation for this is the amorphous regions of the semi-crystalline hard P3HB block blending with the amorphous region of the midblock. P3HB-*b*-P3HHp-*b*-P3HB is elastomeric, exhibits strain-hardening with no visible yield point. SAXS characterization showed that ordering occurs

in the melt for this tri-BCP but is seemingly lost upon cooling due to disruptive/breakout crystallization of P3HB. Further experiments including *in-situ* WAXS is ongoing.

In general, the work presented in this dissertation has advanced the scope of PHA properties. We've produced PHAs with polyolefin-like properties by incorporating a controlled amount of aliphatic comonomers. We've explored the effects of aromatic substituents in this ROP system and produced glassy homopolymers at RT. We've synthesized elastomeric PHAs with high crystallinity from the first synthesis of discrete ABA tri-BCPs. Yet many opportunities in this space remain. First is concerning the currently energy intensive four-step synthesis of $8DL^R$ monomers from succinate. The use of several undesirable reagents (such as excess alkyl halide and oxidizing reagent), overall low yield (~40%), and challenge to scale up inhibits broad implementation of this methodology. Discovery of a more economical and environmentally benign synthesis of this highly valuable monomer is imperative. The development of a chemocatalytic or biocatalytic route to 8DL from the depolymerization of PHAs would be a desirable solution to this problem and would also close the "monomer-polymer-monomer" loop for this class of polyesters and ultimately elevate PHAs to a circular materials economy.

Presently, PHAs suffer from low thermostability towards melt-processing, where decomposition via crotonization can occur while in the melt under compression-molding conditions. Discovering PHA materials with the desired robust mechanical properties coupled with increased thermostability is a major challenge that still needs to be addressed. Designing PHAs with new topologies, such as cyclic, is one solution to increase thermostability by removing the chain-ends of the polymer. Adding an α-substitution could increase PHAs thermostability by shutting down the crotonization that occurs via abstraction of the acidic α-proton.

Finally, synthetic PHAs are currently limited to properties of thermoplastics, elastomers, and thermoplastic elastomers. Designing PHAs to display higher performance properties, such as reprocessable thermosets and adhesives, will broaden the PHA-based materials applicability and thus implementation.

Society is not ready to part with plastics, and in most cases plastic is the cheapest, most robust, lightweight, and durable material option. As fundamental discovery and industrial application of circular plastics begins to take hold, there are several applications where a recycling infrastructure (whether chemical or mechanical) won't have an effect on mitigating plastic waste or capturing material value. Materials that are contaminated by food or human waste like ketchup packets or diapers, materials often lost to the environment like fishery products and seed coatings, or materials essential to our health and safety like wipes or disposable syringes – these are all examples of plastic applications that are important but require creative solutions to ensure we don't just keep accumulating plastic waste. Ideally, these materials can serve their purpose and upon disposal, degrade safely in our landfills without outside intervention. The materials listed above have vastly different performance requirements, and this dissertation work has shown that PHAs as a polymer class can be designed and synthesized for many different applications. This tunable, high precision, chemocatalytic synthetic platform of PHAs has increased the scope of material properties of this diverse polyester class, and I believe this is just the beginning.

Appendix A

Experimental Details and Supporting Information for Chapter 3

A.1. Materials and Instruments.

All syntheses and manipulations of air- and moisture-sensitive chemicals and materials were carried out in flame-dried Schlenk-type glassware on a dual-manifold Schlenk line or in an inert gas (Ar or N_2)-filled glovebox. NMR-scale reactions were conducted in Teflon-valve-sealed J. Young-type NMR tubes. HPLC-grade organic solvents were first sparged extensively with nitrogen during filling 20 L solvent reservoirs and then dried by passage through activated alumina (for dichloromethane, DCM) followed by passage through Q-5 supported copper catalyst (for toluene and hexanes) stainless steel columns. Benzene-d_6 was dried over sodium/potassium alloy and filtered, whereas CD_2Cl_2 and $CDCl_3$ were dried over CaH_2, vacuum-distilled and stored activated Davison 4 Å molecular sieves. NMR spectra were recorded on a Varian Inova or Bruker AV-III 400 MHz spectrometer (400 MHz, ^{1}H; 100 MHz, ^{13}C). Chemical shifts for ^{1}H and ^{13}C spectra were referenced to internal solvent resonances and are reported as parts per million relative to $SiMe_4$.

Yttrium chloride, lanthanum chloride, and 1,1,3,3-tetramethyldisilazane were purchased from Sigma-Aldrich Chemical Co. and used as received. Benzyl alcohol was purchased from Alfa Aesar Chemical Co., purified by distillation over CaH_2, and stored over activated Davison 4 Å molecular sieves. Dimethyl succinate, sodium methoxide, and 3-chloroperoxybenzoic acid (mCPBA, 70-75%) were purchased from Fisher Scientific Co. and used as received. Iodomethane, iodoethane, and iodobutane was purchased from Alfa Aesar Chemical Co. and used as received. The following complexes or compounds were prepared according to their respective literature procedures: $Y[N(SiHMe_2)_2]_3(THF)_2$, $La[N(SiHMe_2)_2]_3(THF)_2$,[1] racemic

yttrium complexes **1**–**5** and **6**,[2] *rac*-4,8-dimethyldioxocane-2,6-dione (*rac*-8DL^{Me}), *rac*-4,8-diethyldioxocane-2,6-dione (*rac*-8DL^{Et}), and *rac*-4,8-dibutyldioxocane-2,6-dione (*rac*-8DL^{Bu}).[2a, 2b, 3]

General Polymerization Procedures. Polymerizations were performed in 5.5 mL glass reactors inside the inert glovebox at room temperature (~ 23 °C). The reactor was charged with a predetermined amount of monomer [*rac*-8DL^{R} or mixture of *rac*-8DL^{Me} and *rac*-8DL^{R} (R = Et or ^{n}Bu)] and solvent (as specified in the polymerization tables) in a glovebox, and the mixture of catalyst and/or initiator in solvent was stirred at room temperature for 10 min in another reactor. The polymerization was initiated by rapid addition of the catalyst solution to the monomer solution. After a desired time period, the polymerization was immediately quenched by addition of 0.5 mL of benzoic acid/chloroform (10 mg/mL) and a 0.02 mL of aliquot was taken from the reaction mixture and prepared for ^{1}H NMR analysis to obtain the percent monomer conversion data. The quenched mixture was then precipitated into 50 mL of cold methanol while stirring, filtered, washed with cold methanol to remove any unreacted monomer, and dried in a vacuum oven at room temperature overnight to a constant weight.

Multi-gram scale polymerizations (run 1, 2, 4, 5, Table 3.3) were run in 50 mL glass reactor jars inside the inert glovebox at room temperature (~23 °C) at a scale of ~25 mmol 8DL (~4.5 g). [8DL] = 1M in dichloromethane. Once reaction reaches completion, quenched by precipitation in 5% HCl in methanol. The quenched mixture was then precipitated into 200 mL of cold methanol while stirring and filtered. The precipitated polymer was redissolved in a small amount of dichloromethane and reprecipitated a minimum of three times. Polymer samples were dried in a vacuum oven at 50 °C overnight to a constant weight before characterization and analysis.

Polymer Characterizations. Measurements of polymer absolute weight-average molecular weight (M_w), number-average molecular weight (M_n), and molecular weight distributions or dispersity indices ($Đ = M_w/M_n$) were performed via gel-permeation chromatography (GPC). The GPC instrument consisted of an Agilent HPLC system equipped with one guard column and two PLgel 5 μm mixed-C gel permeation columns and coupled with a Wyatt DAWN HELEOS II multi (18)-angle light scattering detector and a Wyatt Optilab TrEX dRI detector; the analysis was performed at 40°C using chloroform as the eluent at a flow rate of 1.0 mL min^{-1}, using Wyatt ASTRA 7.1.2 molecular weight characterization software. The refractive index increment (d*n*/d*c*) was determined to be 0.0254 ± 0.0004 mL/g for P3HB, 0.0364 ± 0.0017 mL/g for P3HV, and 0.0292 ± 0.0010 mL/g for P3HHp, obtained by batch experiments using Wyatt Optilab TrEX dRI detector and calculated using ASTRA software. Polymer solutions were prepared in chloroform and injected into *d*RI detector by Harvard Apparatus pump 11 at a flow rate of 0.3 mL/min. A series of known concentrations were injected and the change in refractive index was measured to obtain a plot of change in refractive index versus change in concentration ranging from 0.4 to 5.0 mg/mL. The slope from a linear fitting of the data was the d*n*/d*c* of the polymer.

The isolated low molecular weight samples were analyzed by matrix-assisted laser desorption/ionization time-of-flight mass spectroscopy (MALDI−TOF MS); the experiment was performed on Microflex-LRF mass spectrometer (Bruker Daltonics, Billerica, MA) operated in positive ion, reflector mode using a Nd:YAG laser at 355 nm and 25 kV accelerating voltage. A thin layer of a 1% NaI solution was first deposited on the target plate, followed by 0.6 μl of both sample and matrix (dithranol in chloroform). External calibration was done using a peptide calibration mixture (4 to 6 peptides) on a spot adjacent to the sample. The raw data was processed in the FlexAnalysis software (version 3.4.7, Bruker Daltonics).

Melting transition (T_m) and glass transition (T_g) temperatures were measured by differential scanning calorimetry (DSC) on an Auto Q20, TA Instrument. All T_m and T_g values were obtained from a second scan after the thermal history was removed from the first scan. The second heating rate was 10 °C/min and cooling rate was 10 °C/min unless indicated otherwise in the polymerization tables. Decomposition temperatures (T_d, defined by the temperature of 5 % weight loss) and maximum rate decomposition temperatures (T_{max}) of the polymers were measured by thermal gravimetric analysis (TGA) on a Q50 TGA Analyzer, TA Instrument. Polymer samples were heated from ambient temperatures to 700 °C at a heating rate of 10 °C min^{-1}. Values of T_{max} were obtained from derivative (wt %/°C) vs. temperature (°C) plots, while T_d and T_{onset} values (initial and end temperatures) were obtained from wt % vs. temperature (°C) plots.

Tensile stress/strain testing was performed by an Instron 5966 universal testing system (10 kN load cell) on dog-bone-shaped test specimens (ASTM D638 standard; Type V) prepared *via* compression molding using a Carver Bench Top Laboratory Press (Model 4386) equipped with a two-column hydraulic unit (Carver, Model 3912, maximum force 24000 psi). Isolated polymer materials were loaded between non-stick Teflon paper sheets into a stainless-steel mold with inset dimensions 30 × 73.5 × 0.87 mm fabricated in-house, and compressed between two 6″ × 6″ steel electrically heated platens (EHP) clamp force 5000 psi, at temperature 10-30 °C higher than each material's respective T_m. Specimens for analysis were generated *via* compression molding and cut using an ASTM D638-5-IMP cutting die (Qualitest) to standard dimensions. From each compression molding procedure using the stainless-steel mold described, two ASTM D638-5 standard dog-bone shaped specimens could be cut, and 3-4 dong-bone specimens for each sample were prepared for the analysis. Mechanical behavior was averaged for all the specimens

measured for each individual species investigated. Thickness (0.86 ± 0.01 mm), width (3.18 mm), and grip length (26.4 ± 0.2 mm) of the measured dog-bone specimens were measured for normalization of data by the Bluehill measurement software (Instron). Test specimens were affixed into the screw-tight grip frame. Tensile stress and strain were measured to the point of material break at a grip extension speed of 10.0 mm/min at ambient conditions.

Table S3.1. Selected results of *rac*-8DL^{Et} polymerization [a]

Run	Catalyst (Cat)	[8DL]/[Cat]	Time (min)	Conv.[b] (mol%)	M_n [c] (kg/mol)	$Đ$ [c] (M_w/M_n)	I^* [d] (%)	P_m [e]	[*mm*] [e] (%)	T_g [f] (°C)	T_m [f] (°C)
1	**1**	100/1	120	87	13.8	1.19	128	0.91	85	-15.7	-
2	**1**	100/1	360	98	18.9	1.16	104	0.90	85	-15.5	-
3	**2**	100/1	360	98	19.8	1.13	100	0.91	86	-15.0	-
4	**3**	100/1	20	97	32.5	1.23	60	0.96	95	-18.0	108
5	**3**	200/1	60	100	48.7	1.23	82	0.96	95	-17.4	108
6	**3**	400/1	180	74	55.2	1.21	108	0.96	95	-17.0	108
7	**4**	20/1	48 (h)	<20	n.d.	n.d.	n.d.	n.d.	n.d.	n.d.	n.d.
8	**6**	100/1	15	100	23.6	1.11	85	0.86	75	-14.9	-

[a] Conditions: *rac*-8DL^{Et} = 0.160 g (0.80 mmol), [*rac*-8DL^{Et}] = 1.0 M in 0.8 mL DCM; r.t.; catalyst to BnOH initiator ratio fixed at 1/1, and the catalyst amount varied according to the [*rac*-8DL^{Et}]/[cat] ratio; n.d. = not determined. [b] Monomer conversion measured by ^{1}H NMR spectra of the quenched solution in benzoic acid/chloroform. [c] Weight-average molecular weights (M_w), number-average molecular weights (M_n), and dispersity indices ($Đ = M_w/M_n$) determined by GPC coupled with an 18-angle light scattering detector at 40 °C in chloroform. [d] The initiation efficiency $I^* = M_n$(calcd)/M_n(exptl), where M_n(calcd) = MW(*rac*-8DL^{Et}) × [*rac*-8DL^{Et}]/[cat] × conv (%) + MW of chain-end groups (BnOH)] = 200.23 × [*rac*-8DL^{Et}]/[cat] × conv (%) + 108.14. [e] P_m is the probability of *meso* linkages between 3HV units, and *mm* is isotactic triad made up of two adjacent *meso* diads, determined by ^{13}C{^{1}H} NMR spectroscopy. [f] T_g and T_m measured by DSC with the cooling and second heating rate of 2 °C/min for samples produced by **3**, or 10 °C/min for the samples produced by **1–2** and **6**.

Table S3.2. Selected results of *rac*-8DL^{Bu} polymerization [a]

Run	Catalyst	[8DL]/[Cat]	Time (min)	Conv. (mol%)	M_n (kg/mol)	$Đ$ (M_w/M_n)	I^* (%)	P_m	[*mm*] (%)	T_g (°C)
1	**3**	200/1	35	100	93.9	1.24	54	0.97	93	-30.1
2	**3**	400/1	120	100	140	1.19	73	0.97	94	-29.2
3	**3**	800/1	300	64	126	1.20	104	0.97	94	-29.6
4	**4**	50/1	48 (h)	<6	n.d.	n.d.	n.d.	n.d.	n.d.	n.d.

5	**5**	50/1	20 (h)	58	6.67	1.19	88	0.97	96	-31.7
6	**6**	200/1	14	100	56.3	1.18	91	0.85	74	-30.8

[a] Conditions: *rac*-8DL^{Et} = 0.179 g (0.70 mmol), [*rac*-8DL^{Et}] = 1.0 M in 0.7 mL DCM; r.t. See footnotes under Table S2 for other explanations.

Table S3.3. Conversion data of copolymerizations of *rac*-8DL^{Me} and *rac*-8DL^{Et} with [*rac*-8DL^{Me}+ *rac*-8DL^{Et}]/[3] = 400/1 in Table 3.1

[*rac*-8DL^{Me}]/[*rac*-8DL^{Et}] = 10/1 [8DL^{Me}+ *rac*-8DL^{Et}]/[**3**] = 400/1 (run 8, Table 3.1)			[*rac*-8DL^{Me}]/[*rac*-8DL^{Et}] = 5/1 [8DL^{Me}+ *rac*-8DL^{Et}]/[**3**] = 400/1 (run 10, Table 3.1)			[*rac*-8DL^{Me}]/[*rac*-8DL^{Et}] = 3/1 [8DL^{Me}+ *rac*-8DL^{Et}]/[**3**] = 400/1 (run 12, Table 3.1)		
Time (min)	Conv. (%)		Time (min)	Conv. (%)		Time (min)	Conv. (%)	
	rac-8DL^{Me}	*rac*-8DL^{Et}		*rac*-8DL^{Me}	*rac*-8DL^{Et}		*rac*-8DL^{Me}	*rac*-8DL^{Et}
5	26	11	5	25	8.5	2	13	3.9
10	49	19	10	47	16	5	27	8.1
20	75	26	20	76	28	10	48	15
						20	73	25

[*rac*-8DL^{Me}]/[*rac*-8DL^{Et}] = 2/1 [8DL^{Me}+ *rac*-8DL^{Et}]/[**3**] = 400/1 (run 14, Table 3.1)			[*rac*-8DL^{Me}]/[*rac*-8DL^{Et}] = 1/1 [8DL^{Me}+ *rac*-8DL^{Et}]/[**3**] = 400/1 (run 16, Table 3.1)		
Time (min)	Conv. (%)		Time (min)	Conv. (%)	
	rac-8DL^{Me}	*rac*-8DL^{Et}		*rac*-8DL^{Me}	*rac*-8DL^{Et}
5	25	7.5	2	12	2.9
10	45	13	5	26	6.8
20	72	26	10	47	14
			20	61	18

Table S3.4. Measured tensile behavior of P3HBV [incorporation of *rac*-8DL^{Et} = 7.6%, and M_n = 175 kg/mol ($Đ$ = 1.35)] dog-bone shaped specimens.

specimen	Young's modulus (MPa)	ultimate tensile strength (MPa)	elongation at break (%)

1	1080	25.9	37
2	1180	25.1	30
3	1240	26.3	38
AVG	1166±81	25.8±0.6	35±4

Table S3.5. Measured tensile behavior of P3HBV [incorporation of *rac*-8DL^{Et} = 12.8%, and M_n = 138 kg/mol ($Đ$ = 1.08)] dog-bone shaped specimens.

specimen	Young's modulus (MPa)	ultimate tensile strength (MPa)	elongation at break (%)
1	820	35.0	299
2	839	26.7	230
3	908	30.9	242
AVG	856±46	30.9±4.1	257±37

Table S3.6. Measured tensile behavior of P3HBV [incorporation of *rac*-8DL^{Et} = 19.8%, and M_n = 119 kg/mol ($Đ$ = 1.16)] dog-bone shaped specimens.

specimen	Young's modulus (MPa)	tensile strength at yield (MPa)	elongation at yield (%)	ultimate tensile strength (MPa)	elongation at break (%)
1	612	16.5	11.0	25.2	401
2	722	18.5	11.0	25.0	359
3	672	16.9	11.1	24.7	361
AVG	669±45	17.3±0.9	11.0±0.05	25.0±0.2	374±19

Table S3.7. Measured tensile behavior of P3HBHp [incorporation of *rac*-8DL^{Bu} = 6.3%, and M_n = X kg/mol ($Đ$ = X)] dog-bone shaped specimens.

specimen	Young's modulus (MPa)	ultimate tensile strength (MPa)	elongation at break (%)
1	1140	24.3	50

2	1150	27.1	63
3	945	25.4	60
4	988	24.3	58
AVG	1056±105	25.3±1.3	58±6

Table S3.8. Measured tensile behavior of P3HBHp [incorporation of *rac*-8DL^{Bu} = 10.5%, and M_n =183 kg/mol ($Đ$ = 1.05)] dog-bone shaped specimens.

specimen	Young's modulus (MPa)	ultimate tensile strength (MPa)	elongation at break (%)
1	497	23.5	285
2	541	18.0	128
3	558	21.0	233
AVG	532±31	20.8±2.7	215±80

Table S3.9. Measured tensile behavior of P3HBHp [incorporation of *rac*-8DL^{Bu} = 19.6%, and M_n = 144 kg/mol ($Đ$ = 1.15)] dog-bone shaped specimens.

specimen	Young's modulus (MPa)	tensile strength at yield (MPa)	elongation at yield (%)	ultimate tensile strength (MPa)	elongation at break (%)
1	219	8.79	15.8	20.4	552
2	223	9.14	15.8	20.8	587
3	222	8.88	17.3	20.9	586
4	242	9.55	14.0	19.8	589
AVG	226±9	9.09±0.30	15.7±1.2	20.5±0.4	578±15

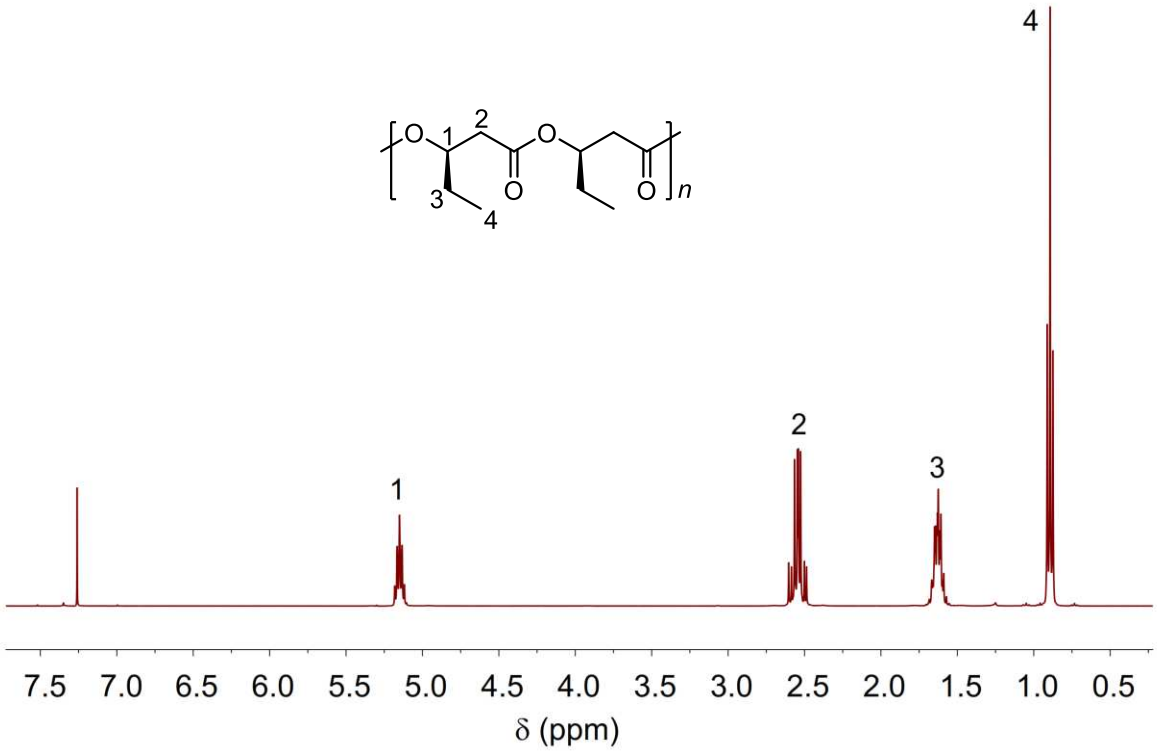

Figure S3.1. ^{1}H NMR spectrum ($CDCl_3$, 298 K, 400 MHz) of P3HV produced with [*rac*-8DL^{Et}]/[3] = 100/1.^{1}H NMR (400 MHz, $CDCl_3$): δ 5.21 – 5.09 (m, 1H, EtC*H*O-C=O), 2.64 – 2.44 (m, 2H, C(=O)CH_2), 1.74 – 1.53 (m, 2H, -CH_2CH$_3$), 0.89 (t, J = 7.4 Hz, 3H, Me).

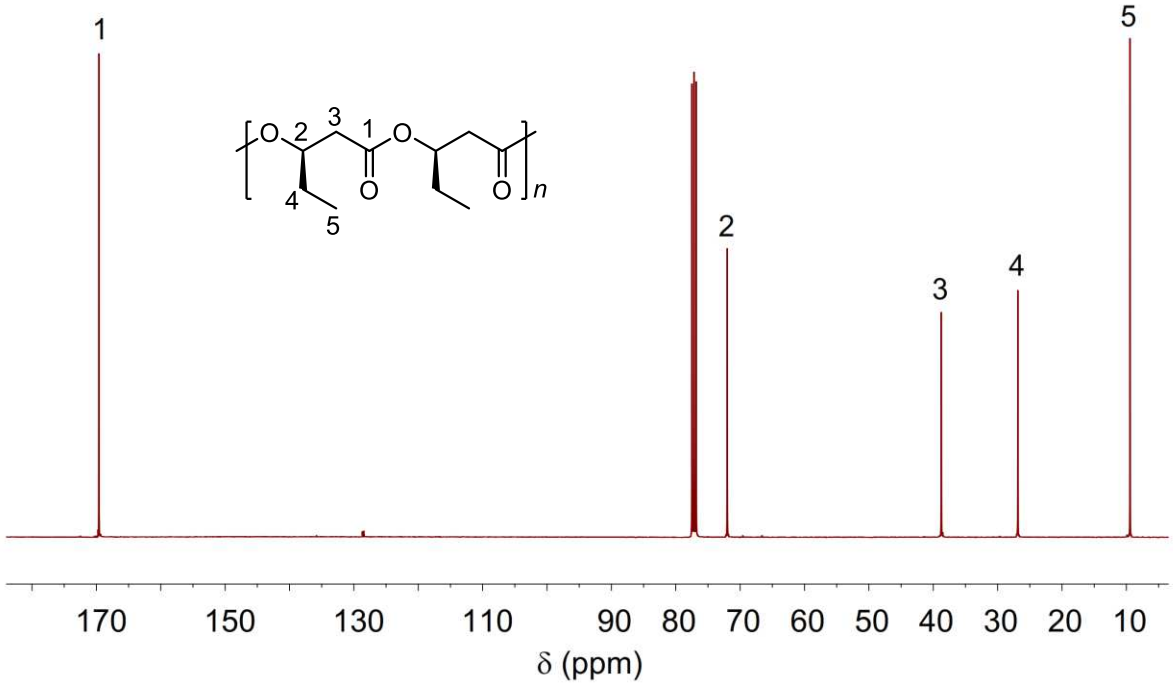

Figure S3.2. ^{13}C NMR spectrum ($CDCl_3$, 298 K, 101 MHz) of P3HV produced with [*rac*-8DL^{Et}]/[3] = 100/1.^{13}C NMR (101 MHz, $CDCl_3$): δ 169.75 (s, *mr* of *C*=O), 169.61 (s, *mm* of *C*=O), 169.56(s, *rm* of *C*=O), 72.01 (m, Et*C*HO-C=O), 38.75 (s, *m* of C(=O)*C*H_2), 38.53 (s, *r* of C(=O)*C*H_2), 26.92 (s, *r* of -*C*H_2CH_3), 26.85 (s, *m* of -*C*H_2CH_3), 9.47 (s, *r* of Me), 9.43 (s, *m* of Me).

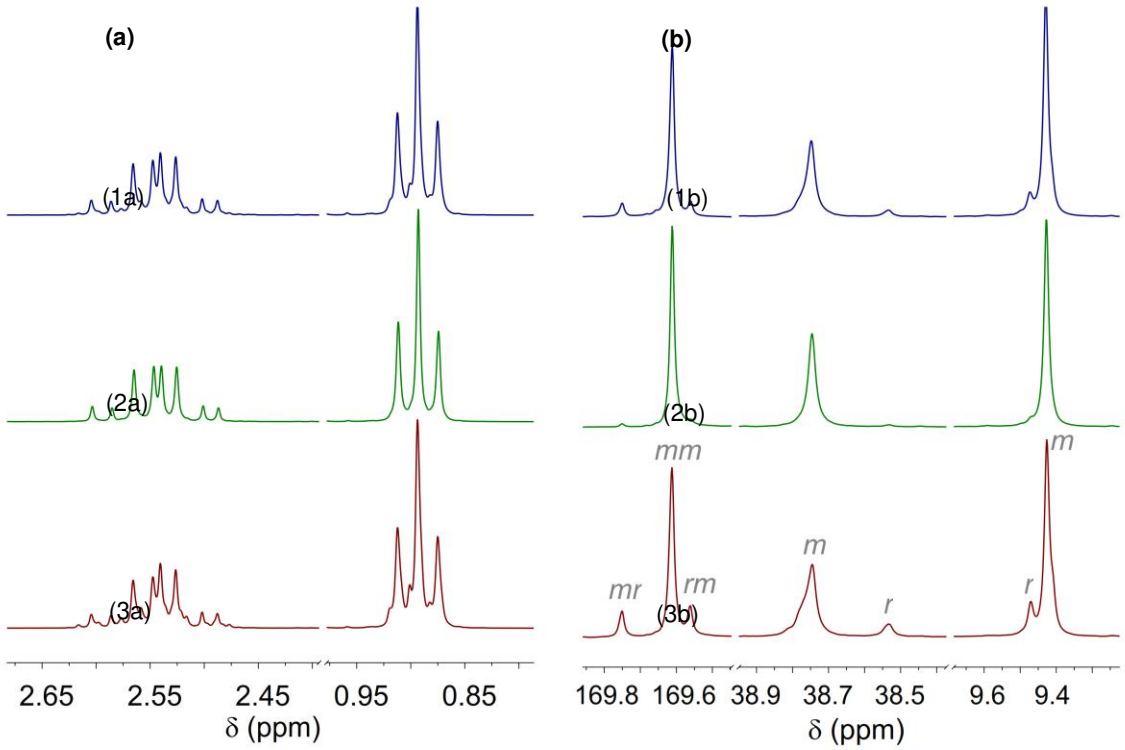

Figure S3.3. Stereomicrostructures of P3HV by the chemical synthesis route. (a) ^{1}H NMR spectra ($CDCl_3$, 298 K, 400 MHz) in the methylene (on backbone) and methyl regions. (b) ^{13}C NMR spectra ($CDCl_3$, 298 K, 101 MHz) in carbonyl, methylene (on backbone) and methyl regions. P3HV produced by [*rac*-8DL^{Et}]/[Y] = 100/1: Y = 1 (1a-b); 3 (2a-b); 6 (3a-b).

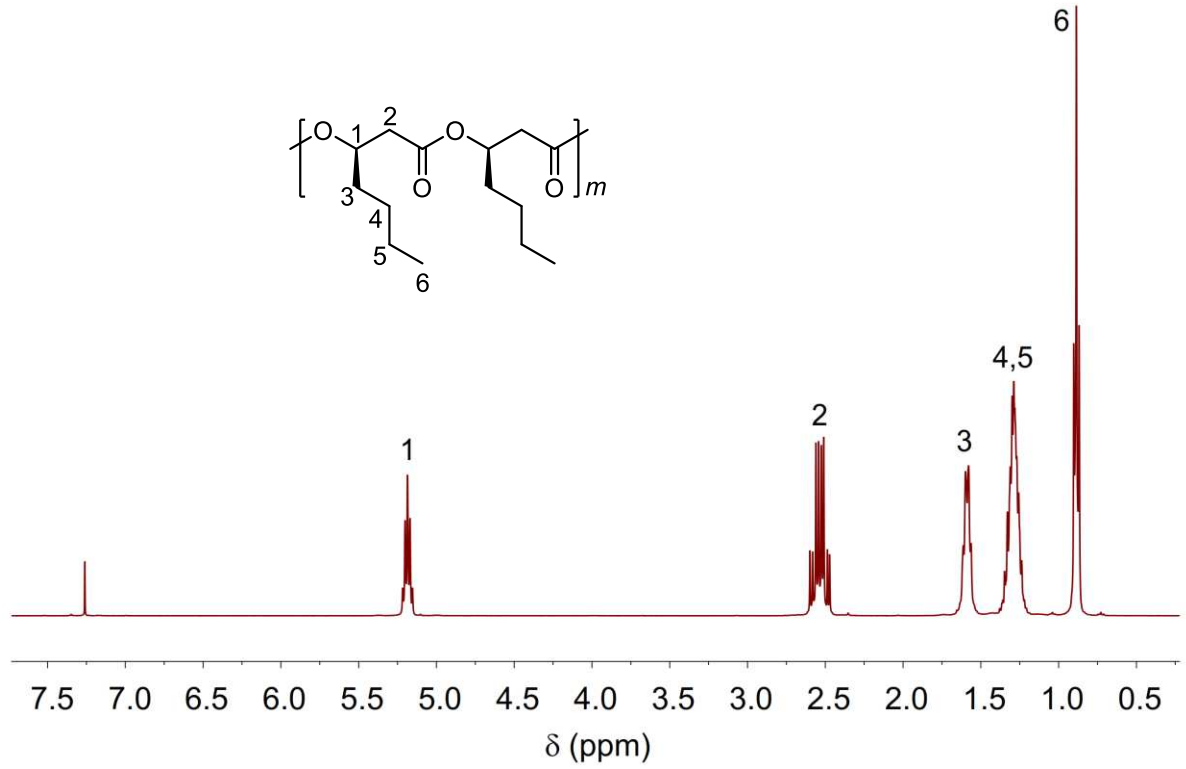

Figure S3.4. ^{1}H NMR spectrum ($CDCl_3$, 298 K, 400 MHz) of P3HHp produced with [*rac*-8DL^{Bu}]/[3] = 200/1.^{1}H NMR (400 MHz, $CDCl_3$): δ 5.25 – 5.13 (m, 1H, BuC*H*O-C=O), 2.64 – 2.42 (m, 2H, C(=O)C*H*$_2$), 1.66 – 1.50 (m, 2H, -C*H*$_2$CH$_2$CH$_2$CH$_3$), 1.40 – 1.18 (m, 4H, -CH$_2$C*H*$_2$C*H*$_2$CH$_3$), 0.89 (t, *J* = 6.8 Hz, 3H, Me).

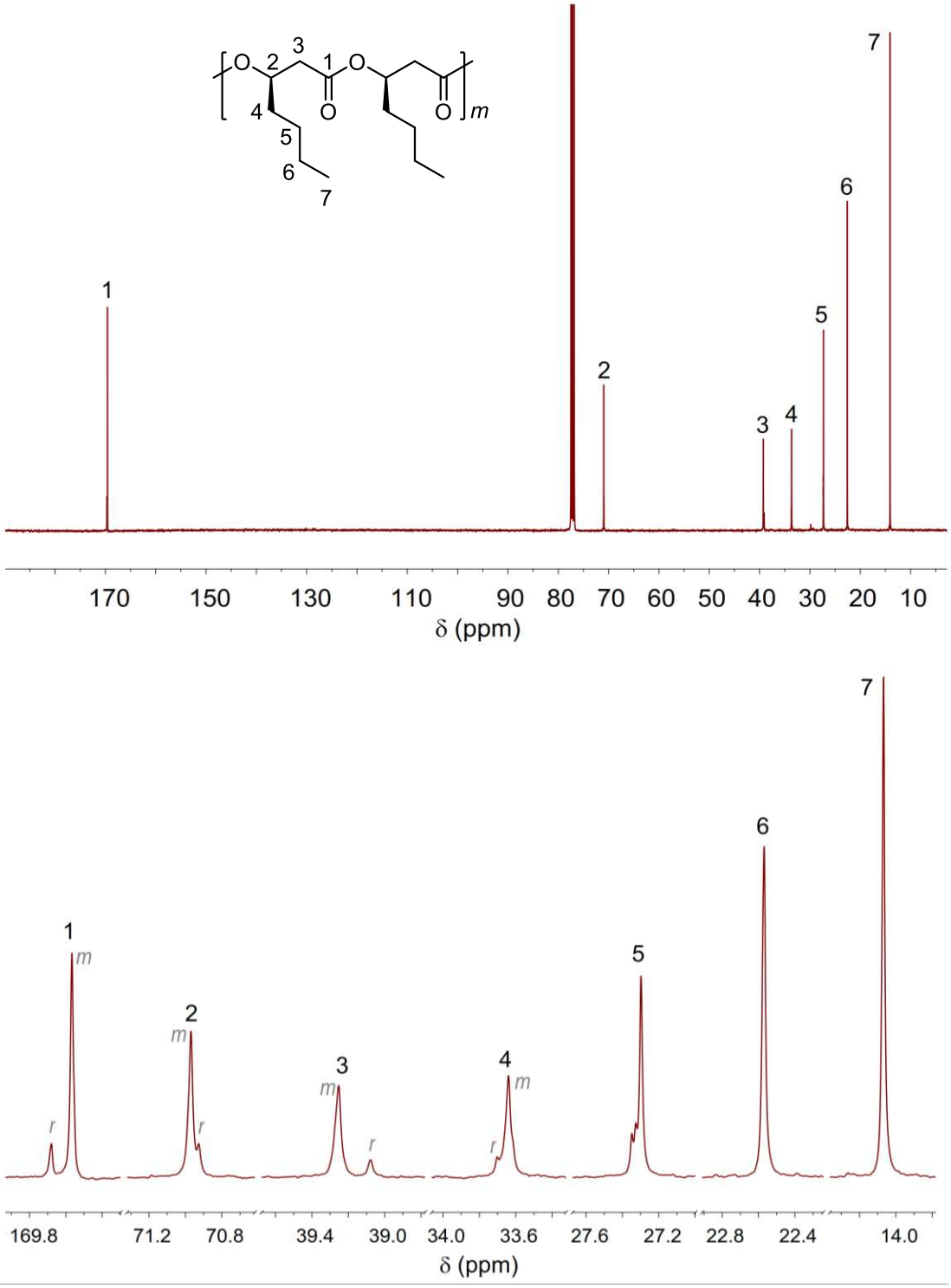

Figure S3.5. ^{13}C NMR spectrum ($CDCl_3$, 298 K, 101 MHz) of P3HHp produced with [*rac*-8DL^{Bu}]/[6] = 200/1.^{13}C NMR (101 MHz, $CDCl_3$): δ 169.68, 169.57, 70.97, 70.93, 39.25, 39.08, 33.70, 33.64, 27.30, 22.57, 14.07.

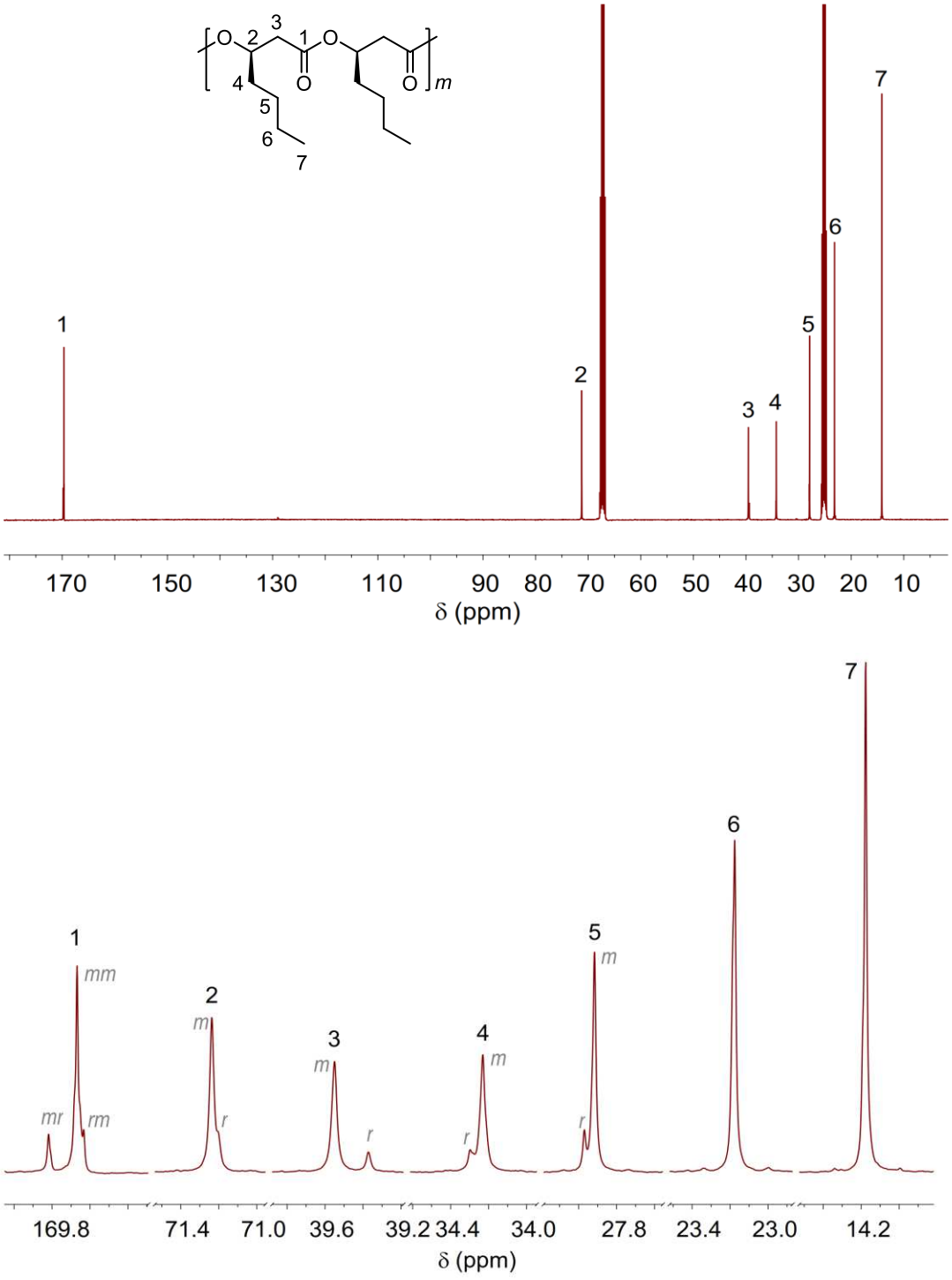

Figure S3.6. ^{13}C NMR spectrum (THF-d_8, 298 K, 101 MHz) of P3HHp produced with [*rac*-8DL^{Bu}]/[6] = 200/1.^{13}C NMR (101 MHz, THF-d_8): δ 169.82, 169.67, 169.63, 71.24, 71.20, 39.55, 39.37, 34.30, 34.23, 27.97, 27.92, 23.18, 14.18.

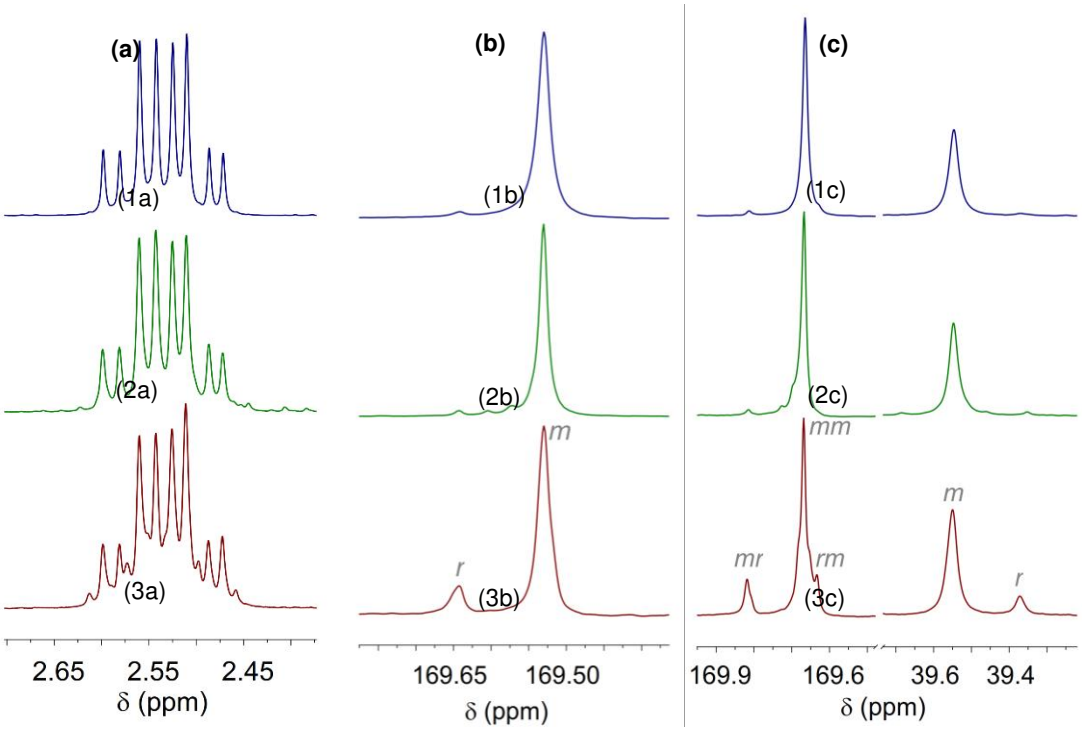

Figure S3.7. Stereomicrostructures of P3HHp by the chemical synthesis route. (a) ^{1}H NMR spectra ($CDCl_3$, 298 K, 400 MHz) in the methylene (on backbone) region. (b) ^{13}C NMR spectra ($CDCl_3$, 298 K, 101 MHz) in the carbonyl region. (c) ^{13}C NMR spectra (THF-d_8, 298 K, 101 MHz) in the carbonyl and methylene (on backbone) regions. P3HHp produced by [*rac*-8DL^{Bu}]/[3] = 200/1 (1a-c); [*rac*-8DL^{Bu}]/[5] = 50/1 (2a-c); and [*rac*-8DL^{Bu}]/[6] = 200/1 (3a-c).

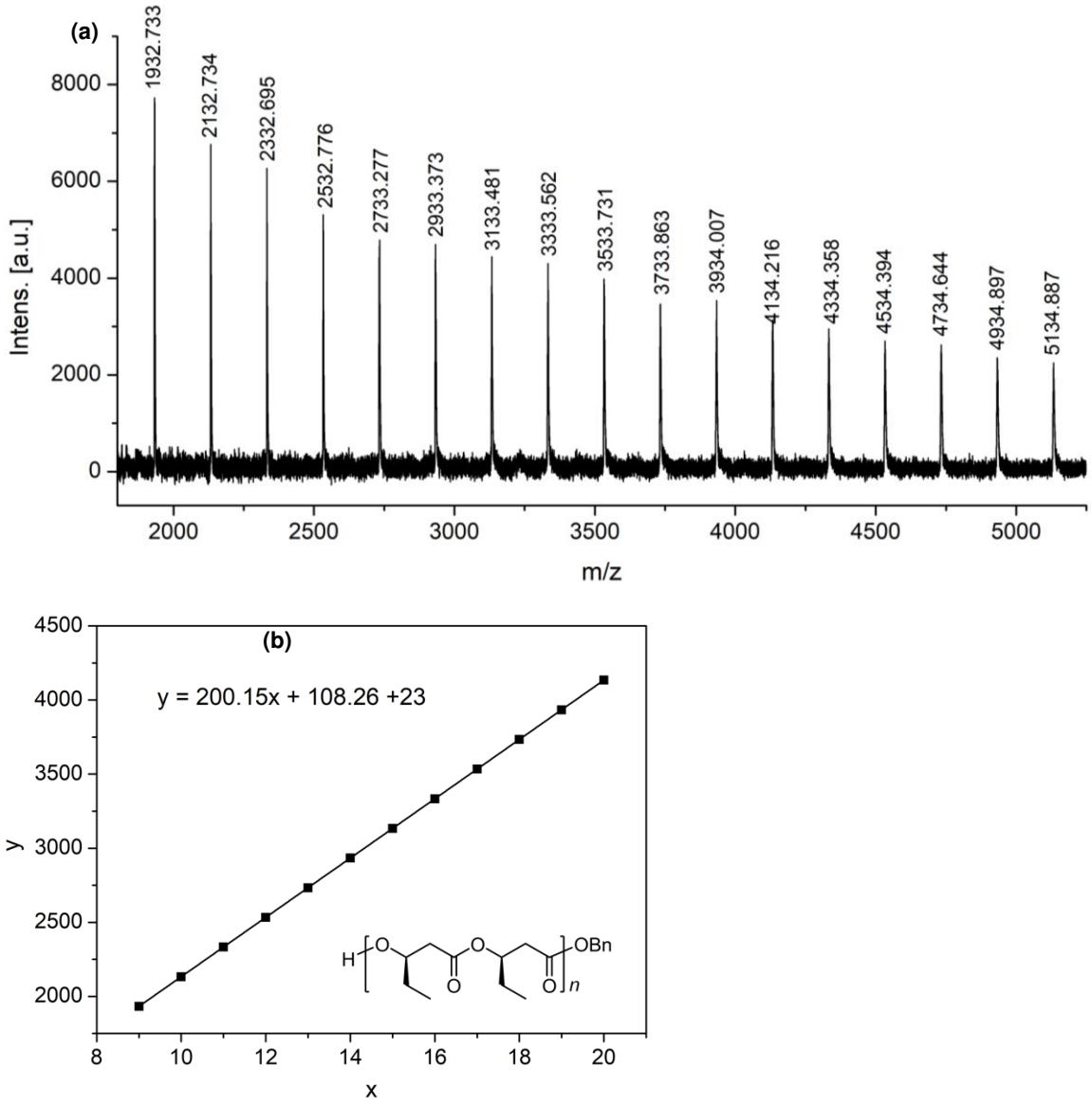

Figure S3.8. (a) MALDI-TOF spectrum of P3HV produced with racemic yttrium complex 3/BnOH ([*rac*-8DL^{Et}]/[3] = 20, 1 min, conversion: 55%); (b) Plot of *m*/*z* values (y) *vs* the number of *rac*-8DL^{Et} repeat units (x).

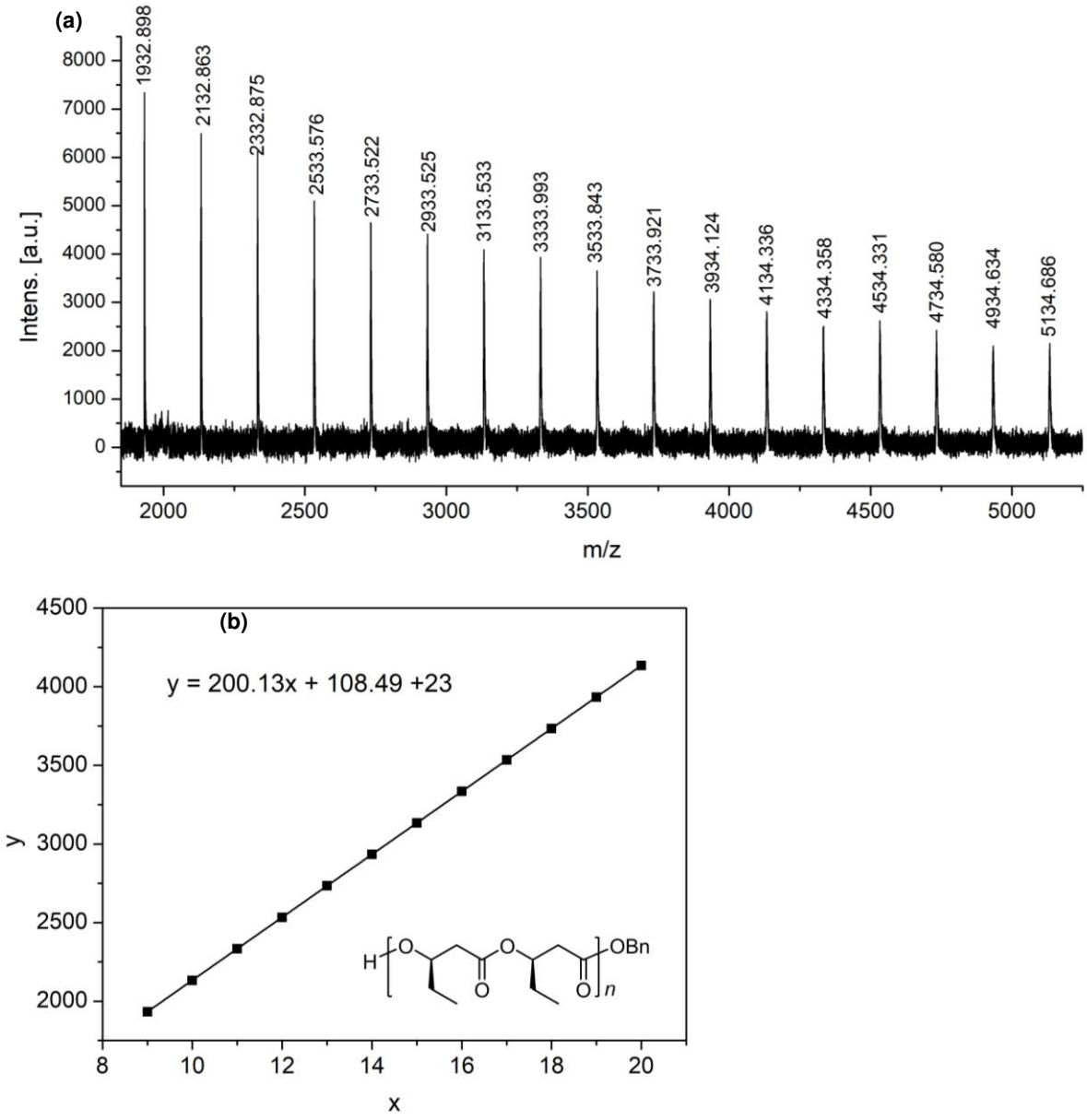

Figure S3.9. (a) MALDI-TOF spectrum of P3HV produced with racemic yttrium complex 3/BnOH ([*rac*-8DL^{Et}]/[3] = 20, 2 min, conversion: 87%); (b) Plot of *m*/*z* values (y) *vs* the number of *rac*-8DL^{Et} repeat units (x).

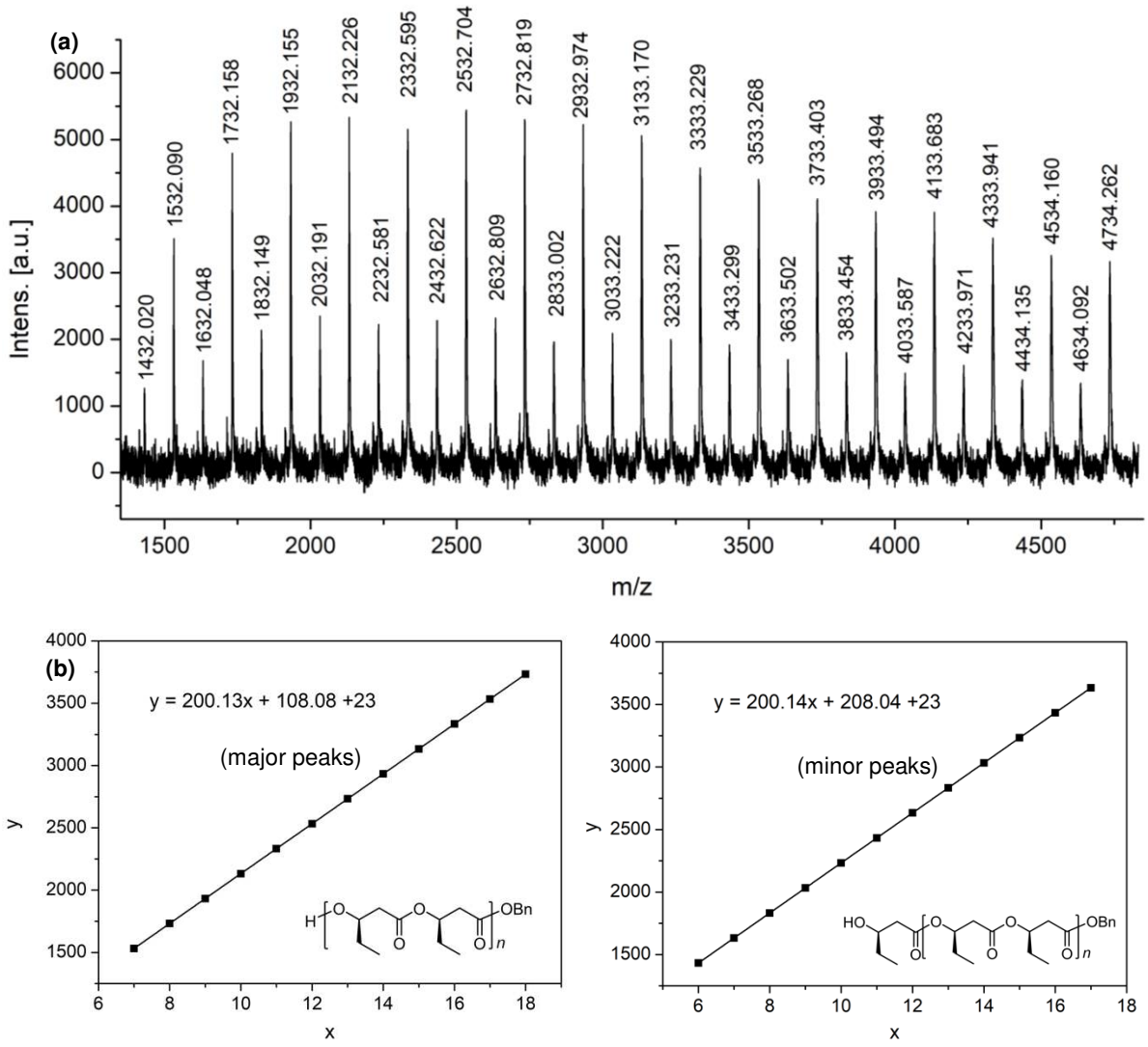

Figure S3.10. (a) MALDI-TOF spectrum of P3HV produced with racemic yttrium complex 3/BnOH ([*rac*-8DL^{Et}]/[3] = 20, 5 min, conversion: 100%); (b) Plot of *m*/*z* values (y) *vs* the number of *rac*-8DL^{Et} repeat units (x).

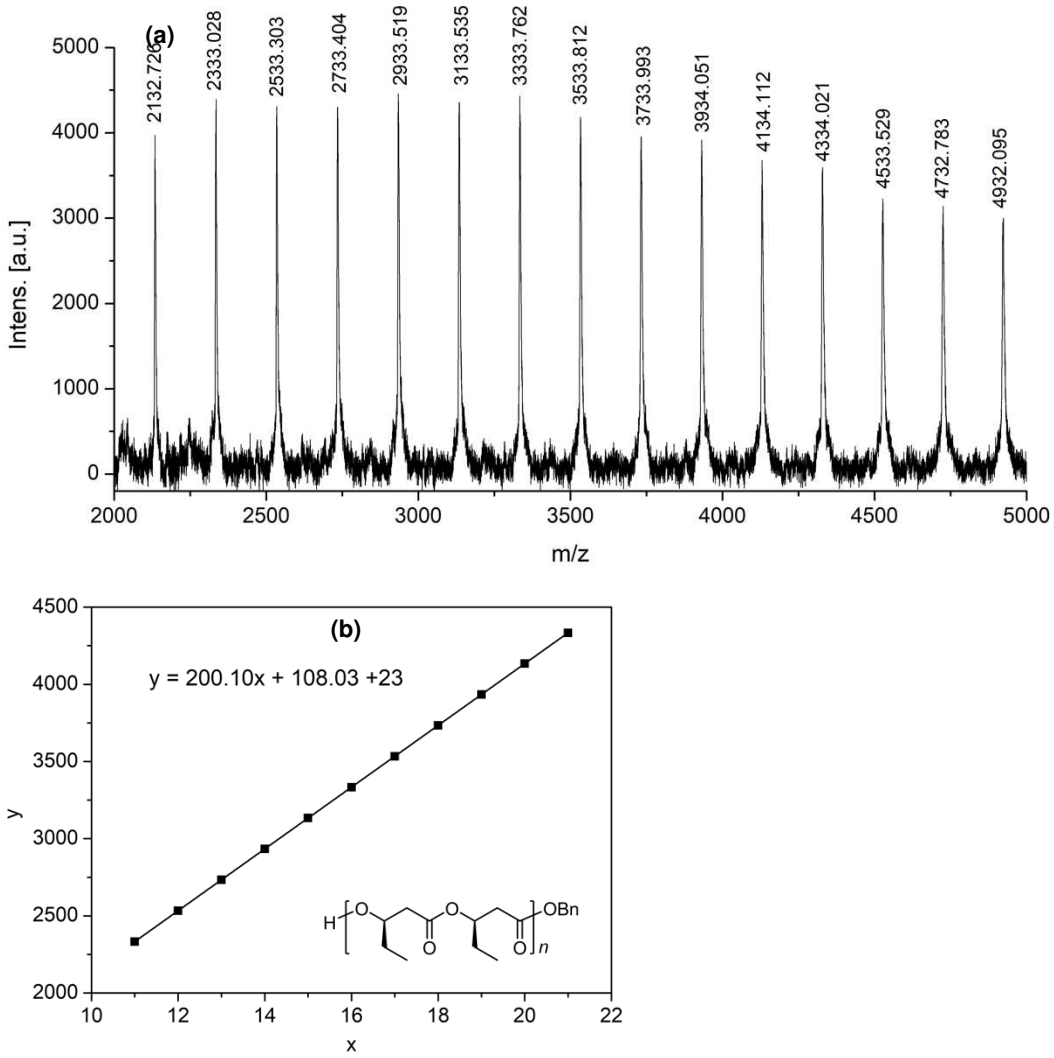

Figure S3.11. (a) MALDI-TOF spectrum of P3HV produced with yttrium complex 3 ([*rac*-8DL^{Et}]/[3] = 100, 30 min, 100% conversion). (b) Plot of *m*/*z* values (y) *vs* the number of *rac*-8DL^{Et} repeat units (x).

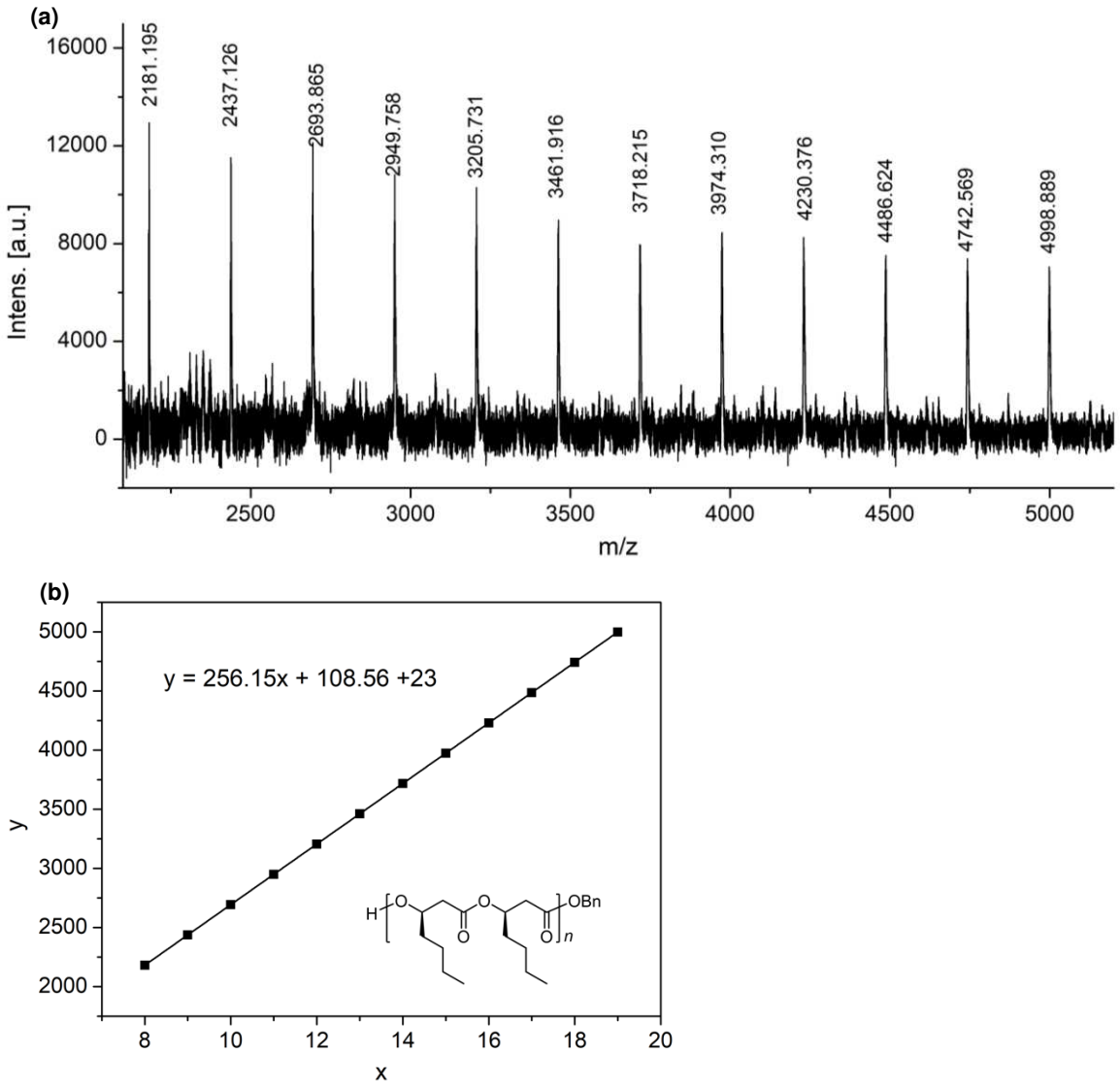

Figure S3.12. (a) MALDI-TOF spectrum of P3HHp produced with racemic yttrium complex 3/BnOH ([*rac*-8DL^{Bu}]/[3] = 20, 1 min, conversion: 74%); (b) Plot of *m*/*z* values (y) *vs* the number of *rac*-8DL^{Bu} repeat units (x).

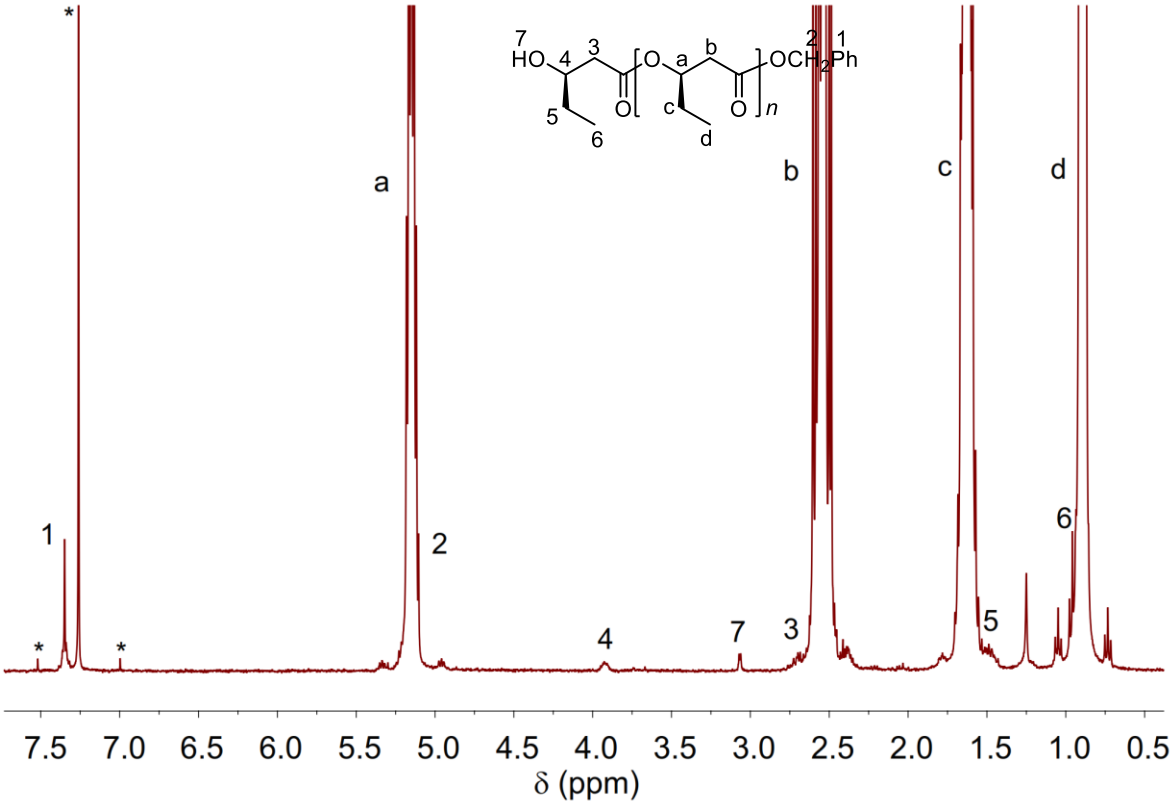

Figure S3.13. ^{1}H NMR spectrum ($CDCl_3$, 298 K, 400 MHz) of P3HV produced with *rac*-8DL^{Et}/3/BnOH (20/1/1, 5 min; *$CHCl_3$), showing chain-end groups.

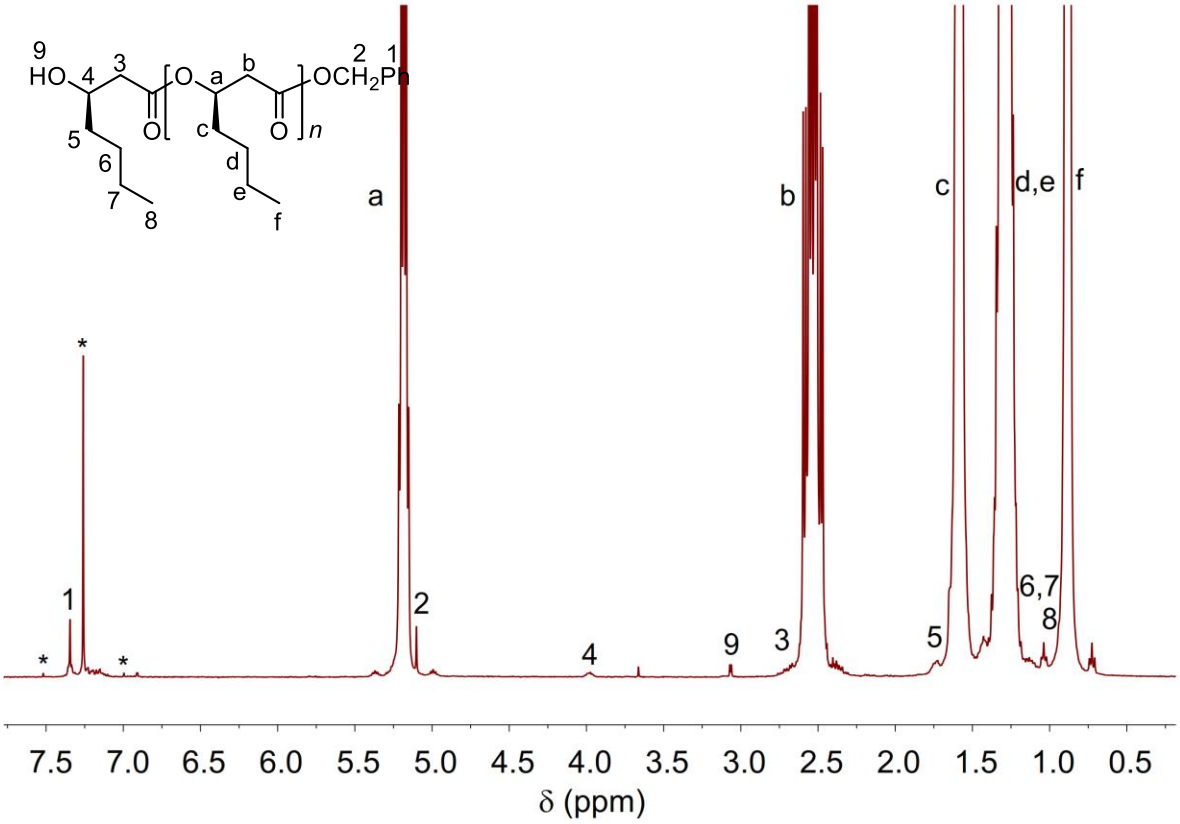

Figure S3.14. ^{1}H NMR spectrum ($CDCl_3$, 298 K, 400 MHz) of P3HHp produced with *rac*-8DL^{Bu}/3/BnOH (20/1/1, 5 min; *$CHCl_3$), showing chain-end groups.

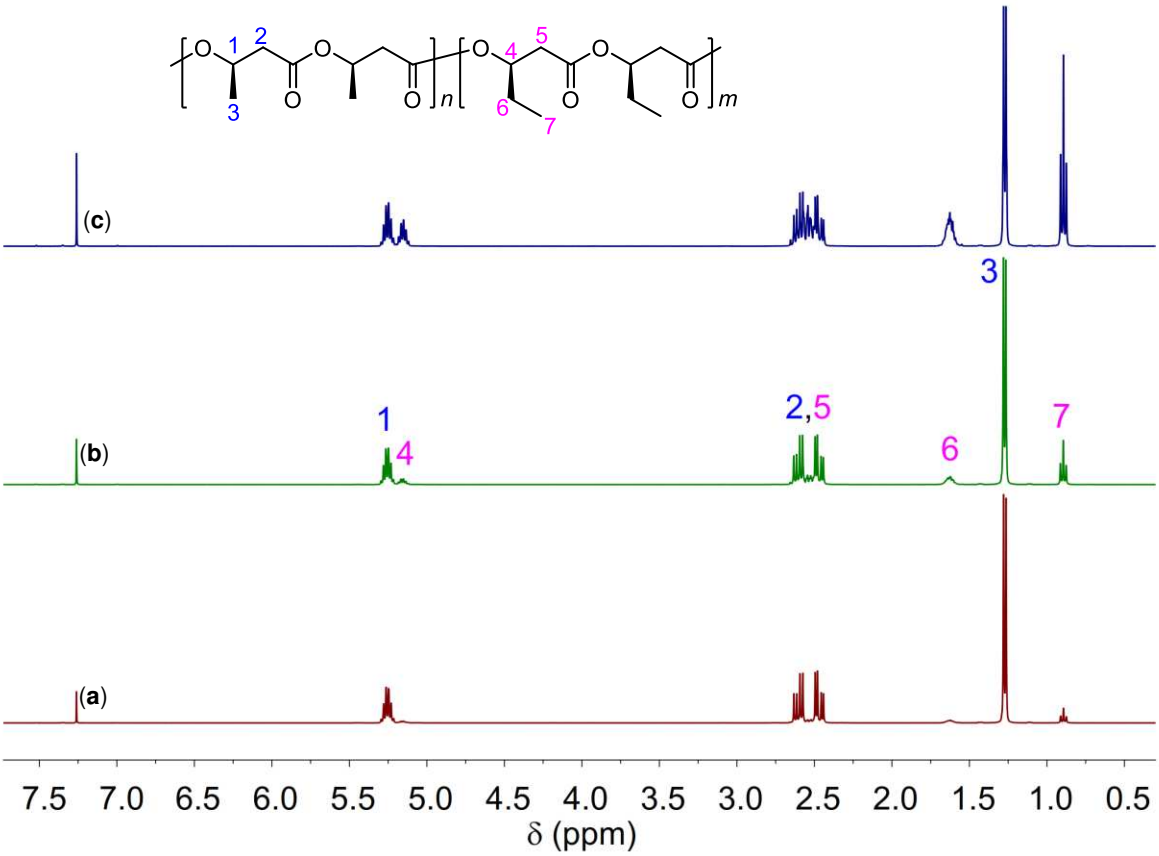

Figure S3.15. Overlay of ^{1}H NMR spectra ($CDCl_3$, 298 K, 400 MHz) of P3HBV with different *rac*-8DL^{Et} incorporations: (a) 6.6% (run 9, Table 3.1); (b) 15.7% (run 13, Table 3.1); and (c) 37.6% (run 17, Table 3.1).

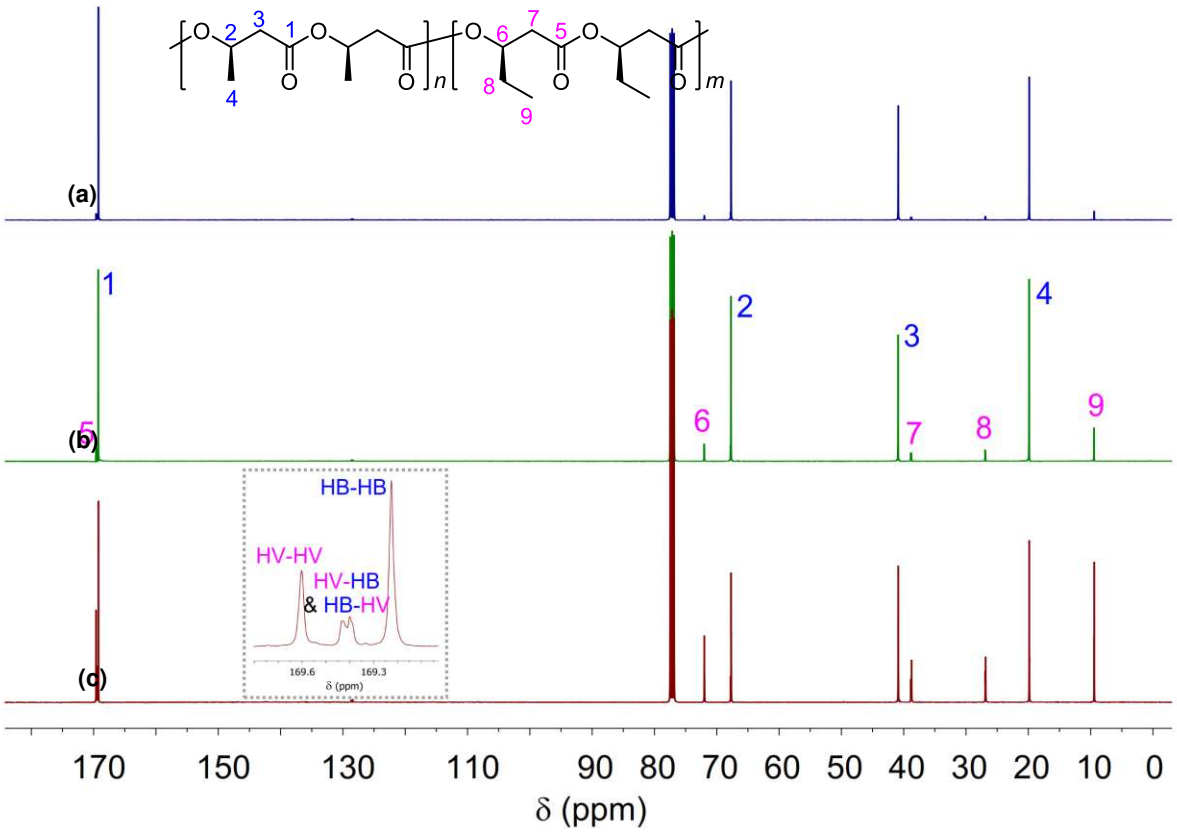

Figure S3.16. Overlay of ^{13}C NMR spectra ($CDCl_3$, 298 K, 101 MHz) of P3HBV with different *rac*-8DL^{Et} incorporations of (a) 6.6% (run 9, Table 3.1); (b) 15.7% (run 13, Table 3.1); and (c) 37.6% (run 17, Table 3.1) and expanded inset of carbonyl region (HB = 3-hydroxybutyrate unit, HV = 3-hydroxyvalerate unit).

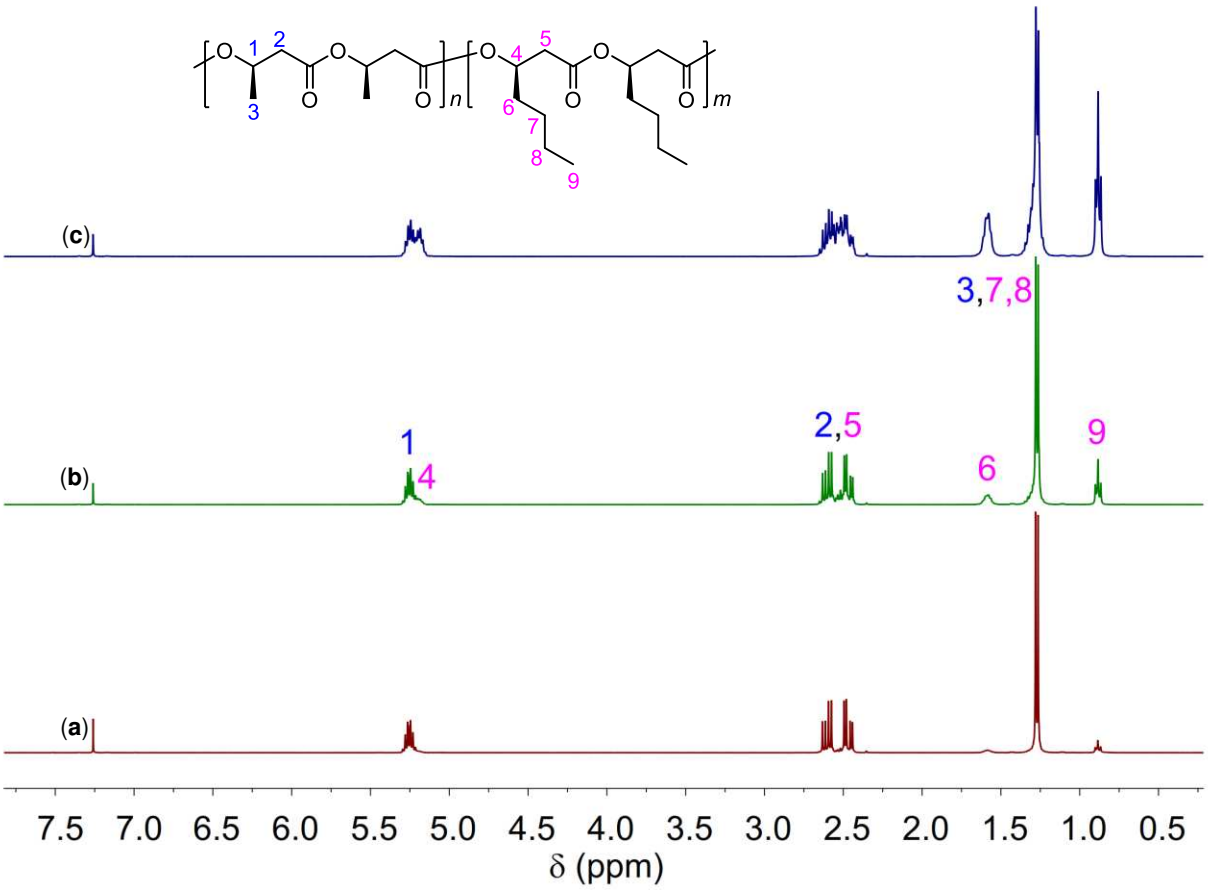

Figure S3.17. ^{1}H NMR ($CDCl_3$, 298 K, 400 MHz) of P3HBHp with different *rac*-8DL^{Bu} incorporations: (a) 7.3% (run 1, Table 3.2); (b) 19.1% (run 3, Table 3.2); and (c) 44.8% (run 5, Table 3.2)

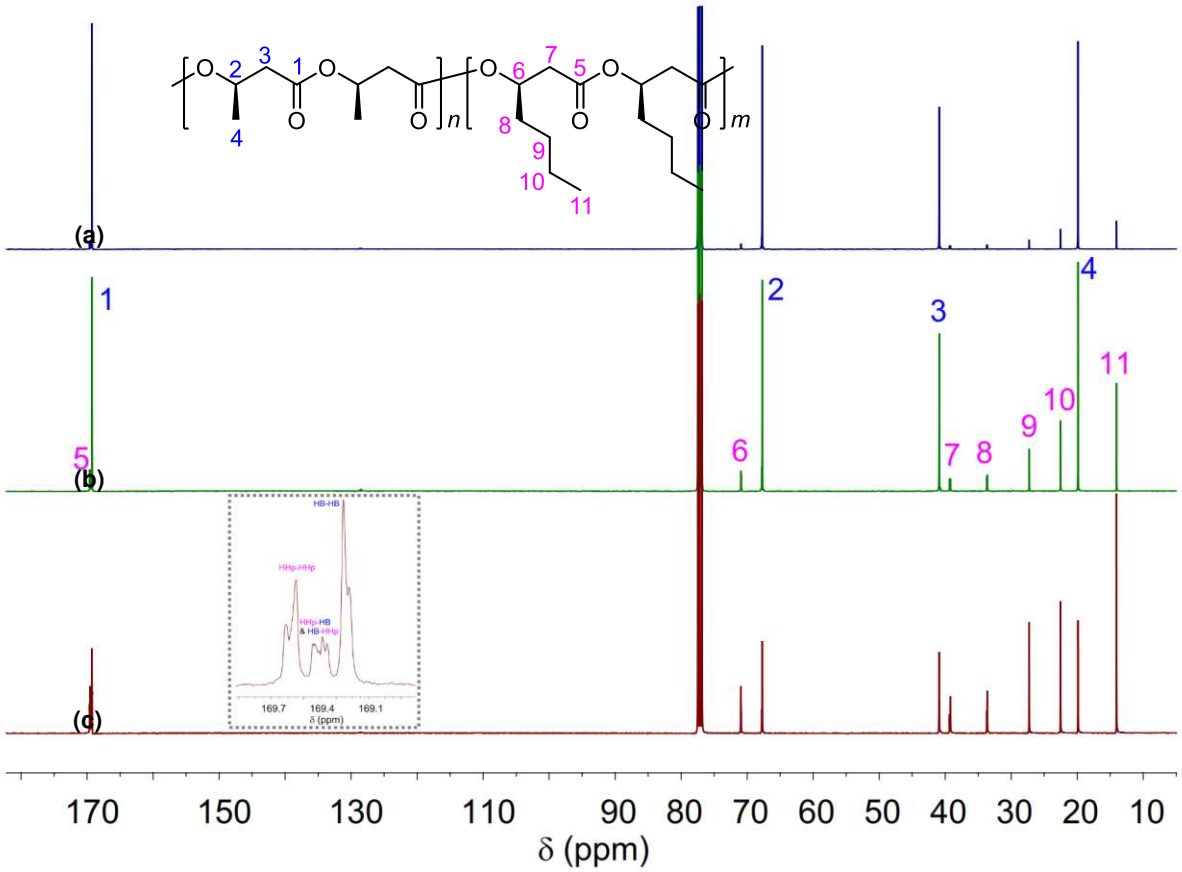

Figure S3.18. Overlay of ^{13}C NMR spectra ($CDCl_3$, 298 K, 101 MHz) of P3HBHp with different *rac*-8DL^{Bu} incorporations of (a) 7.3% (run 1, Table 3.2); (b) 19.1% (run 3, Table 3.2); and (c) 44.8% (run 5, Table 3.2) and expanded inset of carbonyl region (HB = 3-hydroxybutyrate unit, HHp = 3-hydroxyheptanoate unit).

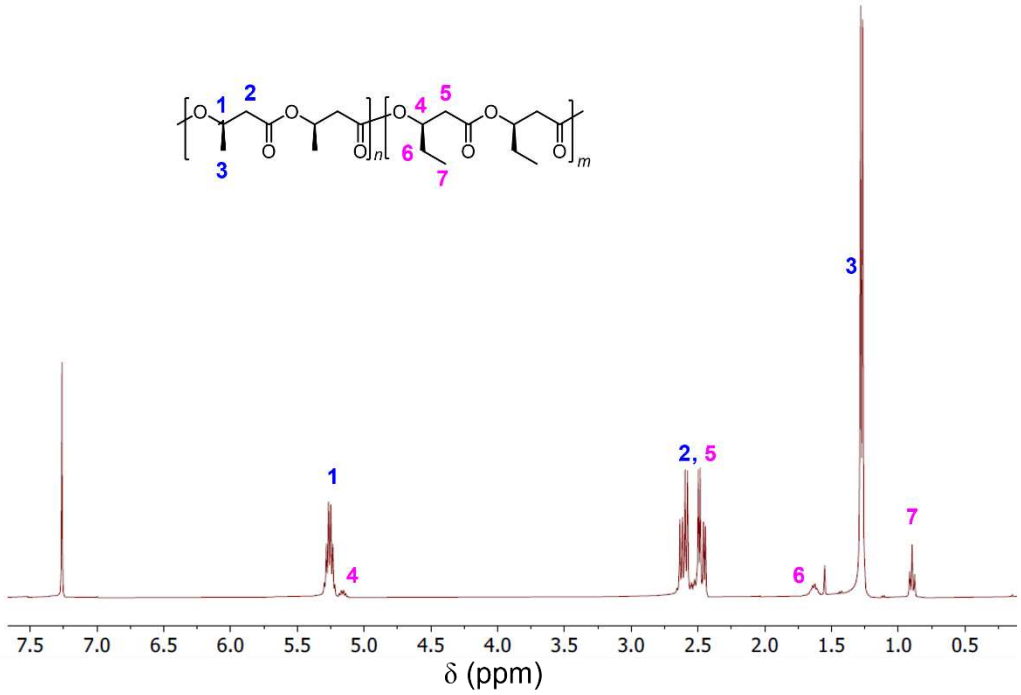

Figure S3.19. ^{1}H NMR ($CDCl_3$, 298 K, 400 MHz) of multi-gram scale P3HBV with 7.6% *rac*-8DL^{Et} incorporation (run 1, Table 3.3)

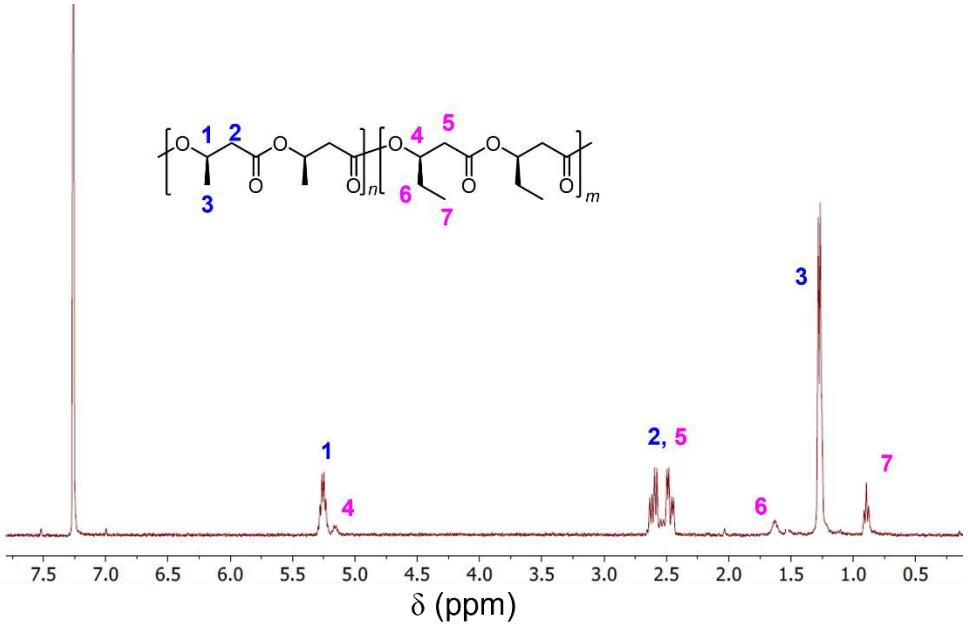

Figure S3.20. ^{1}H NMR ($CDCl_3$, 298 K, 400 MHz) of multi-gram scale P3HBV with 12.8% *rac*-8DL^{Et} incorporation (run 2, Table 3.3)

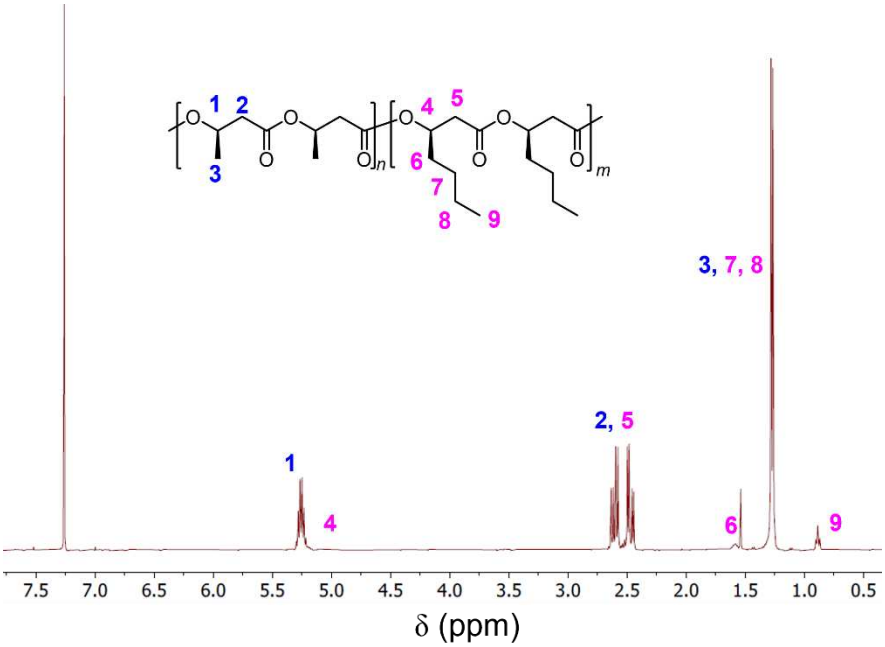

Figure S3.21. ^{1}H NMR ($CDCl_3$, 298 K, 400 MHz) of multi-gram scale P3HBHp with 6.3% *rac*-8DL^{Bu} incorporation (run 4, Table 3.3).

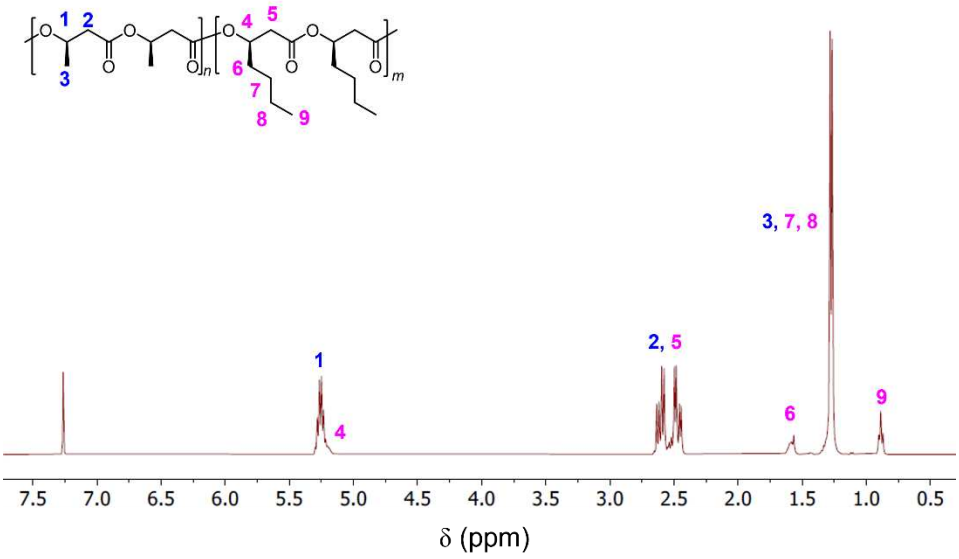

Figure S3.22. ^{1}H NMR ($CDCl_3$, 298 K, 400 MHz) of multi-gram scale P3HBHp with 10.5% *rac*-8DL^{Bu} incorporation (run 5, Table 3.3).

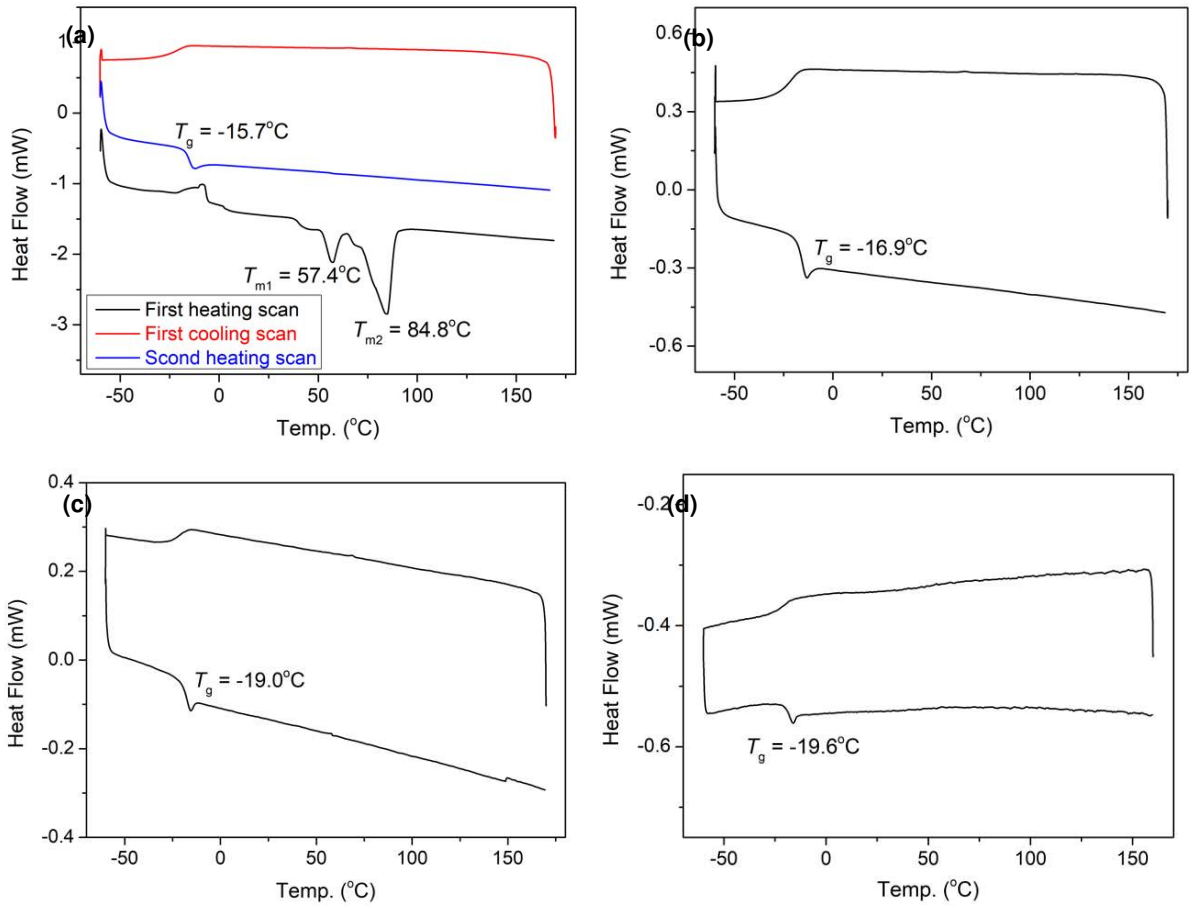

Figure S3.23. DSC curves of P3HV (P_m = 0.91, [*mm*] = 85%) produced by *rac*-8DL^{Et}/1 =100/1 (120 min) with different cooling and second heating rates: (a) 10 °C/min; (b) 5°C/min; (c) 2 °C/min; and (d) 1 °C/min.

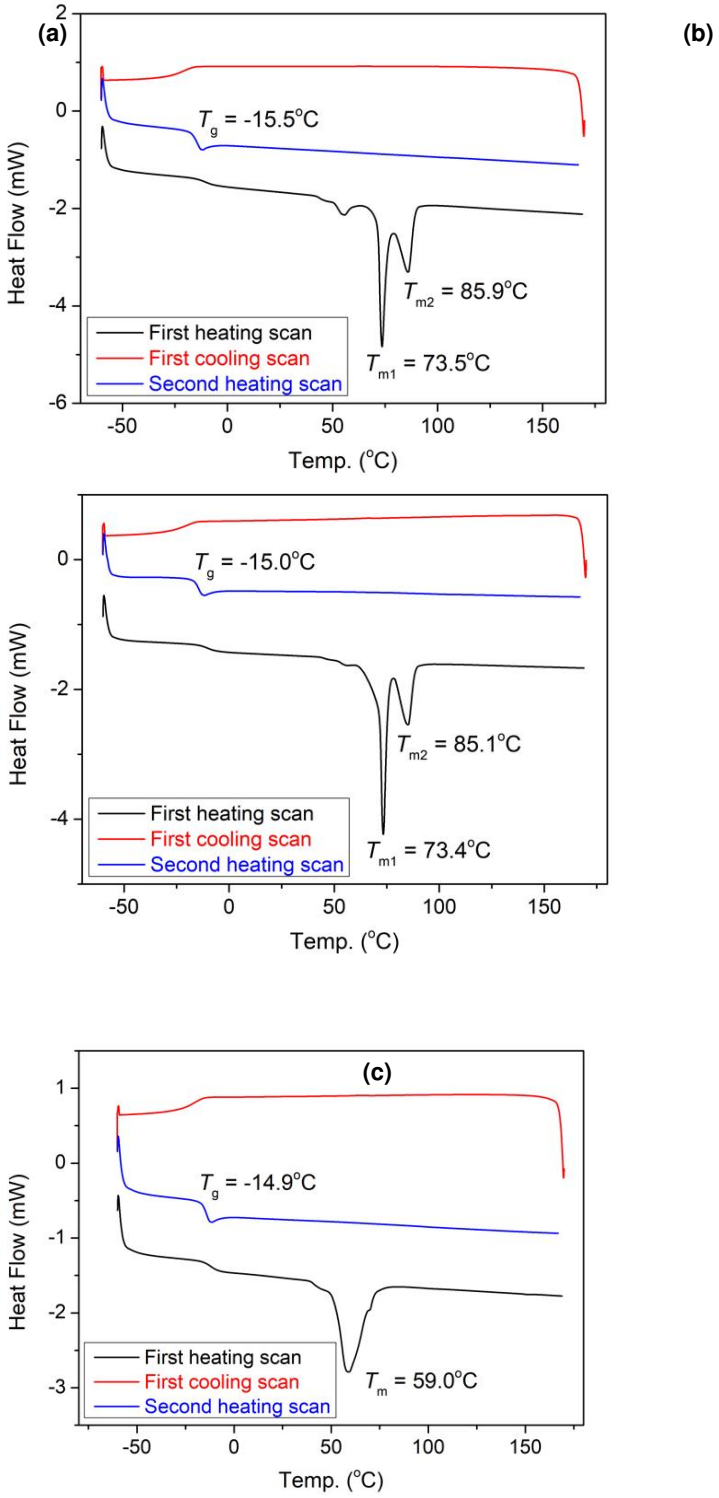

Figure S3.24. DSC curves of P3HV produced by (a) *rac*-8DL^{Et}/1 =100/1 (360 min); (b) *rac*-8DL^{Et}/2 =100/1 (360 min) and (c) *rac*-8DL^{Et}/6 =100/1 (15 min) with different cooling and second heating rate of 10 °C/min.

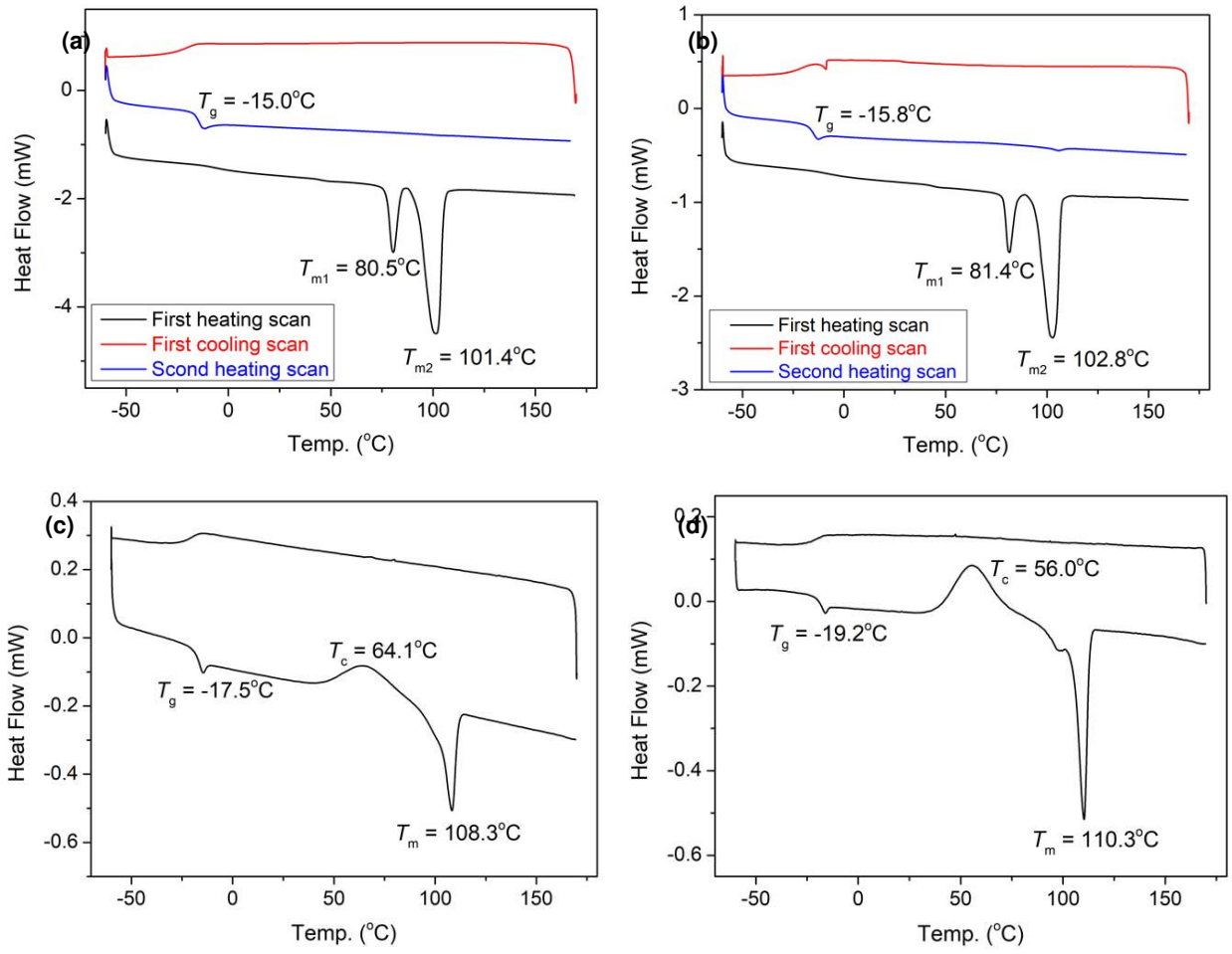

Figure S3.25. DSC curves of P3HV (P_m = 0.97, [*mm*] = 95%) produced by *rac*-8DL^{Et}/3 =100/1 (30 min) with different cooling and second heating rates: (a) 10 °C/min; (b) 5°C/min; (c) 2 °C/min; and (d) 1 °C/min.

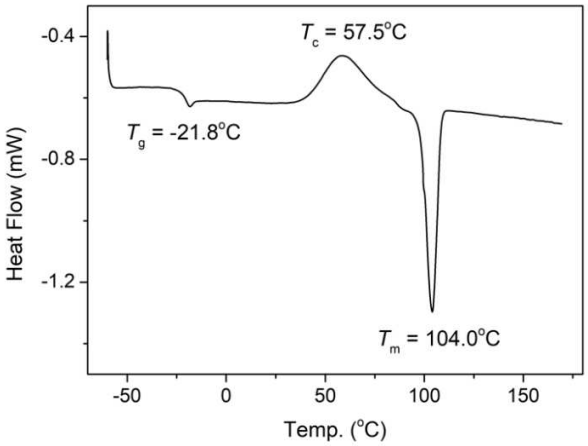

Figure S3.26. DSC curve of P3HV (P_m = 0.94, [*mm*] = 93%) produced by *rac*-8DL^{Et}/5 = 50/1 (20 h) with cooling and second heating rate of 2 °C/min.[2b]

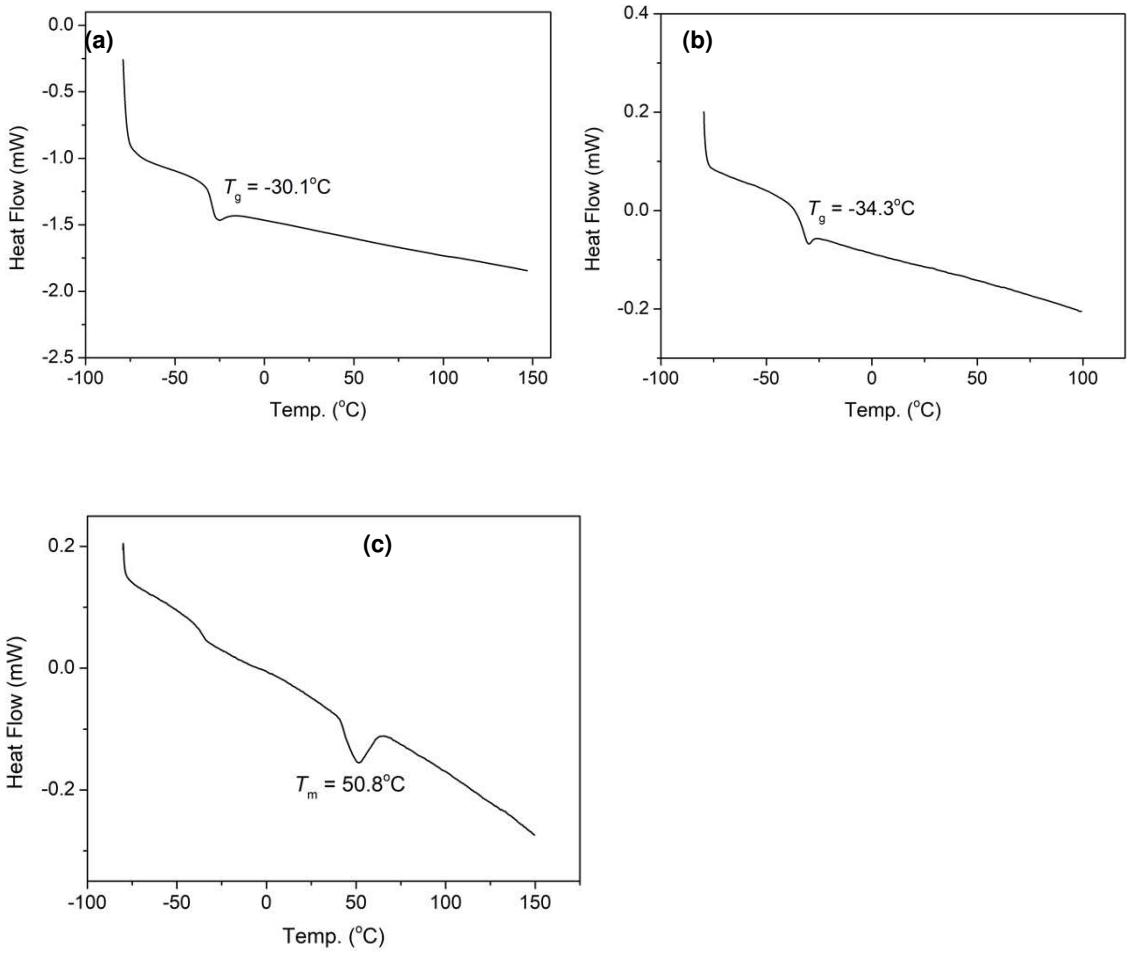

Figure S3.27. DSC curves of P3HHp (P_m = 0.97, [*mm*] = 93%) produced by *rac*-8DL^{Bu}/3 =200/1 with different cooling and second heating rates: (a) 10 °C/min; (b) 2°C/min; and (c) 1 °C/min (curve of the first heating scan).

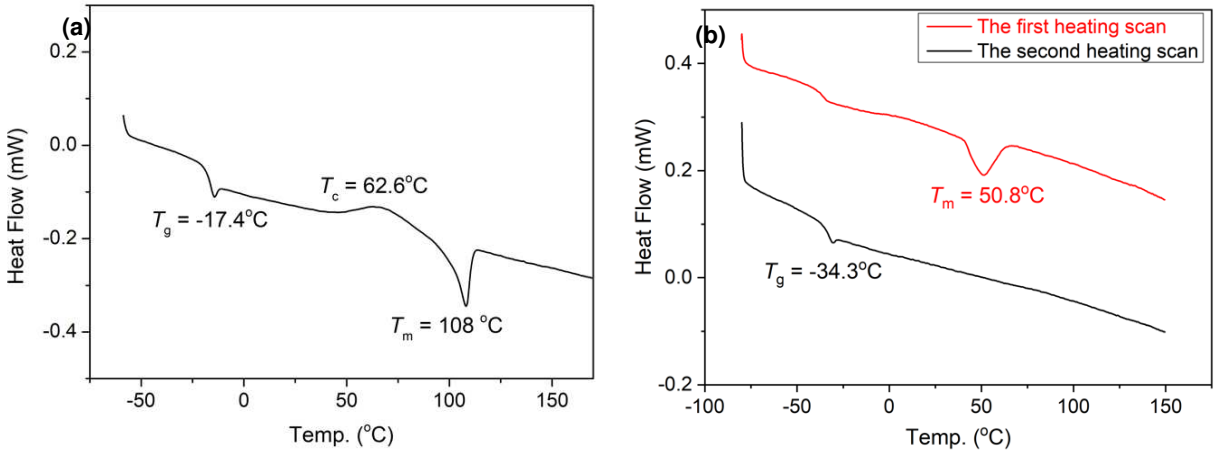

Figure S3.28. (a) DSC curve (the second heating scan) of P3HV obtained by [*rac*-8DL^{Et}]/[3] = 200/1 (cooling and second heating rate = 2 °C/min). (b) DSC curve of P3HHp obtained by [*rac*-8DL^{Bu}]/[3] = 200/1 (cooling and second heating rate = 1 °C/min).

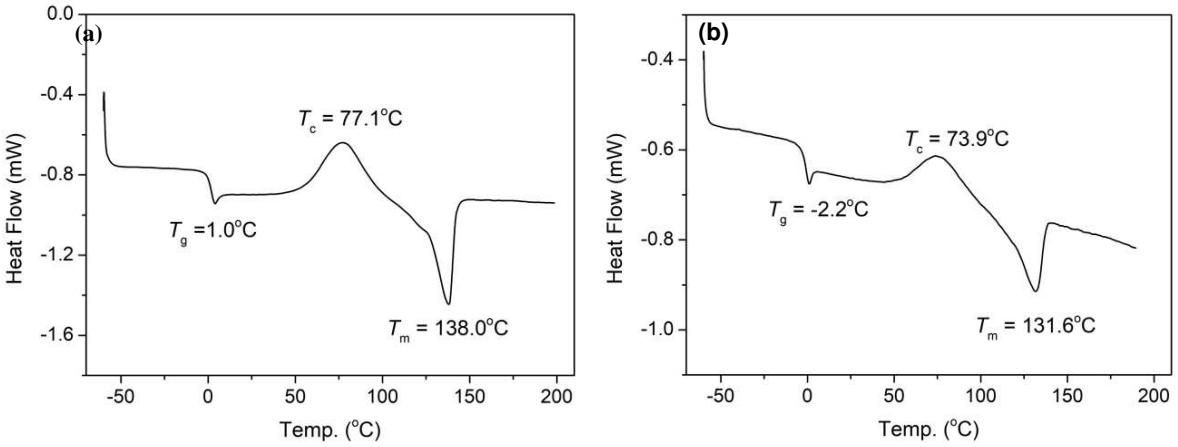

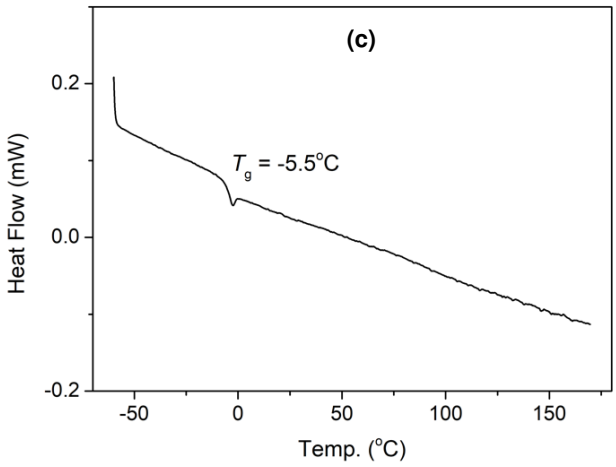

Figure S3.29. DSC curves of P3HBV produced by [*rac*-8DL^{Me}+*rac*-8DL^{Et}]/[3] = 800/1 with *rac*-8DL^{Et} incorporation of: (a) 13.7% (5 °C/min); (b) 19.9% (2 °C/min); and (c) 29.3% (1 °C/min).

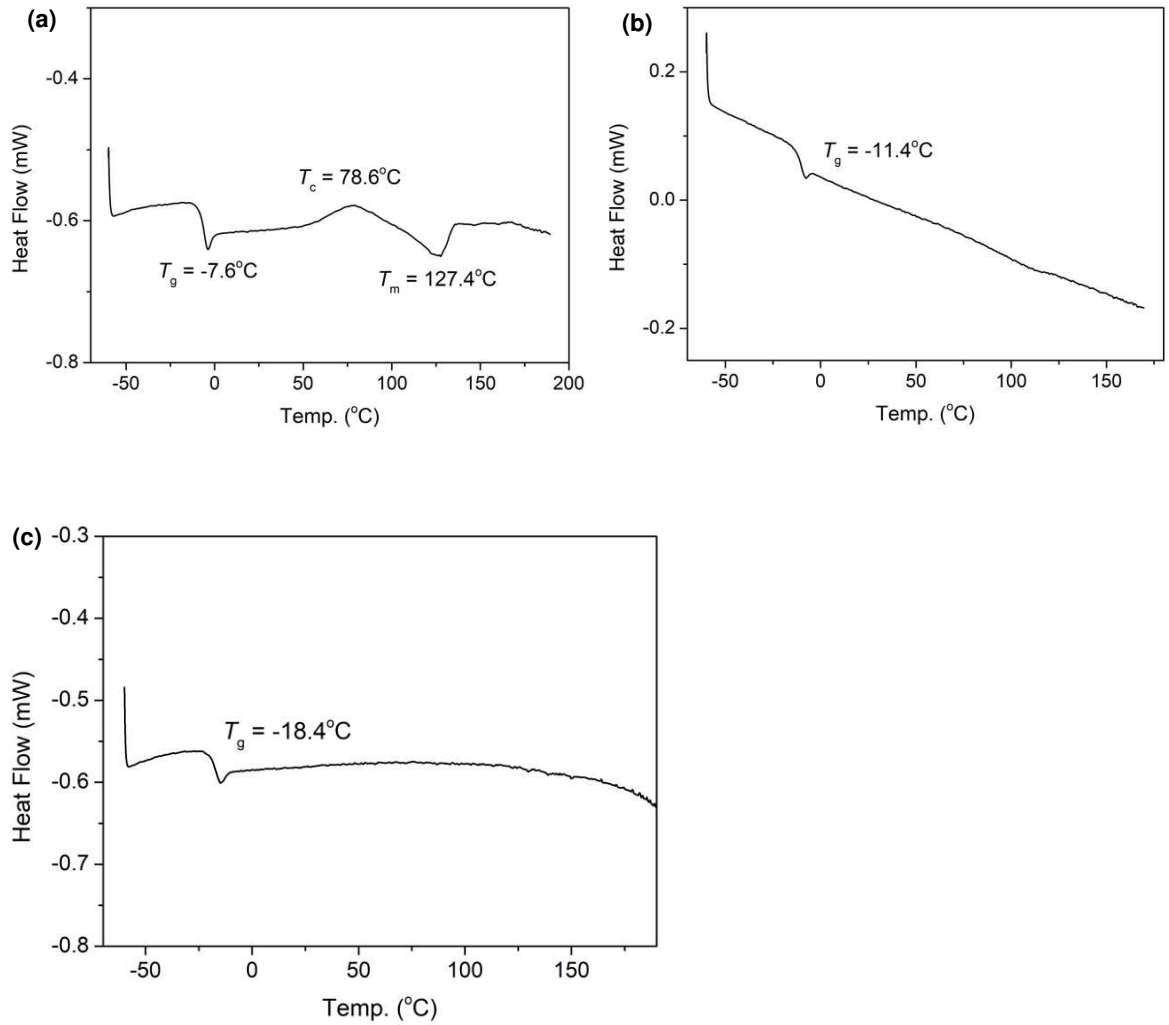

Figure S3.30. DSC curves of P3HBHp produced by [*rac*-8DL^{Me}+*rac*-8DL^{Bu}]/[3] = 800/1 with *rac*-8DL^{Bu} incorporation of: (a) 18.1% (2 °C/min); (b) 25.1% (1 °C/min); and (c) 41.0% (1 °C/min).

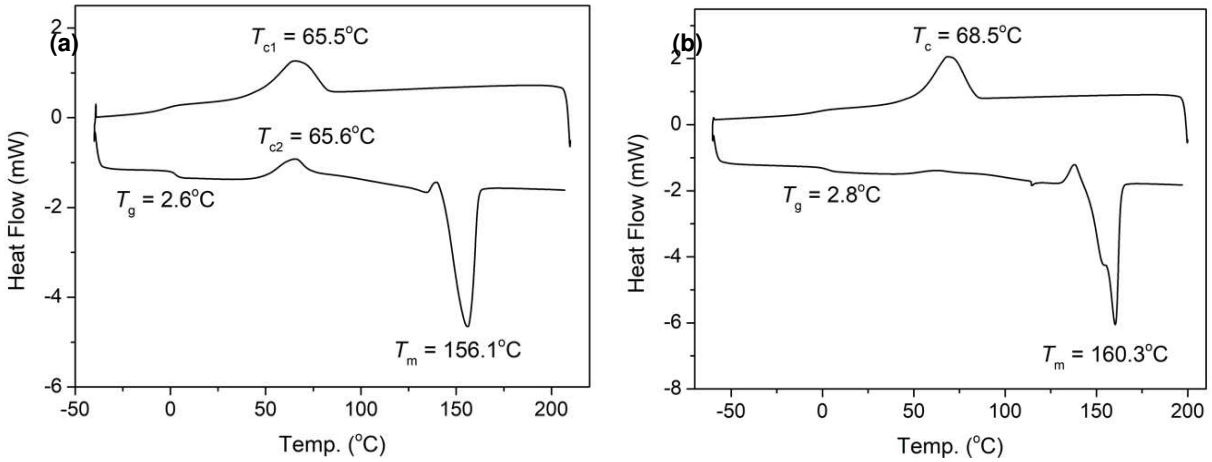

Figure S3.31. DSC curves of copolymers produced by [*rac*-8DL^{Me} + *rac*-8DL^{R}]/[5] = 400/1 with cooling and second heating rate of 10 °C/min. (a) P3HBV with *rac*-8DL^{Et} incorporation of 5.7%; and (b) P3HBHp with *rac*-8DL^{Bu} incorporation of 4.6%.

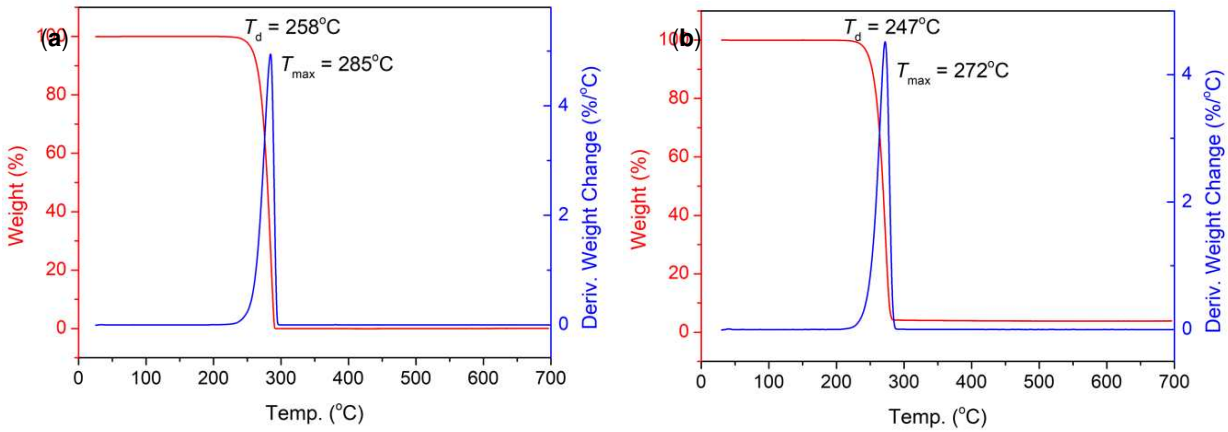

Figure S3.32. TGA and DTG curves of PHAs produced by catalyst 3. (a) P3HV (M_n = 31.8 kg/mol, $Đ$ = 1.18). (b) P3HHp (M_n = 140 kg/mol, $Đ$ = 1.20).

(a) **(b)**

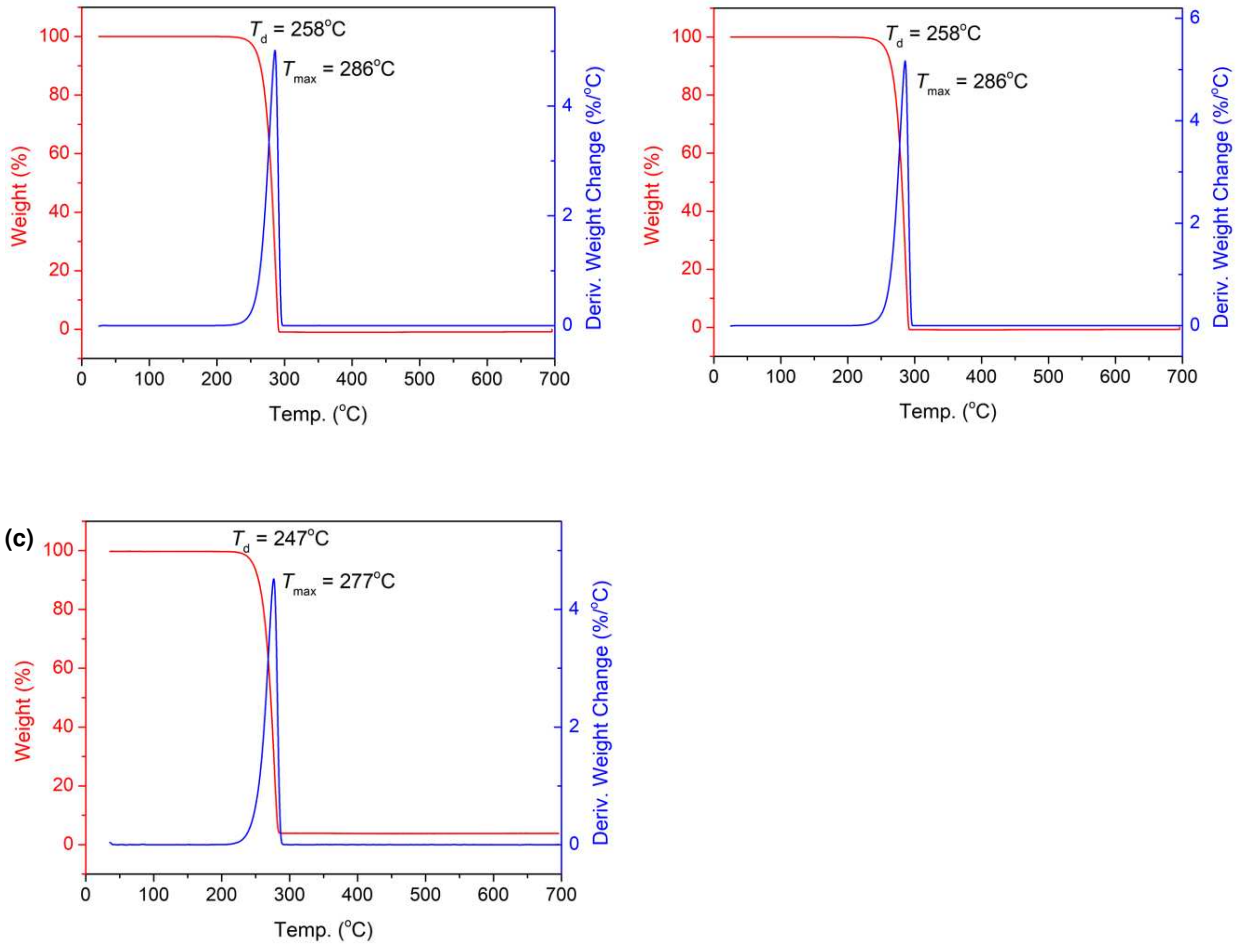

Figure S3.33. TGA and DTG curves of P3HBV produced by [*rac*-8DL^{Me} + *rac*-8DL^{Et}]/[3] = 400/1 with different *rac*-8DL^{Et} incorporations of (a) 6.6% (run 9, Table 3.1); (b) 15.7% (run 13, Table 3.1); (c) 37.6% (run 17, Table 3.1).

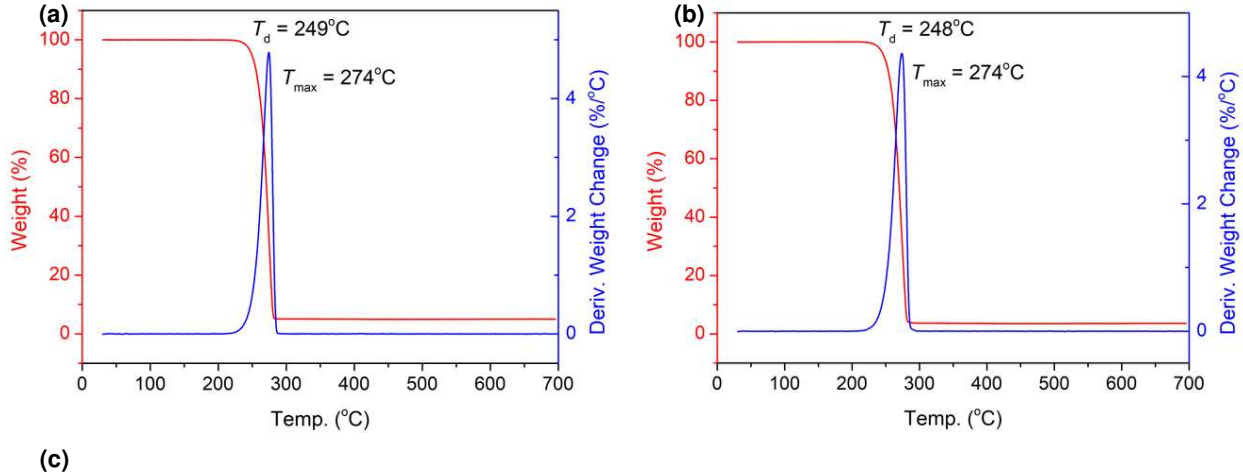

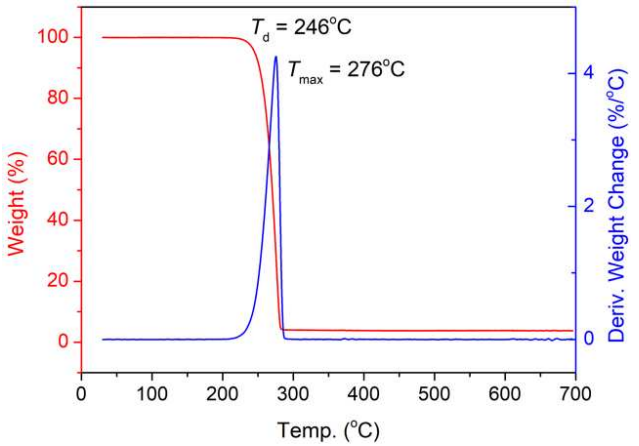

Figure S3.34. TGA and DTG curves of P3HBV produced by [*rac*-8DL^{Me} + *rac*-8DL^{Bu}]/[3] = 400/1 with different *rac*-8DL^{Bu} incorporations of (a) 7.3% (run 1, Table 3.2); (b) 19.1% (run 3, Table 3.2); (c) 44.8% (run 5, Table 3.2).

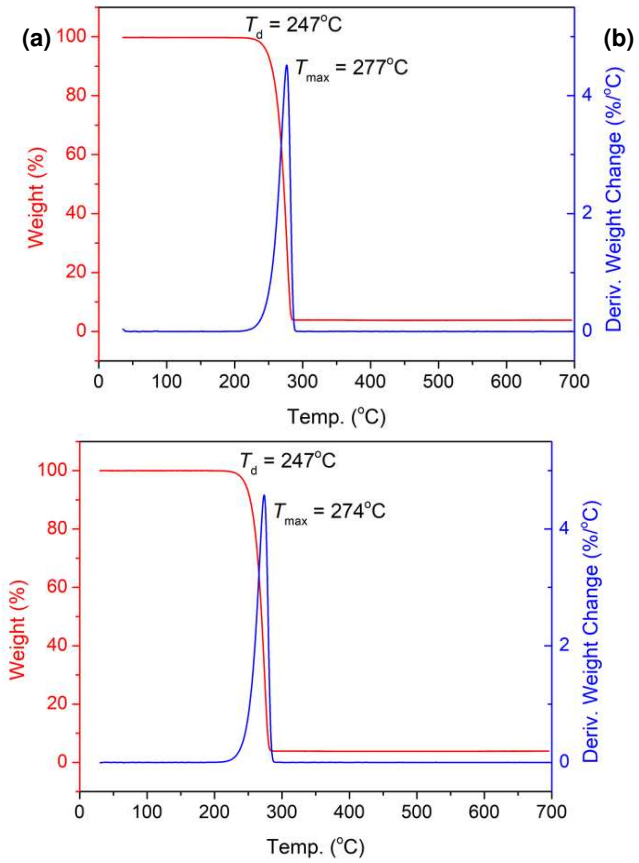

Figure S3.35. TGA and DTG curves of PHAs produced by catalyst 3. (a) P3HBV with *rac*-8DL^{Et} incorporation of 19.9% (M_n = 107 kg/mol, $Đ$ = 1.11). (b) P3HBHp with *rac*-8DL^{Bu} incorporation of 18.1% (M_n = 139 kg/mol, $Đ$ = 1.08).

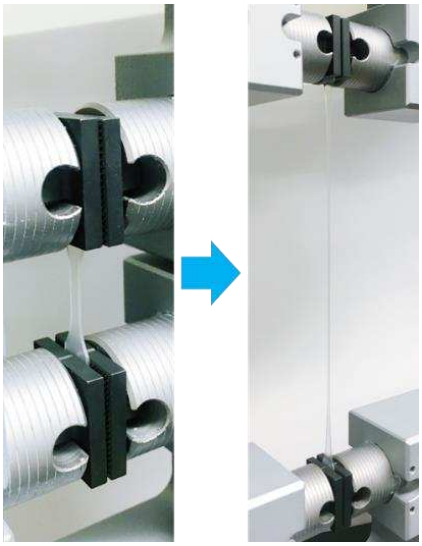

Figure S3.36. Photographs showing tensile test of a P3HBHp specimen with *rac*-8DL^{Bu} incorporation of 19.6%.

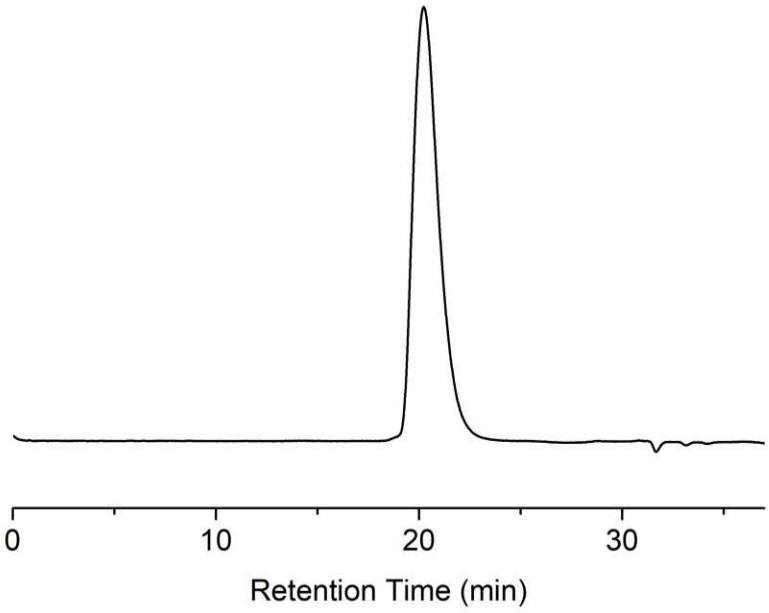

Figure S3.37. GPC trace of P3HV obtained by [*rac*-8DL^{Et}]/[3]/[BnOH] = 200/1/1; M_n = 48.7 kg/mol, $Đ$ = 1.23.

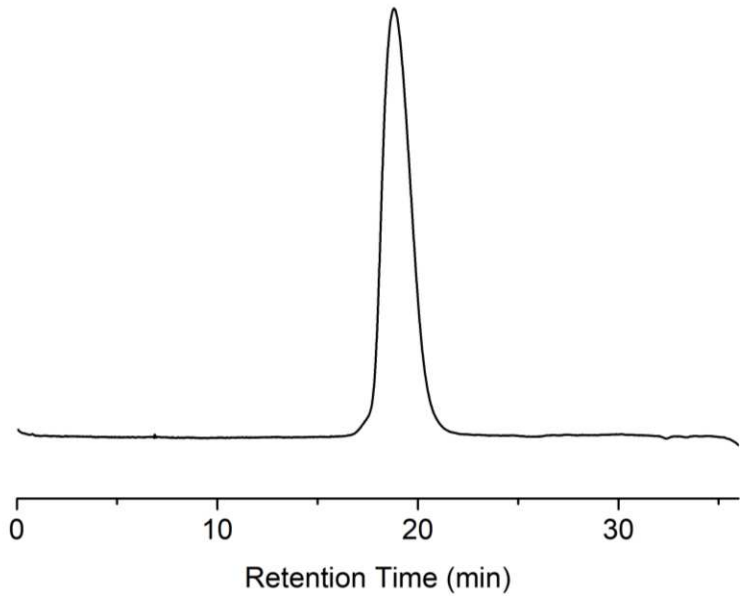

Figure S3.38. GPC trace of P3HHp obtained by [*rac*-8DL^{Bu}]/[3]/[BnOH] = 400/1/1; M_n = 140 kg/mol, $Đ$ = 1.19.

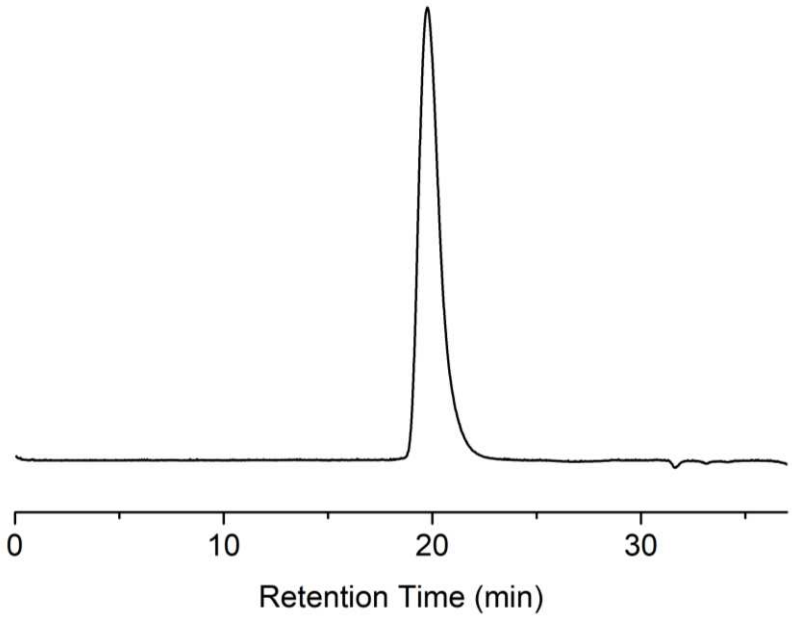

Figure S3.39. GPC trace of P3HBV obtained by [*rac*-8DL^{Me} + *rac*-8DL^{Et}]/[3]/[BnOH] = 400/1/1 and [*rac*-8DL^{Me}]/[*rac*-8DL^{Et}] = 10/1; M_n = 86.6 kg/mol, $Đ$ = 1.18.

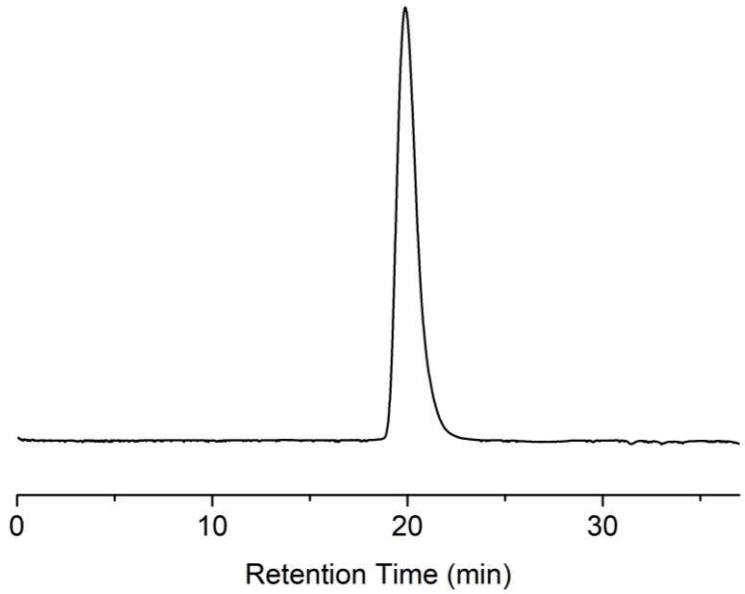

Figure S3.40. GPC trace of P3HBV obtained by [*rac*-8DL^{Me} + *rac*-8DL^{Et}]/[3]/[BnOH] = 400/1/1 and [*rac*-8DL^{Me}]/[*rac*-8DL^{Et}] = 3/1; M_n = 76.6 kg/mol, $Đ$ = 1.18.

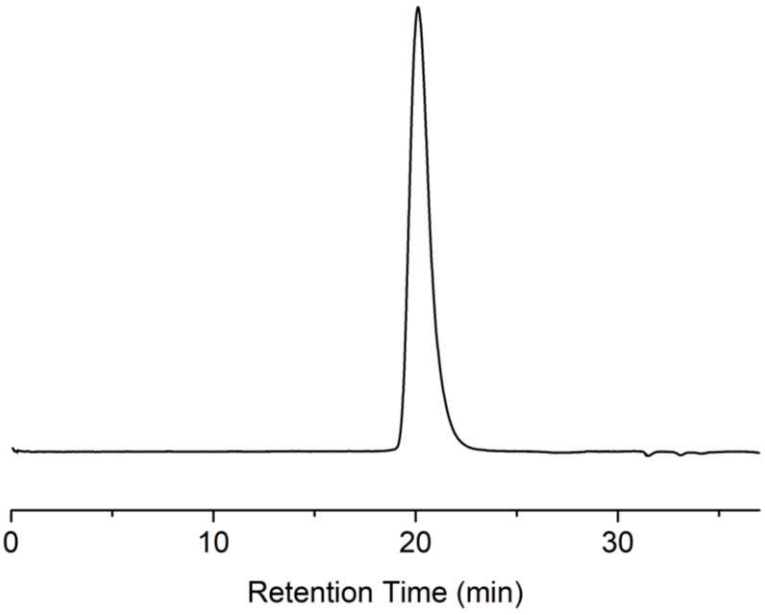

Figure S3.41. GPC trace of P3HBV obtained by [*rac*-8DL^{Me} + *rac*-8DL^{Et}]/[3]/[BnOH] = 400/1/1 and [*rac*-8DL^{Me}]/[*rac*-8DL^{Et}] = 1/1; M_n = 59.6 kg/mol, $Đ$ = 1.21.

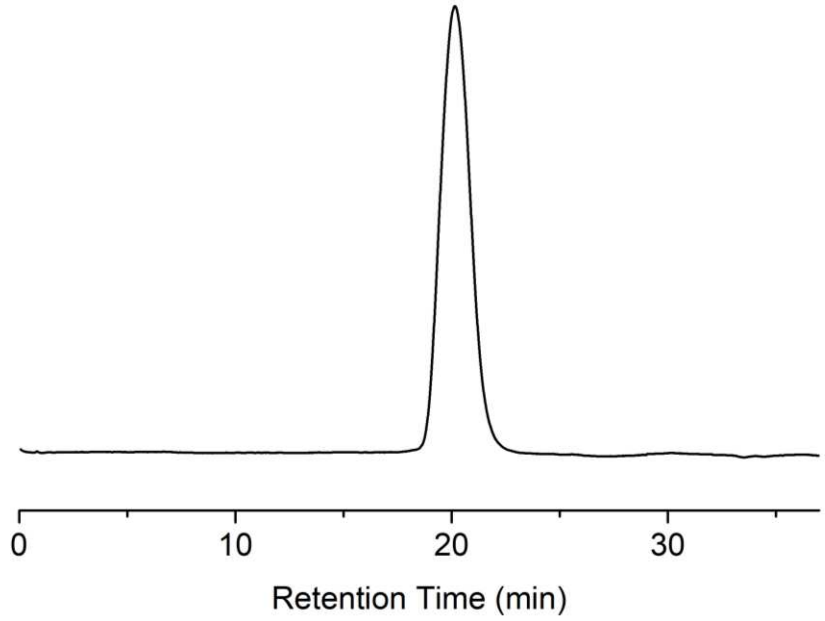

Figure S2.42. GPC trace of P3HBV obtained by [*rac*-8DL^{Me} + *rac*-8DL^{Et}]/[3]/[BnOH] = 800/1/1 and [*rac*-8DL^{Me}]/[*rac*-8DL^{Et}] = 2/1; M_n = 107 kg/mol, $Đ$ = 1.11.

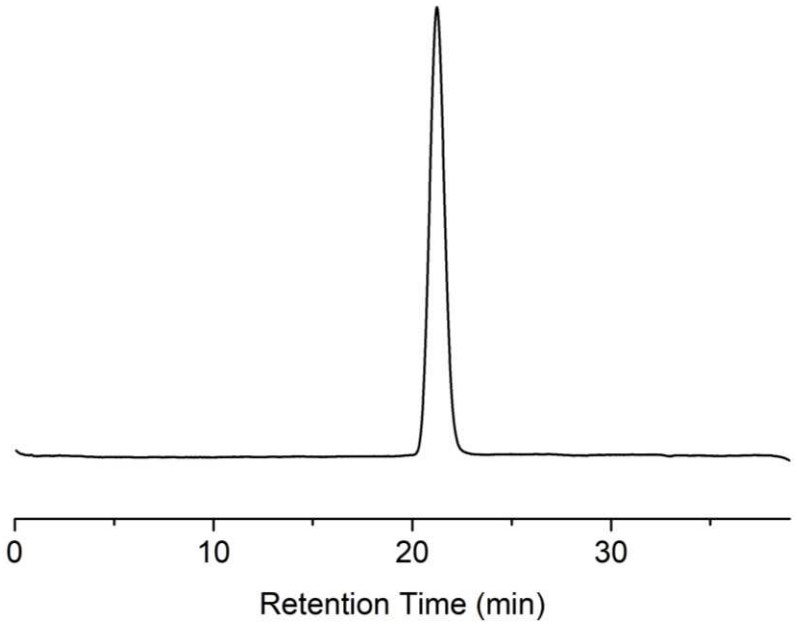

Figure S3.43. GPC trace of P3HBV obtained by [*rac*-8DL^{Me} + *rac*-8DL^{Et}]/[5]/[BnOH] = 400/1/1 and [*rac*-8DL^{Me}]/[*rac*-8DL^{Et}] = 1/1; M_n = 45.0 kg/mol, $Đ$ = 1.01.

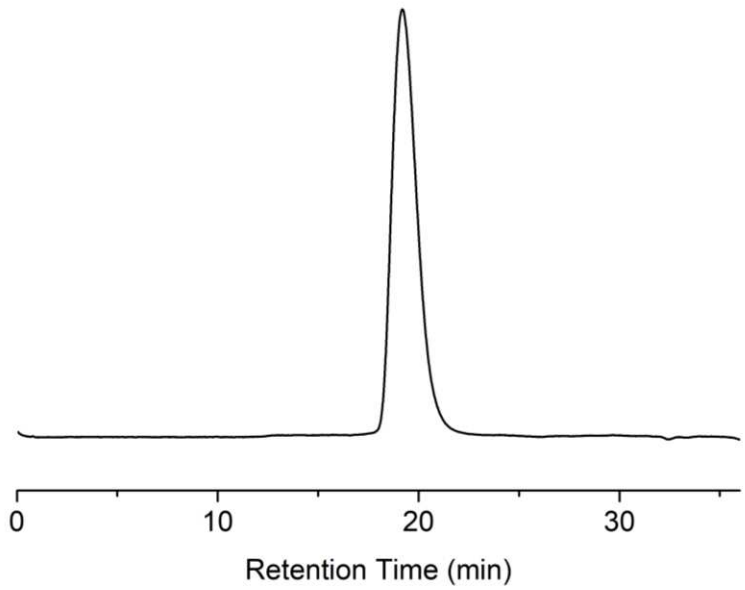

Figure S3.44. GPC trace of P3HBHp obtained by [*rac*-8DL^{Me} + *rac*-8DL^{Bu}]/[3]/[BnOH] = 400/1/1 and [*rac*-8DL^{Me}]/[*rac*-8DL^{Bu}] = 10/1; M_n = 126 kg/mol, $Đ$ = 1.13.

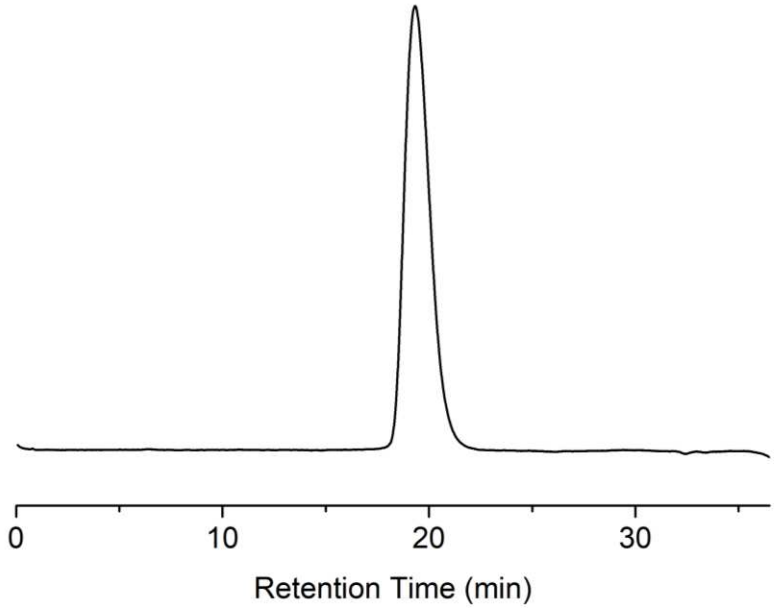

Figure S3.45. GPC trace of P3HBHp obtained by [*rac*-8DL^{Me} + *rac*-8DL^{Bu}]/[3]/[BnOH] = 400/1/1 and [*rac*-8DL^{Me}]/[*rac*-8DL^{Bu}] = 3/1; M_n = 108 kg/mol, $Đ$ = 1.16.

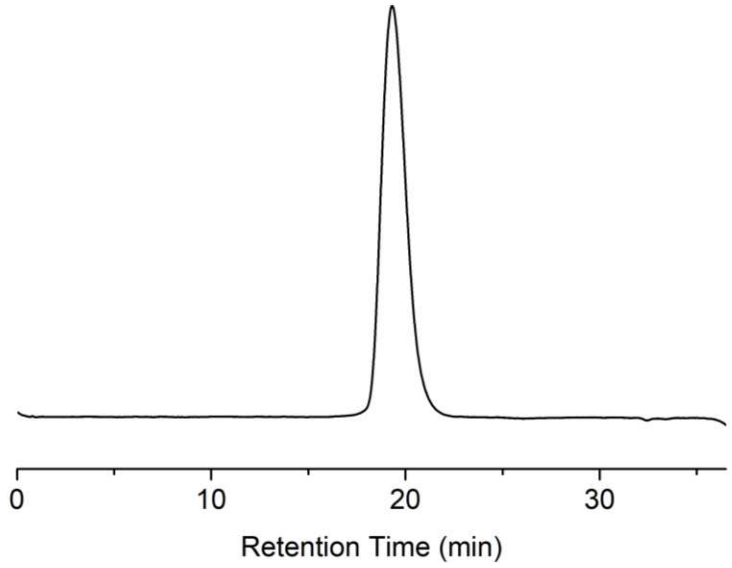

Figure S3.46. GPC trace of P3HBHp obtained by [*rac*-8DL^{Me} + *rac*-8DL^{Bu}]/[3]/[BnOH] = 400/1/1 and [*rac*-8DL^{Me}]/[*rac*-8DL^{Bu}] = 1/1; M_n = 105 kg/mol, $Đ$ = 1.17.

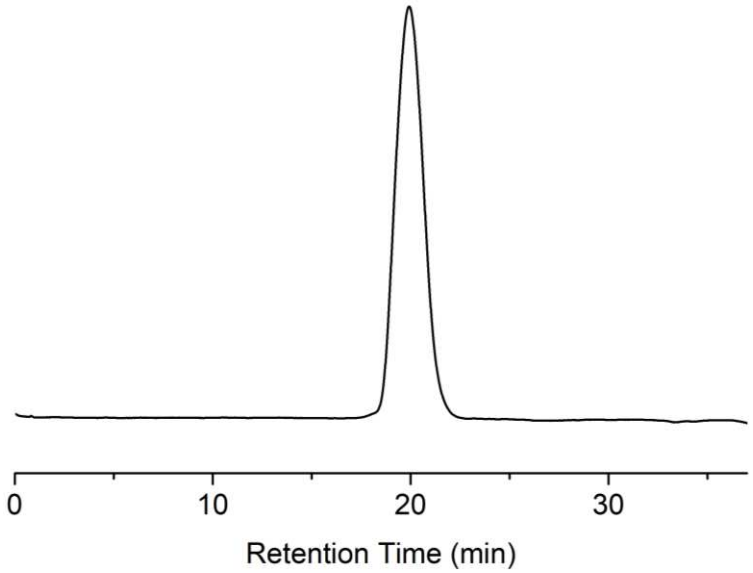

Figure S3.47. GPC trace of P3HBHp obtained by [*rac*-8DL^{Me} + *rac*-8DL^{Bu}]/[3]/[BnOH] = 800/1/1 and [*rac*-8DL^{Me}]/[*rac*-8DL^{Bu}] = 3/1; M_n = 139 kg/mol, $Đ$ = 1.08.

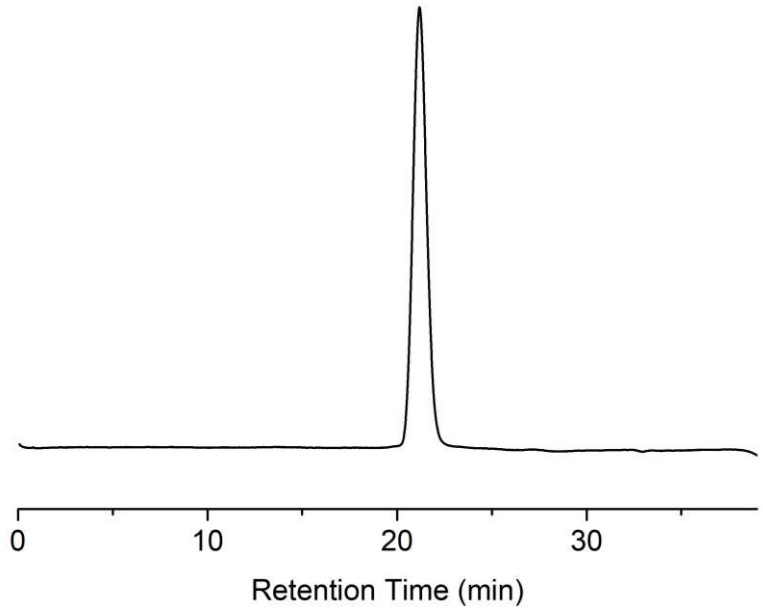

Figure S3.48. GPC trace of P3HBHp obtained by [*rac*-8DL^{Me} + *rac*-8DL^{Bu}]/[5]/[BnOH] = 400/1/1 and [*rac*-8DL^{Me}]/[*rac*-8DL^{Bu}] = 1/1; M_n = 47.2 kg/mol, $Đ$ = 1.01.

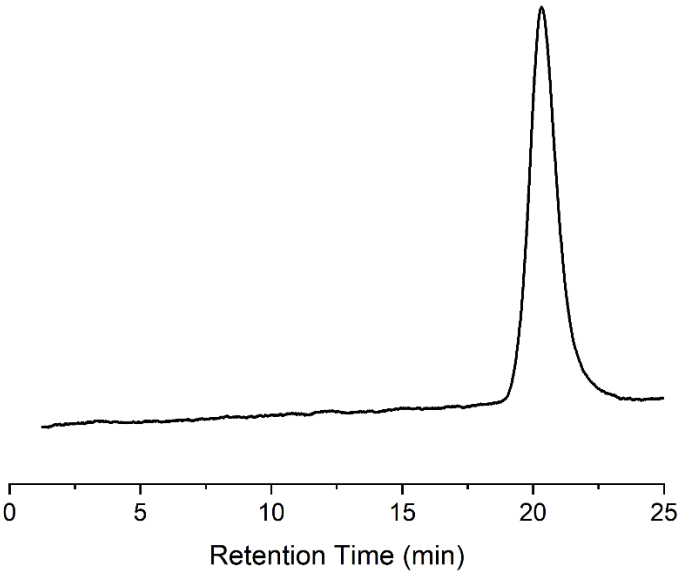

Figure S3.49. GPC trace of P3HBHp obtained by [*rac*-8DL^{Me} + *rac*-8DL^{Et}]/[**3**]/[BnOH] = 800/1/1 and [*rac*-8DL^{Me}]/[*rac*-8DL^{Et}] = 5/1; M_n = 175 kg/mol, $Đ$ = 1.35. (Run 1, Table 3.3)

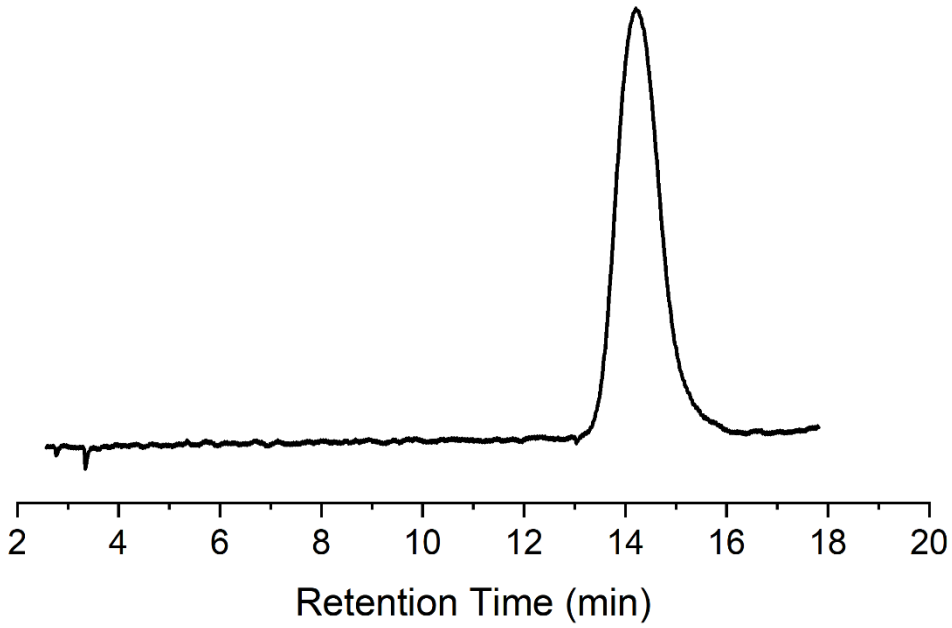

Figure S3.50. GPC trace of P3HBHp obtained by [*rac*-8DL^{Me} + *rac*-8DL^{Et}]/[**3**]/[BnOH] = 800/1/1 and [*rac*-8DL^{Me}]/[*rac*-8DL^{Et}] = 3/1; M_n = 138 kg/mol, $Đ$ = 1.08 (Run 2, Table 3.3)

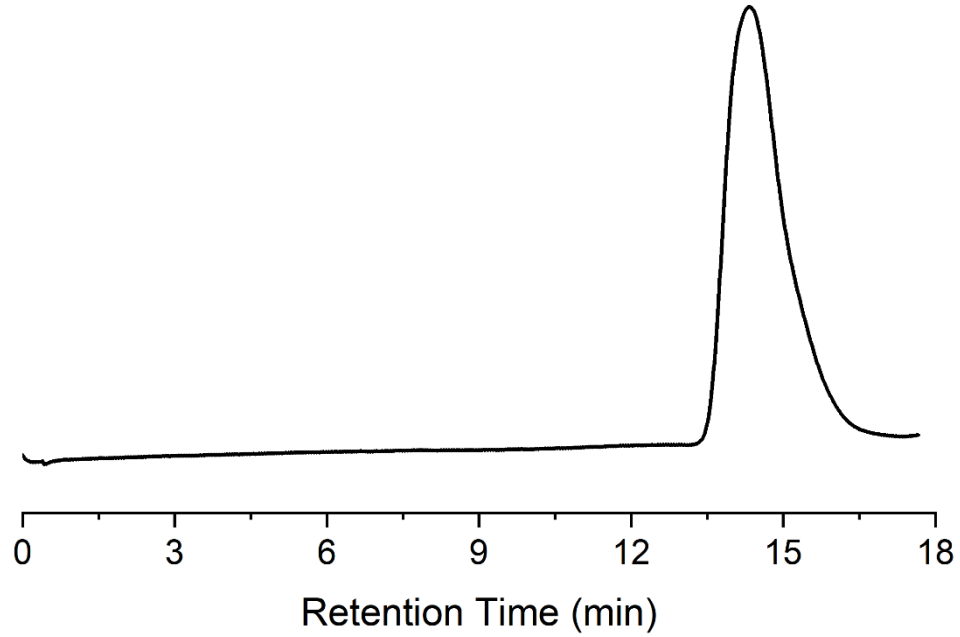

Figure S3.51. GPC trace of P3HBHp obtained by [*rac*-8DL^{Me} + *rac*-8DL^{Bu}]/[**3**]/[BnOH] = 800/1/1 and [*rac*-8DL^{Me}]/[*rac*-8DL^{Bu}] = 10/1; M_n = 169 kg/mol, $Đ$ = 1.01 (Run 4, Table 3.3)

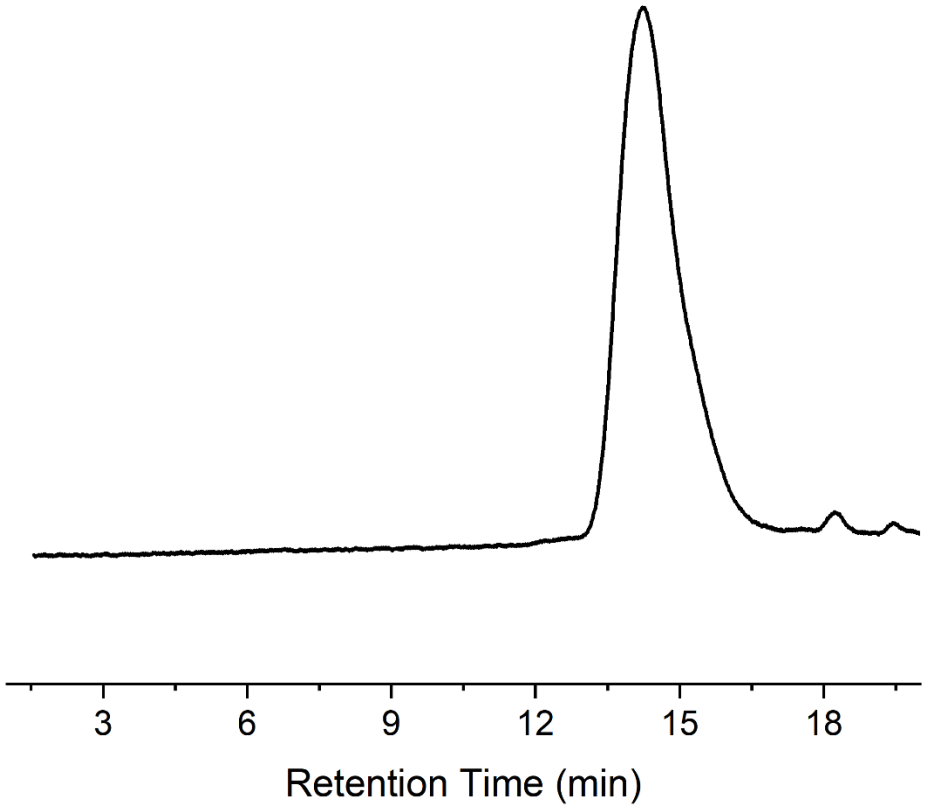

Figure S3.52. GPC trace of P3HBHp obtained by [*rac*-8DL^{Me} + *rac*-8DL^{Bu}]/[**3**]/[BnOH] = 800/1/1 and [*rac*-8DL^{Me}]/[*rac*-8DL^{Bu}] = 5/1; M_n = 183 kg/mol, $Đ$ = 1.05 (Run 5, Table 3.3)

References

[1] a) J. Eppinger, E. Herdtweck, R. Anwander, Polyhedron 1998, 17, 1195-1201; b) R. Anwander, O. Runte, J. Eppinger, G. Gerstberger, E. Herdtweck, M. Spiegler, *J. Chem. Soc., Dalton Trans.* 1998, 847-858.

[2] a) X. Tang, E. Y.-X. Chen, Nat. Commun. 2018, 9, 2345; b) X. Tang, A. H. Westlie, E. M. Watson, E. Y.-X. Chen, *Science* 2019, 366, 754-758; c) M.-H. Lin, T. V. RajanBabu, Organic Letters 2002, 4, 1607-1610; d) Q. Liu, C. Meermann, H. W. Görlitzer, O. Runte, E. Herdtweck, P. Sirsch, K. W. Törnroos, R. Anwander, Dalton Transactions 2008, 6170-6178.

[3] D. Seebach, T. Hoffmann, F. N. M. Kühnle, J. N. Kinkel, M. Schulte, Helv. Chim. Acta 1995, 78, 1525-1540.

[4] SHELXTL, Version 6.12; Bruker Analytical X-ray Solutions: Madison, WI, 2001.

[5] Frisch, M. J.; Trucks, G. W.; Schlegel, H. B.; Scuseria, G. E.; Robb, M. A.; Cheeseman, J. R.; Montgomery, J. A.; Vreven, T.; Kudin, K. N.; Burant, J. C.; Millam, J. M.; Iyengar, S. S.; Tomasi, J.; Barone, V.; Mennucci, B.; Cossi, M.; Scalmani, G.; Rega, N.; Petersson, G. A.; Nakatsuji, H.; Hada, M.; Ehara, M.; Toyota, K.; Fukuda, R.; Hasegawa, J.; Ishida, M.; Nakajima, T.; Honda, Y.; Kitao, O.; Nakai, H.; Klene, M.; Li, X.; Knox, J. E.; Hratchian, H. P.; Cross, J. B.; Adamo, C.; Jaramillo, J.; Gomperts, R.; Stratmann, R. E.; Yazyev, O.; Austin, A. J.; Cammi, R.; Pomelli, C.; Ochterski, J. W.; Ayala, P. Y.; Morokuma, K.; Voth, G. A.; Salvador, P.; Dannenberg, J. J.; Zakrzewski, V. G.; Dapprich, S.; Daniels, A. D.; Strain, M. C.; Farkas, O.; Malick, D. K.; Rabuck, A. D.; Raghavachari, K.; Foresman, J. B.; Ortiz, J. V.; Cui, Q.; Baboul, A. G.; Clifford, S.; Cioslowski, J.; Stefanov, B. B.; Liu, G.; Liashenko, A.; Piskorz, P.; Komaromi, I.; Martin, R. L.; Fox, D. J.; Keith, T.; Al-Laham, M. A.; Peng, C. Y.; Nanayakkara,

A.; Challacombe, M.; Gill, P. M. W.; Johnson, B.; Chen, W.; Wong, M. W.; Gonzalez, C.; Pople, J. A. B.1 ed., Gaussian, Inc., Pittsburgh PA, 2009. .

[6] a) J. P. Perdew, Phys. Rev. B 1986, 34, 7406-7406; b) A. D. Becke, Phys. Rev. A 1988, 38, 3098-3100; c) J. P. Perdew, Phys. Rev. B 1986, 33, 8822-8824.

[7] a) U. Häussermann, M. Dolg, H. Stoll, H. Preuss, P. Schwerdtfeger, R. M. Pitzer, Mol. Phys. 1993, 78, 1211-1224; b) T. Leininger, A. Nicklass, H. Stoll, M. Dolg, P. Schwerdtfeger, J. Chem. Phys. 1996, 105, 1052-1059; c) W. Küchle, M. Dolg, H. Stoll, H. Preuss, J. Chem. Phys. 1994, 100, 7535-7542.

[8] F. Weigend, R. Ahlrichs, Phys. Chem. Chem. Phys. 2005, 7, 3297-3305.

[9] a) J. Tomasi, B. Mennucci, R. Cammi, Chem. Rev. 2005, 105, 2999-3094; b) V. Barone, M. Cossi, J. Phys. Chem. A 1998, 102, 1995-2001.

Appendix B

Experimental Details and Supporting Information for Chapter 4

A.1. Experimental Section

Materials. All syntheses and manipulations of air- and moisture-sensitive chemicals and materials were carried out in flamed Schlenk-type glassware on a dual-manifold Schlenk line or in an inert gas (Ar or N_2)-filled glovebox. HPLC-grade organic solvents were first sparged extensively with nitrogen during filling 20 L solvent reservoirs and then dried by passage through activated alumina (for DCM) followed by passage through Q-5 supported copper catalyst (for toluene and hexanes) stainless steel columns. Benzene-d_6 was dried over sodium/potassium alloy and filtered, whereas CD_2Cl_2 and $CDCl_3$ were dried over CaH_2, vacuum-distilled and stored over activated Davison 4 Å molecular sieves.

Yttrium chloride YCl_3 and lanthanum chloride $LaCl_3$ were purchased from Sigma-Aldrich Chemical Co. and used as received. Benzyl alcohol was purchased from Alfa Aesar Chemical Co., purified by distillation over CaH_2, and stored over activated Davison 4 Å molecular sieves. Dimethyl succinate, sodium methoxide, and 3-chloroperoxybenzoic acid (*m*CPBA, 70–75%) were purchased from Fisher Scientific Co. and used as received. Dimethyl 2,5-dioxocyclohexane-1,4-dicarboxylate was purchased from TCI chemicals and used as received. Benzyl bromide was purchased from Acros Organics and used as received. Literature procedures were employed for the preparation of *rac*-8DL^{Me} [1] and *rac*-8DL^{Bu}.[2] The yttrium and lanthanum complexes were prepared according to their respective literature procedures: $Y[N(SiHMe_2)_2]_3(THF)_2$, $La[N(SiHMe_2)_2]_3(THF)_2$,[3] and complexes **1**,[4] **2**-**4**,[1,3,5] and **5**.[1]

A.1.2. Synthesis of Monomers

Dimethyl 2,5-dioxocyclohexane-1,4-dicarboxylate. A solution of sodium methoxide (185 mL, 5.4 M, 1.0 mol) was added to dimethyl succinate (73.1 g, 0.5 mol) in one portion, and the mixture was heated

under reflux for 24 h. A thick pink-colored precipitate was then formed and remained throughout the reaction. The methanol was removed using evaporator, a 2*N* sulfuric acid solution (500 mL) was added to the residue, and the mixture was stirred vigorously for 4 h. The solid was collected by filtration and washed several times with water. The air-dried product was a pale-buff powder, which was recrystallized from 300 mL ethyl acetate. The filtrate was chilled to give cream to pink-cream colored crystals of the title compound, 37.1 g (65 %). ^{1}H NMR (400 MHz, $CDCl_3$): δ 12.12 (s, 1H), 3.79 (s, 3H), 3.18 (s, 2H).

Dimethyl 1,4-dibenzyl-2,5-dioxocyclohexane-1,4-dicarboxylate. To a stirred suspension of K_2CO_3 (33.6 g, 0.263 mol) in 250 mL DMF under N_2 was added dimethyl 2,5-dioxocyclohexane-1,4-dicarboxylate (20 g, 87.6 mmol). After 15 min stirring at room temperature, benzyl bromide (60.0 g, 0.35 mol) was added dropwise. After 24 h, the mixture was concentrated in vacuo, dissolved in 200 mL of H_2O, and extracted with CH_2Cl_2 (150 mL x 3). The combined organic layers were washed twice with 10% $Na_2S_2O_3$ solution, washed once with saturated NaCl, dried with anhydrous Na_2SO_4, and evaporated. The solid was washed with hexanes to give 34.5 g (96%) of the title compound as a 2:1 mixture of diastereomers. ^{1}H NMR (400 MHz, $CDCl_3$) δ 7.66 (d, *J* = 6.8 Hz, 1H, Ar-*H*), 7.65 – 7.39 (m, 1*H,* Ar-*H*), 7.22 (dd, *J* = 7.4, 4.3 Hz, 5H, Ar-*H*), 7.06 (d, *J* = 7.7 Hz, 1H, Ar-*H*), 6.95 (dd, *J* = 6.3, 2.9 Hz, 2H, Ar-*H*), Major diastereomer: 3.64 (s, 6H, *Me*O), 3.18 (dt, *J* = 13.6, 8.6 Hz, 2H, C*H*$_2$), 2.88 (t, *J* = 16.1 Hz, 2H, C*H*$_2$), 2.68 (d, *J* = 15.2 Hz, 2H, C*H*$_2$), 2.26 (d, *J* = 16.4 Hz, 2H, C*H*$_2$). Minor diastereomer: δ 3.58 (s, 6H, *Me*O), 3.20 (dd, *J* = 36.7, 22.7 Hz, 4H, C*H*$_2$), 2.86 (d, *J* = 15.6 Hz, 2H, C*H*$_2$), 2.68 (d, *J* = 15.2 Hz, 2H, C*H*$_2$).

***Trans*-2,5-dibenzylcyclohexane-1,4-dione.** To a stirred suspension of dimethyl 1,4-dibenzyl-2,5-dioxocyclohexane-1,4-dicarboxylate 5 g, 12.2 mmol) in 5 mL methanol and 15 g crushed ice, 20 mL of concentrated H_2SO_4 was added. After 15 min of stirring at room temperature, the mixture was heated to 100 °C for 48 h. The acidic solution was cooled to room temperature, neutralized with aq. NaOH (pH 6-7), and extracted with CH_2Cl_2 (150 mL x 3). The combined organic layers were washed twice with saturated NaCl, dried with anhydrous Na_2SO_4, and evaporated. The residue was purified by recrystallization in DCM/hexanes to afford 3.07 g (86%) of the title

compound. ^{1}H NMR (400 MHz, $CDCl_3$) δ 7.33 – 7.16 (m, 8H, Ar-*H*), 7.08 (dd, *J* = 16.4, 6.5 Hz, 2H, Ar-*H*), 3.30 – 3.13 (m, 2H, C*H*$_2$), 2.88 – 2.78 (m, 2H, C*H*$_2$), 2.63 (dd, *J* = 11.9, 9.7 Hz, 4H, C*H*$_2$), 2.49 (dd, *J* = 15.0, 11.2 Hz, 2H, C*H*$_2$).

***Trans*-4,8-dibenzyl-1,5-dioxocane-2,6-dione (*meso*-8DL^{Bn}).** To a solution of the *meso*-2,5-dioxocylcolexane-1,4-dicarboxylate (10 g, 34.2 mmol) in 300 mL of CH_2Cl_2 was added *m*-CPBA (25.3 g, 70%, 17.7 mmol) in one portion. The pale-yellow solution was stirred at room temperature in the dark for 48 h. The obtained white suspension was diluted with 200 mL of CH_2Cl_2, washed with saturated $NaHCO_3$ solution (100 mL x 3), which contained 5% $Na_2S_2O_3$, dried with anhydrous Na_2SO_4, and evaporated. After recrystallization of the residue (11.6 g) from hexanes/DCM (5/1) and recrystallization from toluene 7.2 g of pure *meso*-8DL^{Bn} was obtained (65% yield). ^{1}H NMR (400 MHz, $CDCl_3$) δ 7.24 (t, *J* = 7.2 Hz, 5H, Ar-*H*), 7.16 (t, *J* = 6.9 Hz, 5H, Ar-*H*), 5.37 – 5.07 (m, 2H, BnC*H*O-C=O), 3.05 (dd, *J* = 14.1, 7.6 Hz, 2H, C*H*$_2$), 2.90 – 2.76 (m, 4H, C*H*$_2$), 2.50 (dd, *J* = 13.0, 7.5 Hz, 2H, C*H*$_2$).

***Cis*-4,8-dibenzyl-1,5-dioxocane-2,6-dione (*rac*-8DL^{Bn}).** The filtrate from the above purification step of *trans*-2,5-dibenzylcyclohexane-1,4-dione was purified by column chromatography to give the *cis*-dione in ~90% racemic content. To a solution of the *trans*-2,5-dibenzylcyclohexane-1,4-dione (1.5 g, 5.13 mmol) in 100 mL of CH_2Cl_2 was added *m*-CPBA (3.8 g, 70%, 15.4 mmol) in one portion. The yellow solution was stirred at room temperature in the dark for 48 h. The obtained white suspension was diluted with 100 mL of CH_2Cl_2, washed with saturated $NaHCO_3$ solution (50 mL x 3), which contained 5% $Na_2S_2O_3$, dried with anhydrous Na_2SO_4, and evaporated. After recrystallization of the residue from hexanes/DCM and recrystallization from toluene 0.4 g of pure *rac*-8DL^{Bn} was obtained. ^{1}H NMR (400 MHz, $CDCl_3$)

δ7.36 – 7.19 (m, 61H), 5.46 – 5.33 (m, 9H), 3.11 (dd, J = 14.1, 7.6 Hz, 9H), 2.94 (dd, J = 14.1, 6.1 Hz, 9H), 2.71 (dd, J = 11.3, 10.1 Hz, 9H), 2.46 (dd, J = 11.3, 3.5 Hz, 9H).

General polymerization procedures. Polymerizations were performed in 5.5 mL glass reactors inside the inert glovebox at RT. The reactor was charged with a predetermined amount of catalyst and/or initiator and solvent (as specified in the polymerization tables) in a glovebox. The mixture was stirred at RT for 10 min, and the polymerization was initiated by rapid addition to an 8DL monomer. After a desired time period, the polymerization was immediately quenched by addition of 0.5 mL of benzoic acid/chloroform (10 mg mL^{-1}) and a 0.02 mL of aliquot was taken from the reaction mixture and prepared for ^1H NMR analysis to obtain the percent monomer conversion data. The quenched mixture was then precipitated into 50 mL of cold methanol while stirring, filtered, washed with cold methanol to remove any unreacted monomer, and dried in a vacuum oven at RT overnight to a constant weight.

Specific conditions for copolymerization runs summarized in Table 4.3. Statistical copolymerizations: run 15, 8DL = 0.95 mmol [1/1 *rac*-DL^{Me} (0.0819 g) : *meso*-DL^{Bn} (0.154 g)], $V_{solvent}$ = 0.95 mL, RT; run 16, 8DL = 0.80 mmol [5/1 *rac*-DL^{Me} (0.115 g) : *meso*-DL^{Bn} (0.043 g)], $V_{solvent}$ = 0.80 mL, RT; run 19, 8DL = 0.37 mmol [(5/1 *meso*-DL^{Bn} (0.100 g) : *rac*-DL^{Bu} (0.0158 g)], $V_{solvent}$ = 0.4 mL, RT; run 20, 8DL = 0.339 mmol [(10/1 *meso*-DL^{Bn} (0.100 g) : *rac*-DL^{Bu} (0.008 g)], $V_{solvent}$ = 0.4 mL, RT. Sequential block copolymerizations: run 17, 8DL = 0.58 mmol [(1/1 *rac*-DL^{Me} (0.05 g) : *meso*-DL^{Bn} (0.094 g)], RT. Tapered block copolymerization: run 18, 8DL = 0.58 mmol, [(1/1 *rac*-DL^{Me} (0.05 g) : *meso*-DL^{Bn} (0.094 g)], RT.

Absolute Molecular Weight Measurements. Measurements of polymer absolute weight-average molecular weight (M_w), number average molecular weight (M_n), and dispersity indices ($Đ = M_w / M_n$) were performed via gel-permeation chromatography (GPC). The GPC instrument consisted of an Agilent HPLC system equipped with one guard column and three PLgel 5 μm mixed-C gel

permeation columns and coupled with a Wyatt DAWN HELEOS II multi (18)- angle light scattering detector and a Wyatt Optilab TrEX dRI detector; the analysis was performed at 40 °C using chloroform as the eluent at a flow rate of 1.0 mL min^{-1}, using Wyatt ASTRA 7.1.3 molecular weight characterization software. The refractive index increment (d*n*/d*c*) of P3H4PhB was determined to be 0.1079 ± 0.0004 mL g^{-1}, and d*n*/d*c* of P3HHp was determined to be 0.0292 ± 0.0010 mL g^{-1}, obtained by batch experiments using Wyatt Optilab TrEX dRI detector and calculated using ASTRA software. Polymer solutions were prepared in chloroform and injected into dRI detector by Harvard Apparatus pump 11 at a flow rate of 0.30 mL min^{-1}. A series of known concentrations were injected and the change in refractive index was measured to obtain a plot of change in refractive index versus change in concentration ranging from 0.4 to 5.0 mg/mL. The slope from a linear fitting of the data was the d*n*/d*c* of the polymer. Random and diblock specimens d*n*/d*c* values were calculated based on weighted average with respect to co-monomer composition. For GPC data presented in Figure 3, the GPC instrument consisted of an Agilent HPLC system equipped with one guard column and three PL-gel 5 μm mixed-C gel permeation columns running THF as eluent at 1.0 mL/min at 40 °C. The detectors used were a Wyatt Technology TrEX differential refractometer (dRI) and a Wyatt Technology miniDAWN Treos light scattering detector (MALS). The d*n*/d*c* values were determined experimentally, through analysis of known-concentration samples, to be 0.1572 mL g^{-1} for P3H4PhB.

Spectroscopic Characterizations. The isolated low molecular weight samples were analyzed by matrix-assisted laser desorption/ionization time-of-flight mass spectroscopy (MALDI−TOF MS); the experiment was performed on Microflex-LRF mass spectrometer (Bruker Daltonics, Billerica, MA) operated in positive ion, reflector mode using a Nd:YAG laser at 355 nm and 25 kV accelerating voltage. A thin layer of a 1% NaI solution was first deposited on the target plate,

followed by 0.6 µl of both sample and matrix (dithranol in chloroform). External calibration was done using a peptide calibration mixture (4 to 6 peptides) on a spot adjacent to the sample. The raw data was processed in the FlexAnalysis software (version 3.4.7, Bruker Daltonics).

NMR spectra were recorded on a Bruker AV-III 400 MHz spectrometer (400 MHz, ^{1}H; 100 MHz, ^{13}C). Chemical shifts for ^{1}H and ^{13}C spectra were referenced to internal solvent resonances and are reported as parts per million relative to $SiMe_4$. The [*rr*] (the syndiotactic triad made up of two adjacent *rac* diads probability of *rac* linkages between 3HPhB units) value of P3H4PhB was calculated according to the integration area of *rr*, *mr,* and *rm* triads [A([*rr*]), A([*mr*]), A([*rm*])] of the carbonyl group region at δ169.2 ppm, that is [*rr*] = A([rr])/[A([*rr*]), A([*mr*]), A([*rm*])].

Single-crystal X-ray diffraction intensities were collected on a Bruker D8 Venture Diffractometer using CuKa (1.542 Å) radiation at 100 K. Crystallographic data for the structure of *meso*-DL^{Bn} have been deposited with the Cambridge Crystallographic Data Center (CCDC 2004305).

Thermal analysis. Melting transition (T_m) and glass transition (T_g) temperatures were measured by differential scanning calorimetry (DSC) on an Auto Q20, TA Instrument. All T_m and T_g values were obtained from a second scan after the thermal history was removed from the first scan, unless noted otherwise. The second heating rate was 5 °C/min and cooling rate was 5 °C/min unless indicated otherwise in the polymerization tables. This heating and cooling rate was used because of the low crystallinity of the resultant polymer and as a standard condition to compare other chemically synthesized PHAs in our lab. Decomposition temperatures (T_d, defined by the temperature of 5 % weight loss) and maximum rate decomposition temperatures (T_{max}) of the polymers were measured by thermal gravimetric analysis (TGA) on a Q50 TGA Analyzer, TA Instrument. Polymer samples were heated from ambient temperatures to 700 °C at a heating rate

of 10 °C min^{-1}. Values of T_{max} were obtained from derivative (wt %/°C) vs. temperature (°C) plots, while T_d and T_{onset} values (initial and end temperatures) were obtained from wt % vs. temperature (°C) plots.

Mechanical Analysis. Tensile stress/strain testing was performed by an Instron 5966 universal testing system (10 k*N* load cell) on dog-bone-shaped test specimens (ASTM D638 standard; Type V) prepared *via* compression molding using a Carver Bench Top Laboratory Press (Model 4386) equipped with a two-column hydraulic unit (Carver, Model 3912, maximum force 24000 psi). Isolated polymer materials were loaded between non-stick Teflon paper sheets into a stainless-steel mold with inset dimensions 30 × 73.5 × 0.87 mm fabricated in house, and compressed between two 6" × 6" steel electrically heated platens (EHP) clamp force 5000 psi, at temperature 70 °C. Specimens for analysis were cut using an ASTM D638-5-IMP cutting die (Qualitest) to standard dimensions. From each compression molding procedure using the stainless-steel mold described, two ASTM D638-5 standard dog-bone shaped specimens could be cut. To reduce the amount of materials needed for mechanical testing while examining their reprocessability, the measured dog-bone specimens were reprocessed for subsequent trials rather than virgin materials prepared for each measurement. Thus, the workflow would proceed as follows: virgin materials were compression molded to yield two new specimens and measured using the Instron instrument to the point of failure, before reprocessing the material in a subsequent round of compression molding to yield two reprocessed specimens to be again measured to the point of failure. Mechanical behavior was averaged for all the specimens measured for each individual species investigated. Thickness (0.85 ± 0.01 mm), width (3.18 mm), and grip length (26.4 ± 0.2 mm) of the measured dog-bone specimens were measured for normalization of data by the Bluehill measurement software (Instron). Test specimens were affixed into the screw-tight grip frame.

Tensile stress and strain were measured to the point of material break at a grip extension speed of 10.0 mm min^{-1} at ambient conditions.

Additional Figures

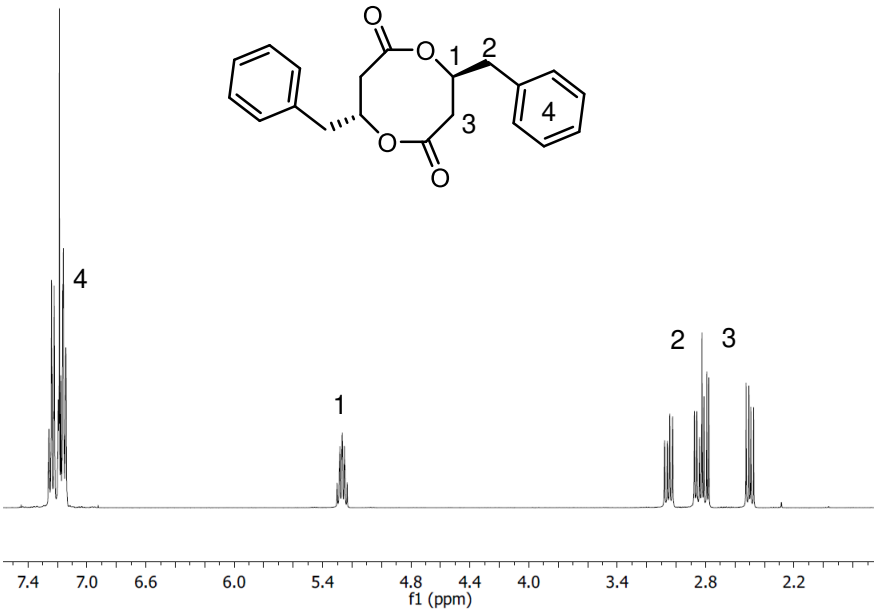

Figure S4.1. ^{1}H NMR ($CDCl_3$, 23 °C) of *meso*-DL^{Bn}.

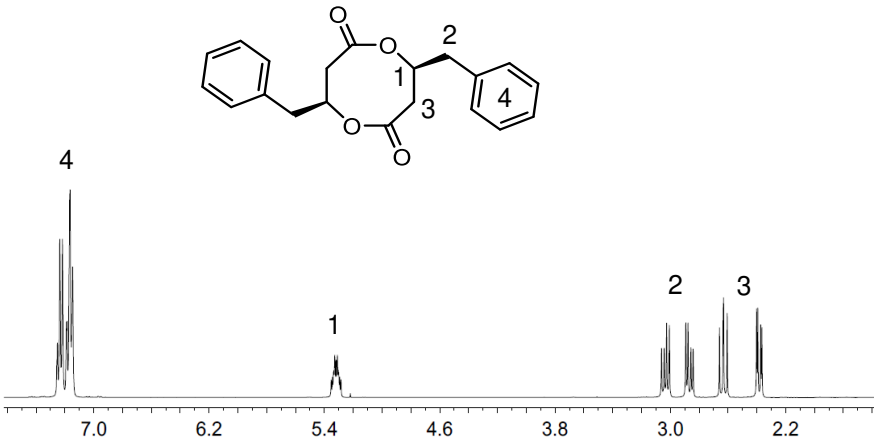

Figure S4.2. ^{1}H NMR ($CDCl_3$, 23 °C) of *rac*-DL^{Bn}.

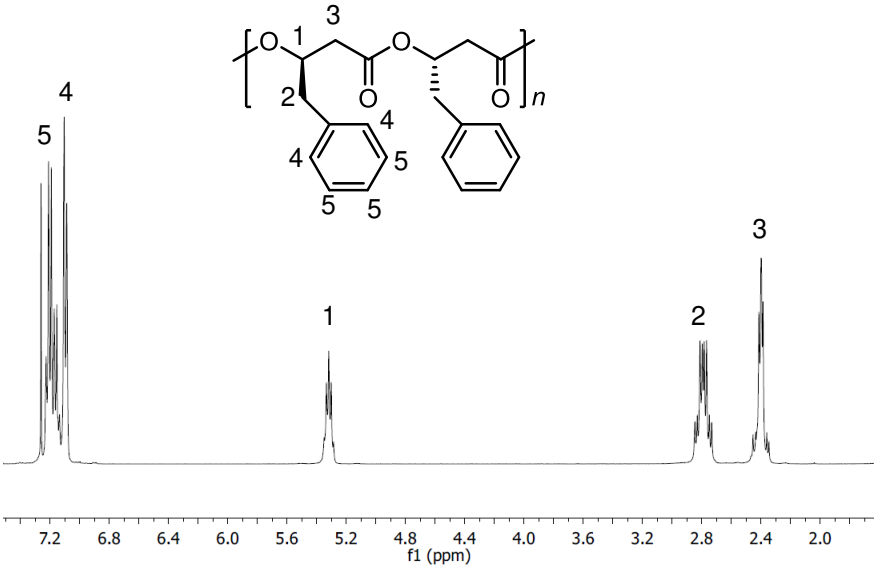

Figure S4.3. ^{1}H NMR ($CDCl_3$, 23 °C) of *st*-P3H4PhB.

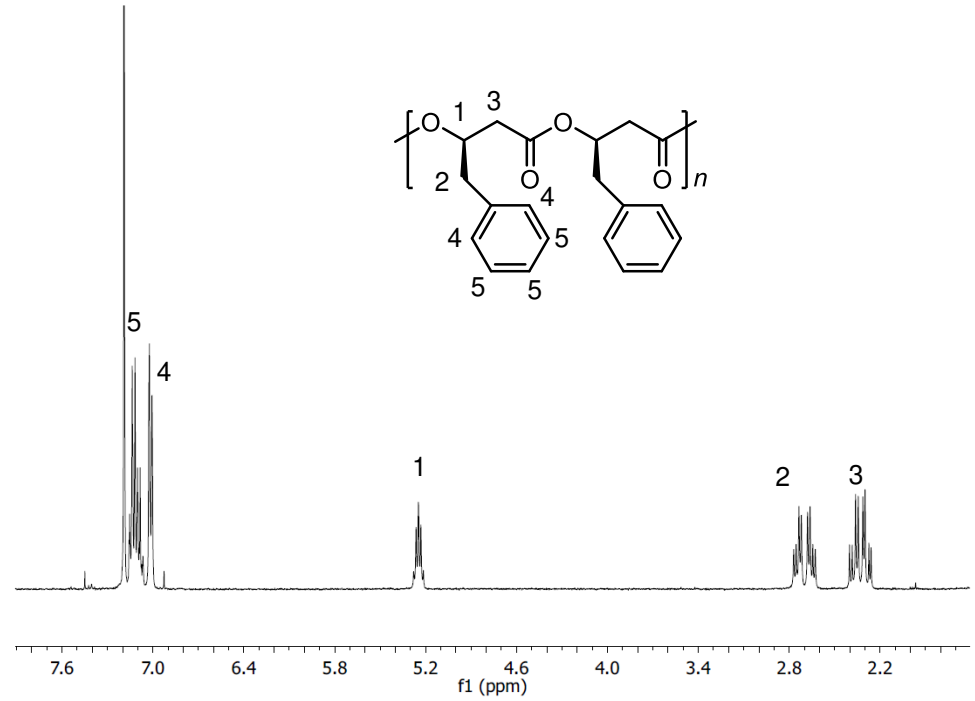

Figure S4.4. ^{1}H NMR ($CDCl_3$, 23 °C) of *it*-P3H4PhB.

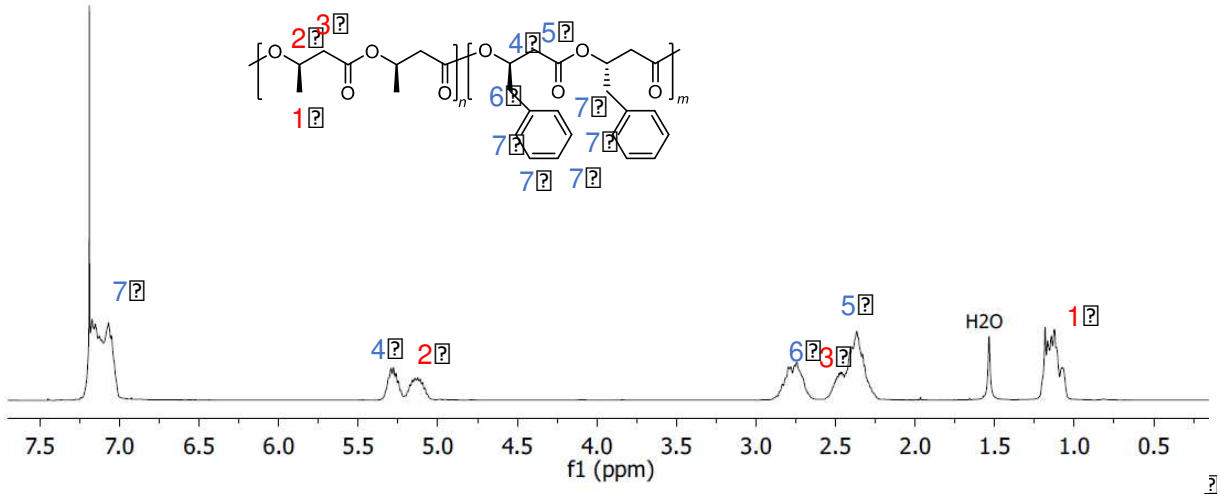

Figure S4.5. ^{1}H NMR ($CDCl_3$, 23 °C) of random copolymer P3H4PhB-*co*-P3HB (48% *rac*-8DL^{Me} incorporation). (Note: H_2O in $CDCl_3$ at 1.56 ppm)

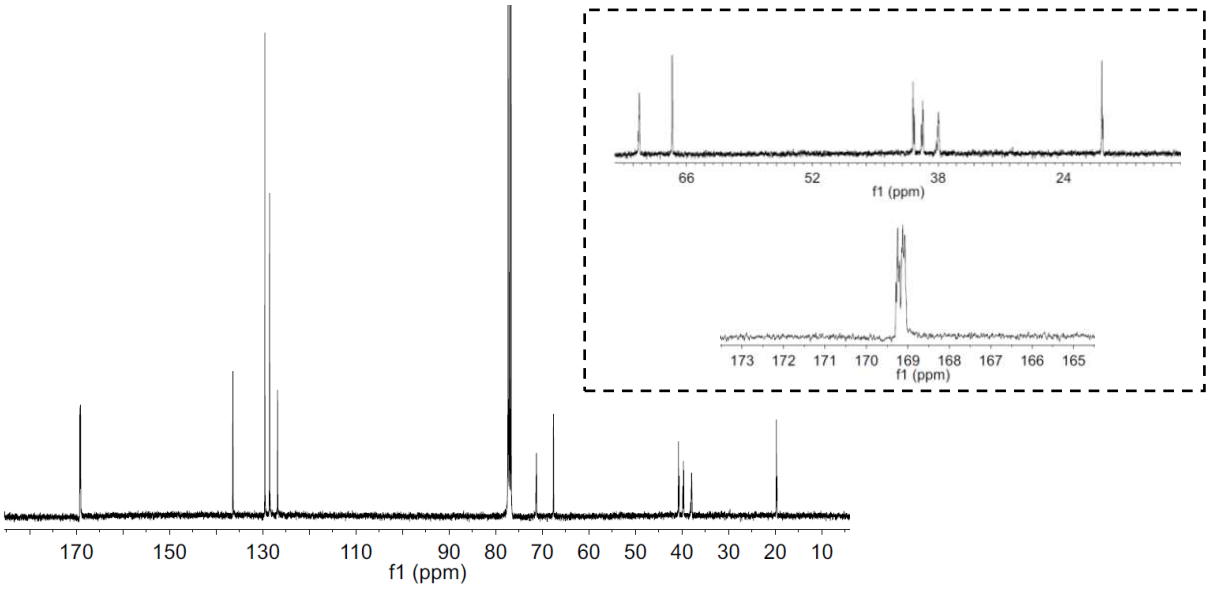

Figure S4.6. ^{13}C NMR ($CDCl_3$, 23 °C) of random copolymer P3H4PhB-*co*-P3HB (48% *rac*-8DL^{Me} incorporation).

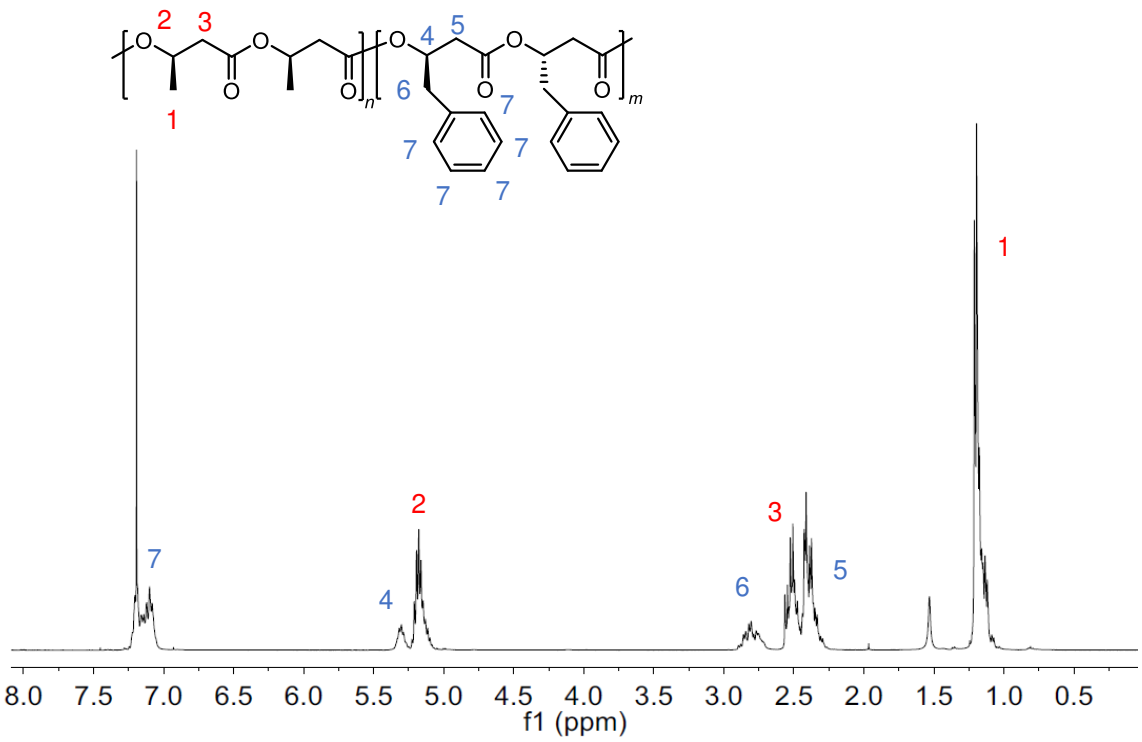

Figure S4.7. ^{1}H NMR ($CDCl_3$, 23 °C) of random copolymer P3H4PhB-*co*-P3HB (80% *rac*-8DL^{Me} incorporation). (Note: H_2O in $CDCl_3$ at 1.56 ppm).

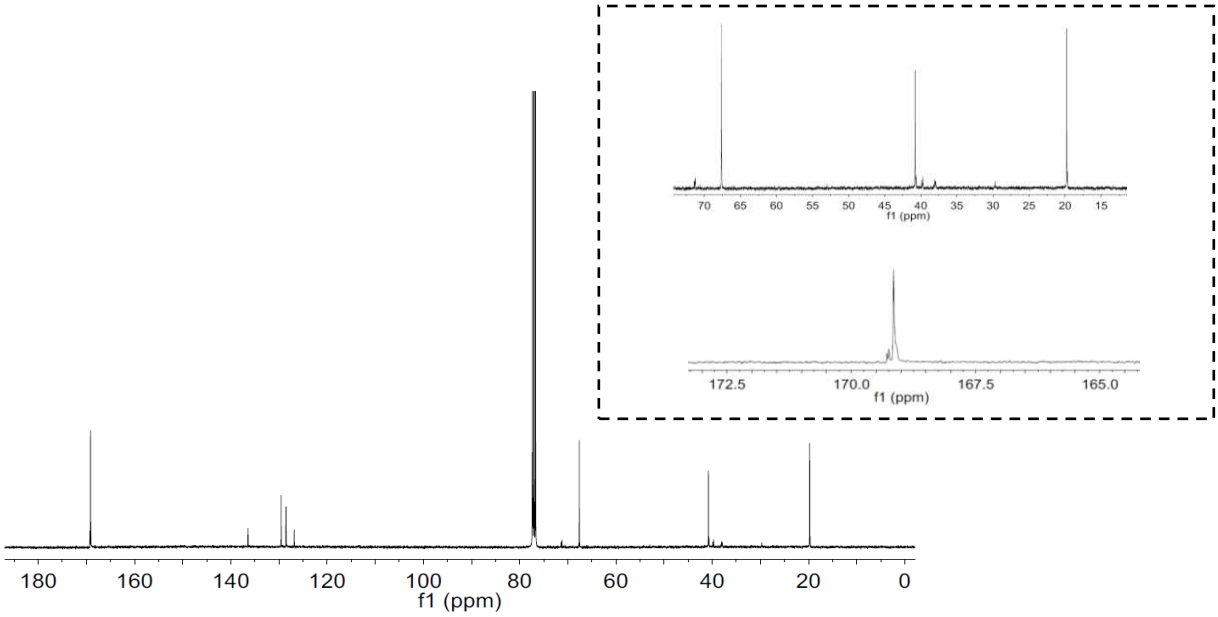

Figure S4.8. ^{13}C NMR ($CDCl_3$, 23 °C) of random copolymer random copolymer P3H4PhB-*co*-P3HB (80% *rac*-8DL^{Me} incorporation).

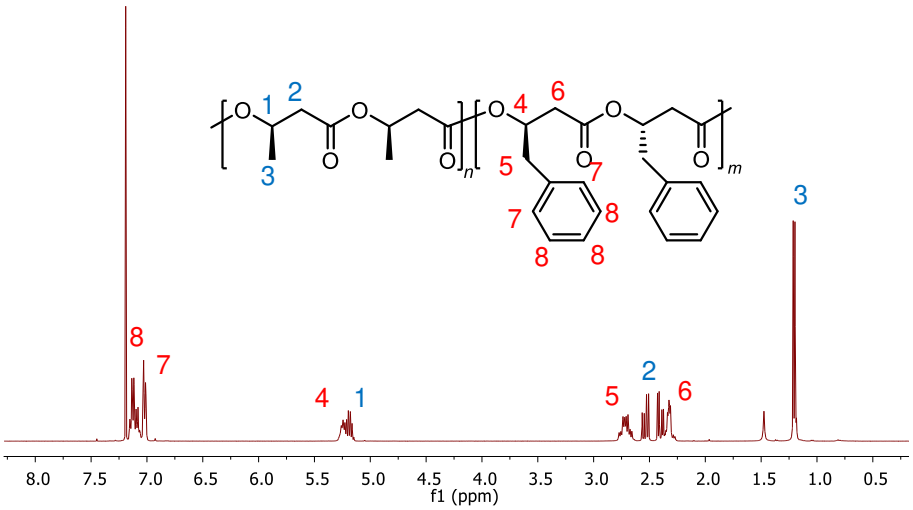

Figure S4.9. ^{1}H NMR ($CDCl_3$, 23 °C) of stereoblock copolymer *it*-P3HB-*b*-*st*-P3H4PhB. (Note: H_2O in $CDCl_3$ at 1.56 ppm).

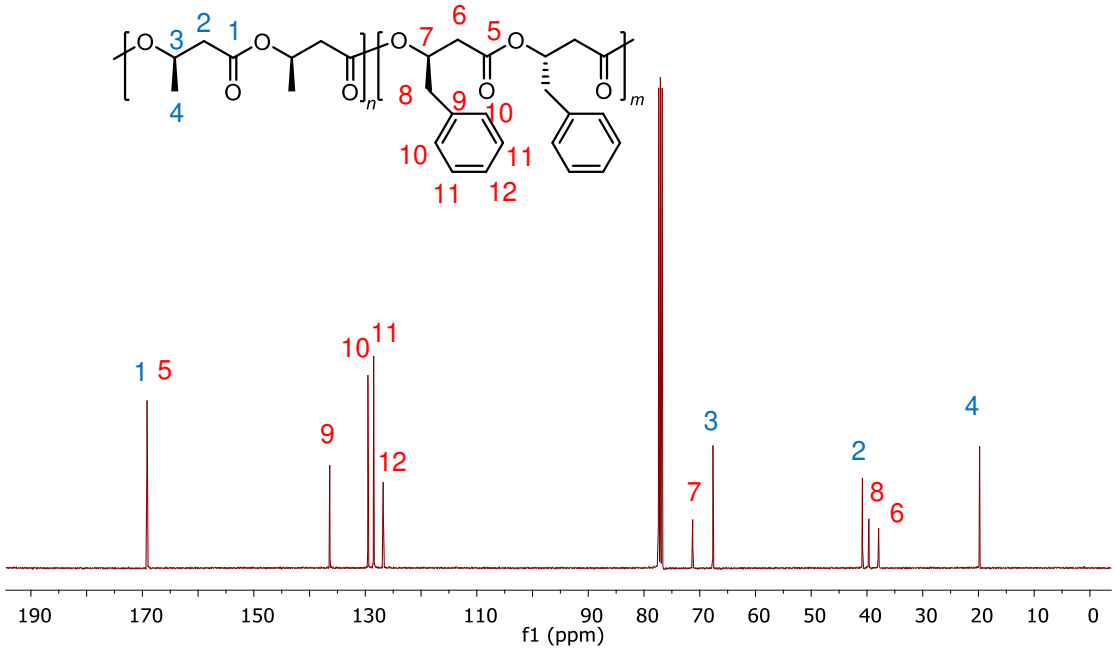

Figure S4.10. ^{13}C NMR ($CDCl_3$, 23 °C) of stereoblock copolymer *it*-P3HB-*b*-*st*-P3H4PhB.

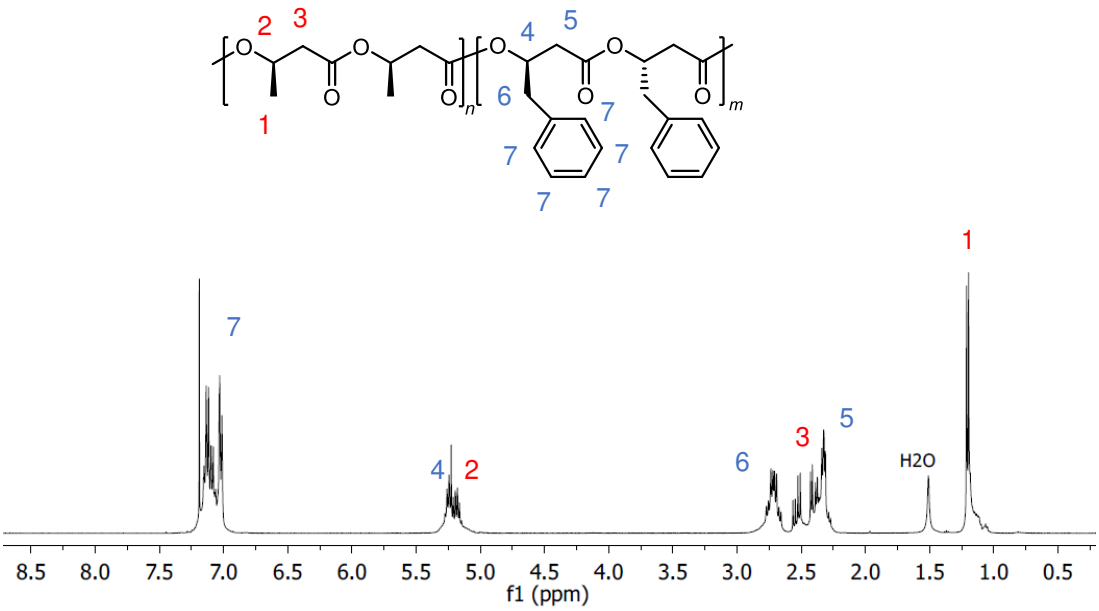

Figure S4.11. ^{1}H NMR ($CDCl_3$, 23 °C) of tapered block copolymer *it*-P3HB-*b*-*st*-P3H4PhB. (Note: H_2O in $CDCl_3$ at 1.56 ppm).

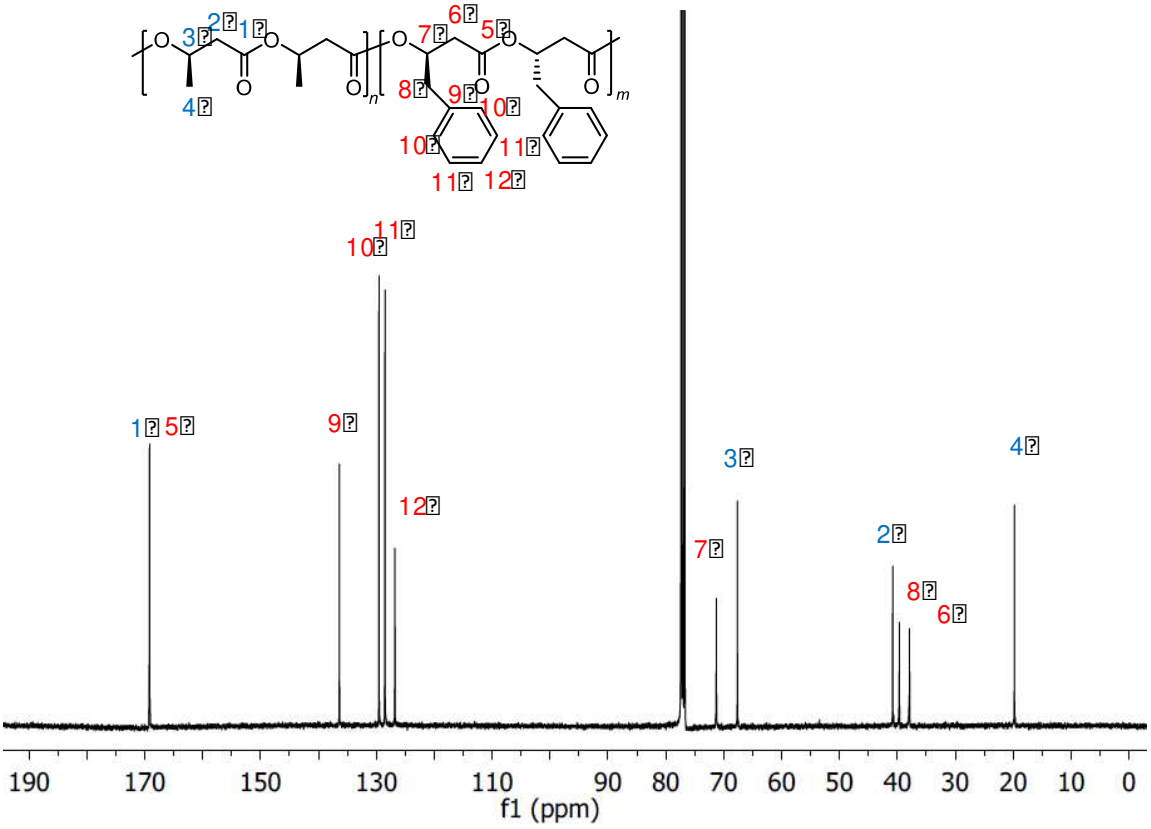

Figure S4.12. ^{13}C NMR ($CDCl_3$, 23 °C) of tapered block copolymer *it*-P3HB-*b*-*st*-P3H4PhB.

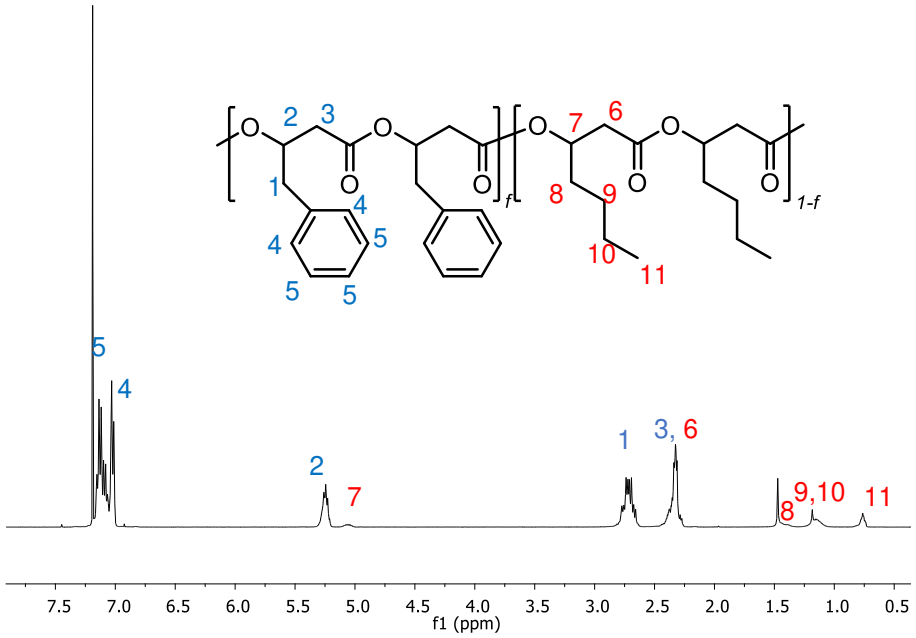

Figure S4.13. ^{1}H NMR ($CDCl_3$, 23 °C) of P3H4PhB-*co*-P3HHp (8.1% *rac*-DL^{Bu} incorporation). (Note: H_2O in $CDCl_3$ at 1.56 ppm).

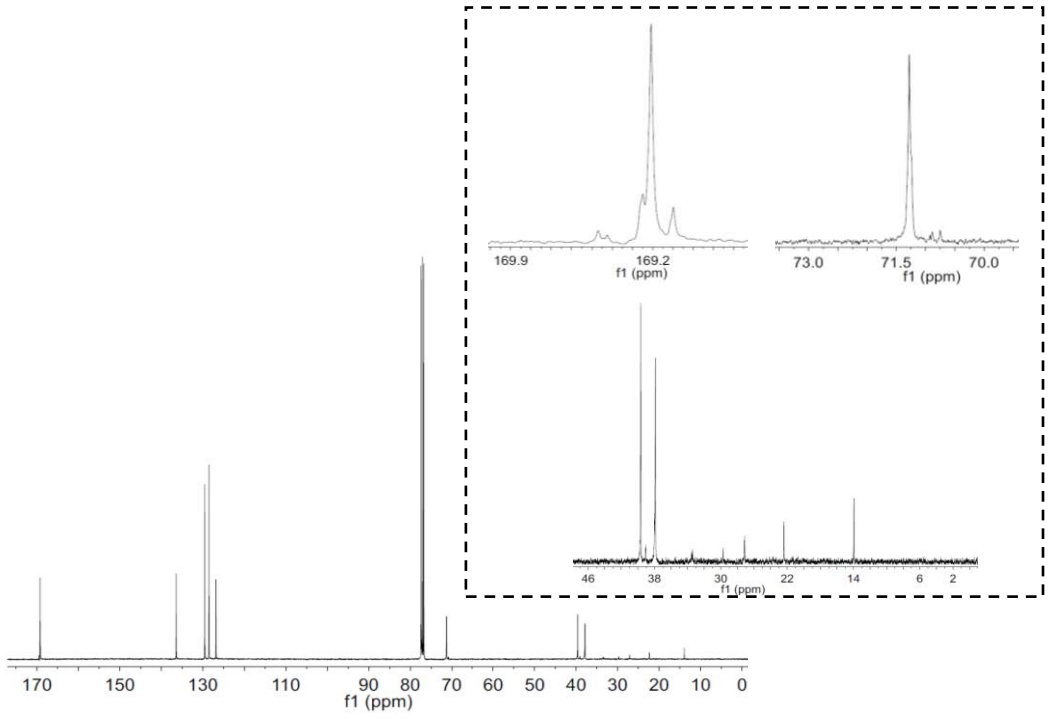

Figure S4.14. ^{13}C NMR ($CDCl_3$, 23 °C) of random copolymer P3H4PhBB-*co*-P3HHp (8.1% *rac*-DL^{Bu} incorporation).

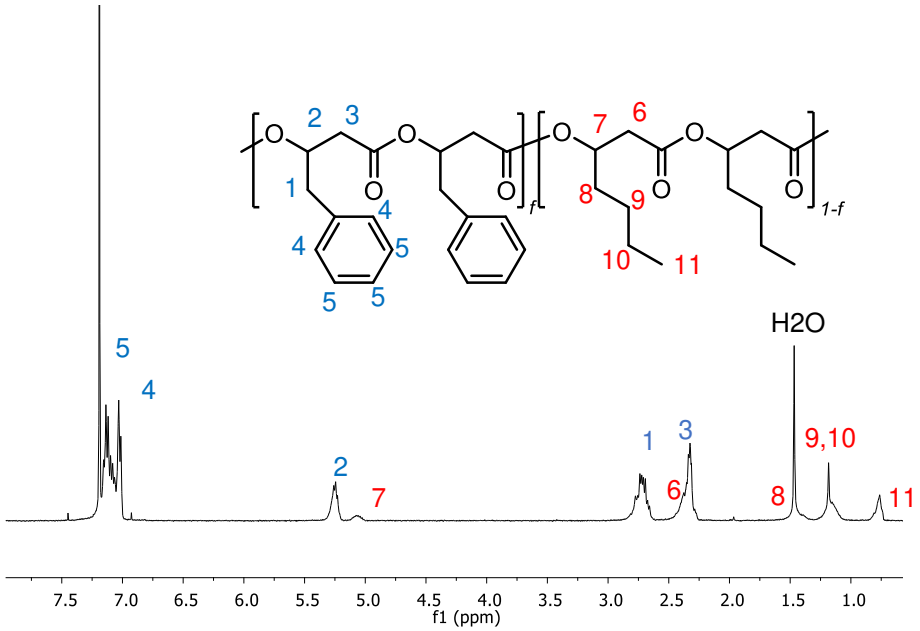

Figure S4.15. ^{1}H NMR ($CDCl_3$, 23 °C) of P3H4PhB-*co*-P3HHp (15.6% *rac*-DL^{Bu} incorporation). (Note: H_2O in $CDCl_3$ at 1.56 ppm)

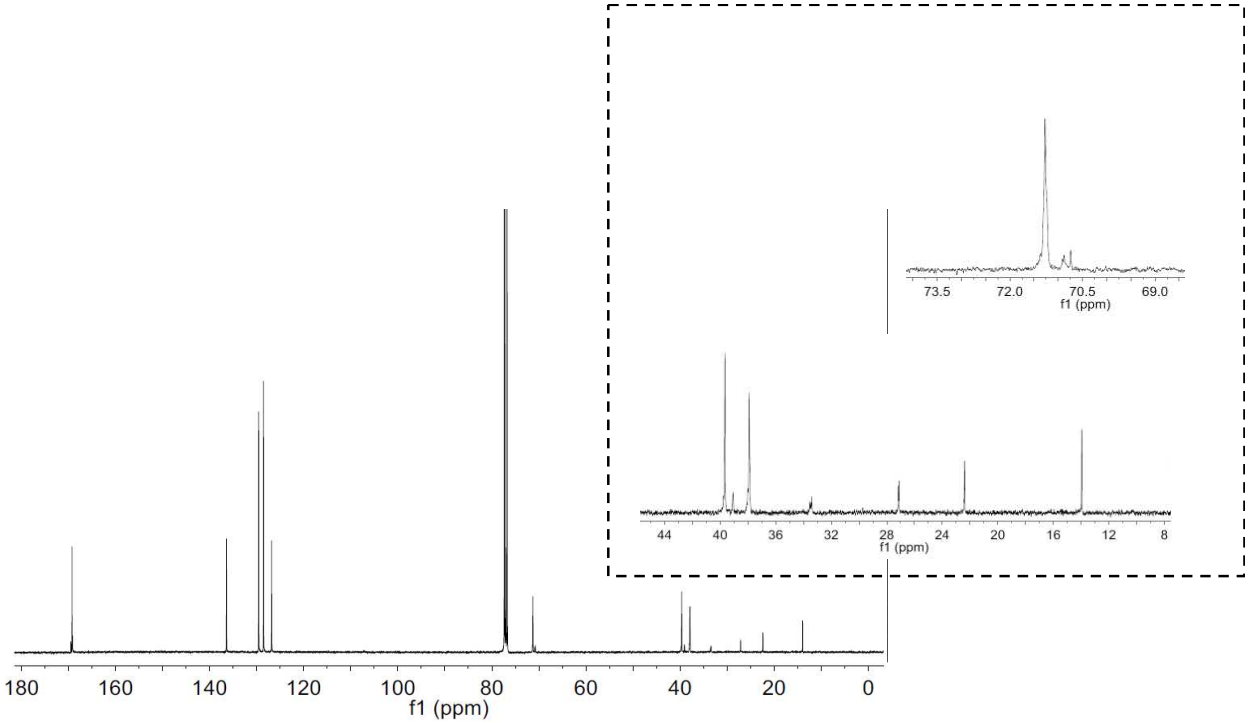

Figure S4.16. ^{13}C NMR ($CDCl_3$, 23 °C) of random copolymer P3H4PhBB-*co*-P3HHp (15.6% *rac*-DL^{Bu} incorporation).

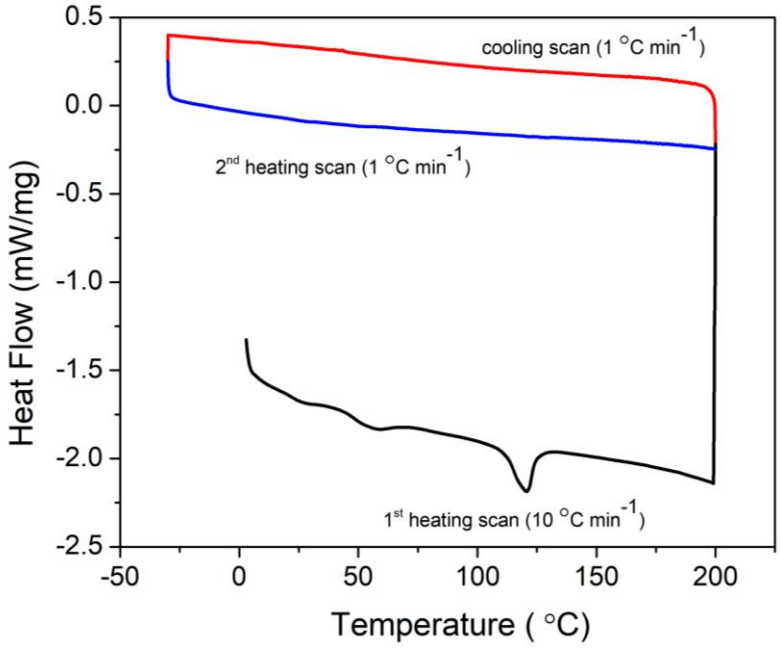

Figure S4.17. DSC curve of *it*-P3H4PhB ([*mm*]>99%). First heating scan (black curve: 10°C min^{-1}) followed by cooling scan (red curve: 1°C min^{-1}) and second heating scan (blue curve: 1°C min^{-1}). An endotherm visible in the first scan at 126 °C for T_m, but no T_c or T_m visible in the cooling or heating scan.

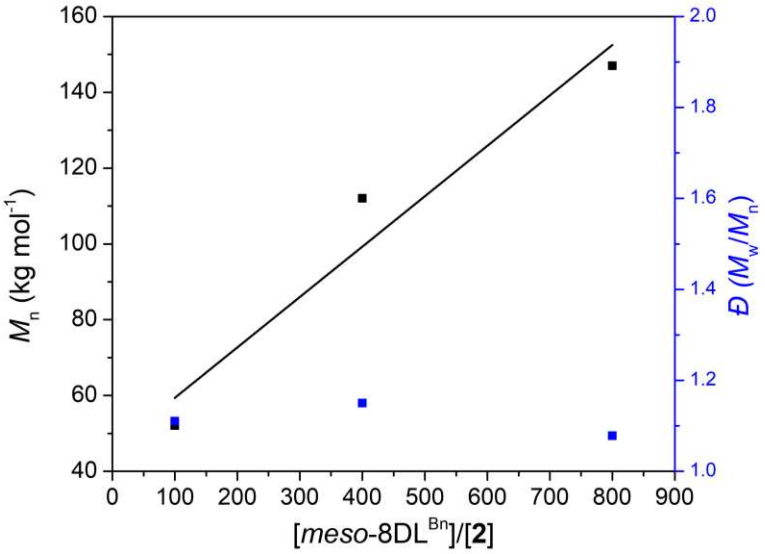

Figure S4.18. Plots of M_n and $Đ$ values of *st*-P3H4PhB produced by racemic complex 2 at varied [*meso*-8DL^{Bn}]/[2] ratios. Conditions: [*meso*-8DL^{Bn}] = 0.77 M (0.100 g in 0.4 mL DCM); RT; [2]/[BnOH] = 1/1).

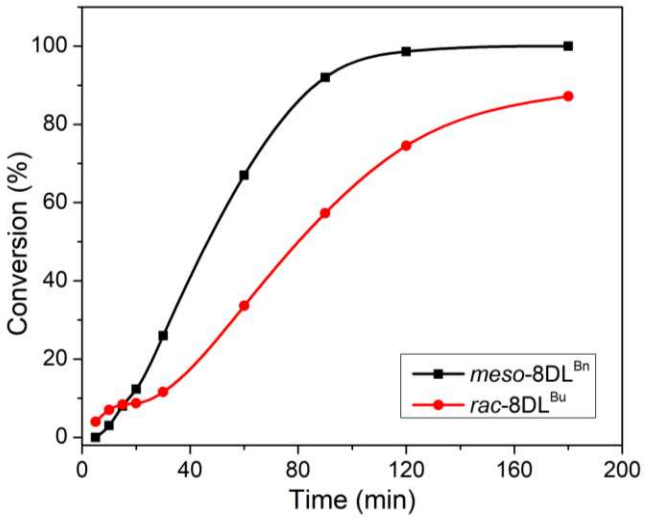

Figure S4.19. Time-conversion plots in the polymerization of *meso*-8DL^{Bn} and *rac*-8DL^{Bu} (5/1 ratio, in DCM, RT, [8DL]/[2]/BnOH = 800/1/1).

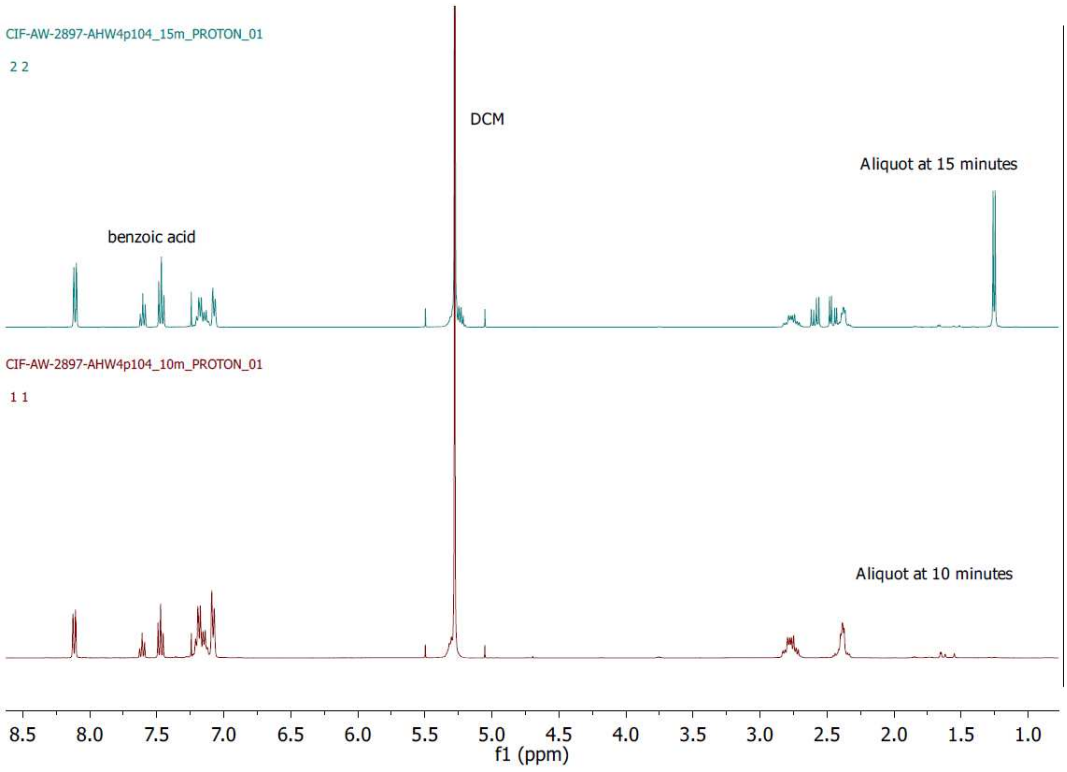

Figure S4.20. ^{1}H NMR of sequential block copolymer produced with *meso*-8DL^{Bn} added first and *rac*-8DL^{Me} added second.

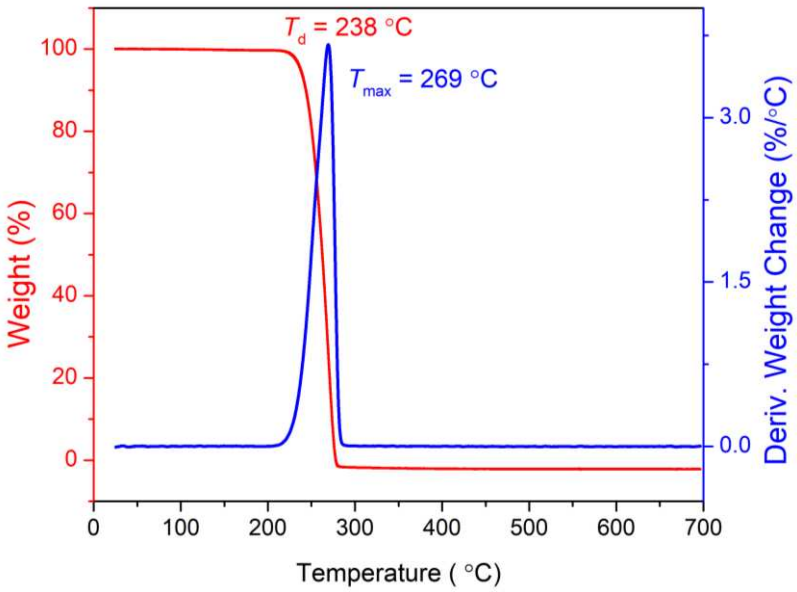

Figure S4.21. TGA curve of random copolymer P3H4PhB-*co*-P3HB (M_n = 58.9 kg mol^{-1}, $Đ$ = 1.16, 48% incorporation of 3HB units).

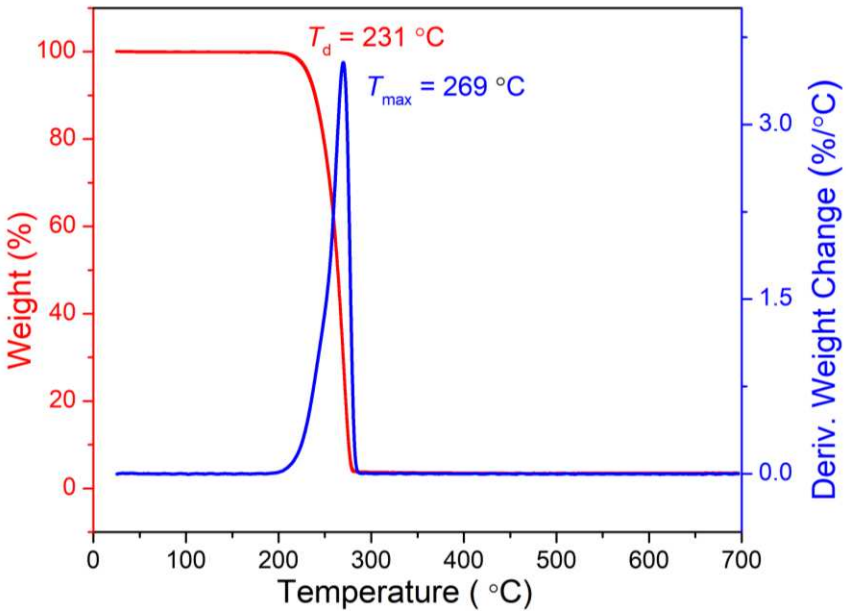

Figure S4.22. TGA curve of random copolymer P3H4PhB-*co*-P3HB (M_n = 93.3 kg mol^{-1}, $Đ$ = 1.11, 80% incorporation of 3HB units).

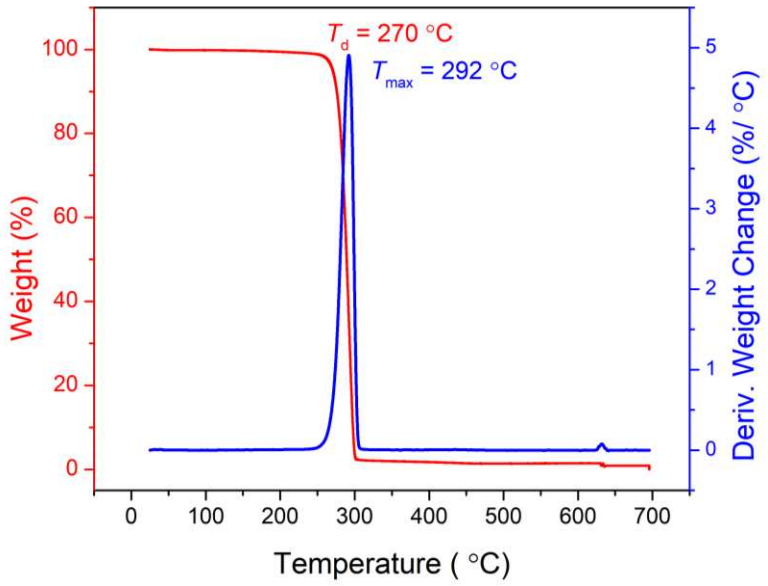

Figure S4.23. TGA curve of *it*-P3H4PhB ([*mm*] > 99%) (M_n = 64.5 kg mol^{-1}, $Đ$ = 1.29).

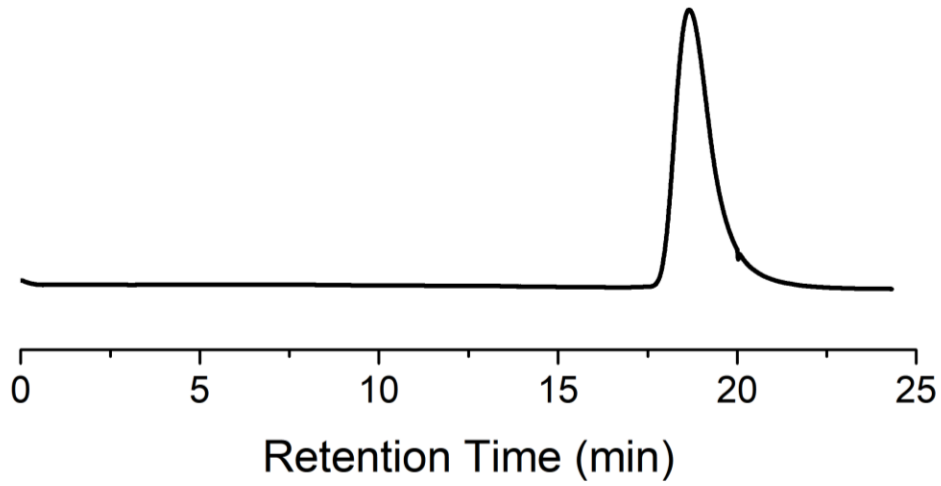

Figure S4.24. GPC trace of *st*-P3H4PhB by [*meso*-DL^{Bn}]/[2] = 400/1 in DCM (M_n = 112 kg mol^{-1}, $Đ$ = 1.15) (Run 3, Table 4.1).

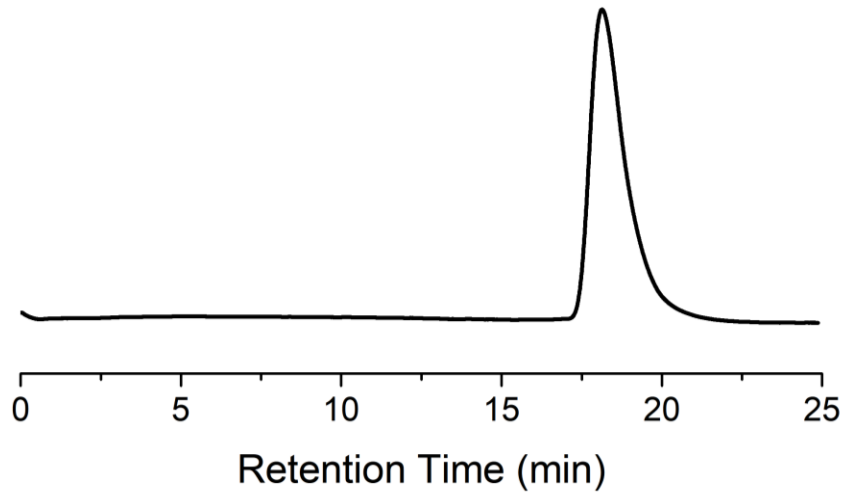

Figure S4.25. GPC trace of *st*-P3H4PhB by [*meso*-DL^{Bn}]/[2] = 800/1 in DCM (M_n = 147 kg mol^{-1}, $Đ$ = 1.19) (Run 4, Table 4.1).

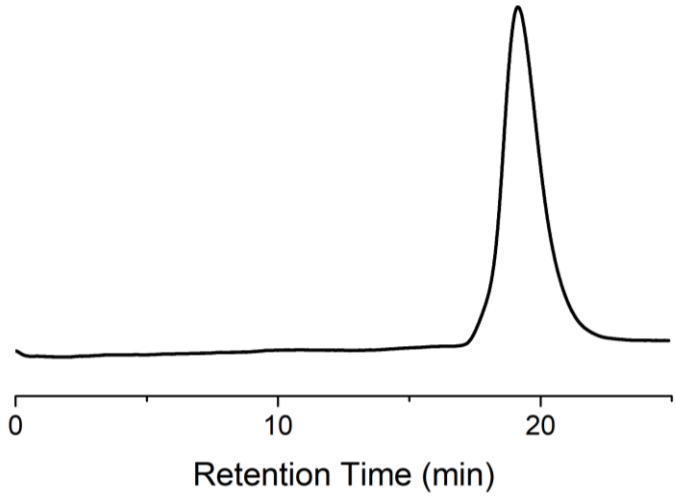

Figure S4.26. GPC trace of *st*-P3H4PhB by [*meso*-DL^{Bn}]/[2] = 400/1 in toluene (M_n = 76 kg mol^{-1}, $Đ$ = 1.16) (Run 10, Table 4.2).

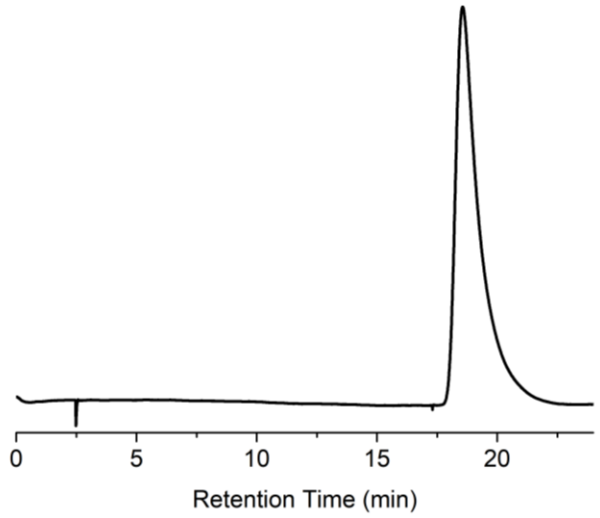

Figure S4.27. GPC trace of *st*-P3H4PhB by [*meso*-DL^{Bn}]/[2] = 800/1 in fluorobenzene (M_n = 119 kg mol^{-1}, $Đ$ = 1.16) (Run 12, Table 4.2).

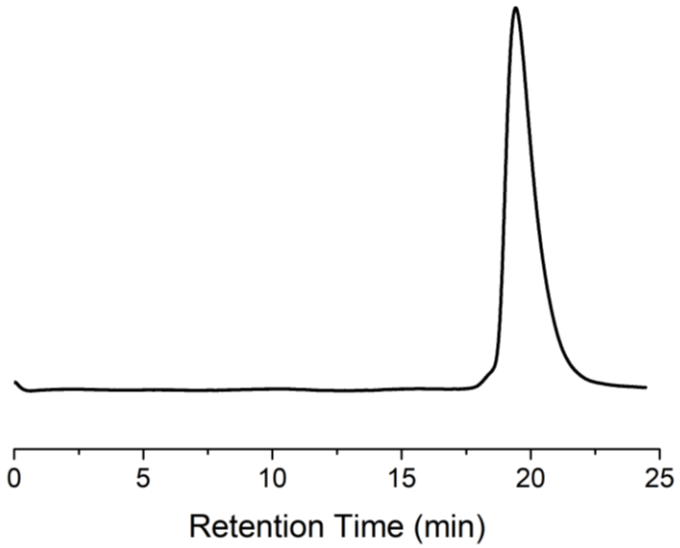

Figure S4.28. GPC trace of *it*-P3H4PhB by [*rac*-DL^{Bn}]/[2] = 100/1 in DCM (M_n = 64.5 kg mol^{-1}, $Đ$ = 1.29).

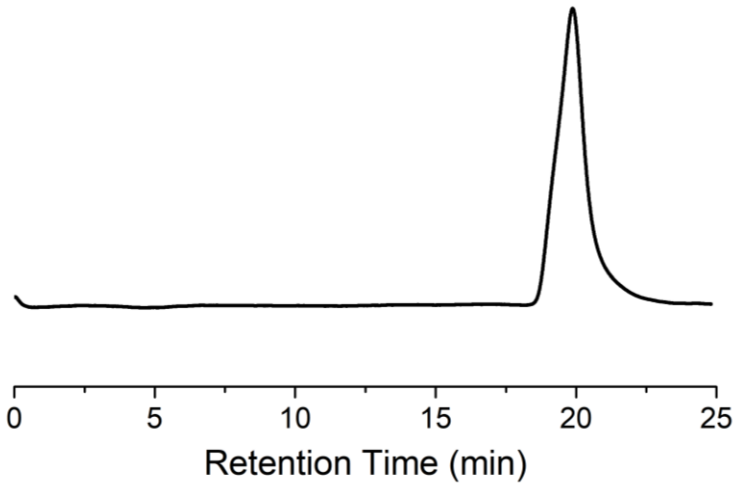

Figure S4.29. GPC trace of stereoblock copolymer *it*-P3HB-*b*-*st*-P3H4PhB by [DL]/[2] = 100/1 (M_n = 84.1 kg mol^{-1}, $Đ$ = 1.08) (Run 17, Table 4.3).

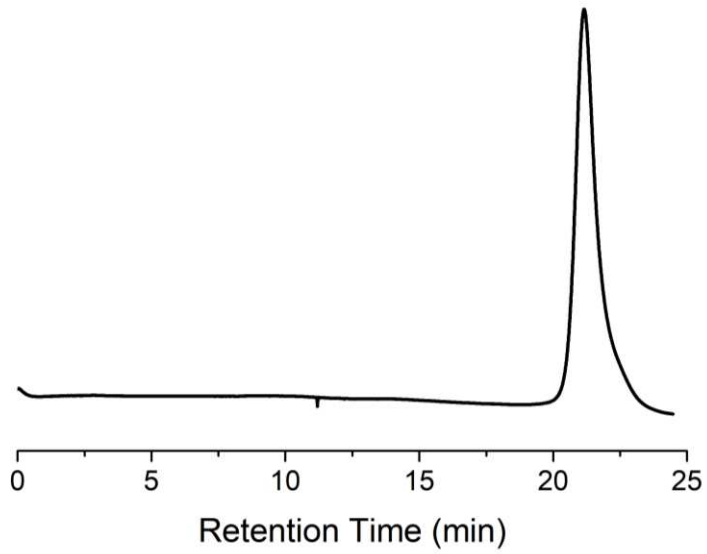

Figure S4.30. GPC trace of tapered stereoblock copolymer *it*-P3HB-*co*-*st*-P3H4PhB by [DL]/[2] = 100/1 (M_n = 18.4 kg mol^{-1}, $Đ$ = 1.22) (Run 18, Table 4.3).

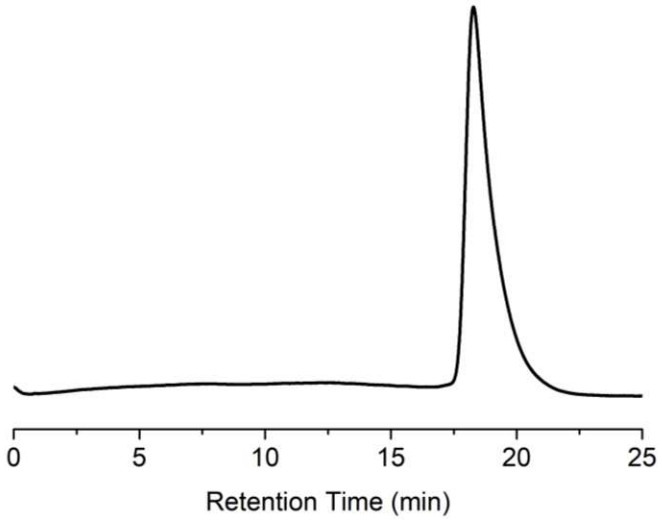

Figure S4.31. GPC trace of P3H4PhB-*co*-P3HHp (5:1) by [DL]/[2] = 800/1 (M_n = 117 kg mol^{-1}, $Đ$ = 1.28) (Run 19, Table 4.3).

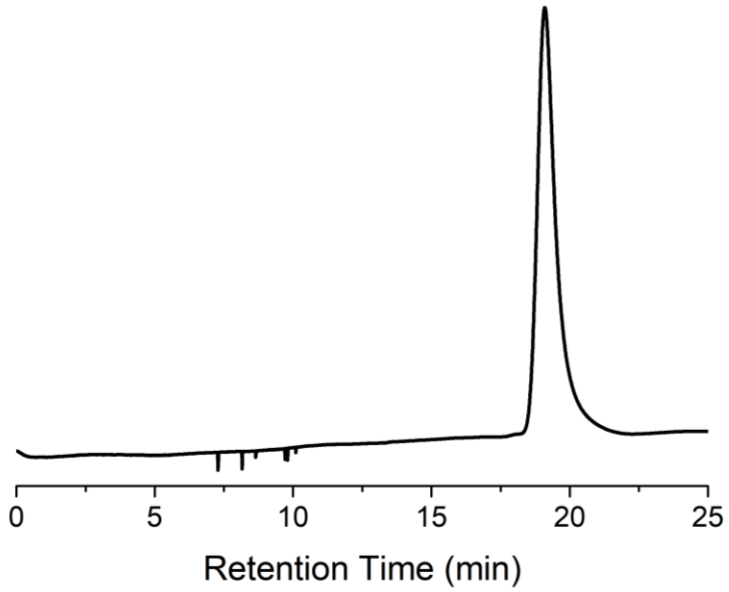

Figure S4.32. GPC trace of P3H4PhB-*co*-P3HHp (10:1) by [DL]/[2] = 800/1 (M_n = 84.0 kg mol^{-1}, $Đ$ = 1.14) (Run 20, Table 4.3).

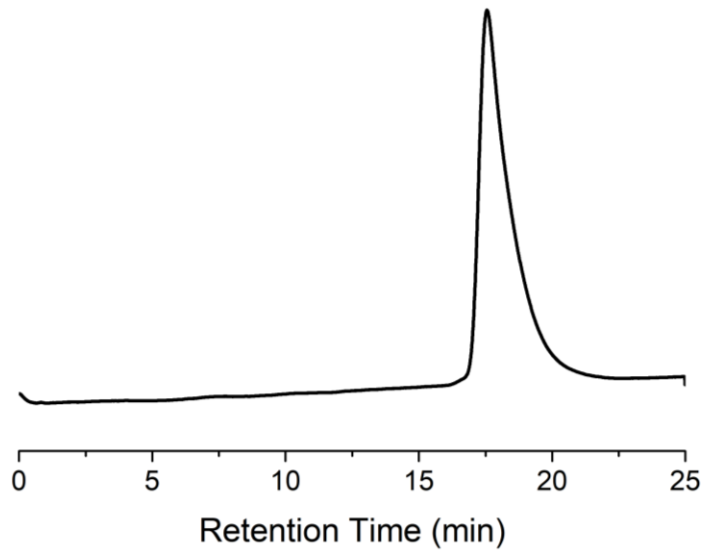

Figure S4.33. GPC trace of large-scale copolymer P3H4PhB-*co*-P3HHp (5:1) by 2 (M_n = 205 kg mol^{-1}, $Đ$ = 1.21).

Additional Tables

Table S4.1. Measured tensile behavior of P3H4PhB-*co*-P3HHp (incorporation of *rac*-DL^{Bu} = 15.6%, M_n = 205 kg mol^{-1}, $Đ$ = 1.21) dog-bone shaped specimens (ASTM D638-5).

Specimen	Modulus of Elasticity (Young's Modulus) (MPa)	Tensile Strength (MPa)	% Elongation at Break
1	1220	19.5	195.0
2	1360	22.7	204.6
3	1510	26.0	173.4
Mean	1363 ± 145	22.7 ± 3.25	191 ± 16

References

[1] Tang, X.; Chen, E. Y.-X. Chemical Synthesis of Perfectly Isotactic and High Melting Bacterial Poly(3-Hydroxybutyrate) from Bio-Sourced Racemic Cyclic Diolide. Nat. Commun. 2018, 9, 2345. https://doi.org/10.1038/s41467-018-04734-3

[2] Tang, X.; Westlie, A. H.; Caporaso, L.; Cavallo, L.; Falivene, L.; Chen, E. Y.-X. Biodegradable Polyhydroxyalkanoates by Stereoselective Copolymerization of Racemic Diolides: Stereocontrol and Polyolefin- Like Properties Research Articles. Angew. Chem. Int. Ed. 2020, 59, 2–12. https://doi.org/10.1002/anie.201916415

[3] Anwander, R.; Runte, O.; Eppinger, J.; Gerstberger, G.; Herdtweck, E.; Spiegler, M. Synthesis and Structural Characterisation of Rare-Earth Bis(Dimethylsilyl)Amides and Their Surface Organometallic Chemistry on Mesoporous MCM-41. J. Chem. Soc. Dalt. Trans. 1998, 5, 847–858. https://doi.org/10.1039/a705608g

[4] Lin, M. H.; RajanBabu, T. V. Ligand-Assisted Rate Acceleration in Transacylation by a Yttrium - Salen Complex. Demonstration of a Conceptually New Strategy for Metal-Catalyzed Kinetic Resolution of Alcohols. Org. Lett. 2002, 4, 1607–1610. https://doi.org/10.1021/ol025809q

[5] Liu, Q.; Meermann, C.; Görlitzer, H. W.; Runte, O.; Herdtweck, E.; Sirsch, P.; Törnroos, K. W.; Anwander, R. Cationic Rare-Earth Metal SALEN Complexes. J. Chem. Soc. Dalt. Trans. 2008, 44, 6170–6178. https://doi.org/10.1039/b808781d

Appendix C

Experimental Details and Supporting Information for Chapter 5

Experimental Section

Materials. All syntheses and manipulations of air- and moisture-sensitive chemicals and materials were carried out in flamed Schlenk-type glassware on a dual-manifold Schlenk line or in an inert gas (N_2)-filled glovebox. HPLC-grade organic solvents were first sparged extensively with nitrogen during filling 20 L solvent reservoirs and then dried by passage through activated alumina (for DCM) followed by passage through Q-5 supported copper catalyst (for toluene and hexanes) stainless steel columns. Benzene-d_6 was dried over sodium/potassium alloy and filtered, whereas CD_2Cl_2 and $CDCl_3$ were dried over CaH_2, vacuum-distilled and stored over activated Davison 4 Å molecular sieves.

Yttrium chloride YCl_3 was purchased from Sigma-Aldrich Chemical Co. and used as received. Benzene dimethanol was purchased from Alfa Aesar Chemical Co., purified by sublimation, and stored in the glovebox. Dimethyl 1,4-dibenzyl-2,5-dioxocyclohexane-1,4-dicarboxylate was purchased from ThermoScientific and used as received. Iodomethane, iodoethane, and iodobutane were purchased from Alfa Aesar Chemical Co. and Oakwood Chemical and used as received. 3-chloroperoxybenzoic acid (*m*CPBA, ≤ 77%) was purchased from Sigma Aldrich. and purified by dissolving in diethyl ether, washing with brine (2x), dried over sodium sulfate, and stored in freezer after diethyl ether removed in vacuo. Literature procedures were employed for the preparation of *rac*-8DL^{Me} [1], *rac*-8DL^{Et}, *rac*-8DL^{Bu}.[2] The yttrium complexes were prepared according to their respective literature procedures: $Y[N(SiHMe_2)_2]_3(THF)_2$, and complex **1**, [1,3,5]

Complex 1 Preparation

The following complexes were prepared according to their respective literature procedures:

$Y[N(SiHMe_2)_2]_3(THF)_2$,

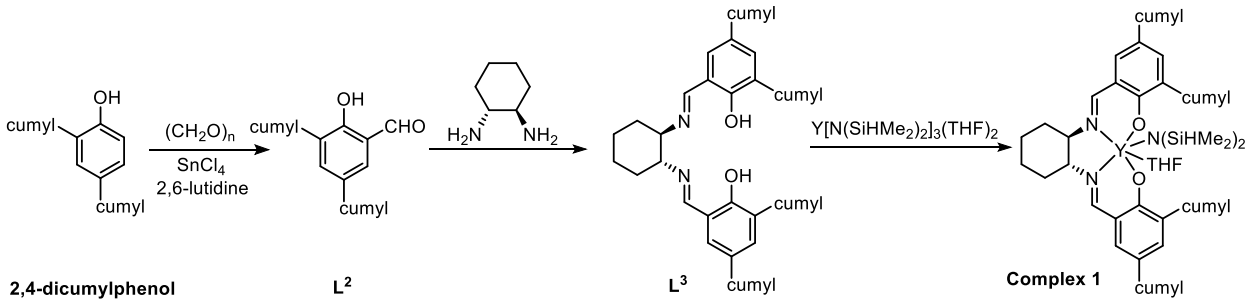

3,5-Dicumylsalicylaldehyde (L^2). 2,4-dicumylphenol (48.6 g, 0.147 mol), 2,6-lutidine (6.9 mL, 0.059 mmol) and 100 mL anhydrous toluene were measured into a side-arm round-bottom flask under nitrogen. Tin(IV) chloride (1.72 mL, 14.7 mmol) was added slowly to the reaction flask. The mixture was stirred at room temperature for 30 min, and then paraformaldehyde (9.74 g, 0.325 mol) was added. The resulting yellowish solution was heated at 100 °C for 8 h, after which time TLC analysis indicated >99% consumption of the phenol. The mixture was allowed to cool to room temperature, and 600 mL water was added to the flask. The aqueous layer was acidified to approximately pH = 2 with 2 N HCl. The aqueous layer was extracted with diethyl ether, and the combined ether extracts were dried over anhydrous Na_2SO_4. The concentrated product was purified using column chromatography. Yield: 57%. ^{1}H NMR (400 MHz, $CDCl_3$): δ 11.25 (s, 1H, OH), 9.77 (s, 1H, CHO), 7.51 (d, J = 2.3 Hz, 1H, Ar-H), 7.38 – 7.09 (m, 11H, Ar-H), 1.73 (s, 6H, Me), 1.64 (s, 6H, Me).

Salcy ligand (L^3). A mixture of 3,5-dicumylsalicylaldehyde (3.8 g, 10.6 mmol) and racemic *trans*-1,2-diaminocyclohexane (0.64 mL, 5.3 mmol) was dissolved in methanol (80 mL), and about 0.2 mL formic acid was added to the solution. The reaction was then heated to reflux for 6 h. Upon cooling, the yellow precipitate was collected by filtration and dried under vacuum. Yield: 95%. ^{1}H

NMR (400 MHz, $CDCl_3$): δ 13.26 (s, 2H, OH), 8.10 (s, 2H, N=C*H*), 7.32 – 7.08 (m, 22H, Ar-H), 6.93 (s, 2H, Ar-H), 3.15 (m, 2H, NC*H*), 1.75 (m, 4H, Cy-H), 1.67 (d, *J* = 2.6 Hz, 12H, -Me), 1.65 (s, 6H, Me), 1.58 (s, 6H, Me), 1.57 – 1.48 (m, 2H, Cy-H), 1.38 – 1.25 (m, 2H, Cy-H).

Yttrium Complex 1. Synthesis of yttrium complex **1** followed the literature procedure[12-13] with minor modifications detailed below. A solution of salcy ligand $\mathbf{L^3}$ (0.500 g, 0.629 mmol) in hexanes (15 mL) was added to a solution of $Y[N(SiHMe_2)_2]_3(THF)_2$ (0.396 g, 0.629 mmol) in hexanes (15 mL) and stirred for 24 h at room temperature. The volatiles were removed in vacuo, and the residue was washed with cold hexanes. The product was obtained as pale yellow solid. Yield: 83%. ^{1}H NMR (400 MHz, C_6D_6): δ 7.82 (s, 1H, N=C*H*), 7.70 (s, 1H, N=C*H*), 7.66 (m, 2H, Ar-H), 7.50 – 7.40 (m, 4H, Ar-H), 7.40 – 7.34 (m, 4H, Ar-H), 7.28 – 7.18 (m, 9H, Ar-H), 7.15 – 7.02 (m, 5H, Ar-H), 4.61 (m, 2H, Si*H*-), 4.38 (m, 1H, NC*H*), 3.36 (s, 4H, THF), 2.12 (m, 1H, NC*H*), 2.10 (s, 3H, Me), 1.95 (s, 3H, Me), 1.80 (s, 3H, Me), 1.72 (d, *J* = 2.4 Hz, 6H, Me), 1.70 (s, 6H, Me), 1.66 (s, 3H, Me), 1.59 – 1.19 (m, 10H, Cy-H, THF), 0.84 – 0.57 (m, 2H, Cy-H), 0.10 (m, 12H, SiMe). ^{13}C NMR (100 MHz, C_6D_6): δ 170.5, 164.6, 164.0, 162.6, 152.1, 151.6, 151.5, 151.4, 138.5, 138.0, 136.6, 136.4, 133.0, 132.9, 132.7, 132.2, 128.4, 128.3, 128.2, 127.2, 126.7, 126.6, 126.0, 125.5, 125.3, 123.2, 122.8, 72.1, 69.4, 65.4, 43.4, 43.4, 42.6, 33.6, 33.2, 33.0, 31.4, 31.3, 28.6, 27.7, 27.3, 25.9, 25.6, 24.9, 3.2, 2.9.

General polymerization procedures. Polymerizations were performed in 5.5 mL glass reactors inside the inert glovebox at RT. The reactor was charged with a predetermined amount of catalyst and/or initiator and solvent (as specified in the polymerization tables) in a glovebox. The mixture was stirred at RT for 10 min, and the polymerization was initiated by rapid addition to an 8DL monomer. After a desired time period, the polymerization was immediately quenched by addition of 0.5 mL of benzoic acid/chloroform (10 mg mL^{-1}) and a 0.02 mL of aliquot was taken from the

reaction mixture and prepared for ^{1}H NMR analysis to obtain the percent monomer conversion data. The polymerization was then precipitated into cold acidic methanol (5% HCl) and washed three times by reprecipitating into cold methanol while stirring to remove any unreacted monomer and residual catalyst, and dried in a vacuum oven at 50 °C overnight (> 12 h) to a constant weight.

Absolute Molecular Weight Measurements. Measurements of polymer absolute weight-average molecular weight (M_w), number average molecular weight (M_n), and dispersity indices ($Đ = M_w / M_n$) were performed via gel-permeation chromatography (GPC). The GPC instrument consisted of an Agilent HPLC system equipped with one guard column and three PLgel 5 µm mixed-C gel permeation columns and coupled with a Wyatt DAWN HELEOS II multi (18)- angle light scattering detector and a Wyatt Optilab TrEX dRI detector; the analysis was performed at 40 °C using chloroform as the eluent at a flow rate of 1.0 mL min^{-1}, using Wyatt ASTRA 7.1.3 molecular weight characterization software. The refractive index increment (d*n*/d*c*) was determined to be 0.0254 ± 0.0004 mL/g for P3HB, 0.0364 ± 0.0017 mL/g for P3HV, and 0.0292 ± 0.0010 mL/g for P3HHp, obtained by batch experiments using Wyatt Optilab TrEX dRI detector and calculated using ASTRA software. Polymer solutions were prepared in chloroform and injected into *d*RI detector by Harvard Apparatus pump 11 at a flow rate of 0.3 mL/min. A series of known concentrations were injected and the change in refractive index was measured to obtain a plot of change in refractive index versus change in concentration ranging from 0.4 to 5.0 mg/mL. The slope from a linear fitting of the data was the d*n*/d*c* of the polymer. Random and block specimens d*n*/d*c* values were calculated based on weighted average with respect to co-monomer composition.

Spectroscopic Characterization. NMR spectra were recorded on a Bruker AV-III 400 MHz spectrometer (400 MHz, ^{1}H; 100 MHz, ^{13}C). Chemical shifts for ^{1}H and ^{13}C spectra were referenced to internal solvent resonances and are reported as parts per million relative to $SiMe_4$.

Thermal analysis. Melting transition (T_m) and glass transition (T_g) temperatures were measured by differential scanning calorimetry (DSC) on an Auto Q20, TA Instrument. All T_m and T_g values were obtained from a second scan after the thermal history was removed from the first scan, unless noted otherwise. The second heating rate was 5 °C/min and cooling rate was 5 °C/min. This heating and cooling is a standard condition to compare other chemically synthesized PHAs in our lab. Decomposition temperatures (T_d, defined by the temperature of 5 % weight loss) and maximum rate decomposition temperatures (T_{max}) of the polymers were measured by thermal gravimetric analysis (TGA) on a Q50 TGA Analyzer, TA Instrument. Polymer samples were heated from ambient temperatures to 700 °C under N_2 at a heating rate of 10 °C min^{-1}. Values of T_{max} were obtained from derivative (wt %/°C) vs. temperature (°C) plots, while T_d and T_{onset} values (initial and end temperatures) were obtained from wt % vs. temperature (°C) plots.

Mechanical Analysis. Tensile stress/strain testing was performed by an Instron 5966 universal testing system (10 k*N* load cell) on dog-bone-shaped test specimens (ASTM D638 standard; Type V) prepared *via* compression molding using a Carver Bench Top Laboratory Press (Model 4386) equipped with a two-column hydraulic unit (Carver, Model 3912, maximum force 24000 psi). Isolated polymer materials were loaded between non-stick Teflon paper sheets into a stainless-steel mold with inset dimensions 30 × 73.5 × 0.87 mm fabricated in house, and compressed between two 6” × 6” steel electrically heated platens (EHP) clamp force 5000 psi, at melting temperature determined by DSC. Specimens were held in melt for 5 min before compression and heat was turned off to slow cool after 3 min of compression. Specimens for analysis were cut using an ASTM D638-5-IMP cutting die (Qualitest) to standard dimensions. From each compression molding procedure using the stainless-steel mold described, two ASTM D638-5 standard dog-bone shaped specimens could be cut. To reduce the amount of materials

needed for mechanical testing while examining their reprocessability, the measured dog-bone specimens were reprocessed for subsequent trials rather than virgin materials prepared for each measurement. Thus, the workflow would proceed as follows: virgin materials were compression molded to yield two new specimens and measured using the Instron instrument to the point of failure, before reprocessing the material in a subsequent round of compression molding to yield two reprocessed specimens to be again measured to the point of failure. Mechanical behavior was averaged for all the specimens measured for each individual species investigated. Thickness (0.85 ± 0.01 mm), width (3.18 mm), and grip length (26.4 ± 0.2 mm) of the measured dog-bone specimens were measured for normalization of data by the Bluehill measurement software (Instron). Test specimens were affixed into the screw-tight grip frame. Tensile stress and strain were measured to the point of material break at a grip extension speed of 10.0 mm min^{-1} at ambient conditions.

Dynamic Mechanical Analysis

Storage modulus (*E*'), loss modulus (*E*") and tan delta (*E*"/*E*') trace for tri-BCP P3HB-b-P3HHp-b-P3HB (64% midblock) were measured on a Q800 DMA Analyzer (TA Instruments) in a tension film mode. Temperature-ramp frequency sweep experiments were performed from -50 ^{o}C to 200 ^{o}C at a heating rate of 5 ^{o}C/min and were pulled at 0.3 % strain with a frequency of 1 Hz. Film thickness was also measured for normalization of the data by the Q-series measurement software (TA Instruments). Specimens were mounted to screw-tight grips (maximum 2 N).

SAX/WAXS characterization.

Carried out by SLAC – waiting for them to send me their experimental

Additional Tables

Table S5.1. Conversion and molecular weight data for ROP of *rac*-8DL^{Et} with **1** and BDM from Fig 1A (black) and B.[a]

Time (s)	*rac*-8DL^{Et} conv.[b] (%)	M_n [c] (g/mol)	$Đ$ [c] (M_w/M_n)
20	20.6	22880	1.15
80	28.6	26880	1.07
100	30.5	27530	1.11
360	45.3	34770	1.08
900	67.7	44610	1.20
1200	78.4	46840	1.13

[a] Conditions: *rac*-8DL^{Et} = 0.50 mmol in CH_2Cl_2, $V_{solvent}$ = 1.0 mL, [8DL] = 0.5 M; r.t.; catalyst to BDM initiator ratio fixed at 2/1, and [*rac*-8DL^{Me}+*rac*-8DL^{Et}]/[I]=400. [b] Monomer conversions measured by ^{1}H NMR. [c] Determined by GPC coupled with an 18-angle light scattering detector at 40 °C in chloroform.

Table S5.2. Conversion and molecular weight data for ROP of *rac*-8DL^{Bu} with **1** and BDM from Fig 1A (red) and C.

Time (s)	*rac*-8DL^{Et} conv. (%)	M_n (g/mol)	$Đ$ (M_w/M_n)
60	8.6	18360	1.06
100	10.3	19360	1.16
300	15.9	27240	1.15
720	28.6	52870	1.08
1800	53.4	93670	1.08
2400	62.0	121200	1.06

[a] Conditions: *rac*-8DL^{Bu} = 0.40 mmol in CH_2Cl_2, $V_{solvent}$ = 0.8 mL, [8DL] = 0.5 M; r.t.; catalyst to BDM initiator ratio fixed at 2/1, and [*rac*-8DL^{Me}+*rac*-8DL^{But}]/[I]=400. [b] Monomer conversions measured by ^{1}H NMR. [c] Determined by GPC coupled with an 18-angle light scattering detector at 40 °C in chloroform.

Table S5.3. Small scale tri-BCP.

Run	Midblock	[*rac*-DL] /[**I**] [a]	$M_{n,P3H(V/HHp)}$ [b] (kg mol^{-1})	$M_{n,P3HB}$ [b] (kg mol^{-1})	$M_{n,total}$ [b] (kg mol^{-1})	*% Midblock*	$Đ$ [b] (M_w/M_n)
1	P3HV	600/1	60	90	150	40	1.08
2	P3HHp	1800/1	227	98	325	70	1.08

[a] Conditions: Run 1: [*rac*-8DL^{Et}+ *rac*-8DL^{Me}] = 0.87 mmol in DCM, $V_{solvent}$ = 0.29 mL, [*rac*-8DL^{Et}] = 1 M; RT. Run 2: [*rac*-8DL^{Bu}+ *rac*-8DL^{Me}] = 0.87 mmol in DCM, $V_{solvent}$ = 0.29 mL, [*rac*-8DL^{Bu}] = 1 M; RT.; catalyst to BDM initiator ratio fixed at 2/1, and [*rac*-8DL^{Me}+*rac*-8DL^{But}]/[I]=400. [b] Monomer conversions measured by ^{1}H NMR. [c] Determined by GPC coupled with an 18-angle light scattering detector at 40 °C in chloroform.

Table S5.4. Mechanical data for P3HB-*b*-P3HV-*b*-P3HB

specimen	Young's modulus (MPa)	ultimate tensile strength (MPa)	elongation at break (%)

1	583	25.6	331.6
2	672	27.6	347.1
AVG	627±63	26.6±1.4	339±11

Table S5.5. Mechanical data for P3HB-*b*-P3HHp-*b*-P3HB (64% midblock)

specimen	Young's modulus (MPa)	ultimate tensile strength (MPa)	elongation at break (%)
1	0.311	8.05	330
2	0.53	7.06	313
3	0.51	6.0	228
AVG	0.45±0.09	7.03±1.0	290±45

Table S5.6. Mechanical data for P3HB-*b*-P3HHp-*b*-P3HB (80% midblock)

specimen	Young's modulus (MPa)	ultimate tensile strength (MPa)	elongation at break (%)
1	1.77	4.72	431
2	1.50	3.32	304
3	1.41	3.62	405
AVG	1.56±0.18	3.9±0.74	380±67

Table S5.7. Mechanical data for P3HB-*b*-P3HBHp-*b*-P3HB (70% midblock)

specimen	Young's modulus (MPa)	ultimate tensile strength (MPa)	elongation at break (%)
1	502	17.9	309
2	439	13.2	235
3	474	12.9	282
AVG	471±32	14.7±2.8	275±37

Table S5.8. Mechanical data for P3HB-*co*-P3HHp (40% 3HHp)

specimen	Young's modulus (MPa)	ultimate tensile strength (MPa)	elongation at break (%)

1	382	0.019	598
2	373	0.020	842
3	11.7	0.040	608
AVG	255±211	0.026±0.012	683±138

Table S5.9. Tri-BCP series sent to SLAC for SAX and WAXS analysis

Sample Name	Midblock	% midblock	M_n total[a] (kg/mol)	$Đ$[a] (M_w/M_n)	T_m (°C) [b]
A	P3HV	45	169	1.02	151
B	P3HV	80	173	1.05	148
C	P3HHp	70	90	1.01	142
D	P3HHp	78	92	1.01	142

[a] Determined by GPC coupled with an 18-angle light scattering detector at 40 °C in chloroform. [b] Determined by DSC second heating scan (5 °C/min)

Additional Figures

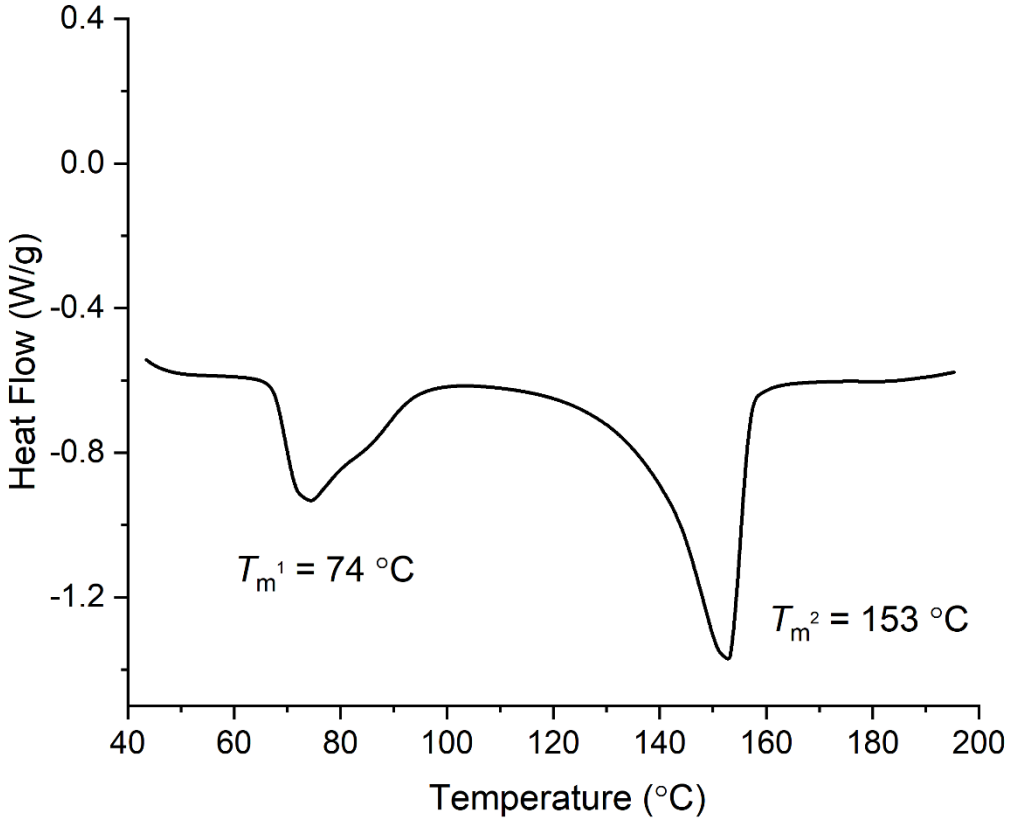

Figure S5.1. DSC of P3HB-*b*-P3HV-*b*-P3HB (first heating scan (black) = 10 °C/min and cooling and second heating scan (red) = 1 °C/min).

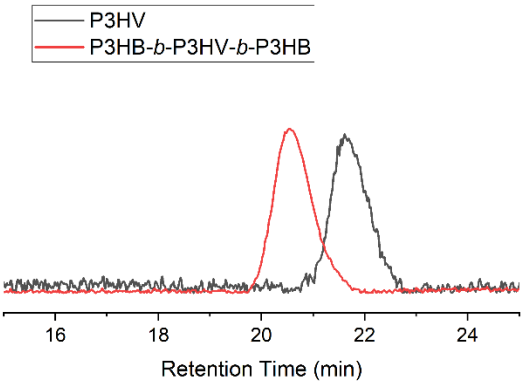

Figure S5.2. GPC trace overlay of Table S5.3, run 1. Black curve: P3HV midblock (M_n = 60 kg mol^{-1}, $Đ$ = 1.10); red curve: tri-BCP, (M_n = 150 kg mol^{-1}, $Đ$ = 1.08). Midblock =40%

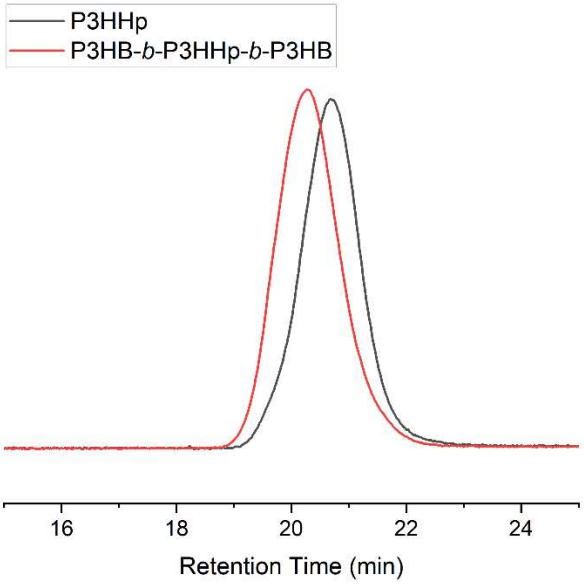

Figure S5.3. GPC trace overlay of Table S5.3, run 2. Black curve: P3HV midblock (M_n = 227 kg mol^{-1}, $Đ$ = 1.07); red curve: tri-BCP, (M_n = 325 kg mol^{-1}, $Đ$ = 1.08). Midblock =70%

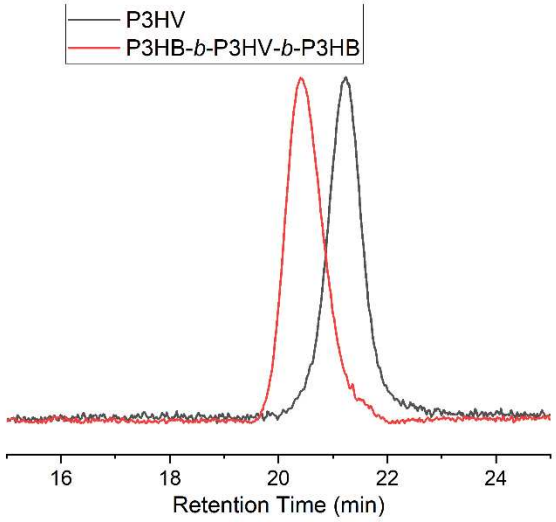

Figure S5.4. GPC trace overlay of sample 1 from Table 5.1. Black curve = P3HV midblock (M_n = 84.4 kg/mol, $Đ$ = 1.03), red curve = triblock (M_n = 144 kg/mol, $Đ$ = 1.14.) Midblock = 58%

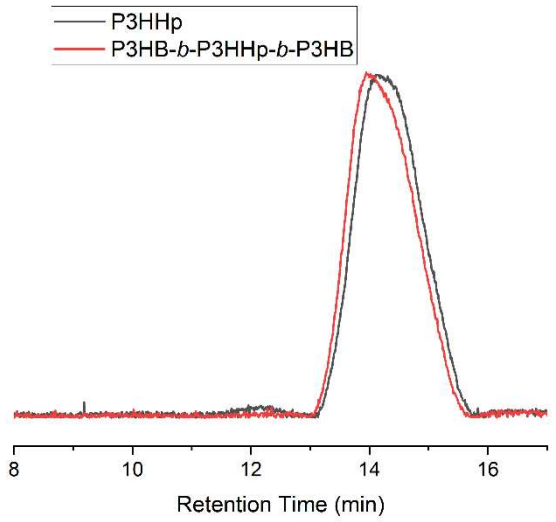

Figure S5.5. GPC trace overlay of Sample 3, Table 5.1. Black curve: P3HHp midblock (M_n = 172 kg mol^{-1}, $Đ$ = 1.05); red curve: triblock, (M_n = 200 kg mol^{-1}, $Đ$ = 1.05). Midblock =86%

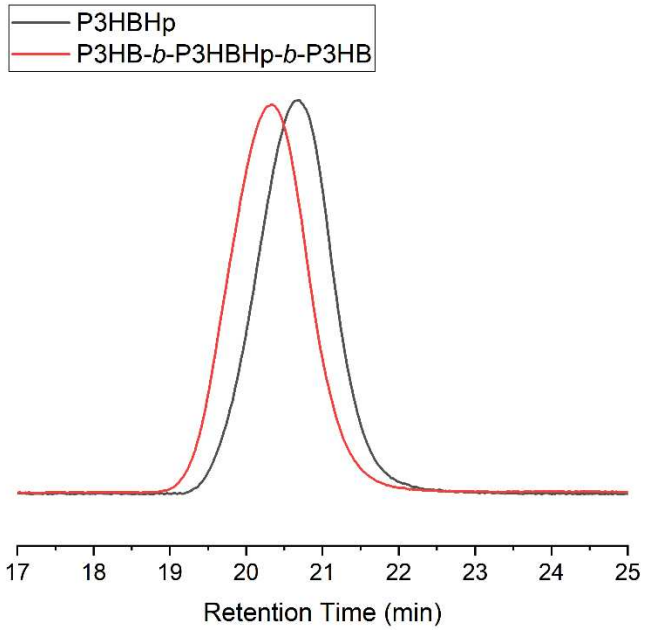

Figure S5.6. GPC trace overlay of Sample 4, Table 5.1. Black curve: P3HBHp midblock (M_n = 164 kg mol^{-1}, $Đ$ = 1.13); red curve: triblock, (M_n = 230 kg mol^{-1}, $Đ$ = 1.13). Midblock =71%

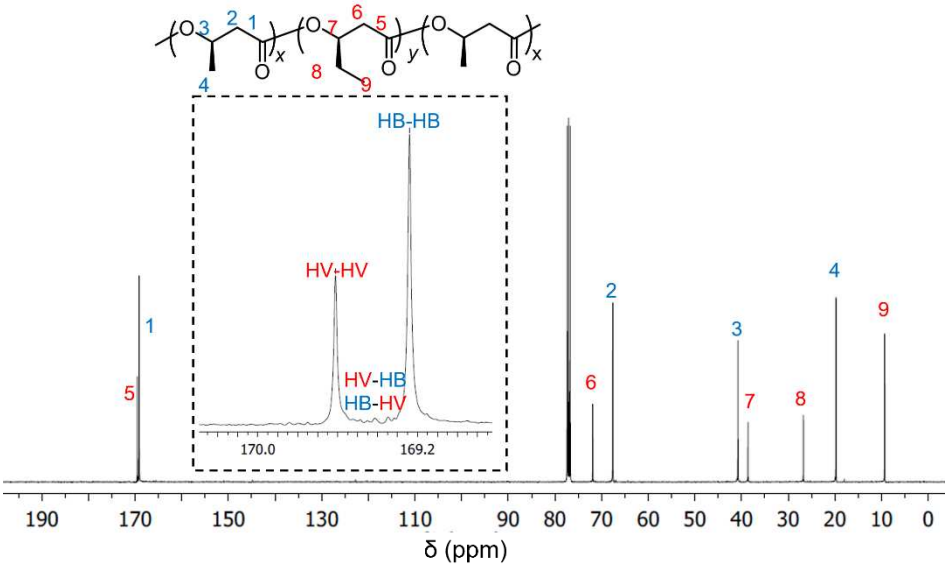

Figure S5.7. ^{13}C-NMR ($CDCl_3$, 100MHz) of Sample 1, Table 5.1.

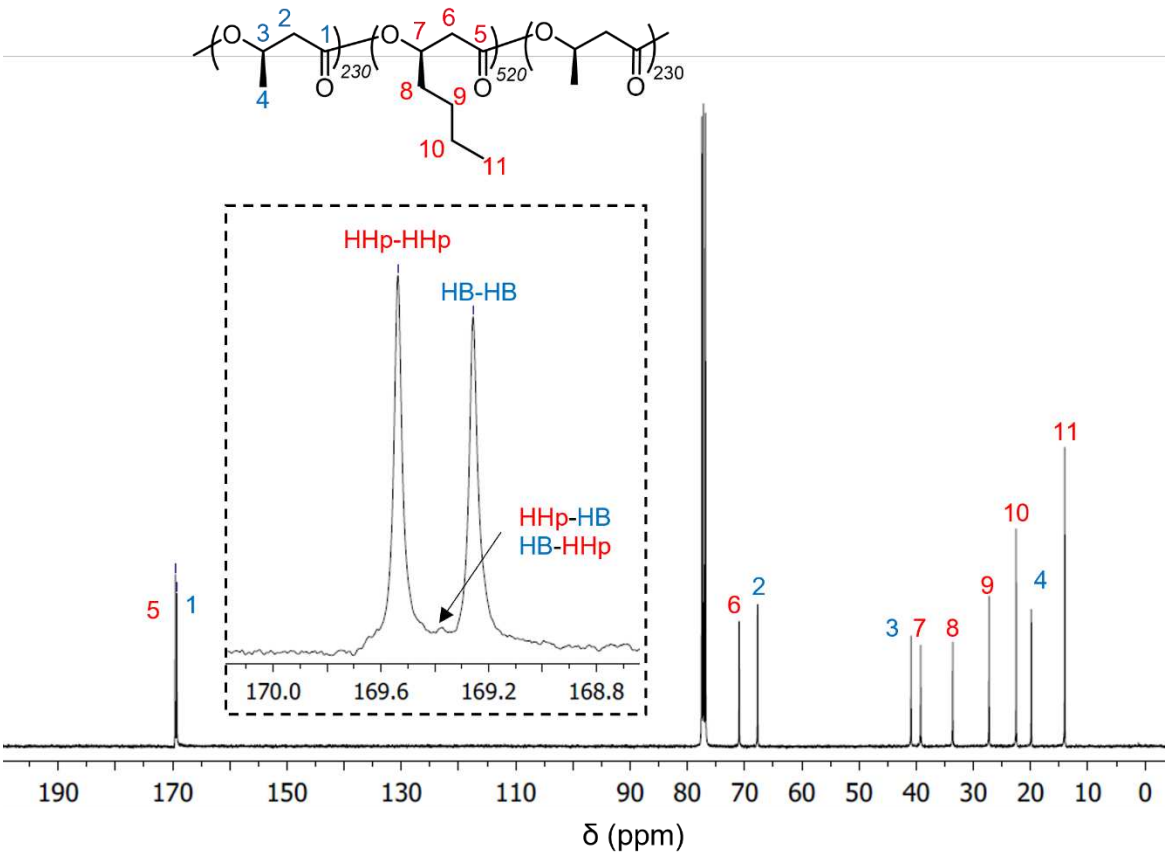

Figure S5.8. ^{13}C-NMR ($CDCl_3$, 100MHz) of Sample 2, Table 5.1

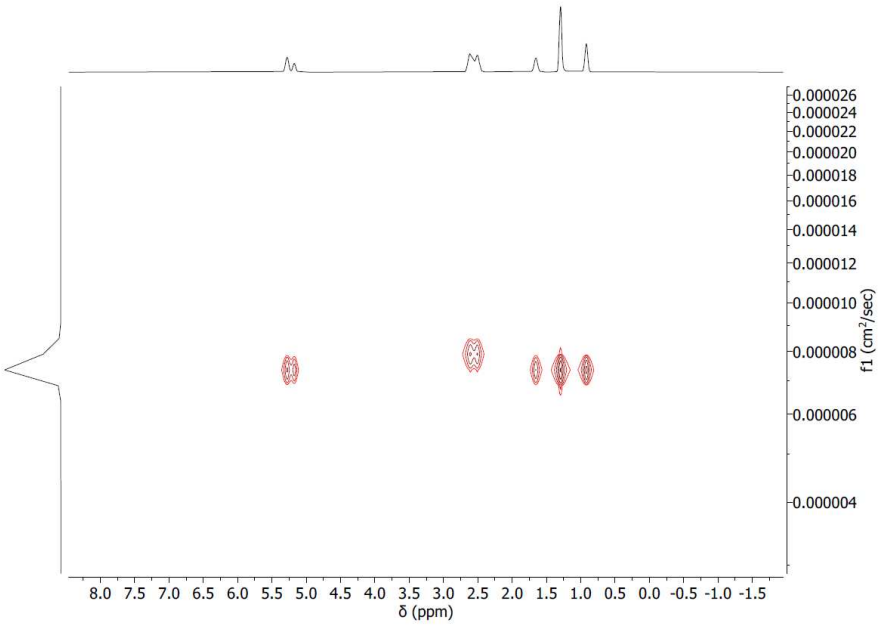

Figure S5.9. DOSY ($CDCl_3$, 500MHz) of P3HB-*b*-P3HV-*b*-P3HB Sample 1, Table 5.1

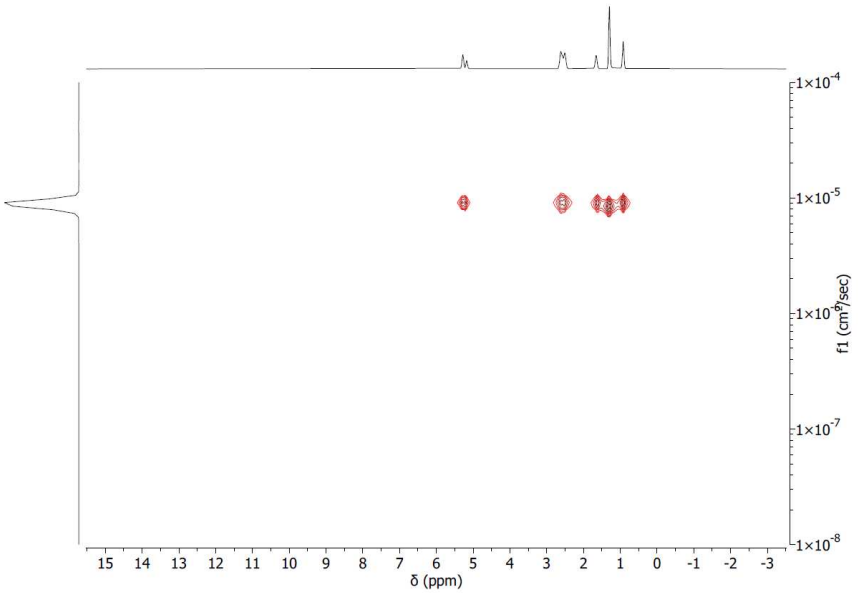

Figure S5.10. DOSY ($CDCl_3$, 500MHz) spectrum of P3HB-*b*-P3HHp-*b*-P3HB: Sample 2, Table 5.1

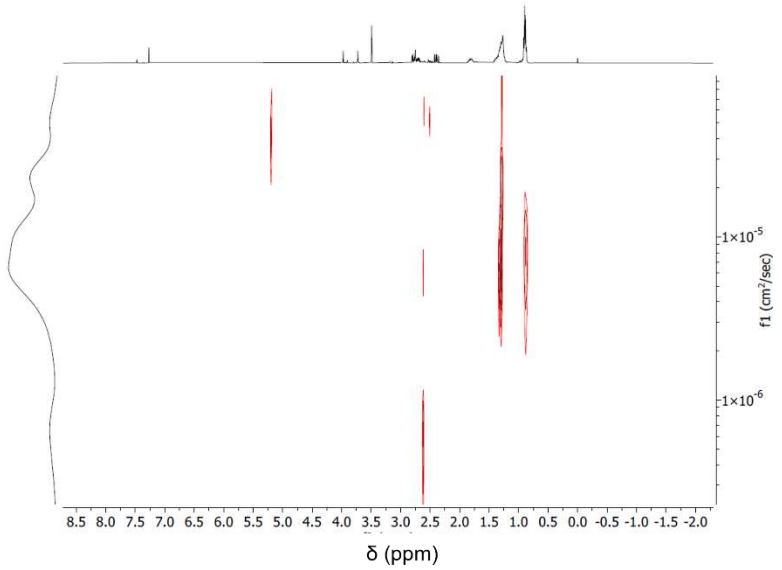

Figure S5.11. DOSY ($CDCl_3$, 500MHz) spectrum of a mixture of P3HB and P3HHp homopolymer

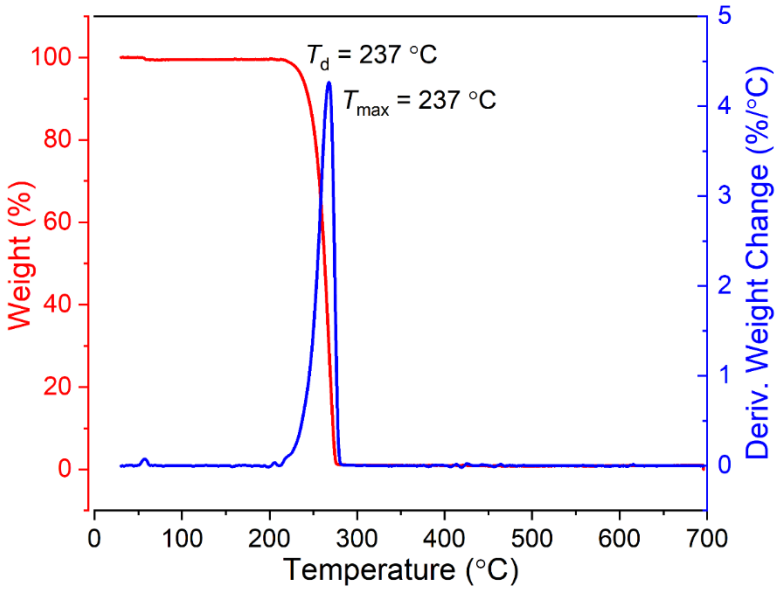

Figure S5.12. TGA of P3HB-*b*-P3HHp-*b*-P3HB (64% midblock), Sample 2, Table 5.1

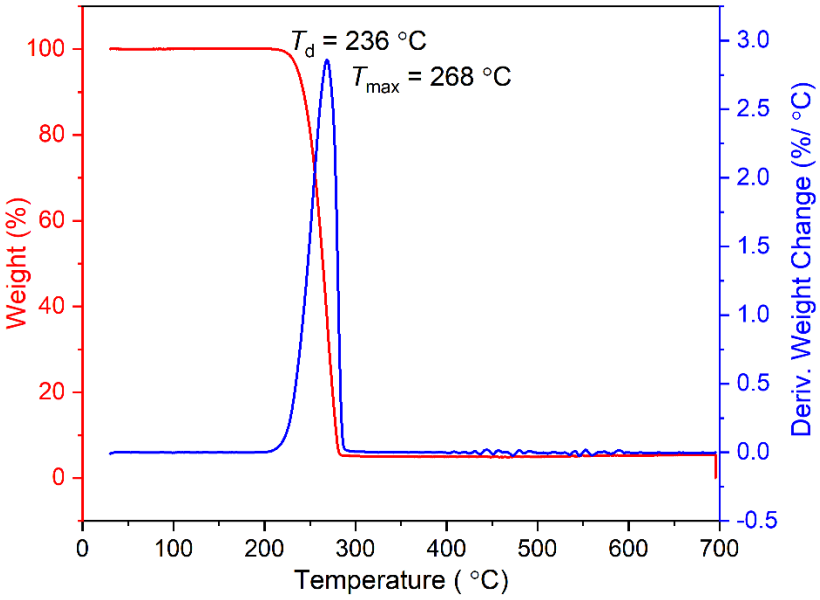

Figure S5.13. TGA of P3HB-*b*-P3HHp-*b*-P3HB (85% midblock), Sample 3, Table 5.1

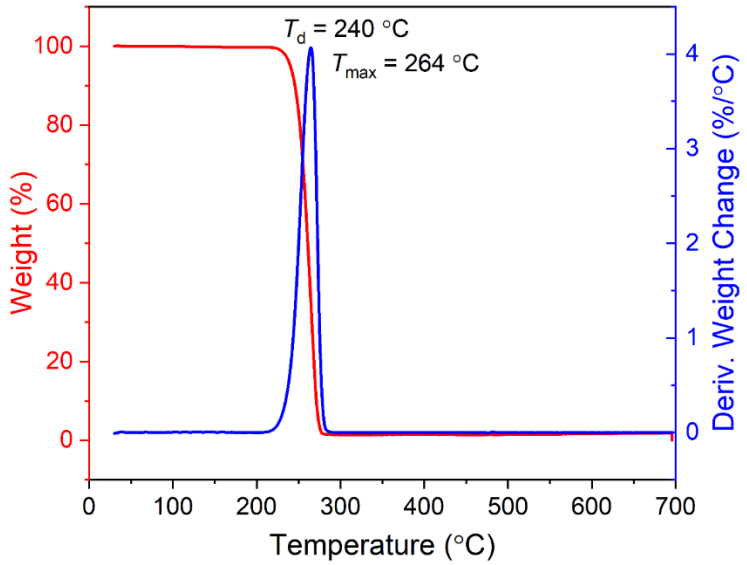

Figure S5.14. TGA of P3HB-*b*-P3HBHp-*b*-P3HB (71% midblock), Sample 4, Table 5.1

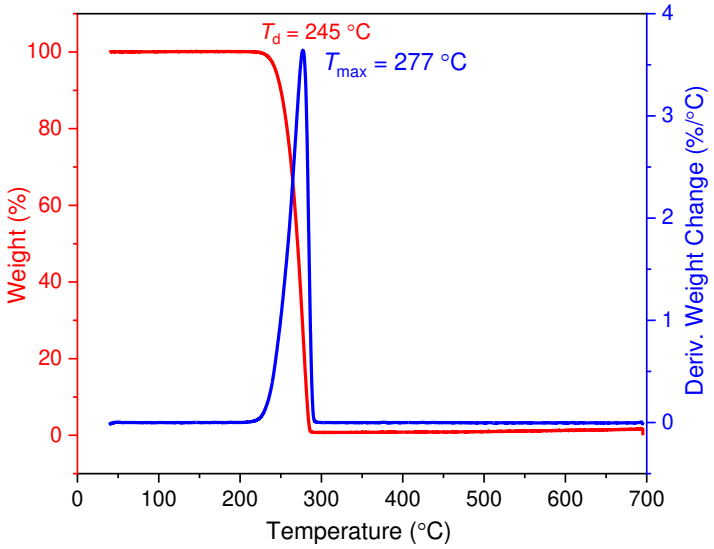

Figure S5.15. TGA of tri-BCP P3HB-*b*-P3HHp-*b*-P3HB (~70% midblock). TGA with no isothermal hold. Washed sample 5 times, dried at 50 °C under vacuum overnight (>12 h)

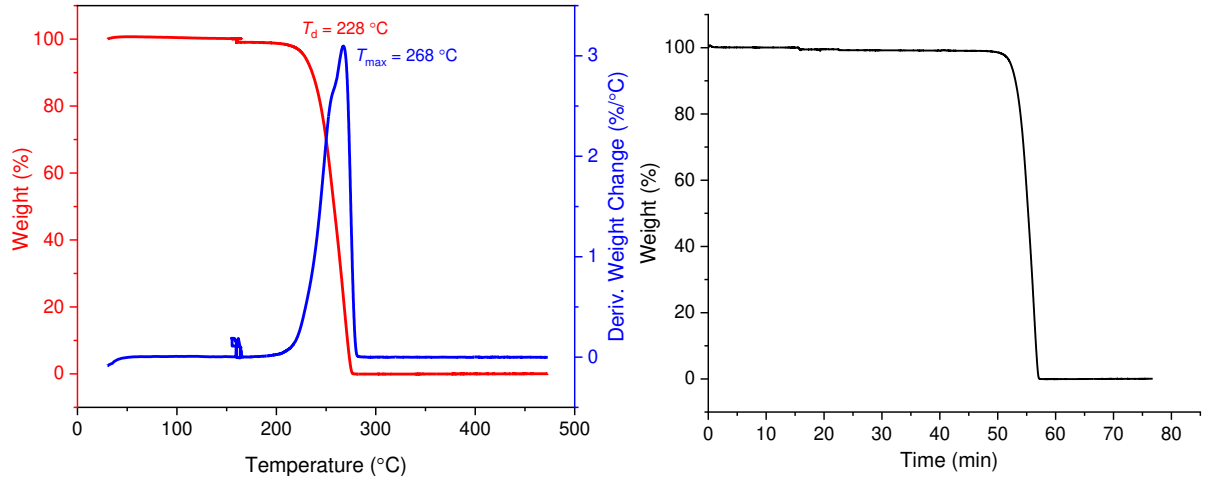

Figure S5.16. TGA of tri-BCP P3HB-*b*-P3HHp-*b*-P3HB (~70% midblock). TGA with an isothermal hold at 160 °C for 45 min. 1% weight loss during hold. Washed sample 5 times, dried at 50 °C under vacuum overnight (>12 h)

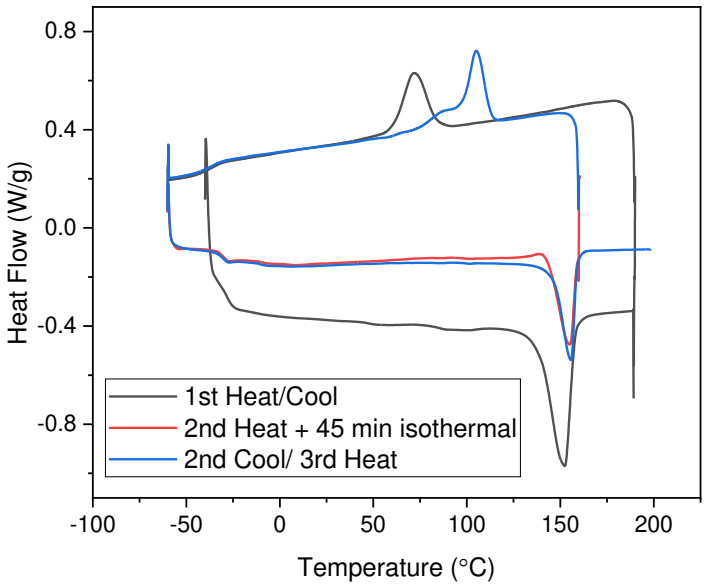

Figure S5.17. DSC of tri-BCP P3HB-*b*-P3HHp-*b*-P3HB (~70% midblock) with isothermal hold. First heating scan to 180 °C at 10 °C/min, cool to -60 °C at 5 °C/min, heat to 160 °C at 5 °C/min and isothermal hold for 45 min, cool to -60 °C at 5 °C/min, heat to 200 °C at 5 °C/min. 2nd heating scan: T_m = 155 ° C, ΔH = 23.8 J/g. 3rd heating scan: T_m = 155 ° C, ΔH = 28.7 J/g

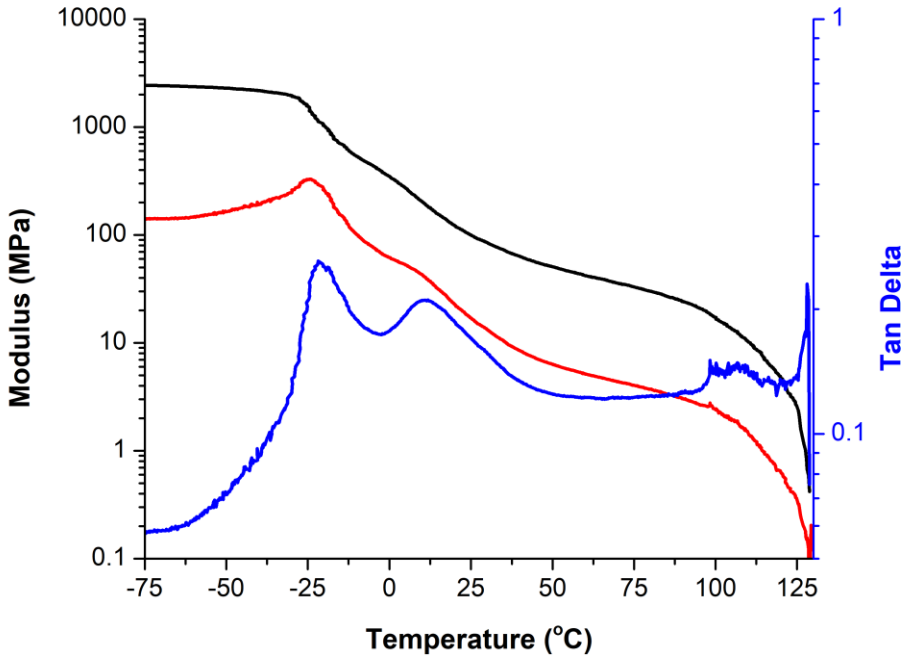

Figure S5.18. DMA of P3HB-*b*-P3HHp-*b*-P3HB (64% midblock) tri-BCP

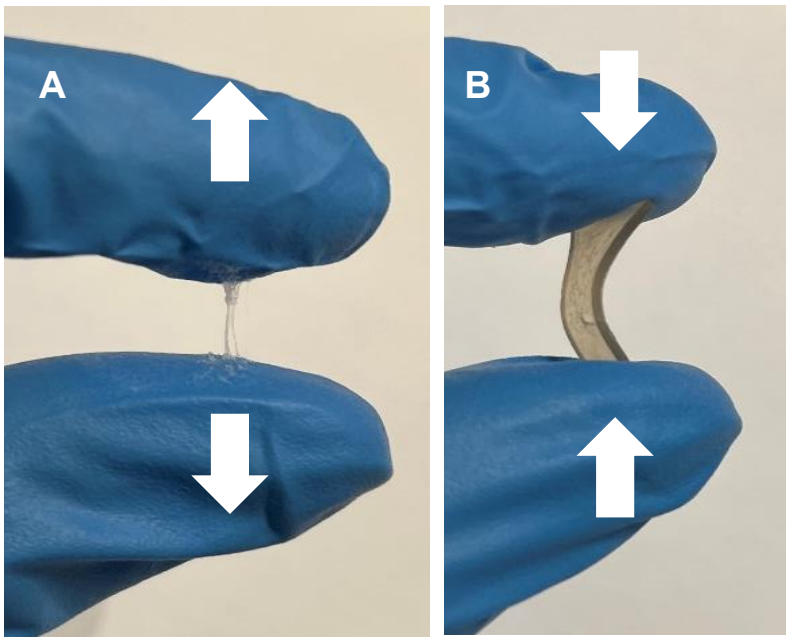

Figure S5.19. A. Pulling apart P3HB-*co*-P3HHp (60% 3HHp incorp.) random copolymer. B) Bending piece of P3HB-*b*-P3HHp-*b*-P3HB (64% midblock) tri-BCP film.

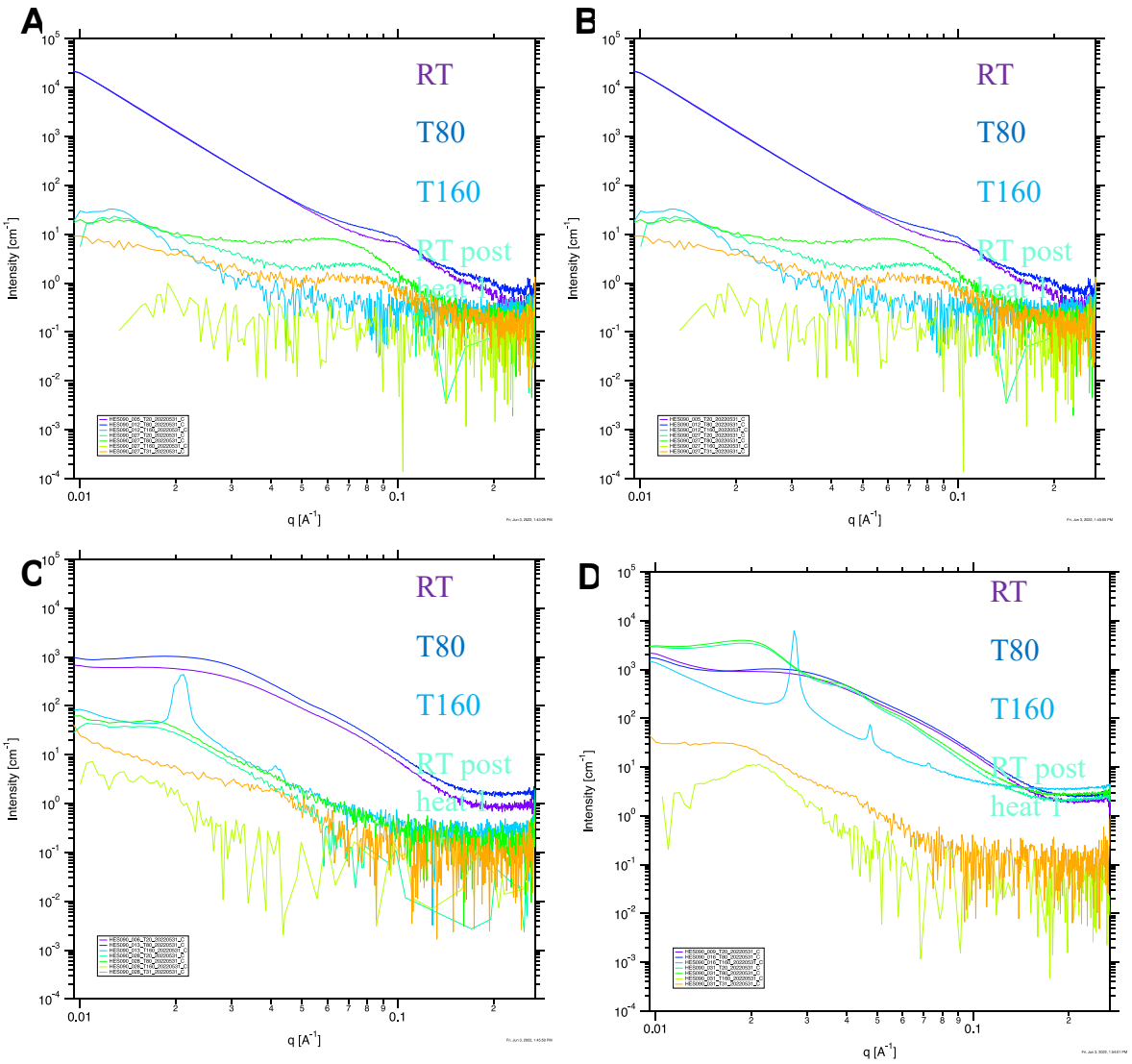

Figure S5.20. A) P3HB-*b*-P3HV-*b*-P3HB (45% midblock). B) P3HB-*b*-P3HV-*b*-P3HB (80% midblock). C) P3HB-*b*-P3HHp-*b*-P3HB (70% midblock). D) P3HB-*b*-P3HHp-*b*-P3HB (77% midblock)

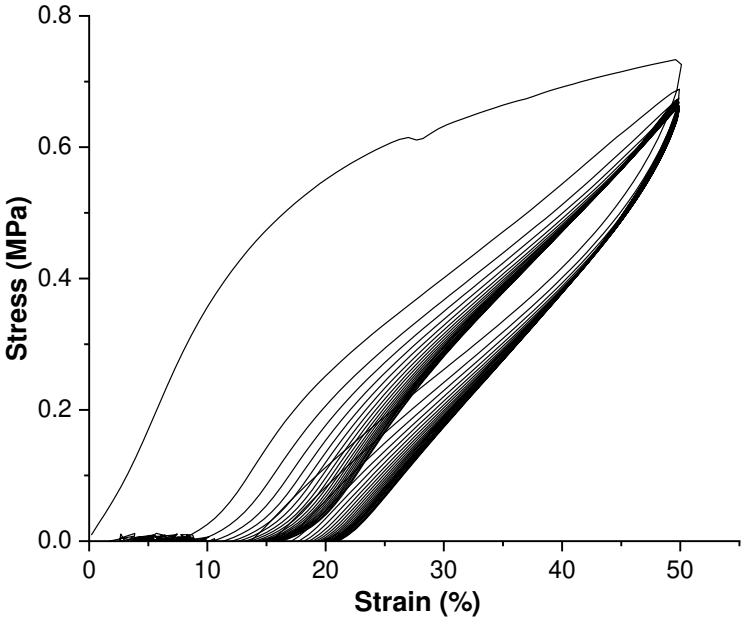

Figure S5.21. Hysteresis of P3HB-*b*-P3HHp-*b*-P3HB (86% midblock), Sample 3, Table 5.1. 60% elastic recovery after 20 cycles.